SANDIA REPORT
SAND2011-0673
Unlimited Release
Printed February 2011

Advances in Process Intensification through Multifunctional Reactor Engineering

Timothy J. O'Hern, Walt Gill, Lindsey R. Evans, James E. Miller, Marcia A. Cooper

Prepared by
Sandia National Laboratories
Albuquerque, New Mexico 87185 and Livermore, California 94550

Sandia National Laboratories is a multi-program laboratory managed and operated by Sandia Corporation, a wholly owned subsidiary of Lockheed Martin Corporation, for the U.S. Department of Energy's National Nuclear Security Administration under contract DE-AC04-94AL85000.

Approved for public release; further dissemination unlimited.

Sandia National Laboratories

Issued by Sandia National Laboratories, operated for the United States Department of Energy by Sandia Corporation.

NOTICE: This report was prepared as an account of work sponsored by an agency of the United States Government. Neither the United States Government, nor any agency thereof, nor any of their employees, nor any of their contractors, subcontractors, or their employees, make any warranty, express or implied, or assume any legal liability or responsibility for the accuracy, completeness, or usefulness of any information, apparatus, product, or process disclosed, or represent that its use would not infringe privately owned rights. Reference herein to any specific commercial product, process, or service by trade name, trademark, manufacturer, or otherwise, does not necessarily constitute or imply its endorsement, recommendation, or favoring by the United States Government, any agency thereof, or any of their contractors or subcontractors. The views and opinions expressed herein do not necessarily state or reflect those of the United States Government, any agency thereof, or any of their contractors.

Printed in the United States of America. This report has been reproduced directly from the best available copy.

Available to DOE and DOE contractors from
U.S. Department of Energy
Office of Scientific and Technical Information
P.O. Box 62
Oak Ridge, TN 37831

Telephone: (865)576-8401
Facsimile: (865)576-5728
E-Mail: reports@adonis.osti.gov
Online ordering: http://www.doe.gov/bridge

Available to the public from
U.S. Department of Commerce
National Technical Information Service
5285 Port Royal Rd
Springfield, VA 22161

Telephone: (800)553-6847
Facsimile: (703)605-6900
E-Mail: orders@ntis.fedworld.gov
Online ordering: http://www.ntis.gov/help/ordermethods.asp?loc=7-4-0#online

SAND2011-0673
Unlimited Release
Printed February 2011

Advances in Process Intensification through Multifunctional Reactor Engineering

Timothy J. O'Hern, Walt Gill
Engineering Sciences Center

Lindsey R. Evans, James E. Miller
Materials Sciences and Engineering Center

Marcia A. Cooper
Energetic Components Realization Center

Sandia National Laboratories
P.O. Box 5800
Albuquerque, NM 87185

Abstract

A multifunctional reactor is a chemical engineering device that exploits enhanced heat and mass transfer to promote production of a desired chemical, combining more than one unit operation in a single system. The main component of the reactor system under study here is a vertical column containing packing material through which liquid(s) and gas flow cocurrently downward. Under certain conditions, a range of hydrodynamic regimes can be achieved within the column that can either enhance or inhibit a desired chemical reaction. To study such reactors in a controlled laboratory environment, two experimental facilities were constructed at Sandia National Laboratories. One experiment, referred to as the Two-Phase Experiment, operates with two phases (air and water). The second experiment, referred to as the Three-Phase Experiment, operates with three phases (immiscible organic liquid and aqueous liquid, and nitrogen). This report describes the motivation, design, construction, operational hazards, and operation of the both of these experiments. Data and conclusions are included.

Acknowledgment

The financial support of the US Department of Energy, Energy Efficiency and Renewable Energy Office (DOE/EERE), Industrial Technologies Program, Dickson Ozokwelu, contract monitor, is acknowledged. Additional support has been provided by CR&L/CDTECH. Bill Prymak at the DOE Golden Field Office was also a great support with project management issues.

This work was done with the close collaboration of our industrial partners Chemical Research and Licensing (CR&L) and ABB Lummus, cooperating together through their partnership Catalytic Distillation Technology CDTECH®. Will Cross, Richard Foley, and Larry Smith were particularly helpful in defining and initiating this project. Will Cross provided excellent technical interaction over the course of the project, and Richard Foley kept both technical and administrative function operating smoothly.

This program ran over the 2004-2010 time frame and a number of individuals were involved. In particular, Donovan Peña was key in developing the fluorescein mass transfer measurement. John Torczynski was instrumental in the flow loop design. Professor Steve Ceccio of the University of Michigan visited and installed the electrical impedance diagnostic on the gas-liquid two-phase experiment, and provided valuable consultation on the project. The authors especially want to acknowledge the excellent technical support at Sandia National Laboratories of Tom Grasser, Jeremy Barney, Bennie Belone, and Shane Adee in the setup and operation of the experiment. Katie Sy, Mai Luu, and Joel Hartenberger all performed experiments while student interns at Sandia. Thanks also to the Sandia peer reviewers who provided valuable comments.

Sandia is a multiprogram laboratory operated by Sandia Corporation, a Lockheed Martin Company, for the United States Department of Energy's National Nuclear Security Administration under Contract DE-AC04-94AL85000.

Contents

Nomenclature **11**

Executive Summary **13**

1. Introduction **15**
- 1.1 Introduction 16
- 1.2 Literature Review 16

2. Two-Phase Experiments **23**
- 2.1 Two-Phase, Non-Reactive, Fixed-Bed Experiment 23
  - 2.1.1 Previous methods for determining trickle-pulse transition 23
  - 2.1.2 Previous work studying wall effects 25
- 2.2 Experimental Facility 26
- 2.3 Packings 29
- 2.4 Results 31
  - 2.4.1 Pulse flow in beds of large particles 31
  - 2.4.2 Time-averaged, bed pressure drop 33
  - 2.4.3 Pulse pressure drop and transition boundary 35
  - 2.4.4 Flow characteristics at trickle-pulse transition 40
- 2.5 Conclusions 43

3. Three-Phase Experiments **45**
- 3.1 Reactor Description and Components 45
  - 3.1.1 Column 47
  - 3.1.2 Problems and Repairs 50
- 3.2 Separator 51
- 3.3 Gas sub-system 51
  - 3.3.1 Heat Exchangers 51
  - 3.3.2 Knockout Tank 51
- 3.4 Liquid sub-system 51
- 3.5 Liquids tested 52
- 3.6 Operations and Control 52
- 3.7 Mass Transfer Measurements 54
  - 3.7.1 Background 54
  - 3.7.2 Implementation in Multiphase Reactor 60
- 3.8 Results 63
  - 3.8.1 Hydrodynamic Data 63
  - 3.8.2 Mass Transfer Data 71

4. Conclusions **91**

Appendix A. Two-Phase Operating Procedures **92**

Appendix B. Two-Phase Viscosity Memo **96**

Appendix C. Two-Phase Resin Memo **99**

Appendix D. AIChE 2005 two-phase paper **105**

Appendix E. 2005 ASME two-phase paper **114**

Appendix F. Two-Phase Data Sets 123

Appendix G. Three-Phase Equipment List 165

Appendix H. Three-Phase Safety Considerations.....166

H.1 Pressure Ratings 166

H.1.1. Internal Pressure 167

H.1.2. External pressure 167

H.1.3. Separator Tank Pressure Ratings.....168

H.2 Chemical Hazards and Mitigation 169

H.2.1 Occupational Exposure Limits and Ventilation System.....169

H.2.2 Vacuum purge requirements.....170

H.2.3 Flammability limits 170

H.2.4. Creating a nonflammable mixture with a single component fuel.....172

H.2.5. Component concentrations in the vapor blend 174

H.2.6. Conclusions 177

Appendix I. Three-Phase Operations.....178

5. References.....184

Figures

Figure 1.1. Flow Regime Map of Blok et al. (1983).....17
Figure 2.1: Two-phase experiment schematic 27
Figure 2.2: Photograph showing major component of two-phase experiment. 28
Figure 2.3: Pressure histories near trickle-pulse transition for (A) d = 0.64 cm, L = 6.91 kg/ m^2s, (B) d = 1.27 cm, L = 38.7 kg/ m^2s, (C) d = 2.54 cm, L = 56.9 kg/ m^2s. 32
Figure 2.4: Normalized bed pressure drop versus gas mass flux for (A) d = 0.64 cm (B) d = 1.27 cm (C) d = 2.54 cm. Circled symbols denote pulse inception. 34
Figure 2.5: Determination of maximum average pulse pressure drop: *d* = 1.27 cm, L = 43.3 kg/ m^2s, G = 0.49 kg/m^2s. 35
Figure 2.6: Normalized pressure across pulse versus gas mass flux for (A) d = 0.64 cm; D/d = 15 (B) d = 1.27 cm; D/d = 7.5 (C) d = 2.54 cm; D/d = 3.75. Circled symbols denote pulse inception.....38
Figure 2.7: Flow map showing trickle-pulse transition for all beads. Solid symbols correspond to pulse flow, and open symbols correspond to trickle flow.....39
Figure 2.8: Conductance data showing radial variation of liquid distribution at location C1. d = 0.64 cm, G = 0.236 kg/m^2s, and L = 11.6 kg/m^2s. Data are scaled so that pure liquid = 1 and pure gas = 0. 41
Figure 2.9: Pressure measurements at locations L2 and L3 with *d* = 0.64 cm and *L* = 11.5 kg/m^2s. (A) Pulses first observed (B) Higher gas mass flux G.....41
Figure 2.10: RMS of pressure at locations L2 and L3. d = 0.64 cm.....42
Figure 3.1. Process and Instrumentation Diagram.....46
Figure 3.2. Experimental Layout (Dimensioned Footprint for Three-Phase System).....47
Figure 3.3. Schematic of the Glass Column 48
Figure 3.4. Illustration of the Teflon Sample Ring (left, sketch; right, installed on column). 49
Figure 3.5. The pKa values and peak absorption maxima of fluorescein structures 55
Figure 3.6. Boundary layer diagram for mass transfer with reactive extraction. Adapted from van Woezik and Westerterp (2000).....56
Figure 3.7. Absorbance spectra of three different concentrations (100, 28, and 0 μM) of fluorescein in 0.1M NaOH. The peak *absorbance* at 492 nm was chosen for detection. 57
Figure 3.8. Calibration plot of fluorescein in 0.1M and 1M NaOH relating concentration of fluorescein (μM) to the peak intensity at 492 nm, showing the range over which fluorescein absorbance is linearly related to concentration. 57
Figure 3.9. Integral method kinetic plots collected on a batch reactor with 25.6 μM fluorescein diacetate, 1M NaCl, and 0.1M NaOH at 400 rpm. 59
Figure 3.10. First-order rate equation for stirred batch reactor with varying BHT concentration, based on measured FDA. kt = -ln(FDA/FDA_0) 60
Figure 3.11. FDA mass transfer at varying BHT concentration. 60
Figure 3.12. Time for injected slug of NaF to become well-mixed in column.....61
Figure 3.13. Holdup experiment run during mass transfer test series. Lower layer is aqueous liquid containing sodium fluorescein (green), upper layer (clear) is toluene. 62
Figure 3.14. Blok et al (1983) correlation for column packed with spheres. 63

Figure 3.15. The pulse flow regime for the three phase column with water and air and 6.4 cm spheres as packing. The black dots visible in the center plot indicate the test points. 64
Figure 3.16. The pulse flow regime for the three phase column with water, isododecane and nitrogen. The black dots visible in the center plot indicate the test points. 65
Figure 3.17. Isododecane holdup in WMFP packing when only isododecane and nitrogen are present. 66
Figure 3.18. Water holdup in WMFP packing when only water and nitrogen are present. Note the color contour scale is the same as in the previous holdup figure. 67
Figure 3.19. Isododecane holdup in WMFP packing when isododecane, water and nitrogen are present. Note the color contour scale is the same as in the previous holdup figures. 68
Figure 3.20. Water holdup in WMFP packing when isododecane, water and nitrogen are present. Note the color contour scale is the same as in the previous holdup figures. 69
Figure 3.21. Toluene holdup in WMFP packing when toluene, water and nitrogen are present. Note the color contour scale is the same as in the previous holdup figures. 70
Figure 3.22. Toluene holdup in WMFP packing when toluene, water and nitrogen are present. Note the color contour scale is the same as in the previous holdup figures. 71
Figure 3.23. First order rate equation based on measured FDA in toluene. kt = -ln(FDA/FDA_0). 73
Figure 3.24. First order rate equation for varying organic volume, based on measured FDA in toluene at 20 C. kt = -ln(FDA/FDA_0). 73
Figure 3.25. First order rate equation for fluorescein diacetate (FDA) used in 3-phase system. kt = -ln(FDA_t/FDA_0). 75
Figure 3.26. Time trace of column pressure at top, middle, and bottom of column during 3/18/2010 run. Aqueous flow 28.3 L/min, toluene flow 18.4 L/min, nitrogen gas flow of 3 scfm. 76
Figure 3.27. Periodogram of column pressure during 3/18/2010 run. Aqueous flow 28.3 L/min, toluene flow 18.4 L/min, nitrogen gas flow of 3 scfm. 77
Figure 3.28. Mass transfer data showing concentration of FDA and Na2F during 3/18/2010 run. Aqueous flow 28.3 L/min, toluene flow 18.4 L/min, nitrogen gas flow of 3 scfm. 78
Figure 3.29. First order rate equation for FDA based on measured [NaF] during 3/18/2010 run. kt = -ln(FDA/FDA_0).Aqueous flow 28.3 L/min, toluene flow 18.4 L/min, nitrogen gas flow of 3 scfm. 78
Figure 3.30. Time trace of column pressure at top, middle, and bottom of column during 3/24/2010 run. Aqueous flow 28.3 L/min, toluene flow 18.4 L/min, nitrogen gas flow of 3 scfm. 79
Figure 3.31. Periodogram of column pressure during 3/24/2010 run. Aqueous flow 28.3 L/min, toluene flow 18.4 L/min, nitrogen gas flow of 3 scfm. 80
Figure 3.32. Mass transfer data showing concentration of FDA and Na2F during 3/24/2010 run. Aqueous flow 28.3 L/min, toluene flow 18.4 L/min, nitrogen gas flow of 3 scfm. 80
Figure 3.33. First order rate equation for FDA based on measured [NaF] during 3/24/2010 run. kt = -ln(FDA_t/FDA_0).Aqueous flow 28.3 L/min, toluene flow 18.4 L/min, nitrogen gas flow of 3 scfm. 81

Figure 3.34. Time trace of column pressure at top, middle, and bottom of column during 3/25/2010 run. Aqueous flow 28.3 L/min, toluene flow 18.4 L/min, and no nitrogen gas flow. 82
Figure 3.35. Periodogram of column pressure during 3/24/2010 run. Aqueous flow 28.3 L/min, toluene flow 18.4 L/min, no nitrogen gas flow. 82
Figure 3.36. Mass transfer data showing concentration of FDA and Na2F during 3/25/2010 run. Aqueous flow 28.3 L/min, toluene flow 18.4 L/min, no nitrogen gas flow. 83
Figure 3.37. First order rate equation for FDA based on measured [NaF] during 3/24/2010 run. $kt = -\ln(FDA_t/FDA_0)$. Aqueous flow 28.3 L/min, toluene flow 18.4 L/min, no nitrogen gas flow. 84
Figure 3.38. Time trace of column pressure at top, middle, and bottom of column during 4/28/2010 run. Aqueous flow 28 L/min, toluene flow 6 L/min, nitrogen gas flow 11 scfm. 85
Figure 3.39. Periodogram of column pressure during 4/28/2010 run. Aqueous flow 28 L/min, toluene flow 6 L/min, nitrogen gas flow 11 scfm. 85
Figure 3.40. Mass transfer data showing concentration of FDA and Na2F during 4/28/2010 run. Aqueous flow 28 L/min, toluene flow 6 L/min, nitrogen gas flow 11 scfm. 86
Figure 3.41. First order rate equation for FDA based on measured [NaF] during 4/28/2010 run. $kt = -\ln(FDA_t/FDA_0)$. Aqueous flow 28 L/min, toluene flow 6 L/min, nitrogen gas flow 11 scfm. 87
Figure 3.42. Mass transfer data showing concentration of FDA and Na2F during 5/18/2010 run. Aqueous flow 28 L/min, toluene flow 1.6 L/min, nitrogen gas flow 4 scfm. 88
Figure 3.43. First order rate equation for FDA based on measured [NaF] during 5/18/2010 run. $kt = -\ln(FDA_t/FDA_0)$.Aqueous flow 28 L/min, toluene flow 1.6 L/min, nitrogen gas flow 4 scfm. 88
Figure H.1. Lower flammability limit of toluene and isododecane in air at standard pressure as a function of temperature. 172
Figure H.2. Concentration of a) toluene and b) isododecane in reactant mixture as a function of added nitrogen. 173
Figure H.3. Concentration of a) toluene and b) isododecane in reactant mixture as a function of subtracted air. 174
Figure H.4. Method of partial pressures and upper flammability limit. 177

Tables

Table 2.1: Experimental Parameters 28
Table 2.2: Details of Packed Beds 29
Table 2.3: Partial list of packing types in literature. 29
Table 2.4: Polypropylene sphere size and required quantity 30
Table 3.1. Component Sizes for Experiment Layout 45
Table 3.2. Liquid Properties 52
Table 3.3. Data and control instrumentation 53
Table 3.4. Holdup data for one set of conditions 62
Table 3.5. Data for determining Intrinsic Rate Constant 74
Table 3.5. Test matrix and results. 90
Table H.1. Borosilicate glass material properties (Avallone and Baumeister, 1996) 166
Table H.2. Properties of 304 stainless steel. 168
Table H.3. Required end plate thicknesses. 169
Table H.4. Longitudinal stresses in cylinder due to vacuum and 2-in thick end plate. 169
Table H.5. Properties of volatile compounds: toluene, isododecane, benzene. † 100°C 171
Table H.6. Concentration of components in experimental blend. 175
Table I.1. Valve Positions of "Normal Shutdown Mode" 182
Table I.2. Valve Positions of "Normal Operating Mode" 183

Nomenclature

a_v	Specific surface area of dry packing and column interior walls
d_{c0}	Diameter of equivalent flow channels (Sicardi et al., 1979)
d	Particle or packing bead diameter
D	Column diameter
D_h	Bed hydraulic diameter
Fr	Froude number = ratio of inertial to gravity forces
g	Gravitational acceleration
G	Gas mass flux (kg/m^2s)
h	Bed height
h_t	Total liquid holdup
L	Liquid mass flux (kg/m^2s)
N	Number of particles in a packed bed
Re	Reynolds number = ratio of inertial to viscous forces ($\rho UL/\mu$)
U	Velocity
V_b	Volume of column filled with bead particles
V_s	Volume of a single bead particle
w	Superficial velocity
We	Weber number = ratio of inertial to surface tension forces

Greek

β	Liquid Holdup
β	Combined column Re (Helwick et al., 1992)
ε	Holdup
ε	Bed void fraction
ε_0	Dry bed porosity
η	Packing density
μ	Dynamic viscosity
ν	kinematic viscosity ($=\mu/\rho$)
ρ	Density
τ	Drag force
Θ	Tortuosity

Subscripts

c	critical value
g	gas phase
l	liquid phase
t	total

This page intentionally left blank

Executive Summary

This study is part of a larger experimental effort funded by the Chemicals Subprogram of the Industrial Technologies Program at the U.S. Department of Energy, Energy Efficiency and Renewable Energy Program Office, to aid the development of new generations of multifunctional chemical reactors by advancing the art of process intensification, and, in particular, by exploiting the benefits of reactor operation in the pulse-flow hydrodynamic regime. Sandia National Laboratories has teamed with CR&L and ABB Lummus through their joint venture Catalytic Distillation Technologies (CDTECH), to optimize the reaction of acid-catalyzed C4 paraffin/olefin alkylation. Issues to be addressed include developing a scientific understanding of how the pulse-flow hydrodynamic regime is affected by the scale-up from bench-scale to industrially relevant sizes with fixed beds of structured packing materials. More specifically, the effects of vessel size, packing material, feed materials, and flow rates on the transition from trickle flow to pulse flow, the pulse characteristics, and the mass transfer between the liquid phases are of particular importance.

This page intentionally left blank

1. Introduction

This study is part of a larger experimental effort funded by the Chemicals Subprogram of the Industrial Technologies Program at the U.S. Department of Energy, Energy Efficiency and Renewable Energy Program Office, to aid the development of new generations of multifunctional chemical reactors by advancing the art of process intensification. In particular, the benefits of reactor operation in the pulse-flow hydrodynamic regime are the focus of this work. Sandia National Laboratories has teamed with CR&L and ABB Lummus through their joint venture Catalytic Distillation Technologies (CDTECH), to optimize the reaction of acid-catalyzed C4 paraffin/olefin alkylation. Issues to be addressed include developing a scientific understanding of how the pulse-flow hydrodynamic regime is affected by the scale-up from bench-scale to industrially relevant sizes with fixed beds of structured packing materials; more specifically, the effects of packing material, feed materials, and flow rates on the transition from trickle flow to pulse flow, the pulse characteristics, and the mass transfer between the liquid phases are of particular importance.

The chemical industry uses cocurrent down flows of three phases through packed beds for a variety of applications including hydrogenation and hydrodesulphurization of petroleum fractions, hydrocracking, hydrorefining, and the oxidation of organic pollutants in waste waters and flue gases (Bartelmus et al., 1998; Burghardt et al., 2002; Gianetta and Specchia, 1992). Such down flows are known to have a range of hydrodynamic operating regimes from trickle flow to pulse flow to spray or bubble flow, depending on the flow rates of the individual phases (Beimesch and Kessler, 1971; Tosun, 1984). The operating regime determines which physical processes (i.e. heat transfer, mass transfer, gravity, etc.) will dominate the flow. For example, reactor operation in the pulse flow regime can enhance heat and mass transfer between the phases which can promote reactions that are typically limited by mixing processes (Burghardt et al., 1999). Operation in such a regime that has been optimized for a particular application is commonly referred to as process intensification (Nigam and Larachi, 2005). The current project seeks to gain scientific knowledge and engineering experience that will result in a new generation of multifunctional reactors designed for the most efficient of process intensification strategies. Such new technologies are identified in "Technology Vision 2020: The U. S. Chemical Industry" (American Chemical Society, 1996) to provide for new, emerging process chemistries.

This report covers both two-phase and three-phase flow experiments. A cocurrent down flow was studied for two phases, namely air as the gas phase and water as the liquid phase. A range of hydrodynamic regimes was studied as a function of bed packing, liquid and gas flow rates, and liquid viscosities. Such regimes and the factors affecting these regimes have been studied extensively in the two-phase literature (Blok et al., 1983; Talmor, 1977ab; Tosun, 1984; Shiney and Varma, 1995) yet predictions generally still depend heavily on empirical correlations due to the complicated interactions of gravity, surface tension, viscosity, and pressure. General understanding of these processes when an additional phase is added is currently lacking.

C4 alkylation is a process in which the benefits of operating within the pulse flow operating regime show promise. Current alkylation technology uses high energy mixers and mechanical devices (Shorey, 2005) which could be replaced with a packed bed of cocurrently downward flowing liquids and gas. For this application, an organic liquid and an aqueous liquid would flow downward through a packed bed. At some location within the bed, the organic liquid would

begin to flash vaporize, forming a gas phase in addition to the two liquids. Liquid-liquid mixing between the liquids initiates the alkylation reaction. This reaction can have a number of undesirable byproducts which may be minimized by enhancement of the mass transfer that occurs in the pulse flow regime.

SNL has joined with CDTECH to develop a unique experimental facility in which quantitative measurements in a three-phase, fixed bed reactor can be taken. It has been operated with a chemical surrogate system that models the liquid-liquid mass transfer that occurs in C4 alkylation. The surrogate system contains an indicator chemical (fluorescein diacetate) that provides qualitative visual and quantitative measurements of the liquid-liquid mass transfer. This project enhanced the understanding of how mass transfer between the phases is affected by operation (and optimization) of the pulse flow regime. Operational parameters such as the phase flow rates and bed packing characteristics were explored.

This report provides documentation of several experimental facilities and operations including two- and three-phase, fixed-bed experiments. Initial construction took place from December 2005 to March 2006, and experiments continued through early 2010. Major components of the experiment are discussed along with operational procedures and experimental hazards and mitigations.

1.1 Introduction

The flow of gases and liquids through columns packed with solid materials undergo significant flow transitions depending on operating conditions. At low gas and liquid flow rates, trickle bed operation is observed, in which a continuous liquid phase trickles through the packing material, surrounded by a continuous gas phase. At low liquid flow rates but high gas flow rates, mist flow operation occurs. In this regime the liquid takes the form of discrete droplets suspended in the continuous phase gas flow. Increasing the liquid flow rate results in blockage of the channels within the packing, finally blocking the entire column diameter and starting the inception of alternating gas and liquid pulses. This is the pulse flow regime. Increasing the liquid flow rate further increases the pulse frequency and when the pulses are no longer distinguishable (approximately 10 Hz) the column transitions to the bubble flow regime. In this regime dispersed gas bubbles are suspended in the continuous phase liquid.

Existing research on the packed bed reactors has focused on predicting and modeling the transition between the gas continuous (trickle) regime and the pulse flow regime. This includes characterizing the operating behavior including the pulse velocity, pulse frequency, holdup, and pulse height. Only in the more recent literature have a few studies started to address bed operating in the pulse flow regime at higher pressures like those expected in industrial applications (Al-Dahhan and Dudukovic, 1994).

1.2 Literature Review

Weekman and Meyers (1964) seem to be the first to examine flow behavior in gas-liquid cocurrent downflow packed bed reactors. Since then, numerous authors have examined flow characteristics and transitions, flow regime mapping, diagnostics, and industrial applications. A few of these papers are summarized below.

Blok et al. (1983) describe the different flow regimes in packed bed operation including the trickle and mist flow, pulsing and bubble flow. The transition from pulse flow to bubble flow is said to occur when the pulse frequency exceeds 10 Hz, after which point the pulses can no longer be distinguished. They carried out an experimental study on the transition limit, total liquid holdup and the pressure drop. The experiments were carried out using air and water with column diameters of 5, 10, and 20 cm, all 1 m in length. Packing consisted of 2.5 and 4 mm Raschig Rings. They injected tracers and used a colorimeter to measure residence times. They measured the pulse frequency with a microphone or a conductivity cell. Pressure taps along the column measured the pressure. In the pulsing regime the liquid holdup was found to be more dependent on the gas flow rate than on the liquid flow rate. They determined an empirical relation between holdup, packing characteristics, and gas flow rate. In their system the transition to pulsing flow always occurred at the same real liquid velocity and so from this they investigate the Froude number as is encountered in gravity waves. They plotted the experimental data U_g/S versus $U_L/[\varepsilon(d_p)^{1/2}]$ yielding a constant Fr =0.09. Also, they indicate the transition is independent of column diameter up to 0.3 m. Figure 1 shows the flow regime map from Blok et al. (1983).

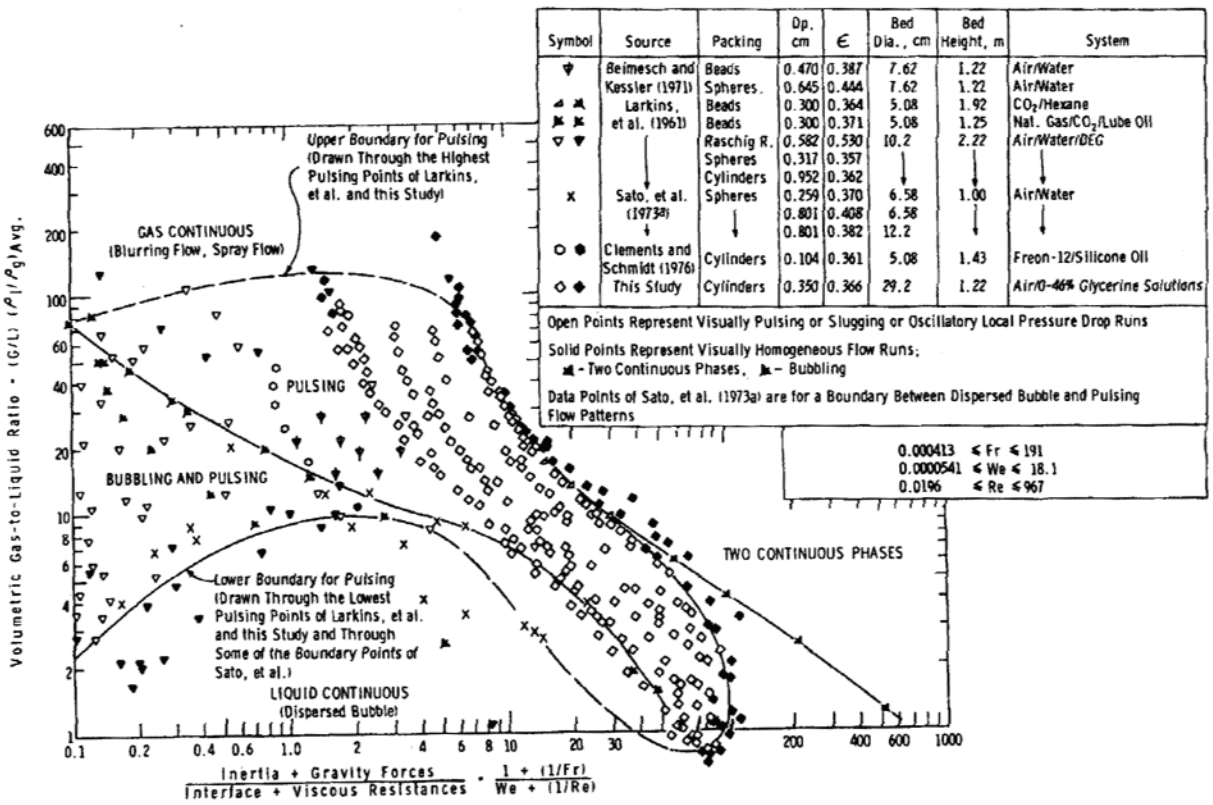

Figure 1.1. Flow Regime Map of Blok et al. (1983)

Helwick et al. (1992) focused on the intermittency of the pulses during the pulse-flow regime in gas-liquid cocurrent packed beds. They carried out an experimental study in a cylindrical acrylic column with a length of 1.3 m and an inner diameter of 7.62 cm. The packing was 0.318 cm

diameter nonporous, polished acrylic spheres filling 1.25 m of the column. Pure water and air comprised the liquid and gas phases. Several layers of porous monolith were installed in the inlet section to evenly distribute the inlet streams. The ratio of column to particle diameter was approximately 24. The water stream was recirculated while the air was vented after exiting the column. The inlet air pressure was 100 psig. Instantaneous pressure measurements were recorded as a function of time at sampling frequencies of 125-200 Hz at 1 m from the column inlet. The pressure gauges could detect pressures between 0-10 psig. Flow visualization with a video camera was also used to provide crude measurements of pulse height and pulse velocity. Data were presented for four gas fluxes of 0.33, 0.345, 0.40, and 0.524 kg/m^{2}s. The pressure traces showed that the pulses occur at irregular time intervals that decreased as the inlet gas flow rate increased, indicating that within the pulse flow regime the heat and mass transfer rates depend on the frequency of the pulses. The pressure traces also indicated a decrease in pressure after passage of the pulse, indicating a loss of liquid holdup. The pressure increased as the holdup increased until a pulse was formed. Histograms were created of the time intervals between the pulses recorded for a period of 660 s. Rapid succession of pulses on the order of 1 Hz was observed for the three lowest gas flow rates along with apparently random long time periods between the pulses. This was not observed at the highest gas flow rate where regular pulsing was observed. Helwick et al. suggest a two-state process at the lowest flow rates. Their paper included a qualitative discussion of how pulses are formed. They extended this discussion to a model for the induction time between pulses that scales with 1/(β-1) where β represents a combined Reynolds number $Re_l Re_g/(Re_l Re_g)_c - 1$. The *c* subscript indicates the critical values at which pulses are first observed. Helwick et al. stress that it is not enough to know that the column is operating in the pulse flow regime, but rather the induction time between the pulses is also critical information.

Xiao et al. (2000) carried out an experimental study focused on the liquid holdup for reactors operating in the pulse flow regime. The liquid holdup provides information on the degree of wetting of the solid phase and is related to the liquid film thickness around a bed particle. The local liquid holdup depends on time and position yet here the bed-averaged holdup was considered. They measured the dynamic liquid holdup by a draining method in a column with an inner diameter of 10 cm and a packed height of 1 m. It was packed with non-porous ceramic and glass beads with 2-3 mm diameter. The liquid phase was water with varying amounts of carboxymethylcellulose and the gas phase was air. The column inlet and outlet valves were shut simultaneously to collect the whole bed's liquid holdup by allowing it to drain for over 30 minutes. The holdup was measured as a function of the liquid viscosity and gas and liquid superficial velocities. Local liquid holdup was measured with a point conductance probe at a specific axial height in the column. Neither inlet flow stream was recirculated. The liquid superficial velocity varied between 0.008-0.016 m/s and the gas superficial velocity varied between 0.07-0.36 m/s. Pulsing was first observed at the bottom of the packing and increased up the packing as the flow rates were increased. They attributed the occurrence of pulsing to the requirement of both sufficient liquid flux and gas compressibility. For a given packing and liquid-solid surface properties, the ratio of gas-to-liquid interstitial velocity affects the characteristics of pulsing flow. Under pulse flow conditions, the gas superficial velocity has a strong effect and the liquid superficial velocity has a minimal effect of the liquid holdup. Increasing the liquid viscosity by a factor of two increased the liquid holdup less than 4%. The surface properties of the packing affected the holdup significantly. The authors proposed a correlation between the liquid holdup and the ratio of flow velocities of the form

$$\beta = A_1 + A_2 \left(\frac{U_g}{U_l}\right)^{A_3} \quad (1)$$

where A_1, A_2, A_3 are fitting parameters. The holdup is observed to increase as the ratio of U_g/U_l decreases.

Bartelmus et al. (1998) indicate that the pulsing flow regime appears when the liquid flow rate exceeds a critical value and that the heat and mass transfer coefficients are significantly larger than in the gas-continuous flow regime. Also, perfect wetting of the bed solids is observed. The first pulses are observed at the bottom of the packing since the gas velocity is higher there due to the pressure drop along the column. The travelling plug of liquid is observed to take in liquid at its front and leave it behind at its rear while the size of the plug remains virtually constant. Bartelmus et al. sought to characterize the pulse characteristics; frequency, velocity, and structure including the size of the liquid-rich and gas-rich zones. A detailed literature review on pulse velocities and correlations was also included. They carried out an experimental study in a Perspex column with an inner diameter of 5 cm and 1.5 m in length. Nitrogen was the inlet gas stream which was temperature controlled and saturated in a scrubber. The gas vented at the bottom of the column and the liquid was recirculated. Two different packings consisted of glass spheres 3 and 1.5 mm in diameter which yielded porosities of 0.38 and 0.372 and specific surfaces of 1240 1/m and 2512 1/m, respectively. The liquid phase was water solutions with ethanol or glycerol. Pulse velocity was measured either visually with a video camera and a ruler attached to the column or with two wire-gauze conductance probes located 0.8 m and 0.9 m from the top of the column. The data that were used to create pulse velocity correlations were taken with a ratio of column to particle diameter of 17 and 33.

The pulse velocity was observed to increase with an increase in both the liquid and gas flow rates. A maximum value was reached at high gas flow rates. This pulse velocity is related to the real phase velocities rather than the superficial velocities, requiring a measurement of the liquid holdup.

$$U_{gr}=U_g/(\varepsilon-\varepsilon_{lt}) \quad (2)$$

$$U_{lr}=U_l/\varepsilon_{lt} \quad (3)$$

They calculated the real gas and liquid velocities with these equations solving for the total liquid holdup from correlations, correcting for the fluid properties to that of pure water. They show, as did Xiao et al., that the liquid flow velocity cannot be neglected as an influence on the pulse parameters. Additional tests with larger packing diameters of 5 mm showed that the correlation is not valid when the column diameter to packing diameter of is reduced to 10. They concluded that the pulse velocity depends on the real velocities of the liquid and gas phases in addition to the packing type.

Andreussi et al. (1988) developed a non-intrusive probe made of two ring electrodes that were flush-mounted to the inner diameter of the column to measure the mean liquid holdup under different flow conditions. The probes were made of stainless steel. The conductance between the electrodes is proportional to the mean liquid holdup if the distance between the probes is large compared to the characteristic size of the cross-section occupied by the liquid.

Schmit et al. (2001) carried out experiments to illustrate the use of X-ray tomography in multiphase reactors. The experiments were carried out in counter-current air/water flows in a 6-in diameter column with random plastic packing. A 450 kV X-ray source was used and individual slices through the column were recorded. Numerous rotations and table positions were used to establish a full data set, such that the total scan time was 3-5 min with 1-3 min of reconstruction time. They encountered difficulties in obtaining holdup data from the reconstructed images, and were forced to use the transmission data and found significant error as compared to average holdup predictions. They attributed this error to not being time-averaged and also including the dynamic and static liquid holdup at a specific axial location along the column.

Boyer and Fanget (2002) describe a gamma-ray tomographic system to measure the gas/liquid flow distribution in a 6 cm diameter column operating in the trickle bed regime. They used gamma rays because the relatively low power of X-rays was not sufficient to be detected across the column when packed with a fixed bed of particles.

Boelhouwer et al. (2002) studied the effect of cycling the liquid flow rate to force the column into the pulse flow regime. Previous studies indicated that better performance and component selectivity was achieved by cycling the liquid flow off and on as opposed to cycling it between a lower and higher flow setting. They describe liquid-rich "shock waves" that move down the bed and in the cases of extreme liquid flow rates, pulses are initiated within the "shock waves". Increasing flow rates resulted in the entire column switching between the trickle bed regime and the pulse flow regime. They carried out an experimental study in a column 3.2 m in height using two modes (fast or slow) of cycling the liquid feed. The column was Plexiglas and had an inner diameter of 11 cm and a packed height of 3.2 m. The packing was 6 mm diameter glass spheres with a porosity of 0.37 and a specific surface area of $630 m^{-1}$. The process fluids were air regulated between 2 and 7 bars and water. They measured the cross-sectionally averaged liquid holdup with 8 sets of conductance probes at different axial positions. They indicated a decrease in pulse strength as it travels down the column due to a loss of liquid at the tail of the pulse. While the strength of the pulse decays, the pulse velocity remains constant down the column as long as a pulse plateau is observed. The pulse tail increases as the pulse travels down the bed. They found this decrease in pulse duration to be related to unit traveled distance. Smaller superficial liquid velocities are required to operate in the pulse flow regime when cycling the liquid feed in the fast mode. When the liquid-induced cycling is active, the inception point of the pulses is fixed. This is not true in the natural pulsing flow where the inception point affects the increase in velocity at the end of the column and a wider variation in pulse velocities is recorded when measuring at a fixed axial location along the column.

Reinecke and Mewes (1996) experimentally studied the pulse flow regime using capacitance tomography in an air/water packed acrylic column with an inner diameter of 12 cm. It had a packed height of 2 m and the packings used were 10 mm diameter ceramic spheres. Their results indicated a three-dimensional structure to the pulses and a significant wall effect that they speculated would be different depending on the column dimensions. As the pulse width decreases the wall effect is also observed to decrease and the pulse behavior is dominated by momentum forces.

Iliuta and Larachi (2004) carried out numerical modeling to predict the transition to the pulse flow regime in trickle bed reactors with fine particulates suspended in the liquid phase. They assumed that the parameters of the pulse flow regime occur on a shorter time scale while the effects of particle accumulation on the packing occurs on a longer time scale, thus enabling the two solutions to be superimposed.

Sicardi et al. (1979) combined the results of different researchers to determine the dimensional groups that determine the transition boundary between flow regimes. They drew analogies with the formation of large waves in annular two-phase flow in tubes. They completed a flow map using their experimental data and others in the literature between the low- and high-interaction flow regimes. Packing wettability is difficult to quantify yet an important parameter. They do indicate a dependence of transition on the ratio of column diameter to packing diameter. In the early data, the effect of gas pressure on the regime transition was not considered. They carried out an experimental study in an air/water system. The water was recirculated and the air was not. They measured inlet gas and liquid flowrates and monitored pressures along the column. The total liquid holdup and mean residence time were measured using conductivity sensors. The inception of pulsing was seen to occur when a critical liquid flow rate was obtained. They discussed the channel model which considers the packed column as parallel and interconnecting channels with an equivalent mean diameter $d_{c0}=4\varepsilon_o/a_v$. The liquid holdup can be incorporated by $\varepsilon=\varepsilon_0-h_t$. This model works well in representing the trickle flow regime. They had good success in correlating the different data as a function of the drag force τ_p versus the gas velocity for all the packings and systems considered. The drag force at the inception of pulsing increases with an increase in the gas velocity. They also investigated the effect of energy dissipation in the bed due to the occluded channels. They used the ratio W_{tp}/W_w (ratio of total power dissipated in the column at pulse inception normalized by total power dissipated in the same wetted column at the same gas flow rate, but zero liquid flow rate) that is independent of packing geometry. The energy dissipation ratio was shown to decrease as the gas velocity increases.

The paper of Sicardi and Hoffman (1980) extends the considerations of Sicardi et al. (1979) to irregularly shaped channels by introducing the tortuosity factor $\Theta = 2b/d_{c0}$ (ratio of constriction height to channel diameter) where $0 < \Theta < 1$. They also consider the Weber number (ratio of inertial to surface tension forces). They suggest that the mechanism for the formation of large waves in the presence of high gas velocity is similar to the initiation of roll waves.

Gianetta and Specchia (1992) presented a review on the state of art of trickle bed reactors, including an extensive list of references. They discuss common applications and advantages/disadvantages of trickle bed reactors. They proposed a flow regime map and identified the important parameters of 1) gas and liquid physical characteristics 2) size and porosity of the packing 3) ratio of column diameter to packing diameter.

Burghardt et al. (1999) stated that the pulse flow regime is excellent for processes in which mass transfer is the rate-limiting step since in this regime the mass transfer coefficients are several times higher than in the trickle flow regime. This study addresses the transition between gas continuous flow and pulsing flow and also characterizes parameters of the pulses: pulse velocity, pulse frequency and pulse structure. Pulse flow is initiated when a certain limiting liquid flow rate is exceeded and the channels in the bed become blocked. They indicate that the most important parameters to consider are the phase flow rates, physiochemical properties and the size

and shape of the packing. They use the model of Grosser et al. (1988) to correlate with their experimental data and say the other models are not sufficient. They indicate that the effectiveness of the Grosser et al. model is highly dependent on accurate values of the liquid holdup. Significant scatter was seen in the pulse velocity and frequency measurements. The frequency is higher in the area where the pulses are formed and lower at the bottom of the column due to coalescence. At higher values of the liquid flow rate they observe secondary pulses in addition to the main pulses. They say that these secondary pulses adversely affect the column performance since they carry less liquid than the main pulse. Only at low liquid flow rates is there a single pulse frequency. As the liquid flow rate increases, the pulse frequency increases and reaches a limiting value that depends on the gas flow rate. Surface tension affects these results and correlations used in their analysis. They also quantified the pulse height. Generally speaking, the higher the gas velocity, the lower the height of the whole pulse and of the liquid-rich zone.

Burghardt et al. (2002) studied the effect of system pressure on the transition point, pulse velocity and frequency. They found that the pulse flow regime could not always be achieved under high pressure conditions, because the high pressure decreases the liquid holdup and therefore requires much high liquid flowrates to achieve the same flow conditions seen at atmospheric pressure. However, when pulsing occurs in pressurized beds, they observed that the pulse frequency is higher, the pulses are shorter, and they contain more liquid.

2. Two-Phase Experiments

2.1 Two-Phase, Non-Reactive, Fixed-Bed Experiment

Cocurrent multiphase downflows in a trickle bed were examined through two experimental efforts carried out at Sandia National Laboratories. The first experiment was a two-phase, non-reactive, fixed-bed column operating with cocurrent downward flows of air and water. The purpose of this experiment was to investigate the hydrodynamics of the pulse-flow regime, the trickle-pulse regime transition, how to detect regime transition, and how these operating regimes are impacted by the bed properties. The second experiment consisted of a three-phase, reactive, fixed-bed column operating with downward flow of a surrogate chemical system. Operating the column with this surrogate chemical system enables investigation of how the hydrodynamics in and near the pulse-flow regime and the bed properties affect the chemical kinetics and mass transfer. Additional bench-top experiments in which accurate kinetics studies could be carried out were performed in support of the surrogate mass transfer technique. These experiments will be described in the following sections.

This section presents results from the two-phase, non-reactive experiment operating with air and water in fixed-beds of spherical particles. Several hydrodynamic regimes, which have been extensively studied over the past several decades are possible in such experiments (see the reviews of Charpentier, 1976; Satterfield, 1975; and Tosun, 1984). Our focus is on the pulse-flow regime as it is a crucial process intensification strategy due to the possibility of increased throughput without flooding (Blok et al., 1983), increased mass and heat transfer rates (Boelhouwer et al., 2002), and complete wettability of the packing (Burghardt et al., 1999) for petrochemical reactions and hydrotreating (Sicardi et al., 1979).

Industrial units sometimes operate within the pulse-flow regime or near the trickle-pulse regime transition (Satterfield, 1975) requiring an accurate definition of the transition boundary for given packed-bed properties, column dimensions, and flow streams. Previous studies defining this transition boundary have typically been carried out in beds of particles with characteristic particle dimensions orders of magnitude smaller than the confining column diameter ($D/d \gg 1$). The results presented here further investigate the trickle-pulse flow boundary and the experimental methods used to detect transition in beds of spherical particles with values of D/d between 3.75 and 15.

2.1.1 Previous methods for determining trickle-pulse transition

Several methods have been used in laboratory experiments to detect the trickle-pulse regime transition. The most common method is visual observation through a transparent column of either glass (Wilhite et al., 2003; Bartelmus et al., 1998) or plastic (Boelhouwer et al., 2002; Burghardt et al., 2002, 2004; Helwick et al., 1992; Chou et al., 1977). While this method is simple to implement in the laboratory, it is highly subjective, resulting in different interpretations of the operating regime amongst researchers (Attou and Ferschneider, 2000). Other experimental

techniques to detect pulse flow include implementing microphones (Blok et al., 1983), video imaging (Weekman and Meyers, 1964), lightbulb and photocells (Blok et al., 1983; Weekman and Meyers, 1964), pressure transducers (Helwick et al., 1992; Chou et al., 1977), impact plates (Weekman and Meyers, 1964), anemometers (Boelhouwer et al., 2002), and conductance measurements with a point probe (Xiao et al., 2000), a ring (Boelhouwer et al., 2002), or a wire mesh (Burghardt et al., 2002; Bartelmus et al., 1998).

Despite the relatively large number of studies focused on the trickle-pulse transition boundary, no quantitative measure of this important regime transition has been established. In beds of particles with large values of D/d, the transition is easily identifiable, and visual observation may be acceptable. However, in the industrially relevant situations of columns operating with highly viscous fluids or with beds of large particles with relatively low values of D/d, visual observation becomes very difficult in addition to being impractical to implement. An experimental study has been carried out with packed beds consisting of different-sized spherical beads in order to better understand how different experimental methods can be used to identify the conditions of transition from trickle flow to pulse flow. These data from wall-mounted pressure transducers and conductance probes generate a more robust definition of the trickle-pulse transition than has previously appeared in the literature (Cooper et al., 2005, Appendix D).

A multifunctional reactor operating with air and water was constructed to explore the hydrodynamic operating regimes and system operation in a safe laboratory environment. The different hydrodynamic regimes that exist in gas-liquid downward flows through fixed beds of particles have been studied for the past several decades. Much of the early work is reviewed in Charpentier (1976), Satterfield (1975), and Tosun (1984). More recent work has focused on a better physical understanding of the conditions leading to the transition between (Sicardi et al., 1979; Burghardt et al., 1999; Sicardi and Hofmann, 1980; Attou and Ferschneider, 2000) and the characterization of these different operating regimes (Boelhouwer et al., 2002; Helwick et al., 1992; Saez and Carbonell, 1985; Xiao et al., 2000). Those experiments were carried out in beds of small particles so that the wall effects were negligible and the bed void fraction was considered homogeneous. Even with particle beds that can be easily characterized, the complicated fluid dynamics have typically resulted in the derivation of empirical relations for dynamic liquid holdup and bed pressure drop from experimental data. In beds of large particles, radial variation of the bed void fraction invalidates the assumption of a homogeneous bed of particles. This additional complication in characterizing the particle bed with two-phase flows has not yet been adequately addressed in the literature.

There are four generally accepted hydrodynamic regimes in two-phase, cocurrent flow through fixed beds: trickle flow, pulse flow, bubble flow and spray flow (Attou and Ferschneider, 2000; Tosun, 1984). However, other investigators have defined only two regimes (high and low interaction) (Sicardi et al., 1979) or up to five regimes (bubbling/pulsing flow in addition to the four listed above; Talmor, 1977). The conditions for operation within each of the regimes have historically been presented on flow maps with a variety of axis coordinates. The original flow maps (Weekman and Meyers, 1964; Satterfield, 1975) were presented in terms of the superficial mass fluxes where the two phases consisted of air and water. Charpentier (1976) later accounted for liquids other than water and gases other than air with a modification to the superficial mass fluxes. Correction factors based on the ratio of liquid properties such as density, viscosity, and surface tension, as well as the ratio of the gas-to-air density, all raised to some empirical power,

were developed. Talmor (1977) applied more physical understanding of the driving and resistance forces that determine the operating regime in the derivation of his flow map, instead of relying on empirical corrections as was done previously. The driving forces consist of gravity and inertia, and the resistance forces consist of viscous and surface-tension forces. The effects of the particle size and shape, if considered, are typically included in the flow map through a constant value for the bed void fraction (Sicardi et al., 1979) or some form of a modified hydraulic radius (Talmor, 1977).

Of the four major flow regimes, pulse flow has gained the most attention in recent years due to the possibility of increased throughput without flooding (Blok et al., 1983), increased mass and heat transfer rates (Boelhouwer et al., 2002), and complete wettability of the packing (Burghardt et al., 1999) for petrochemical reactions like hydrodesulphurization and hydrotreating (Sicardi et al., 1979). In the creation of the above-mentioned flow maps, particular attention was placed on the boundary between trickle flow and pulse flow due to industrial units operating in pulse flow or near the transition (Satterfield, 1975). However, data from fixed beds operating with cocurrent downflows of gas and liquid have generally been collected with packing particles that have a characteristic size that is orders of magnitude smaller than the column diameter. In this case, the transition between the trickle-flow and pulse-flow regimes is distinct.

When the particle size approaches the confining column size, the mean bed void fraction is greater than the range of void fractions, 0.36-0.40, of an infinite bed of randomly packed spheres (Valtsifer and Zvereva, 1999). In this case, the void fraction near the wall increases and the flow is affected (Winterberg and Tsotsas, 2000; Chu and Ng, 1989; Cohen and Metzner, 1981). This problem is different than that of regular, high-void-fraction packings (voidage up to 0.70) being tested due to the development of more active catalysts which are allowing commercial units to operate at higher flow rates and lower pressure drops (Miller and Kaibel, 2004). These high-void-fraction packings are composed of many smaller empty spaces while beds of spheres with diameters on the order of the column diameter are composed of fewer, but larger, empty spaces. Rather than studying the irregular and difficult-to-characterize high-void-fraction packings, an experimental study has been carried out with packed beds consisting of different-sized spherical beads in order to better understand the effect that the walls can have on the trickling and pulsing regimes of two-phase flow. The results are illustrated in terms of the total bed pressure drop and the local pressure variations within the bed.

2.1.2 Previous work studying wall effects

The wall effect on flow through packed beds has been extensively studied for single-phase flow where the competing effects of increased void fraction near the wall and wall friction determine the resulting pressure drop. The Ergun equation, which relates the pressure drop to the rate of fluid flow through the packed bed, is typically modified for the effect of non-uniform void fraction (Niven, 2002). Below some critical value of D/d, the effect of the wall becomes significant, and the Ergun equation no longer represents the measured pressure drop. The critical diameter ratio where wall effects become important is largely disputed in single-phase flows. Mehta and Hawley (1969) suggest a critical diameter ratio less than 50:1, Cohen and Metzner, (1981) suggest a ratio less than 30:1 for Newtonian fluids, and Chu and Ng (1989) suggest that the wall effect may become important for ratios less than 25:1 and most certainly become important for ratios less than 8:1. Methods to resolve the wall effect have implemented a

modified hydraulic radius (Eisfeld and Schnitzlein, 2001), or a relationship for the radial variation of void fraction either through a mathematical function (Chu and Ng, 1989; Winterberg and Tsotsas, 2000) or division of the column cross-section into two (Nield, 1983; Tosun and Mousa, 1986) or three (Nield, 1983; Cohen and Metzner, 1981) regions of different void fractions. A large collection of data was effectively correlated for D/d ratios between 1.624 and 250 for a single phase flowing through a packed bed (Eisfeld and Schnitzlein, 2001) using the hydraulic radius concept. The data collapse onto a single curve relating the modified pressure drop

$$\psi = \frac{\Delta P}{\rho_L w_L^2} \frac{d}{h} \frac{\varepsilon^3}{(1-\varepsilon)} \tag{4}$$

to the modified particle Reynolds number

$$Re_{\bar{d}} = \frac{\rho_L w_L d}{\mu_L}(1-\varepsilon)\ , \tag{5}$$

where ρ_L is the liquid density, w_L is the liquid superficial velocity, μ_L is the liquid viscosity, h is the bed height, d is the particle diameter, and $\bar{\varepsilon}$ is the mean bed void fraction.

While there are many studies investigating the wall effect on the hydrodynamic behavior of single-phase flow through packed beds, only a few studies (Attou and Ferschneider, 2000; Talmor, 1977) have mentioned this issue for downward cocurrent two-phase flow, and no studies have been devoted entirely to determining how the confining walls influence the hydrodynamic regimes of two-phase flow. This study addresses the lack of experimental data in columns with low D/d ratios and cocurrent gas-liquid downflows. Observations of the flow regimes, including pressure histories, and total bed pressure drop as a function of particle size are presented below. The scope of this study is not to develop additional empirical relations but to focus on characteristics of the operating regimes and to observe how they change as the particle size increases.

2.2 Experimental Facility

The two-phase experiment (Figures 2.1 and 2.2) consisted of a transparent, polycarbonate column (I.D. 9.53 cm, 2.5 m high, wall thickness 3.2 mm) with deionized water supplied to the top of the column via a Magnatex liquid pump (model MMP21-R25) and air supplied from the building supply via an Alicat mass flow controller (model MCR-1000SLPM-D/5M 5IN). A liquid return line at the pump discharge was present for all tests. Pressure transducers were installed downstream of the pump and along the column as indicated in Figure 2.1. A needle valve was located between the inlet to the liquid return line and the column inlet and a ball valve was located in the liquid return line. Both valves aided in throttling the flow to the column. The column was filled with packed beds of various materials described below. A liquid holding tank below the column held the liquid.

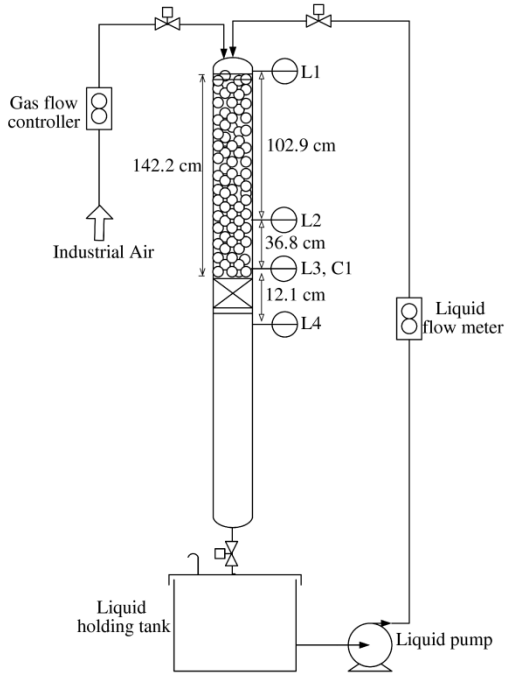

Figure 2.1: Two-phase experiment schematic

The bottom of each bed was fixed 1 m from the bottom of the column and held in place by a ring supporting a 3.8-cm-thick barrier layer of highly porous filtration media (203 m^2/m^3). The beads were randomly packed by dropping them into the column from above until the bed height equaled nominally 1.4 m. Deionized water and air both entered the column at a constant flow rate through the top flange and flowed downward through the packed bed into the holding tank. The air vented to the surroundings, and the liquid was recirculated to the top of the column. A centrally-located spray nozzle at the top of the column was used to distribute the water. Table 2.1 shows the liquid properties and the experimental conditions examined in this work. Four pressure transducers mounted along the column wall measured pressure histories at locations L1-L4 as shown in Fig. 2.1. A point conductance probe was installed at location C1 near the bottom of the bed. Details of the circuitry can be found in Cho et al. (2005).

The measured pressures, conductance probe output, and flow rates were recorded by a LabVIEW™ program. The pressure transducers were Omega PX315 diaphragm type, and the liquid flow was monitored using a Controlotron System 1010 magnetic flow meter. Experimental repeatability was within ±8.7% in the pressure drop (measured between locations L1 and L4 in Fig. 2.1), ±0.34% in the superficial mass flux of the liquid phase L, and ±0.29% in the superficial mass flux of the gas phase G. The liquid flow meter had an accuracy of ±0.20 LPM and the gas flow controller had an accuracy of ±7 SLPM based on the manufacturer's specifications.

Appendix A lists the operating procedures for the two-phase column.

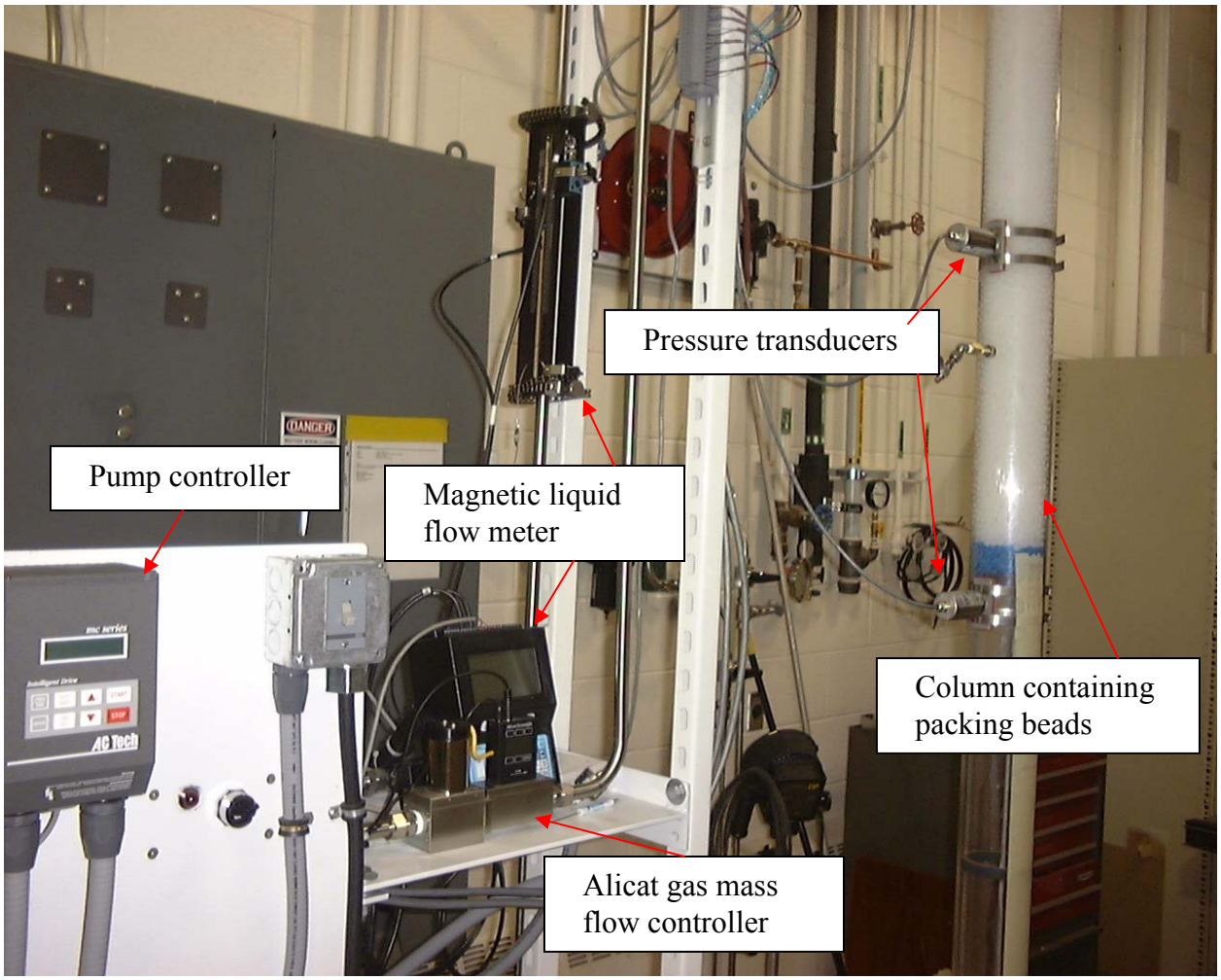

Figure 2.2: Photograph showing major component of two-phase experiment.

Table 2.1: Experimental Parameters

Liquid density (kg/m^3)	ρ_L	997
Liquid viscosity (mPa s)	μ_L	0.856
Liquid mass flux (kg/m^{2}s)	L	0-66
Gas mass flux (kg/m^{2}s)	G	0-1.88

Representative data are shown in Figure 2.3. Further measurements with the two-phase flow system are described in Appendices B (viscosity effects), C (Amberlyst resin packing), D (pulse detection), E (effect of particle-to-column diameter ratio *d/D*), and F (raw data).

Measurements were obtained first with zero gas flow rate to ensure that the beads were completely wetted and maximize experimental repeatability. The gas flow rate was then increased incrementally. The bed pressure drop was determined by calculating the difference in the average pressure at the top (L1) and bottom (L3) measurement locations and was then normalized by the bed height h, gravitational acceleration g, and the water density ρ_L.

2.3 Packings

A total of six packed beds were tested. Four beds consisted of polished, solid, monodisperse, spherical, polypropylene spheres (beads) with diameters equal to 0.64, 0.95, 1.27 and 2.54 cm, one bed consisted of a proprietary developmental woven multifilament polypropylene (WMFP) material, and one bed consisted of industrial resin beads. Bed specifics appear in Table 2.2.

The bed void fraction ε was calculated from the volume of the column filled with particles V_b, the volume of one particle V_s, and the number of particles in the bed N.

$$\varepsilon = 1 - N\frac{V_s}{V_b} \tag{6}$$

This represents the average void fraction throughout the bed and does not provide information regarding local variations in the void fraction.

Table 2.2: Details of Packed Beds

Bead diameter d (cm)	Bed void fraction ε	D/d
0.64	0.403	15.0
0.95	0.411	10.0
1.27	0.422	7.50
2.54	0.464	3.75

A partial list of the packing types appearing in the literature is tabulated in Table 2.3. Overall, the values of D/d range between 7.5 and 30.

Table 2.3: Partial list of packing types in literature.

	Ball dia. d (mm)	Material	D/d	Porosity	Specific surface area (1/m)	Reference
Spheres	10	Ceramic	12			Reinecke and Mewes (1996)
	6	Glass	18.3	0.37	630	Boelhouwer et al. (2002)
	4	Catalyst	9.5	0.385		Iliuta and Larachi (2004)
	3	Glass	17	0.39		Wammes et al. (1991)
	3	Glass	16.7	0.40	1200	Boelhouwer et al. (2002)
	6	Glass	18.3	0.38	620	Boelhouwer et al. (2002)
Raschig Rings	10		11	0.67	924	Boelhouwer et al. (2002)
	10		30.3	0.62	510	Sicardi et al. (1979)
Cylinders	12	Ceramic	25	0.406	291	Sicardi et al. (1979)
	6	Ceramic	25	0.41	616	Sicardi et al. (1979)
	5	Ceramic	22	0.41	906	Sicardi et al. (1979)

The packing density η is defined as the fraction of a volume filled by the spheres. Random close packing of spheres in three dimensions gives packing densities of 0.64 (Jaeger and Nagel, 1992).

This is smaller than the highest packing density of 0.7405 for hexagonal close packing (Steinhaus, 1999).

The number of spheres needed to fill a desired volume of the column is determined from the packing density.

$$N = V\eta / V_s \tag{7}$$

Where N is the number of spheres, η is the packing density, V is the tube volume to be packed with spheres, and V_s is the volume of one sphere. The results are tabulated below for the available polypropylene sphere sizes (from Orange Products, Inc., Allentown, PA). All have a polished surface finish.

Table 2.4: Polypropylene sphere size and required quantity

Ball	Ball		Specific Surface	Quantity
dia. (in)	dia. (mm)	D/d	Area (1/m)	(η=0.64)
0.125	3.175	30.00	1209	414,800
0.1563	3.970	23.99	967	212,200
0.1875	4.763	20.00	806	122,900
0.2188	5.558	17.14	691	77,400
0.236	5.994	15.89	641	61,700
0.250	6.350	15.00	605	51,900
0.275	6.985	13.64	550	39,000
0.2813	7.145	13.33	537	36,400
0.3125	7.938	12.00	484	26,600
0.3149	7.998	11.91	480	26,000
0.3543	8.999	10.58	427	18,300
0.375	9.525	10.00	403	15,400
0.3937	10.000	9.53	384	13,300
0.398	10.109	9.42	380	12,900
0.400	10.160	9.38	378	12,700
0.4375	11.113	8.57	346	9,700
0.5	12.700	7.50	302	6,500
0.5625	14.288	6.67	269	4,600
0.625	15.875	6.00	242	3,400
0.75	19.050	5.00	202	2,000
0.875	22.225	4.29	173	1,200
1.000	25.400	3.75	151	1000
1.125	28.575	3.33	134	600

2.4 Results

2.4.1 Pulse flow in beds of large particles

Pulse flow has been described as repetitive slugs of liquid and gas (Blok et al., 1983) or a phase redistribution of a two-phase mixture (Talmor, 1977). Our observations and those of others (Bartelmus et al., 1998; Ratheesh and Kannan, 2004) were that, at low flow rates, the liquid flowed over the beads in continuous streams (trickle flow). An increase in either the liquid flow rate or the gas flow rate caused alternating liquid-rich and gas-rich regions to form near the bottom of the packed bed (pulse flow). The liquid rich regions were pushed down the column and through the packed bed because of a pressure increase in the gas-rich region above each liquid-rich plug. Further increases in either fluid flow rate resulted in increases in the pulse frequency and the height of the pulse inception point, and decreases in the pulse height and the pulse pressure drop.

The transition between the trickle-flow and pulse-flow regimes is of critical importance for the design of two-phase packed bed columns for commercial applications. Only a few models (Attou and Ferschneider, 2000; Iliuta and Larachi, 2004; Holub et al., 1993) have attempted to predict this flow-regime transition. Sicardi et al. (1979) likened the pulsing phenomenon to the mechanism of annular two-phase flow in straight tubes in order to determine the basic conditions required for pulsing to exist. Most definitions of the flow-regime transition are based on experimental data, which has resulted in a variety of empirical relations.

In all of the above-mentioned models and empirical relations, the effect of the column-to-bead diameter ratio D/d in two-phase flows has not been investigated over a sufficiently large range, unlike the case of single-phase flow in packed beds. This diameter ratio can significantly affect the flow characteristics within the packed bed. In beds with small particles or large D/d ratios, distinct pulses are observed over a wide range of flow rates. Due to the smaller voids between the particles, the liquid tends to plug these channels at relatively low flow rates.

Figure 2.3A shows three pressure histories at the location of L2 in the packed bed of 0.64-cm beads (D/d = 15.0) for the regimes of trickle flow (case 1, low gas mass flux G) and pulse flow (cases 2 and 3, higher G). Only minor pressure fluctuations are observed in the trickle-flow regime (Fig. 2.3A-1) whereas the transition to pulse flow is noted by distinct pressure peaks that occur at fairly regular time intervals (Fig. 2.3A-2) as measured at a constant location within the packed bed. The pressure rises within the pulses are not equal. Immediately after a pulse passes, the pressure decreases to a minimum, indicating a net loss of liquid holdup (Helwick et al., 1992). The pressure then rises as the liquid holdup on the beads increases until the holdup is sufficient to span the column cross section and initiate the formation of the next pulse.

Increasing the gas flow rate increases the number of pulses that travel through the bed per unit time (Fig. 2.3A-3). The induction time between pulses is intermittent and has been shown (Helwick et al., 1992) to scale in a manner similar to that of turbulent bursts in a modified Taylor-Couette flow.

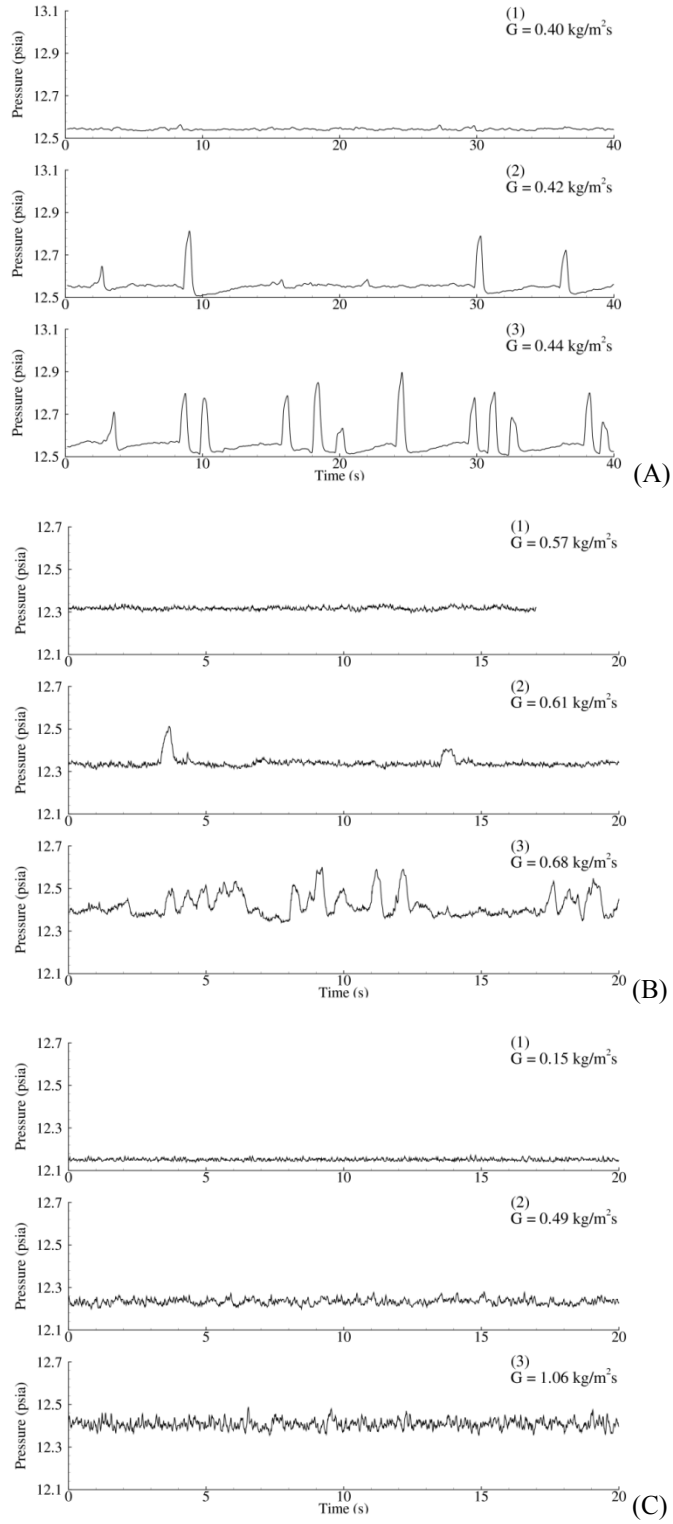

Figure 2.3: Pressure histories near trickle-pulse transition for (A) d = 0.64 cm, L = 6.91 kg/ m^2s, (B) d = 1.27 cm, L = 38.7 kg/ m^2s, (C) d = 2.54 cm, L = 56.9 kg/ m^2s.

Increasing the bead size to 1.27 cm (D/d = 7.50) results in an increased number of small pressure oscillations in the trickle-flow and pulse-flow regimes (Fig. 2.3B). Additionally, the pulses become less obvious visually and in the pressure histories. The pulse irregularity is more prevalent as the bead size increases.

Finally, increasing the bead size to 2.54 cm (D/d = 3.75) results in additional increases in the small-scale pressure oscillations (Fig. 2.3C). No transition to pulsing was observed with the 2.54 cm beads for the experimental flow rates.

Thus, it is shown that a decrease in the D/d ratio results in higher-frequency, smaller-scale pressure oscillations within the packed bed during both the trickle-flow and pulse-flow regimes. Irregularities in the pulse height and frequency increase as the D/d ratio decreases. Significantly higher liquid and gas flow rates are required to achieve transition to pulsing in these large-particle beds.

2.4.2 Time-averaged, bed pressure drop

The nondimensional bed pressure drop as a function of the gas mass flux is shown in Figs. 2.4A-C for three beds with different-sized beads and varying liquid mass fluxes. In all cases, the bed pressure drop increases with an increase in either the liquid or the gas mass flux. The data points where pulsing was first visually observed in Figs. 2.4A-C are noted with circles.

The smallest beads with diameters of 0.64 cm (D/d = 15.0) show a nearly constant increase in the average bed pressure drop with increasing gas mass flux (Fig. 2.3A). These trends have been previously noted in beds of particles with D/d> 15 (Blok et al., 1983; Wammes et al., 1991). At the lowest liquid mass flux, the pressure drop increases at a slower rate when the gas mass flux is low as compared to the rapid increase of the pressure drop at the highest liquid mass fluxes. Higher liquid mass fluxes cause the transition to pulse flow to occur at relatively lower gas mass fluxes, where the inclusion of the pulses within the bed are known to increase the average bed pressure drop over that of trickle flow (Talmor, 1977). The bed pressure drop for the 0.95-cm beads (not shown) appears qualitatively similar to Fig. 2.4A, but slightly lower in magnitude, as expected due to the lower flow restriction provided by the larger beads and the higher bed void fraction.

The bed pressure drop for the 1.27-cm beads (D/d = 7.50) is plotted in Fig. 2.4B, and the same general trend of increasing pressure drop with either liquid or gas flow rate is shown. At the lowest liquid mass fluxes, the pressure drop increases gradually with increasing gas mass flux. As the liquid mass flux increases, a rapid change in the slope of the average bed pressure drop appears at conditions near where the pulses within the bed are visually observed. The presence of such a rapid change of the slope of the bed pressure drop as a function of the gas mass flux has not been previously noted since the literature contains only pressure drop data for two phases flowing in packed beds with larger D/d ratios.

The normalized bed pressure drop for the 2.54-cm beads (D/d = 3.75) is plotted in Fig. 2.4C for three liquid mass fluxes. Due to the large voids between particles, only trickle flow was visually observed for all of the test conditions. Higher liquid and gas flow rates that exceed the current experimental capabilities are required in order to achieve pulse flow. From the pressure data, a

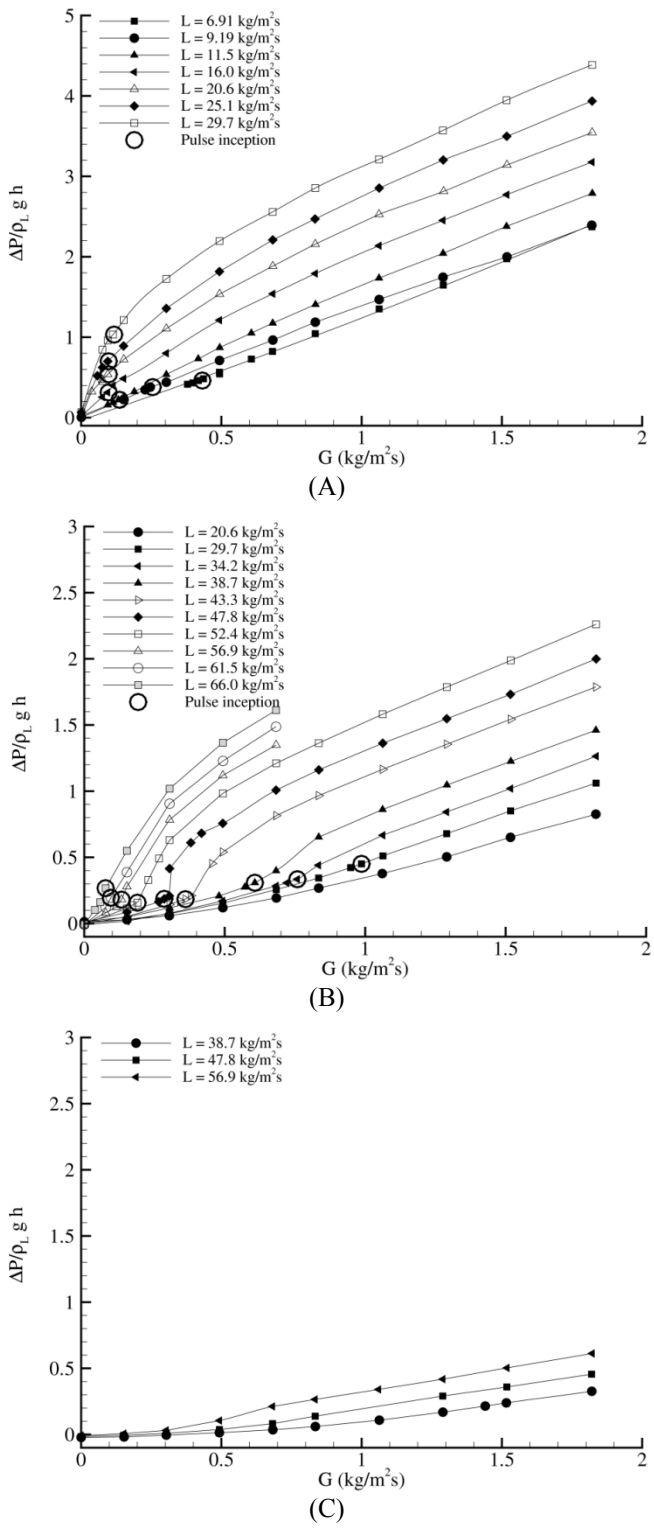

Figure 2.4: Normalized bed pressure drop versus gas mass flux for (A) d = 0.64 cm (B) d = 1.27 cm (C) d = 2.54 cm. Circled symbols denote pulse inception.

slight discontinuity is observed for the highest liquid flow rate tested, which indicates operation near the transition to pulse flow based on the previous results for the 1.27-cm beads. However, due to the significant flow along the inner surface of the tube, it was difficult to visually confirm the presence of pulses within the bed.

2.4.3 Pulse pressure drop and transition boundary

To investigate the origin of the discontinuity in the slope of the average bed pressure drop discussed above, the magnitudes of the pressure oscillations within the bed (from location L2 in Fig. 2.1) were determined and compared to the total bed pressure drop. While it is known that the pulse characteristics depend on their location within the packed bed (i.e., the pulse inception point moves upward in the bed as the flow rates are increased, and the pulse velocity increases as the pulse travels downward through the bed), insight can be gained by a comparison of the flow within the bed to the behavior of the total bed.

The maximum average pressure drop across a pulse is determined from the pressure history at L2 and averaging the three pulses with the greatest change in pressure. An example pressure trace is shown in Fig. 2.5 with the three selected pulses used to determine the maximum average pulse pressure drop noted.

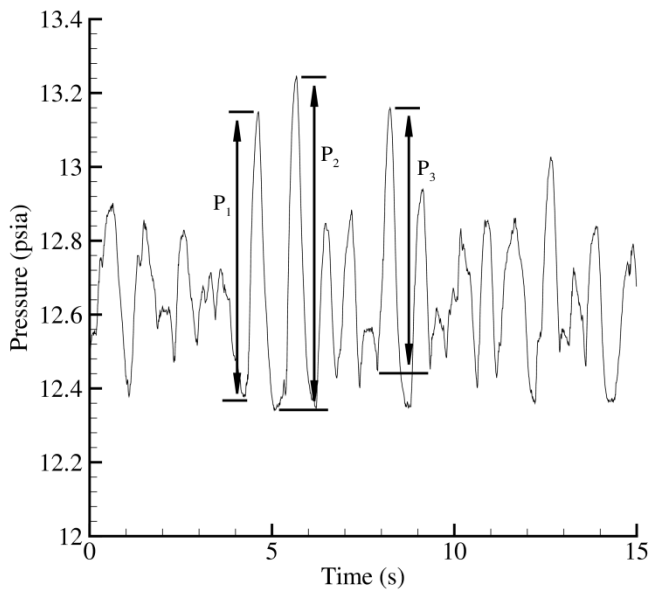

Figure 2.5: Determination of maximum average pulse pressure drop: *d* = 1.27 cm, L = 43.3 kg/ m^{2}s, G = 0.49 kg/m^{2}s.

Figure 2.6 plots the parameter P^*, defined as the maximum average pressure drop across a pulse within the packed bed normalized by the total average bed pressure drop ΔP, as a function of the gas mass flux:

$$P^* = \frac{(P_1 + P_2 + P_3)/3}{\Delta P} . \tag{8}$$

The locations at which pulses were first visually observed are noted on Figs. 2.6A-C by circles surrounding the test conditions. If a data series does not contain a circle (see Figs. 2.6B and C), then transition was not observed, and the bed operated in the trickle-flow regime. In the trickle-flow regime, no significant pressure oscillations were observed, as noted by values of P^* much less than the P^* values in the pulse-flow regime (Fig. 2.6B). As noted previously, the gas-flow rate at which pulsing was first observed decreased with increasing liquid-flow rate. After the initial observation of pulses within the bed, the maximum average pulse pressure drop was found to increase to a maximum fraction of the total bed pressure drop before decreasing. Although the values of P^* decreased, pulses remained present within the bed. If the experimental capabilities enabled higher gas and liquid flow rates, the pulses would continue to be damped out until the bubble-flow regime was reached.

It is interesting to note that the conditions under which pulsing became visually obvious correspond to values of $P^* = 0.2$ for the 0.64-cm beds and increased to $P^* = 0.3$ for the 1.27 cm beads. Transition to pulse flow seems to occur at a consistent value of P^* for a given value of D/d which increases as D/d decreases. This appears to be a condition from which the transition to pulsing can be inferred. For the case of the 2.54-cm beads, the maximum values of P^* did not exceed 0.3, further indicating that the pulse-flow regime was not reached. Values of P^* are not shown for $G < 0.5$ kg/m^{2}s due to the uncertainty in the pressure measurements for the nearly-zero values of the pressure drop (see Fig. 2.6C).

The results of this study clearly show that the particle size can significantly impact flow regimes, so comparisons must be made to a map that incorporates the column diameter and characteristic particle size. The flow map of Talmor (1977) is chosen. The transition boundary results of this study are plotted on the flow map of Talmor (1977) in Fig. 2.7 for the beds with the 0.64-cm, 0.95-cm, and 1.27-cm beads. The results for the 2.54-cm beads are not plotted on the flow map since no transition to pulse flow was observed either visually or by inspection of pressure histories within the bed. An increase in the experimental flow capabilities is needed in order to determine the transition location for these largest particles. The solid symbols in Fig. 2.7 correspond to pulse flow, and the open symbols correspond to trickle flow. The coordinate axes consist of the volumetric gas-to-liquid ratio $(G/L)(\rho_L/\rho_G)$ on the y-axis and a ratio of nondimensional numbers $[1 + (1/Fr)] / [We + (1/Re)]$ on the x-axis. This ratio takes into account the driving forces of gravity and inertia and the viscous and surface-tension resistance forces. The gravity-to-inertia-force ratio is represented by the two-phase Froude number

$$Fr = \frac{[(L+G)v_{LG}]^2}{gD_h}, \tag{9}$$

the viscous-to-inertia-force ratio is represented by the two-phase Reynolds number

$$Re = \frac{D_h(L+G)}{\mu_{LG}}, \tag{10}$$

and the inertia-to-surface-tension-force ratio is represented by the two-phase Weber number

$$We = \frac{D_h (L+G)^2 v_{LG}}{\sigma_L} . \tag{11}$$

In these definitions, the two-phase viscosity μ_{LG} and specific volume v_{LG} correspond to the average properties of the two phases:

$$\mu_{LG} = \mu_L \frac{(L/G)}{1+(L/G)} + \mu_G \frac{1}{1+(L/G)} ,$$

$$v_{LG} = v_L \frac{(L/G)}{1+(L/G)} + v_G \frac{1}{1+(L/G)} . \tag{12}$$

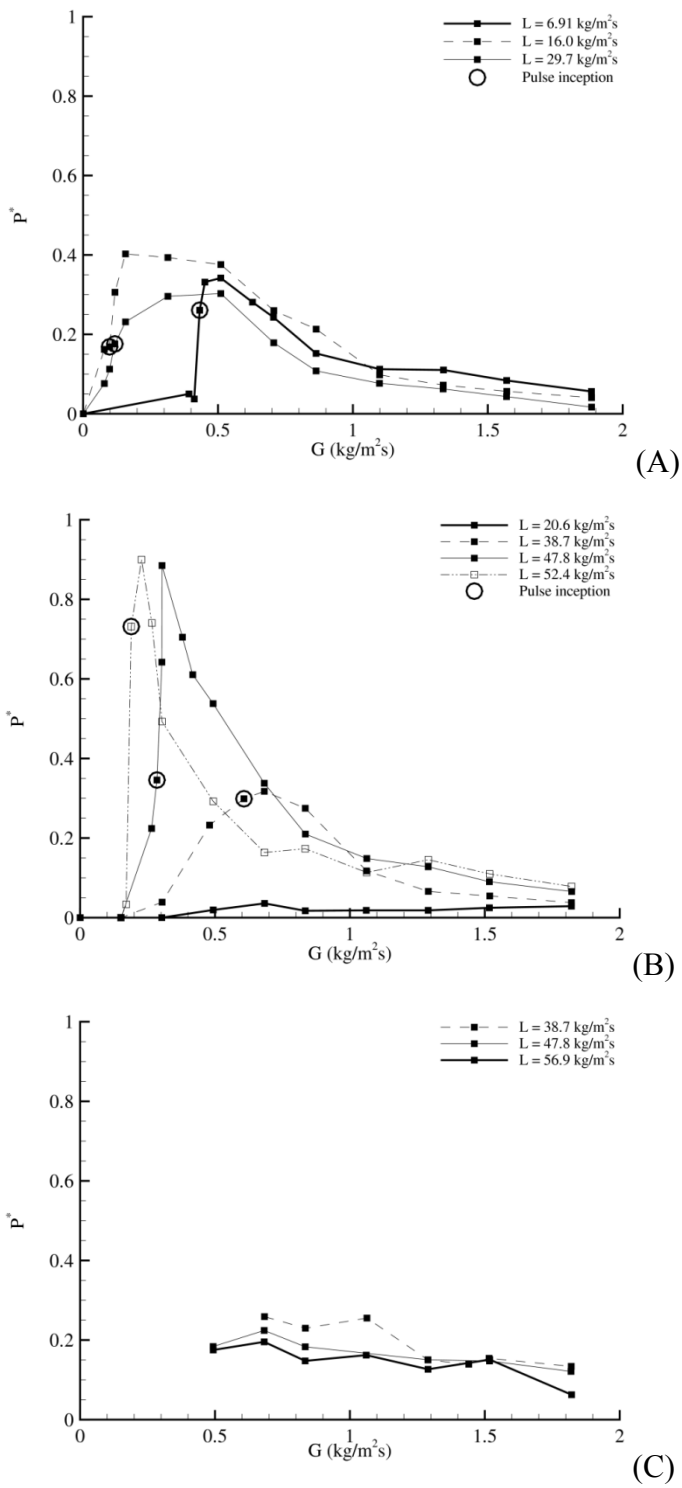

Figure 2.6: Normalized pressure across pulse versus gas mass flux for (A) d = 0.64 cm; D/d = 15 (B) d = 1.27 cm; D/d = 7.5 (C) d = 2.54 cm; D/d = 3.75. Circled symbols denote pulse inception.

The parameter D_h is the bed hydraulic diameter:

$$D_h = \frac{2\varepsilon D}{2+3(1-\varepsilon)(D/d)} . \tag{13}$$

The trickle-pulse boundary of the flow map (Talmor, 1977)) was determined with experimental data for a range of diameter ratios D/d between 83 and 10.7. The transition points for the 0.64-cm and 0.95-cm beads match the transition line as expected since their values of D/d equal 15 and 10. Thus, wall effects and particle diameter variations are effectively captured by the relationship for the bed hydraulic diameter (Eq. 13). Near transition for the 0.64-cm and 0.95-cm beads, $(1/Fr)$~1, We~0.1, and $(1/Re)$~0.001, indicating that the inertia-to-surface-tension-force ratio is dominant. The effect of the column wall is obvious for the 1.27-cm beads with $D/d = 7.5$, for which the transition boundary is shifted towards the origin. The higher-void-fraction bed is not effectively correlated by the coordinates of the flow map. Near transition for 1.27-cm beads, $(1/Fr)$~1, We~1, and $(1/Re)$~0.0001, indicating that the gravity-to-inertia-force ratio is no longer negligible as comparable to the inertia-to-surface-tension-force ratio. In this case, the liquid surface tension is not sufficient to increase the holdup on the beads to enable the liquid to bridge the large open spaces between the beads, but rather this necessary process for pulse flow is inhibited by gravity.

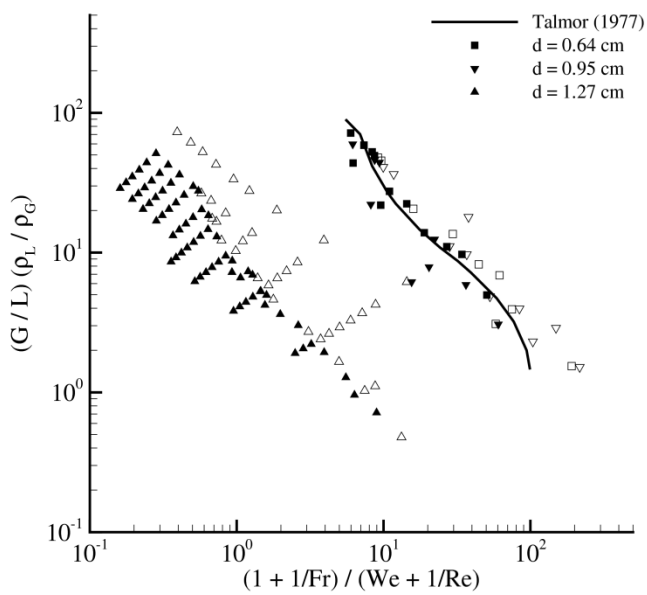

Figure 2.7: Flow map showing trickle-pulse transition for all beads. Solid symbols correspond to pulse flow, and open symbols correspond to trickle flow.

The experimental observations of Tosun (1984) do not support the trickle-pulse transition boundary of Talmor (1977) even though air and water are used and the bed particles have a sufficiently large $D/d = 27$ so that wall effects are negligible. Tosun (1984) does not offer an explanation for this discrepancy but instead concludes that the flow map of Talmor (1977) is unreliable. Instead, Tosun (1984) supports the flow map of Charpentier (1976) which does not account for the bed void fraction or particle size. As stated previously, comparisons of the

experimental data in this study must be made to flow map that accounts for variations in *D*/*d*, such as the flow map of Talmor (1977).

2.4.4 Flow characteristics at trickle-pulse transition

Pulse flow has been described as repetitive slugs of liquid and gas (Blok et al., 1983) or a phase redistribution of a two-phase mixture (Talmor (1977). At low flow rates, the liquid flows over the beads in continuous streams (trickle flow). An increase in either the liquid flow rate or the gas flow rate causes liquid-rich regions to form near the bottom of the packed bed (pulse flow). Further increases in either flow rate increase the pulse frequency and the height of pulse inception within the bed. Observations of the local pressure and conductance probe measurements at the trickle-pulse regime transition follow.

Pulse variations with bed location

The pulses exhibit radial variations across the column cross-section and axial variations as they travel through the packed bed. Previous observations of the radial variations have shown that the center of the column ($0< r/R <0.1$) has a high liquid fraction within the pulse (Beimesch et al., 1971; Weekman and Meyers, 1964). This liquid fraction within the pulse decreases significantly to near-gas-continuous conditions in an annular region ($0.1 <r/R <0.6$). Conductance probe output from three different radial locations appears in Fig. 2.8 for a bed of 0.64-cm-diameter spheres. The results are linearly scaled so that liquid-continuous conditions yield an output of unity, while gas-continuous conditions yield an output of zero. Inspection of Fig. 2.8 shows that a high fraction of liquid appears near the column centerline ($r/R = 0.09$, Fig. 2.8A), significant variations between gas-rich and liquid-rich conditions occur at a slightly larger radius ($r/R = 0.5$, Fig. 2.8B), and a nearly constant low liquid fraction exists at the column wall ($r/R = 1.0$, Fig. 2.8C). Such a nearly constant liquid fraction is due to the increased bed void fraction at the wall, which is known to affect the flow (Winterberg and Tsotsas, 2000; Chu and Ng, 1989; Cohen and Metzner, 1981). This liquid fraction at the wall increases as the value of D/d decreases.

The data of Fig. 2.8 were taken while the pulses traveling through the bed were visually distinct. While the flow down the column walls is mostly liquid, distinct variations are observed in the conductance-probe data that match the corresponding measurements from the wall-mounted pressure transducers. It is clear that the higher concentration of liquid flow down the walls not only inhibits visual observation of the pulses but also acts to dampen the liquid-rich-to-gas-rich oscillations that occur within the bed. The difficulties associated with observing the pulses at the wall increase at higher liquid and/or gas flow rates and with beds of large particles.

The pulses also exhibit axial variations depending on the bed height, as previously noted by Talmor (1977). Figure 2.9 plots the output for the wall-mounted pressure transducers at bed locations L2 and L3 (Fig. 2.1) when pulses are first visually observed (A) and for pulses observed with a higher gas mass flux (B). The pressure variations are greater when measured at axial locations near the middle of the bed (Location L2), yet the pulse profiles are more regular when measured at locations near the bottom of the bed (Location L3). In determining the pulse characteristics, most researchers have taken measurements between the bottom and the middle of the bed. Measurements of pulse parameters without consistency of measurement location would likely impact agreement amongst different groups.

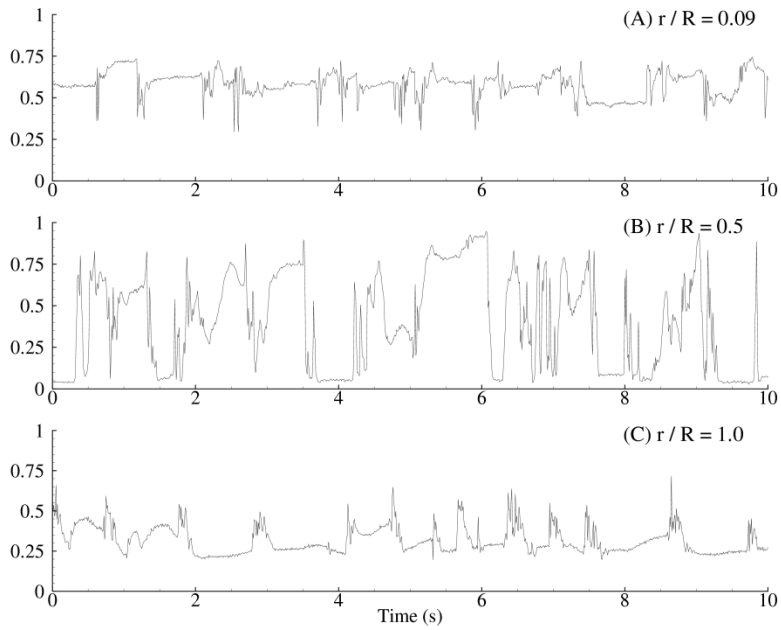

Figure 2.8: Conductance data showing radial variation of liquid distribution at location C1. d = 0.64 cm, G = 0.236 kg/m^{2}s, and L = 11.6 kg/m^{2}s. Data are scaled so that pure liquid = 1 and pure gas = 0.

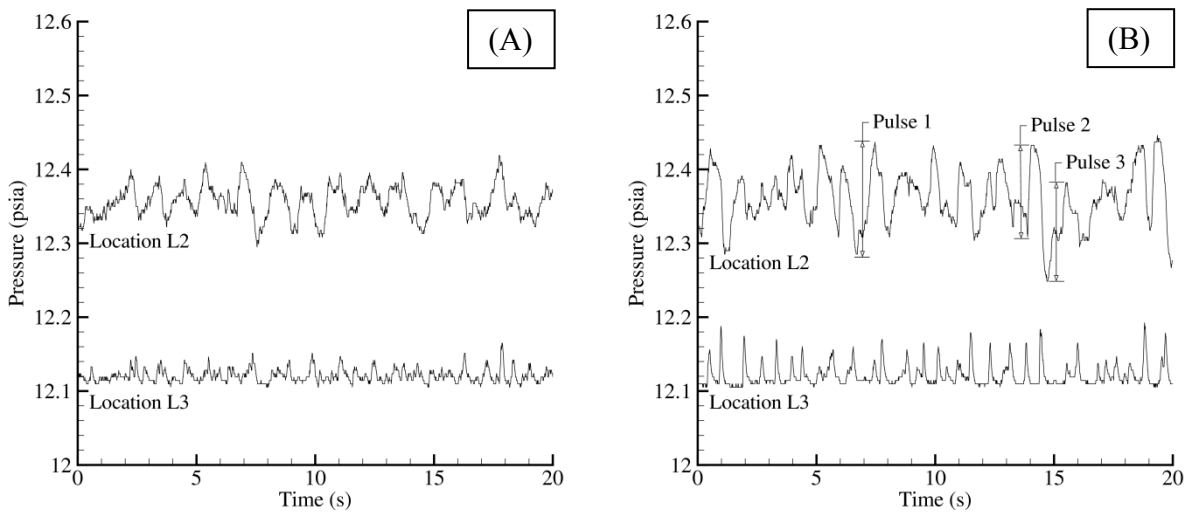

Figure 2.9: Pressure measurements at locations L2 and L3 with *d* = 0.64 cm and *L* = 11.5 kg/m^{2}s. (A) Pulses first observed (B) Higher gas mass flux G.

Using local pressure measurements to detect transition

The most versatile measurement technique to detect the trickle-pulse transition uses wall-mounted pressure transducers. However, because the axial measurement location along the bed has been shown to affect the resulting pulse characteristics, this technique is investigated further.

Chou et al. (1977) used a non-transparent column made of Bakelite and relied on pressure transducers to determine the trickle-pulse transition. They report a distinct jump in the root mean square (RMS) of the time-varying pressure measured at 5% of the bed length above the bottom packing support. In the present study, the RMS values of the local pressure measurements were determined at locations L2 and L3 (28.5% and 2.7% of the total bed length above the bottom packing support, respectively). The results are plotted in Fig. 2.10 as functions of the gas mass flux. The conditions at which pulses were first visually observed are also indicated. No correlation between the RMS values of the local pressure measurements and the conditions at which pulses were first visually observed exists. This is in agreement with the results of Tosun (1984), who noted that significant pressure fluctuations appear within the flow prior to the observation of pulsing.

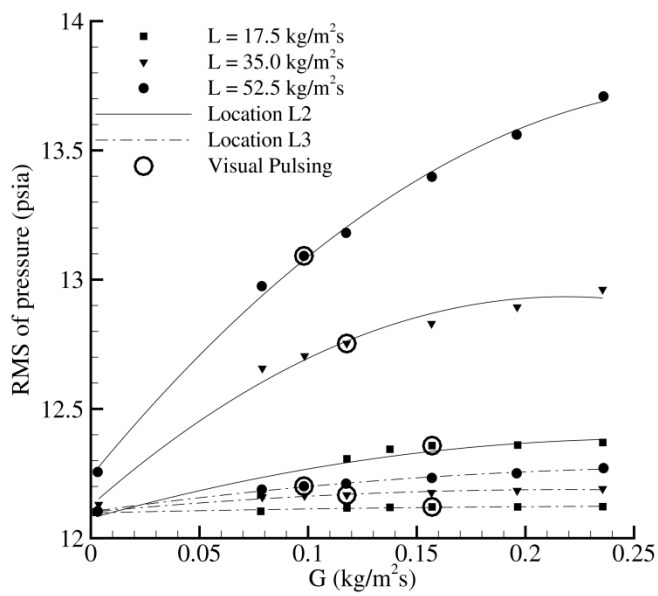

Figure 2.10: RMS of pressure at locations L2 and L3. d = 0.64 cm.

An alternative method to utilizing the local pressure measurements to provide an indication of the trickle-pulse regime transition is to calculate the average maximum pressure drop across a pulse at each location and compare that to the time-averaged pressure drop across the bed. This is investigated for beds with beads of different diameters.

The average maximum pressure drop across a pulse within the bed (from location L2 in Fig. 2.1) was determined and normalized by the time-averaged bed pressure drop ΔP, resulting in the parameter P^*, which was shown in Figs. 2.6A-B as a function of the gas mass flux G. The

average maximum pressure drop across a pulse is determined from the pressure history at L2 by averaging the three pulses with the greatest change in pressure (see Fig. 2.9B where the three pulses selected to determine the average maximum pressure drop are denoted).

The conditions at which pulses were first visually observed are noted on Figs. 2.6A-B by open circles. If a data series does not contain a circle (see Fig. 2.6B), then transition did not occur, and the bed operated in the trickle-flow regime. In the trickle-flow regime, no significant pressure oscillations were observed, as noted by values of P^* much less than the P^* values in the pulse-flow regime (Fig. 2.6B). When pulses occurred within the bed, pulses were first observed at lower gas flow rates as the liquid flow rate was increased. After the initial observation of pulses within the bed, the average maximum pressure drop across a pulse was found to increase to a maximum fraction of the time-averaged bed pressure drop before decreasing. Although the values of P^* decreased, pulses within the bed remained present. If the experimental capabilities enabled higher gas and liquid flow rates, the pulses would continue to be damped out until the bubble-flow regime was reached.

It is interesting to note that the conditions under which pulses became visually obvious correspond to values of $P^* = 0.2$ for beds with large values of D/d and higher values of P^* as the D/d ratio decreases. This appears to be a condition from which the transition to pulsing can be inferred. For the case of the 2.54-cm beads (not shown), the maximum values of P^* did not significantly exceed 0.2, further indicating that the pulse-flow regime was not reached.

Appendices B – F provide additional detail on the two-phase experiments.

2.5 Conclusions

Two-phase experiments were performed in order to investigate experimental methods that can be used to determine the transition boundary between the trickle-flow and pulse-flow hydrodynamic regimes in a packed bed of spherical particles with cocurrent downward flows of air and water, as well to examine the effects of various packing materials on the flow behavior. Tests were performed with different-sized beads with D/d ratios between 15 and 3.75 and measurements obtained with wall-mounted pressure transducers and conductance probes. The trickle-pulse transition boundary was determined for a variety of packed beds and gas and liquid flows, yet no quantitative criteria exist to experimentally determine the operating regime.

Transparent columns are impractical for industrial applications, and beds of large particles or highly viscous liquids complicate the identification of the operating regime. This work has highlighted several key considerations, such as radial and axial variations of the pulse parameters, which must be considered when using conductance probes or pressure transducers to facilitate identification of the operating regime.

An investigation was carried out to experimentally determine the effect that the particle size has on the transition and the characteristics of the pulse-flow regime in two-phase cocurrent downflow of air and water through a fixed bed of particles. Tests were performed with different-sized beads with D/d ratios between 15 and 3.75, which extended the range of previous data for two-phase flow. While the effect of this ratio has been well studied in single-phase flow through packed beds, no previous study has systematically addressed the issue in two-phase flow.

It was shown that increasing the bead diameter generated a rapid increase in the slope of the average bed pressure drop that corresponded to the conditions at which pulsing was visually apparent within the bed. Under these conditions, the maximum average pulse pressure drop became a significant fraction of the total bed pressure drop, and the transition to pulsing occurred at almost a consistent 0.2 for the 0.64-cm beads and 0.3 for the 1.27-cm beads. While it became visually more difficult to identify when transition to pulsing occurred as the bead size increased, analysis of the pressure histories at a location within the bed can be used to determine criteria to define pulsing.

Plotting the pulse-flow-regime transition points for the different bead diameters on the existing flow map of Talmor (1977) shows that the map does not effectively correlate all data with the lower D/d ratios. Further investigation is required in order to account for the increased void fraction and wall effects in fixed beds of large particles.

Thus, the effect of the D/d ratio can be significant in determining the characteristics of the pulse-flow regime and the transition boundary for pulse flow. Experiments have been carried out to illustrate the magnitude of this effect and highlight the importance of carefully determining the packing specifics required in order to achieve the desired pulse characteristics for critical commercial applications.

3. Three-Phase Experiments

This section serves to document the three-phase multifunctional reactor experiment that was fabricated and operated at Sandia National Laboratories, Building 865, Room 19. This section focuses on the design and assembly, hazard mitigation and operation of the experiment, with data included in the following section.

3.1 Reactor Description and Components

The experiment replicates the industrial application case of cocurrent downflow through a fixed, packed bed with two liquids and a gas. Figure 3.1 shows the process and instrumentation diagram for the reactor. The major components are a vertical glass column, a separator, a liquid sub-system, and a gas sub-system which are described in more detail in the following sections.

The experiment is located along the north wall of Building 865 in Room 19. See Figure 3.2 for a dimensioned footprint of the experiment and components. The components shown in the Process and Instrumentation Diagram and their overall dimensions are listed in Table 3.1. Appendix G lists equipment used with the three-phase experiment. Appendix H presents safety information on this experiment.

Table 3.1. Component Sizes for Experiment Layout

Component	Footprint	Height
Column support structure	24-in x 24-in	14 ft
Compressor	23-in x 20-in	19-in
Chiller	28-in x 23-in	40-in
Aqueous liquid pump	10-in x 30-in	10-in
Organic liquid pump	10-in x 30-in	10-in
Heat Exchangers (qty 2)	22.25-in x 1.5-in	2-in
Knockout Tank	4-in Dia.	48-in
UV/VIS	24-in x 24-in	18-in
Peristaltic pumps (qty 6)	12-in x 12-in	12-in
Ventilation Fan	20-in Dia.	48-in
Computer &(2) DAQ	36-in x 36-in	60-in
Vacuum pump	36-in x 24-in	18-in
Separator tank	48-in dia	48-in

Process & Instrumentation Diagram for Three-Phase Multifunctional Reactor
Building 865, Rm 19
Contact: Walt Gill (505.845.3193), Org 1532
Rev. May 08, 2007

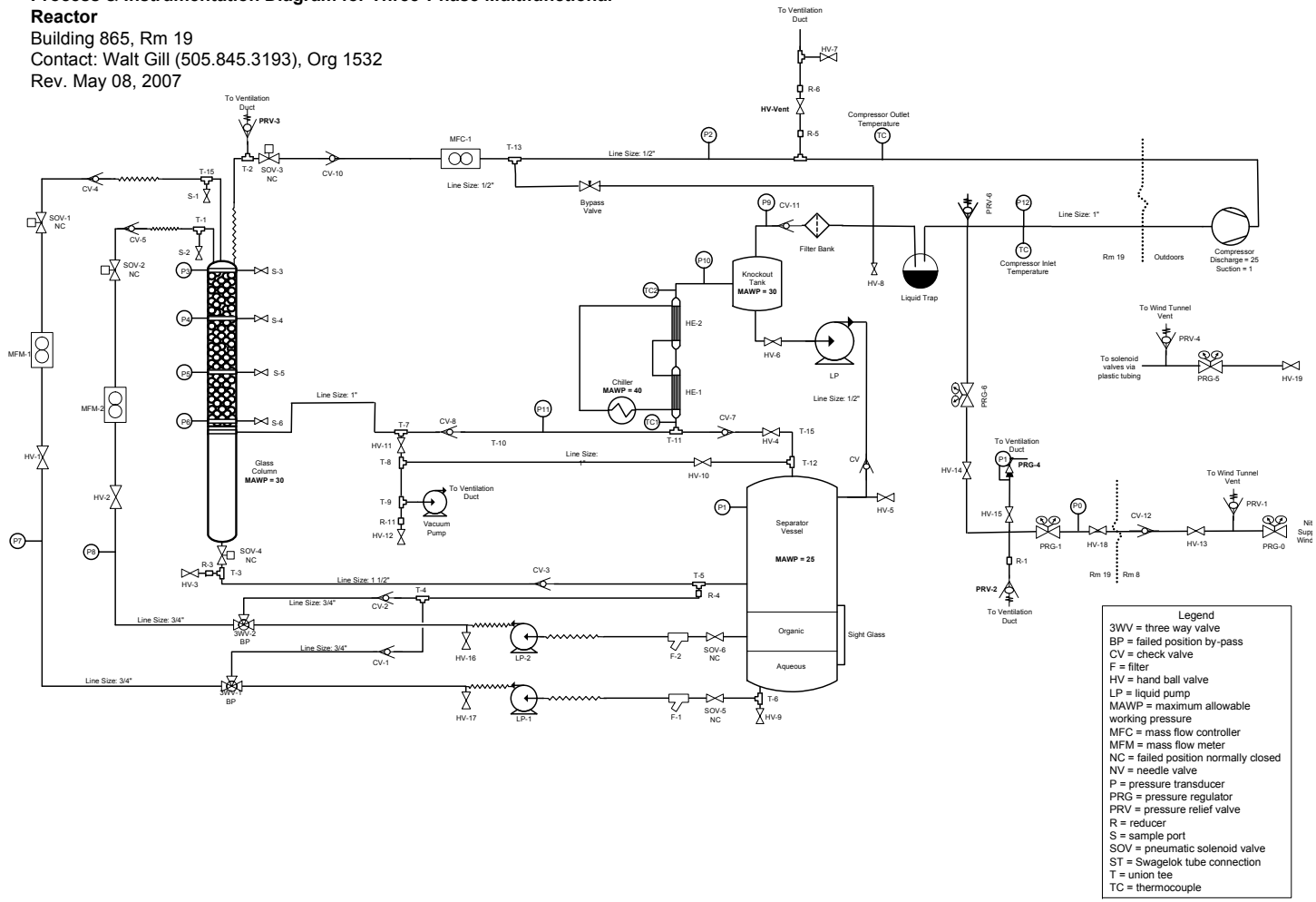

Figure 3.1. Process and Instrumentation Diagram

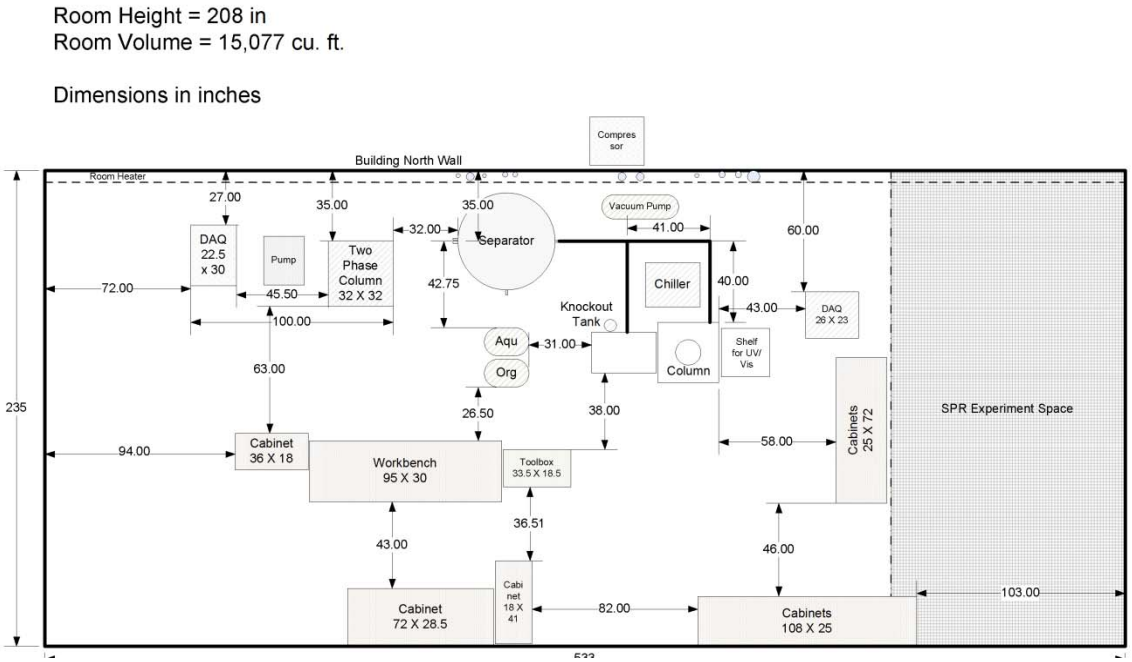

Figure 3.2. Experimental Layout (Dimensioned Footprint for Three-Phase System)

3.1.1 Column

The custom-built column (Figure 3.3) was constructed by Chem Flowtronics, Inc. (Little Falls, NJ). It is constructed from glass and Teflon sections that are bolted together. The inner diameter is 10.2 cm (4 in), the height is 305 cm (10 ft), and it is elevated 122 cm (4 ft) from the ground. A Kee-Clamp super-structure is used to support and elevate the column. Due to the strength of this super-structure, it was also used to support a number of the other experiment components including several of the solenoid valves, the knockout tank, and all plumbing connections to the column.

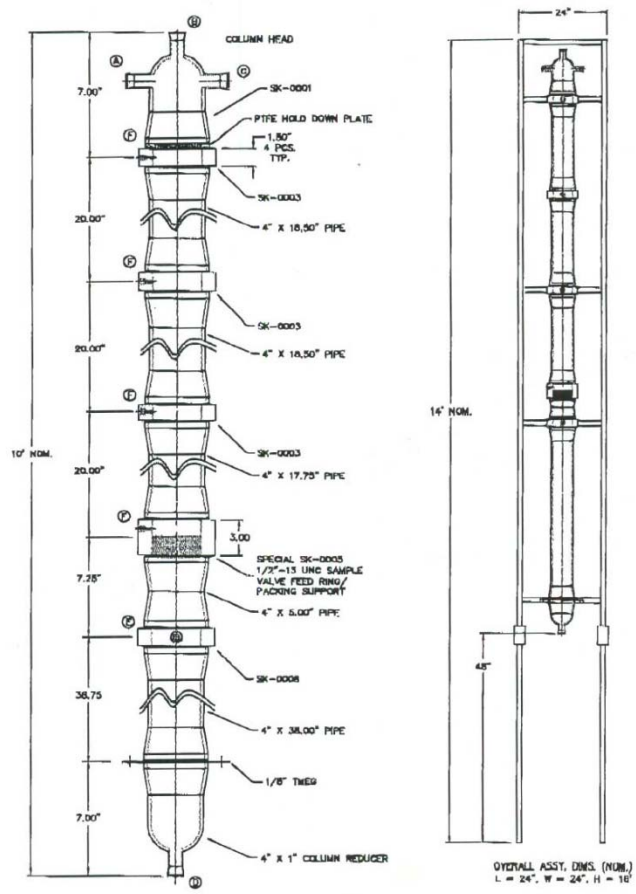

Figure 3.3. Schematic of the Glass Column

As shown in Figure 3.3, a total of five glass column sections, four Teflon sections, and two glass end caps comprise the column. The glass sections are made of borosilicate (Pyrex) glass. The top end cap contains two 3/4-in liquid inlet ports and a 1/2-in gas inlet port. The bottom end cap contains one 1-in liquid outlet port. Column sections 1-4 are 12-in long. The top end cap and column sections 1-4 are separated by 1-1/2-in thick Teflon rings (Figure 3.4Figure). These rings are referred to as the sample rings and were built with three 3/8-in NPT ports (i.e. for pressure transducers, sampling probes, other fittings) and a 1/2-in NPT port for a sample valve (not used in present tests).

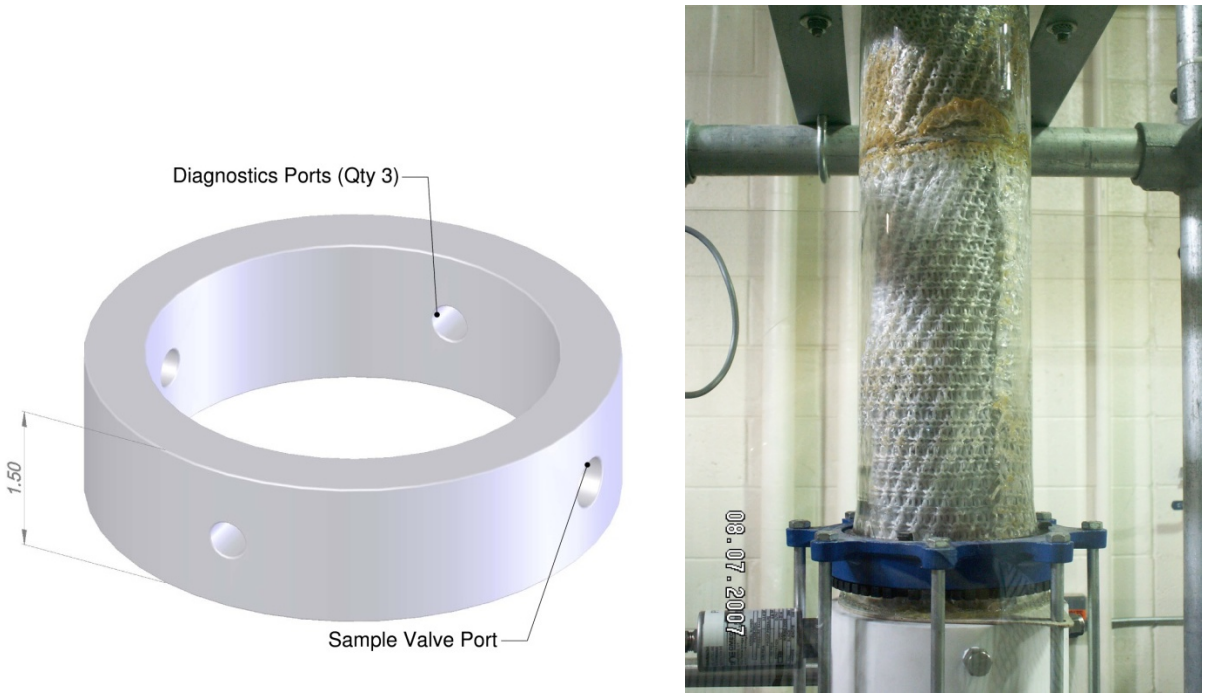

Figure 3.4. Illustration of the Teflon Sample Ring (left, sketch; right, installed on column).

Column section 5 is 57 inches long. It is separated from column section 4 with a 1-1/2-in thick Teflon ring. This ring contains the same ports for diagnostics and the sample valve above a packing support that covers the inner cross-sectional area of the column. The packing support was constructed by drilling an array of 3/8-in through holes through the Teflon. Special care was taken to ensure that all packing installed in the column did not plug these holes. Below the packing support is a 1-in port for the vapor take-off.

Metal flanges compress the sample rings and gaskets between the different glass sections. Bolts around the flange circumference were carefully tightened in a standard torque sequence to compress the gaskets and prevent leaks. When assembled, the portion of the column above the packing support was filled with desired packing and pressure transducers were installed in the sample rings. The portion of the column below the packing support remained empty and was used to collect the liquid that was held up by the packing during holdup experiments.

To properly size the long column section below the packing, the amount of liquid holdup due to the packing was estimated. The intent was that all liquid holdup, once allowed to drain out of the packing, would be fully contained in the non-packed portion of the column. A correlation appears in Wammes et al. (1991) for the dynamic liquid holdup as a function of the liquid Reynolds number.

$$\beta_{dyn} = 3.8\left(\frac{\rho_l v_l d_p}{\eta_l}\right)^{0.55}\left[\frac{d_p^{\,3}\rho_l^{\,2} g}{\eta_l^{\,2}}\left(1+\frac{\Delta P}{\rho_l g L}\right)\right]^{-0.42}\left(\frac{a_v d_p}{\varepsilon}\right)^{0.65} \tag{3.1}$$

The final term, $(a_v d_p/\varepsilon)^{0.65}$, was included by Specchia and Baldi (1977) to account for the effect of different packing materials. It is based on porous and nonporous packings with different geometries and sizes with a nominal diameter between $0.5 < d_p < 50$ mm. Raschig rings were not effectively represented by this relationship (Rao and Drinkenburg, 1985). Equation 3.1 was

determined from data at low superficial gas velocities of $1.9 < v_g < 5.2$ cm/s. As a result, the holdup was found to not depend on the gas flow parameters, explaining why β_{dyn} does not depend on v_g. While operation in the experimental column exceeded this superficial gas velocity range (up to $v_g = 64$ cm/s at 11 scfm gas flow), the above relationship was used to provide a maximum bound on the expected liquid holdup for column design since liquid holdup is known to decrease as the gas velocity increases.

The pressure term appearing in Equation 3.1 is to account for operating the reactor at pressures different from atmospheric. Increasing the reactor pressure acts to decrease the liquid holdup. The experiments of Wammes et al., 1991 show that at $Re_l \approx 6$ the effect of increasing the column pressure from 0.3 MPa to 5.0 MPa results in decreasing the dynamic liquid holdup by only 30%. The holdup for our experiment was calculated by assuming that ΔP in Eq. 3.1 was zero, modeling column operation at near-atmospheric conditions. This term could be included, yet it is not expected to significantly affect the predicted value of the liquid holdup.

The relationship for dynamic holdup (Equation 3.1) is calculated for the column parameters as a function of the liquid Reynolds number.

$$\mathrm{Re}_l = \left(\frac{\rho_l v_l d_p}{\eta_l} \right) \tag{3.2}$$

The static holdup values were assumed to be 10-20% of the dynamic holdup (Wammes et al., 1991). The sum of the static and dynamic holdup equals the total holdup due to the packing. The total liquid holdup was converted into an equivalent volume of liquid by

$$\beta = V_l / \varepsilon V_{bed} \tag{3.3}$$

In all cases of the ratio of aqueous/organic liquid between 90/10 to 10/90, Eq. (3.1) predicts dynamic holdup to not exceed 0.5 gallons assuming the packing is 6 mm diameter spheres and the bed length is 1.5 m long (5 ft). So, including the static holdup, no more than 0.6 gal liquid holdup is expected.

This volume is converted into the total height in the bottom of the column that the liquid would fill during the draining process of a holdup experiment. Considering a column outer diameter of 4 in, the liquid height does not exceed 10 in. It should be noted this is the liquid that is contained within the packing when operating in the pulse flow regime. Values obtained with the column is operating in the trickle flow regime will be a small fraction of these values.

3.1.2 Problems and Repairs

The connections along the column height are a potential source of leaks. Leak prevention is done by carefully tightening the bolts at the joints of the main glass column sections. The column was tightened together from the top and then bolts tightened while working down to the bottom of the column.

Additional places where leaks may be present are through the threads of the ports in the Teflon sample ring. Fittings and diagnostics were carefully threaded into these ports so as not to cross the threads. Teflon is a soft material and the threads can be easily ruined such that leaks can't be fixed. The ports in the top and bottom cover connect to stainless steel Swagelok fittings through Teflon adapters, another potential source of leaks.

3.2 Separator

The custom-built separation tank was constructed by Brown-Minneapolis Tank Company (Albuquerque, NM). It is a vessel constructed of 304 stainless steel, with an overall height of 4 ft and a diameter of 4 ft. The bottom of the vessel is welded on while the top of the vessel is sealed with a bolted flat plate, allowing the tank to be opened for cleaning. The top plate is 1-in thick and weighs approximately 400 lbs. A Viton gasket seals the top flange to the tank. The entire vessel weighs nearly 1500 lbs. A sight glass (125 psig rating) from John Ernst Co. was welded to the side of the vessel for visualization of the two liquid levels. The bolts on the top lid were torqued to 150 ft-lbs following a standard torque sequence.

3.3 Gas sub-system

The gas sub-system consists of the vapor handling lines connecting the vapor take-off of the column to the vapor headspace of the separator, through the knockout tank and compressor then to the top of the column (see Figure 3.1). The system contains multiple pressure relief valves, and regulators to maintain a constant pressure within the flow stream. A knockout tank and chiller combination was designed to condense approximately 70% of the organic vapor absorbed in the gas stream upstream of the compressor. All lines are stainless steel tubing with Swagelok connections.

As shown in Figure 3.1, the gas flow system included two Alicat Model MCR-1000SLPM-D/5M 5IN mass flow controllers, one on the gas supply line to the top of the column, and the other on a recirculating gas bypass loop. The desired flow rate into the column was achieved by adjusting the flow rates of the two mass flow controllers.

3.3.1 Heat Exchangers

Two heat exchangers are located in the gas stream upstream of the knockout tank to cool the gas/vapor so that the vapor can be removed from the gas stream. They were purchased from Exergy, LLC (Garden City, NY).

3.3.2 Knockout Tank

A knockout tank is located in the gas stream between the heat exchangers and the compressor inlet. Its purpose is to remove vaporized liquid entrained in the gas stream. The tank was designed to ASME standards for a working pressure of 30 psig and 50°C and was fabricated at Sandia.

3.4 Liquid sub-system

The liquid sub-system consists of the two liquid lines that draw the aqueous (pure water or NaCl/NaOH solution) and organic (toluene or isododecane) liquids from the separator tank and pump them through magnetic drive pumps (LP-1 and LP-2; all labels refer to Figure 3.1) to the top of the column. Each liquid line contains a particulate filter (F-1, F-2), separator isolation valve (HV-1, HV-2), switching valve for liquid bypass flow (3WV-1, 3WV-2), throttling valve (NV-1, NV-2), mass flow meter (MFM-1, MFM-2), and a column isolation valve (SOV-1, SOV-2).

The bottom of the column drains by gravity directly to the separator vessel through the bottom holdup valve (SOV-4) or can be drained directly through HV-3.

All lines are stainless steel tubing with Swagelok connections.

3.5 Liquids tested

The aqueous phase was always either pure water or water containing sodium chloride (NaCl) and sodium hydroxide (NaOH) for the mass transfer experiments (see Section 3.8). After the fluorescein reaction the water also contains sodium fluorescein.

The organic phase was isododecane for the initial hydrodynamics experiments (pressure and holdup data), and was toluene with fluorescein diacetate and BHT for the mass transfer experiments.

Table 3.2. Liquid Properties

Liquid	*Density (kg/m^3) at 20C*	*Kinematic Viscosity (cSt) at 20C*
Water	998	1.002
Isododecane	746	1.796
Toluene	867	0.68

3.6 Operations and Control

All systems operations were controlled by a LabVIEW program written by Jeremy Barney, entitled CDTECH_3Phase. Most operations were controlled by the LabVIEW program, with only a few valves and switches that had to be manually operated. Table 3.3 shows the measurement devices controlled and monitored by the LabVIEW program. Detailed step-by-step operations are included in Appendix I.

The only problems encountered involved either contamination or excess liquid in the gas flow system. Additional filter banks were added to try to prevent loose particles from reaching the Alicat mass flow controllers. Efforts were made to trap all liquid in the gas line, and the compressor input and output lines were heated to prevent liquid condensation. However, even with these measures, the compressor flow range was limited. More details are in Section 3.8.2 below.

Table 3.3. Data and control instrumentation

Component	*Parameter*	*Save Data?*
MicroMotion Flow Meter (MFM-1 and MFM-2)	volume flow rate (gpm)	Y
	density (kg/m3)	Y
	Temperature (K)	Y
Alicat Flow Controller	volume flow rate (gpm)	Y
	density (kg/m3)	Y
	Temperature (K)	Y
Magnatex Liquid Pump	Speed (Hz)	N
Thermo Chiller	ON/OFF	N
RIX Compressor with Starter	ON/OFF	N
Aqueous Solenoid Valve (SOV-1)	Position	N
Organic Solenoid Valve (SOV-2)	Position	N
Nitrogen Solenoid Valve (SOV-3)	Position	N
Column Solenoid Valve (SOV-4)	Position	N
Aqueous 3-Way Solenoid Valve (3WV-1)	Position	N
Organic 3-Way Solenoid Valve (3-WV-2)	Position	N
Aqueous Pump Solenoid Valve (SOV-5)	Position	N
Organic Pump Solenoid Valve (SOV-6)	Position	N
Separator Pressure (P1)	Pressure (psia)	N
Knockout Tank Pressure (P2)	Pressure (psia)	N
Bed Pressures (P3-6)	Pressure (psia)	Y, graph
Process Temperature (T1, T2)	Temperature (K)	N

3.7 Mass Transfer Measurements

3.7.1 Background

In addition to hydrodynamic studies of the pressure and holdup in the column, the system was designed to allow a particular mass transfer measurement to be made using the hydrolysis reaction of sodium fluorescein. The surrogate chemical system identified for use in the pilot-scale experiment consists of three phases (immiscible aqueous and organic liquid phases and a gas phase), which effectively models the process of sulfuric-acid-catalyzed C4 paraffin/olefin alkylation. Monitoring the progress of an interfacial chemical reaction in the surrogate system provides a quantitative measure of interfacial area. Liquid-liquid mass transfer and hence the rate of mass transfer controlled or influenced reactions such as alkylation are proportional to this interfacial area.

Fluorescein has been widely used as a fluorescent indicator, particularly in biological applications. Fluorescein is yellow-green and fluoresces when excited by light, which provides significant flexibility in its use as an indicator. One method of generating the fluorescein marker is through the hydrolysis of fluorescein esters. Fluorescein diacetate is one particular fluorescein ester. The uncatalyzed hydrolysis of fluorescein diacetate occurs slowly near neutral pH values, but the rate can be increased by using more basic solutions (Guilbault and Kramer, 1964; Wenn et al., 2003). Fluorescein may exist in the dianionic, monoanionic, neutral, lactone, or cationic forms in aqueous solution, depending on the pH (Zanker and Peter, 1958; Leonhardt et al., 1971; Martin and Lindquist, 1975; Invitrogen, 2010). These forms, along with their corresponding pKa values and absorption peak maxima (Leonhardt et al., 1971; Martin and Lindquist, 1975; Invitrogen, 2010; Lindquist, 1960), are illustrated in Figure 3.5. The first reported use of this method was the analysis of enzyme activity (Guilbault and Kramer, 1964). Since then, it has been used in the development of enzyme assays (Huang, 1991ab), estimation of biomass in wastewater and activated sludge (Jorgensen et al., 1992), measurement of total microbial activity in soil (Schnurer and Rosswall, 1982; Adam and Duncan, 2001), determination of total esterase activity in biofilms (Battin, 1997), detection of yeasts in food products (Breeuwer et al., 1995), and measurement of disease suppression in crop container media (Inbar et al., 1991). The reliability of this method in biological applications has also been discussed (Jorgensen et al., 1992; Clarke et al., 2001).

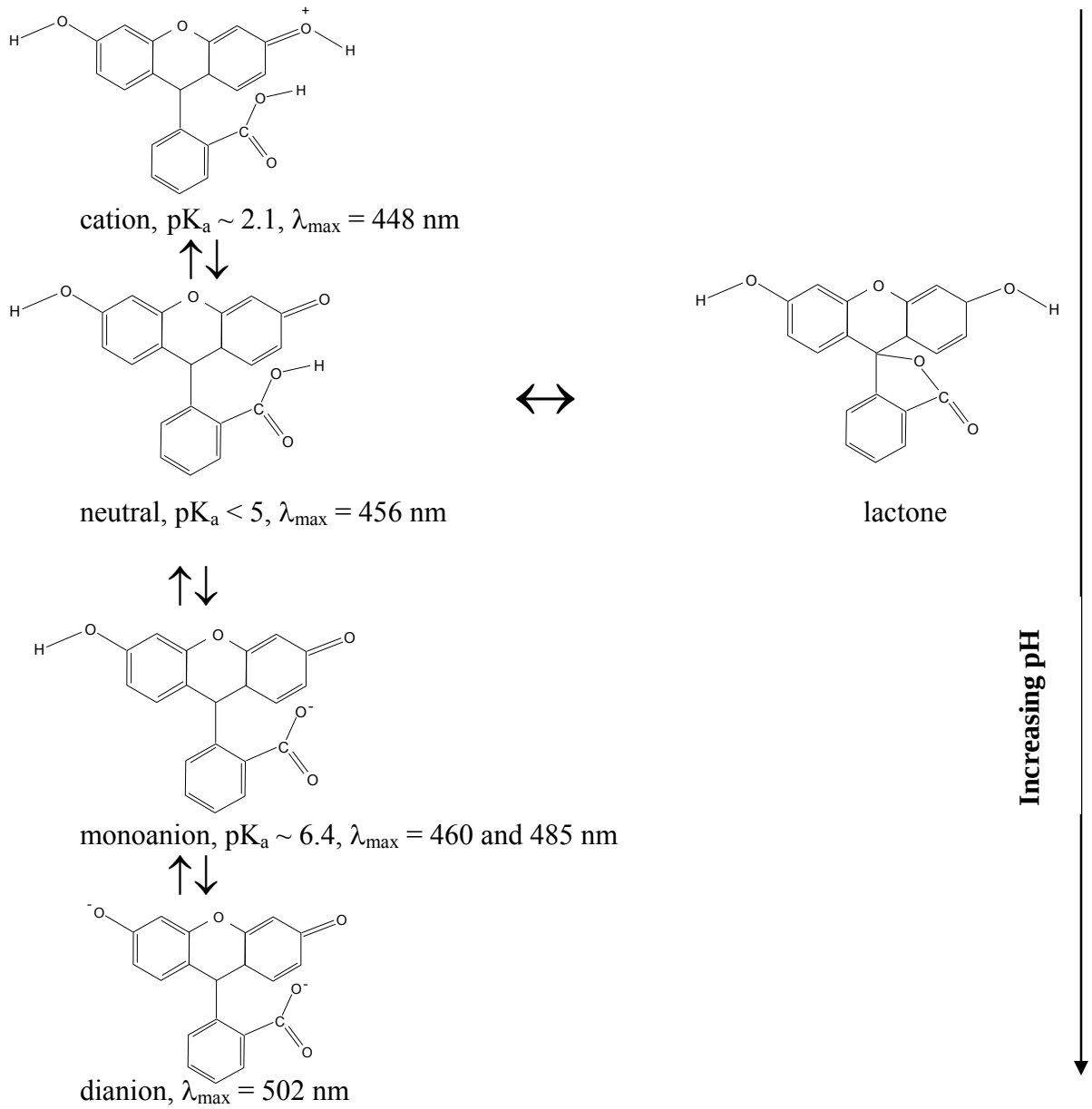

Figure 3.5. The pKa values and peak absorption maxima of fluorescein structures

Only one reference on the use of fluorescein diacetate hydrolysis in industrial applications could be found (Wenn et al., 2003), and it dealt with the construction of mesh micro-contactor devices to study the kinetics of two-phase reactions. The hydrolysis of a fluorescein diacetate/toluene solution with an aqueous sodium hydroxide solution was found to follow pseudo first order kinetics, and the activation energy was determined to be approximately 28 kJ mol^{-1} (Wenn et al., 2003).

There are at least five possibilities to consider for the rate-limiting step (see Figure 3.6): a) reaction in the aqueous phase, b) diffusion in the aqueous phase to and from the interface, c) reaction at the interface, d) diffusion in the organic phase to the interface, or e) reaction in the organic phase.

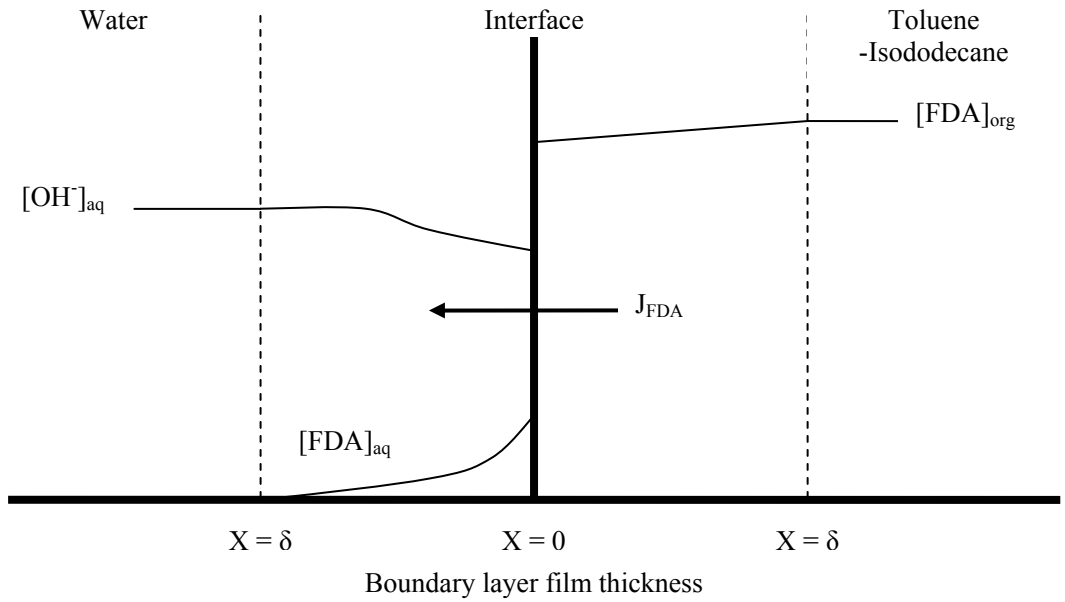

Figure 3.6. Boundary layer diagram for mass transfer with reactive extraction. Adapted from van Woezik and Westerterp (2000).

The organic phase consisted of toluene with fluorescein diacetate and BHT. Initially bench tests were performed using 50% toluene and 50% isododecane, but this was changed to pure toluene when it was discovered that impurities in the isododecane interfered with the fluorescein diacetate hydrolysis reaction. The aqueous phase was deionized water containing NaOH and NaCl.

Lab experiments were performed to better understand the reaction and to prepare solutions for application in the three-phase experiments. Figure 3.7 shows absorbance spectra for different concentrations of fluorescein in 0.1M NaOH, indicating that many peaks were present in both the UV and visible regions. The linearity of peak areas was excellent for all of the major peaks observed. The peak absorbance at 492 nm was chosen for detection. The UV/VIS spectrophotometer is a Shimadzu BioSpec-1601.

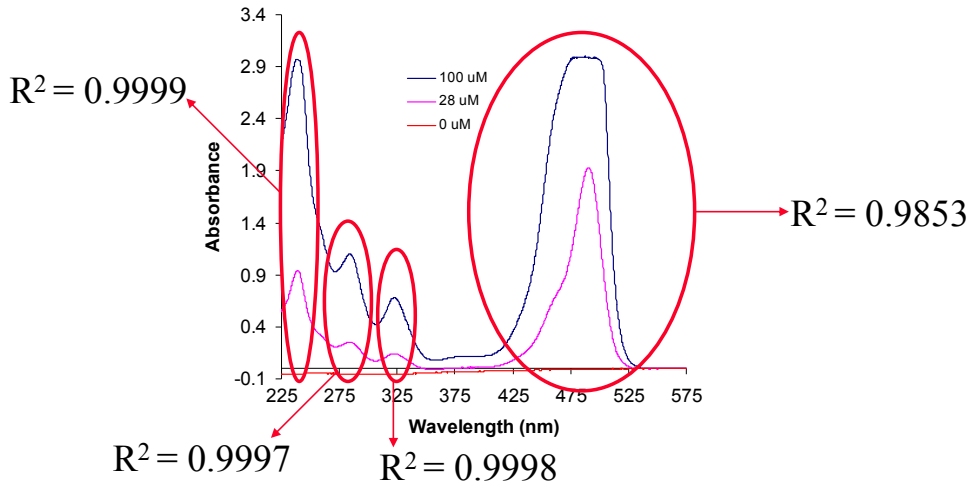

Figure 3.7. Absorbance spectra of three different concentrations (100, 28, and 0 µM) of fluorescein in 0.1M NaOH. The peak *absorbance* at 492 nm was chosen for detection.

Figure 3.8 is a calibration plot of fluorescein in 0.1M and 1M NaOH relating concentration of fluorescein (µM) to the peak intensity at 492 nm. This plot shows the linear range over which fluorescein may be detected. Higher concentrations were tested, and those points were discarded because of nonlinearity. Other than the one bad data point at 30 µM, the 0.1M and 1M NaOH point line up perfectly.

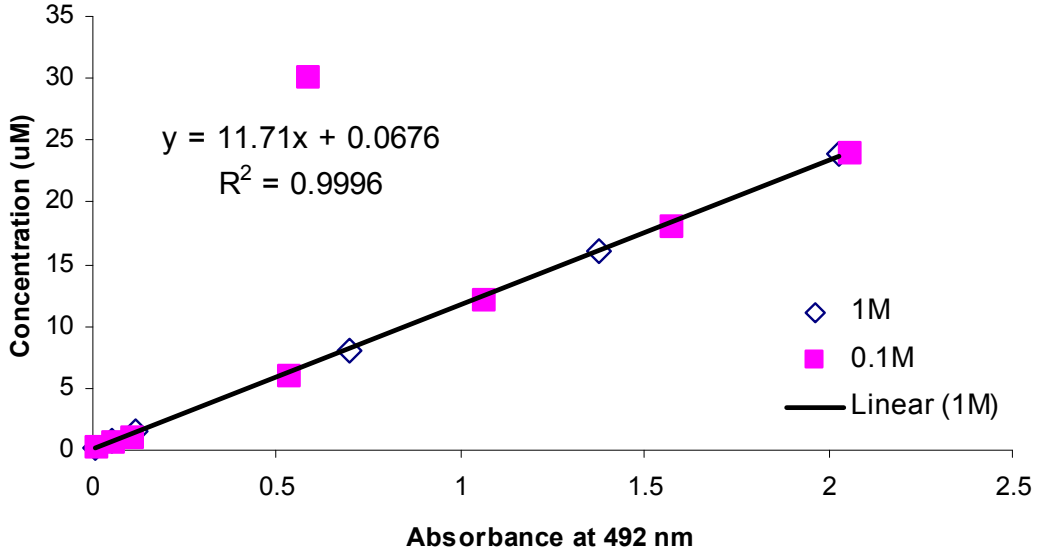

Figure 3.8. Calibration plot of fluorescein in 0.1M and 1M NaOH relating concentration of fluorescein (µM) to the peak intensity at 492 nm, showing the range over which fluorescein absorbance is linearly related to concentration.

In order to increase our understanding of the system, the rate-limiting step during the hydrolysis of fluorescein diacetate had to be determined. The experiment described earlier (Wenn et al., 2003) in which a small amount of fluorescein diacetate is added to an excess amount of well-stirred NaOH solution was repeated in our laboratories in order to validate that the rate-limiting

step is not in the aqueous phase. As stated above, if a rate limiting step is not found in these two cases, then an interfacial process is responsible for the rate-limiting step.

Data were collected and analyzed using the differential method of rate analysis for a batch reactor (Fogler, 1992). The initial general assumption would be that A + B → Products. Using the method of excess, testing would begin with systems containing an excess of B so that C_B remains essentially constant during the course of the reaction. This would imply that equations (3.4) and (3.5) hold.

$$-r_A = k' C_A^{\alpha} \tag{3.4}$$

$$k' = kC_B^{\beta} \cong kC_{Bo}^{\beta} \tag{3.5}$$

After α has been determined, the reaction is carried out in excess A so that equations (3.6) and (3.7) hold.

$$-r_A = k'' C_B^{\beta} \tag{3.6}$$

$$k'' = kC_A^{\alpha} \cong kC_A^{\alpha} \tag{3.7}$$

Combining the mole balance and rate law yields equations (3.8) and (3.9).

$$-\frac{dC_A}{dt} = kC_A^{\alpha} C_B^{\beta} \tag{3.8}$$

$$\ln(\frac{dC_A}{dt}) = \ln k + \alpha \ln C_A + \beta \ln C_{\beta} \tag{3.9}$$

While determining that the reaction is controlled by an interfacial process is sufficient to calculate interfacial areas in the packed column, knowing the particular rate-limiting step of the interfacial process allows us to push the system into an extreme mode where either the interfacial reaction is much faster or much slower than interfacial diffusion. Operating in an extreme mode simplifies data analysis, since the contribution of the insignificant processes can be neglected. Otherwise, the contributions of all interfacial processes must be included when calculating the mass transfer rate of fluorescein diacetate across the interface.

Lewis cell experiments were used to determine rate constants for the surrogate chemical reaction under a baseline set of conditions. Sodium chloride was used as a means to increase the ionic strength and to destabilize the organic/aqueous emulsion that might form during periods of high mixing. The possible influence of NaCl on the rate equation was evaluated. To confirm the reaction rate laws and constants, a modified Lewis cell approach was adopted that exploits the fact that the chemical reaction rate is slower than the rate of solute diffusion in thin liquid layers. Sample batch reactor data are shown in Figure 3.9.

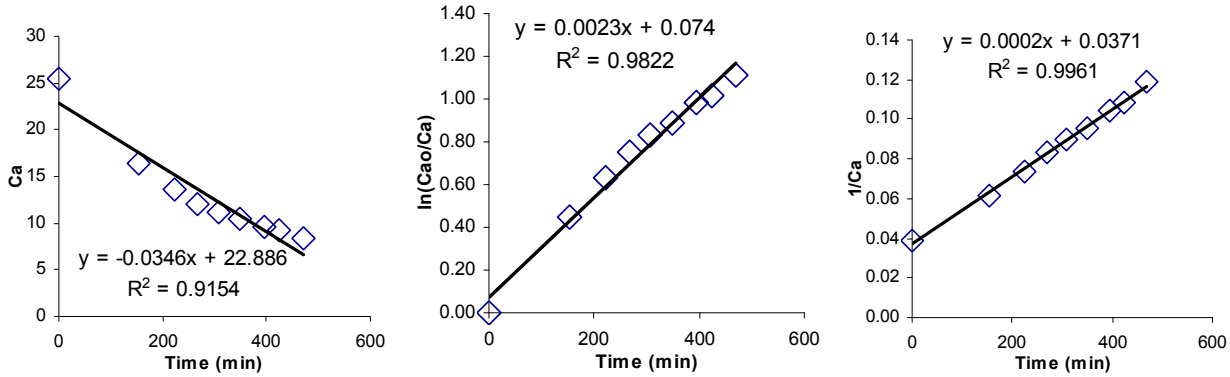

Figure 3.9. Integral method kinetic plots collected on a batch reactor with 25.6 μM fluorescein diacetate, 1M NaCl, and 0.1M NaOH at 400 rpm.

To try to stop auto-oxidation observed in some of the batch tests, butylated hydroxy toluene (BHT) was added as an antioxidant to the organic phase. Results using BHT showed that the auto-oxidative reaction was abated since most triplicate data points were in good agreement and the reaction showed first order kinetics that were expected for the hydrolysis of FDA. The mass transfer test without BHT was slower, and there was greater scatter in duplicate data points than in the standard test runs with BHT.

Stirred batch reactor tests were run using different BHT concentrations to determine if a change in BHT has a significant effect on reaction rate, as shown in Figures 3.10 and 3.11. Twenty ml of organic and 50 ml of aqueous solutions were placed in a crimped sealed vial and magnetically stirred at 400 rpm and samples were taken at various time intervals. Before taking a sample, stirring was stopped for 10 minutes to allow for a good break between the organic and aqueous phases. Except for the test at 15 ppm BHT Run#1, the samples were placed back into the test vial and stirring restarted. For the 15 ppm BHT Run#1 test, new vials were used for each one of the data points, but a poor correlation of the data set was obtained. There was some minor difference in the calculated rate constants between each of the data sets and it appears that a change in BHT concentration will have a negligible impact on the reaction rate. It is important that at least some BHT is present in the organic phase. All subsequent tests were run with a BHT concentration of 15ppm.

Using the 1st order rate constants from the different mass transfer tests, an intrinsic rate constant can be calculated for the fluorescein hydrolysis reaction. The intrinsic rate constant is a function of the 1st order rate constant, the interfacial mass transfer area, and the volume of the organic phase. The average intrinsic rate constant calculated from the mass transfer data is approximately 8.97×10^{-9} (L/mm^2/hr). Using an average 1st order rate constant of 0.052/hr for the stirred batch reactor tests, the calculated interfacial area is about 111,500 mm^2 with an average drop diameter of 0.54 mm. The drop size is calculated based on the drop that gives the same volume/area ratio. Thus, magnetically stirring increased the interfacial mass transfer area by about 15 times over the area of the standard static mass transfer tests (7088 mm^2).

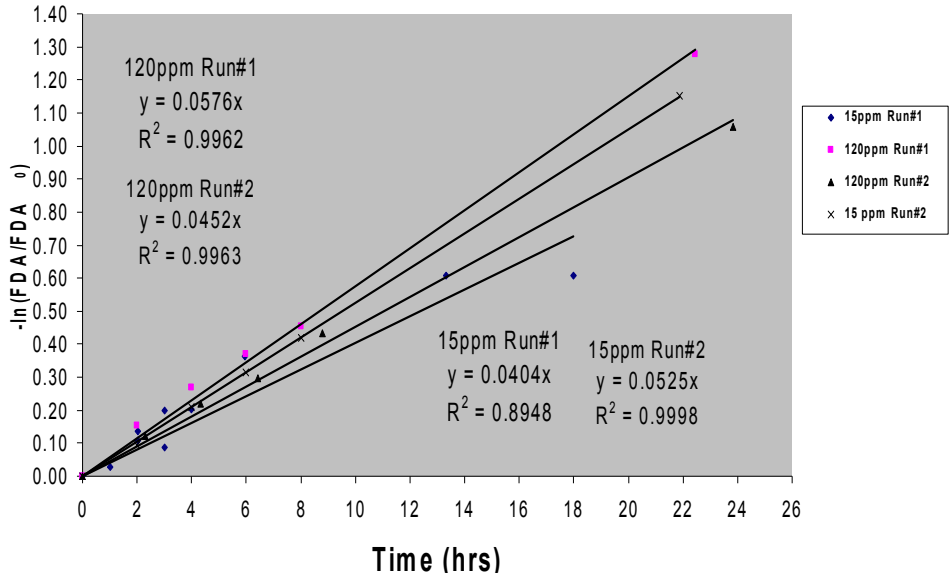

Figure 3.10. First-order rate equation for stirred batch reactor with varying BHT concentration, based on measured FDA. kt = -ln(FDA/FDA$_0$)

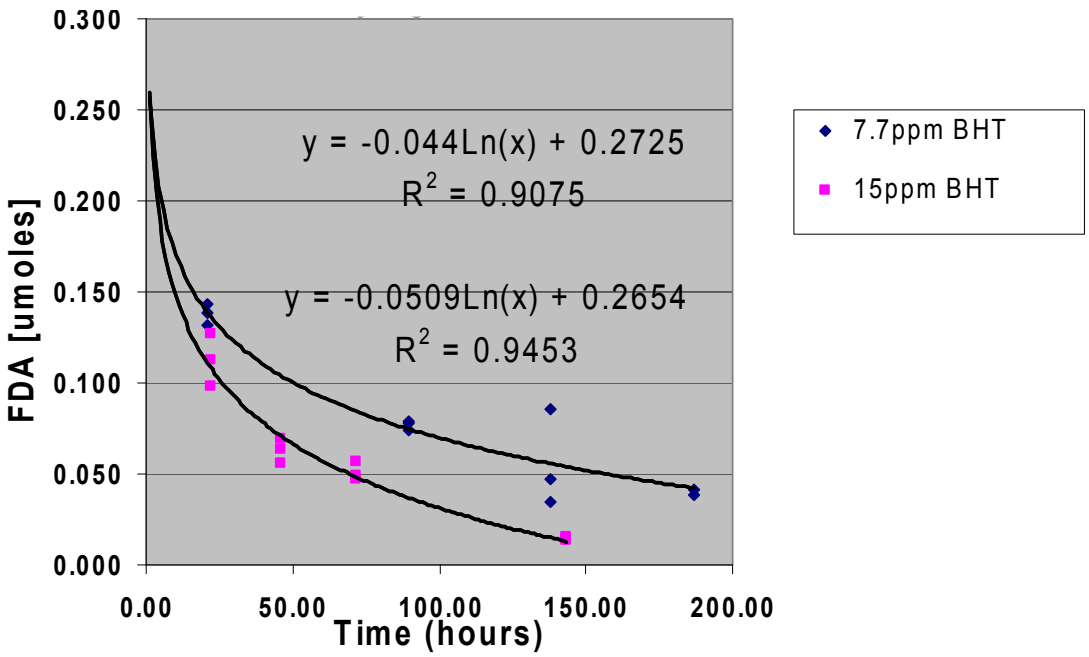

Figure 3.11. FDA mass transfer at varying BHT concentration.

3.7.2 Implementation in Multiphase Reactor

Eighty gallons of toluene were obtained in specialized containers (Fisher Scientific "Now-Pak" 19 liter bag-in-drum containers) that allow direct transfer from the container to the flow loop without unsealing the container. This avoids safety issues in pouring or pumping toluene in the presence of oxygen. All toluene transfer operations were made with adequate ventilation, no hot work allowed in vicinity, and continuous monitoring of organic concentration in the air.

The mixture of nitrogen gas, water (aqueous phase) and isododecane (organic phase) were tested and several operating points were confirmed in the first of a number of packing materials to be tested. The mixing of the reaction product NaF in the ancillary equipment (separation tank and piping) could influence evaluation of the reaction rate constant. To quantify the mixing of NaF in the ancillary equipment, a large quantity of NaF (18,500 μMoles) was injected just downstream of the column under high (11.5 L/min) aqueous flow conditions, organic flow of 3.46 L/min, and N2 flow of 3.55 scfm. Under these conditions the NaF reached well mixed condition (30 μMolar) in 2 minutes or less (see Figure 3.12). Given the speed in which the NaF became well mixed within the tank and piping, its effect on the reaction rate calculations should be negligible.

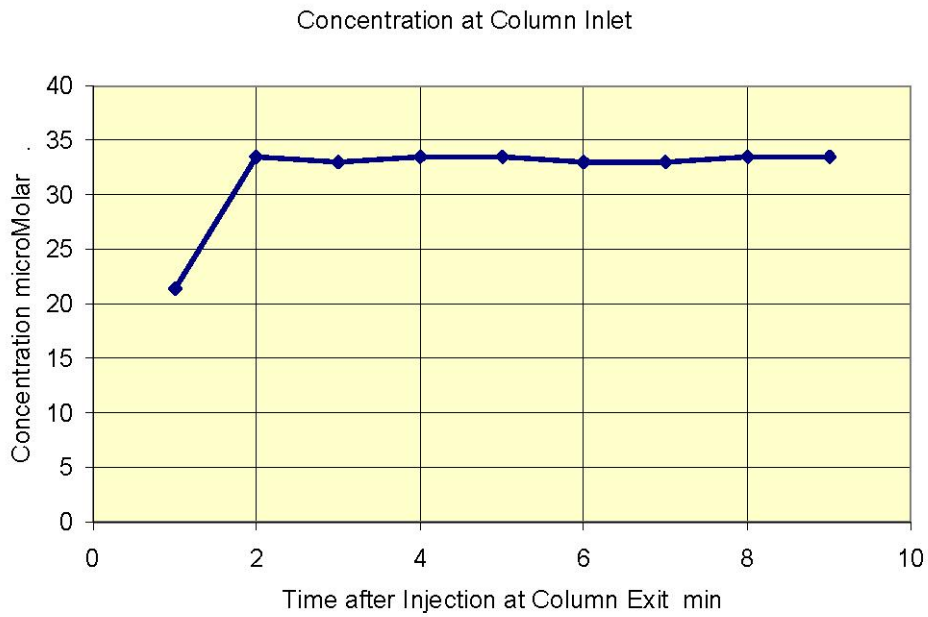

Figure 3.12. Time for injected slug of NaF to become well-mixed in column.

Flow visualization of pulsing in the packed column was attempted by dyeing the water green (using sodium fluorescein) but it was still difficult to distinguish the green aqueous from the clear organic liquids. Holdup measurements were performed, and results will be given in Section 3.8.1. Knowing the rate constant (above) and the volume of the organic, given by a holdup test, the interfacial mass transfer area can be determined. This information can be used to evaluate the mixing capability of a packing operated under various flow regimes. On example of holdup data is shown in Table 3.4 which indicates that for this condition, the isododecane was preferentially held up in the column, but that on the centerline (where the sample was extracted) the ratio was reversed. Figure 3.13 shows the holdup conditions for one set of flow conditions.

Table 3.4. Holdup data for one set of conditions

	Vol% Isododecane	Vol% H2O
Flow	35%	65%
Holdup	84%	16%
Sample	16%	84%

Residence time in column: Isododecane = 72 sec, Water = 7.5 sec

Figure 3.13. Holdup experiment run during mass transfer test series. Lower layer is aqueous liquid containing sodium fluorescein (green), upper layer (clear) is toluene.

3.8 Results

3.8.1 Hydrodynamic Data

Hydrodynamic data to identify pulse flow regimes was taken for water and air with sphere packing for comparison with the two-phase data. The regime was found to agree with what has been observed in our experiments and that correlated by Blok et al. (1983). Pulse flow regimes and holdup characteristics for woven multifilament polypropylene (WMFP) packing using water, isododecane and nitrogen were then determined. The pulse flow regimes did not correlate with previous experiments and were not well predicted by the Blok correlation. Holdup characteristics of the isododecane showed a marked dependence on flow rates of the isododecane and air. The WMFP packing displayed preference for the isododecane over water. Finally, holdup characteristics for toluene, water and nitrogen were observed. Again the WMFP packing had a high affinity for toluene. The same sort dependence of the toluene holdup on the toluene and nitrogen flow was observed.

I. Identification of pulse flow regimes.

Water and Air in Sphere packing:
Blok et al (1983) present a correlation for the transition between trickle and pulse flow for a column packed with spheres. In Figure 3.14 it has been evaluated for the current setup, as well as for spheres 10 times larger and 10 times smaller than the diameter tested.

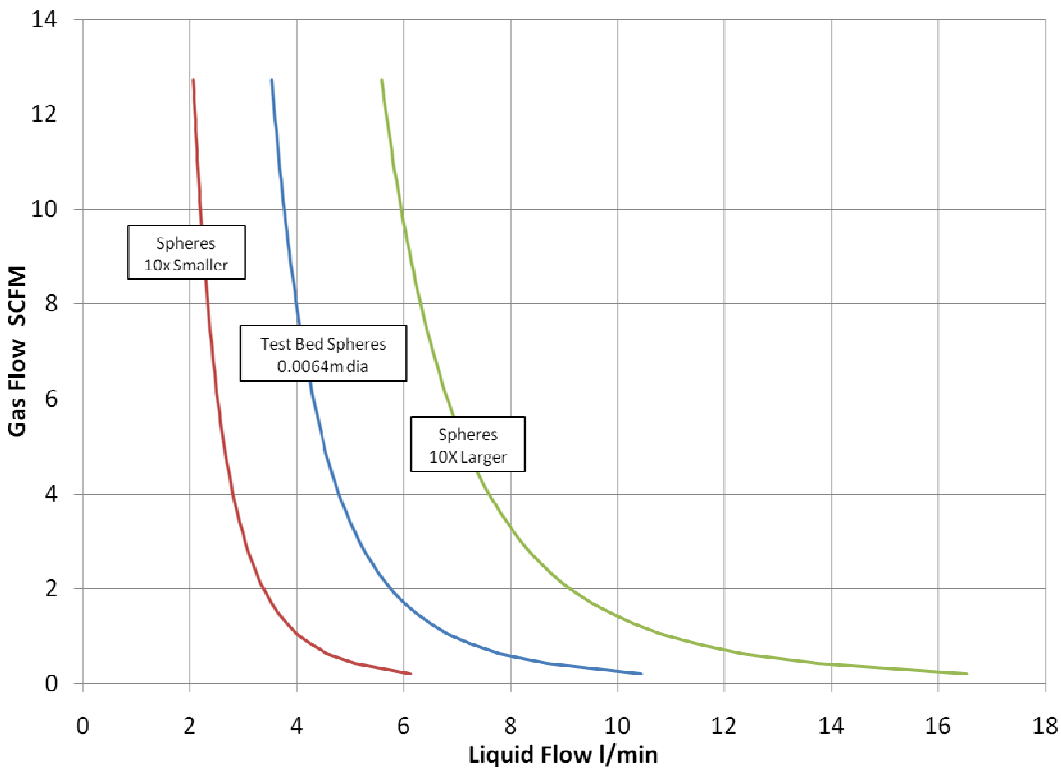

Figure 3.14. Blok et al (1983) correlation for column packed with spheres.

Experiments were run over a wide range of air and liquid flow rates and the pressure wave forms in the column were recorded. The results are plotted in Figure 3.15, where the RMS of the pressure signal about the average is used as an indicator of pulse flow. The upper left hand plot is an example of the time history of the pressure in the column and the upper right hand shows a frequency plot of the same data. The pulsing is obvious with a frequency of about 1 Hz, which is in agreement with Blok for these conditions.

In the lower regions of the figure, the wave form and frequency decomposition is shown for a trickle flow. The ~1 Hz frequency is still evident, but the RMS is an order of magnitude lower. The dark blue contour corresponding to the RMS between 0.03 and0.04 psi roughly coincides with the Blok limit.

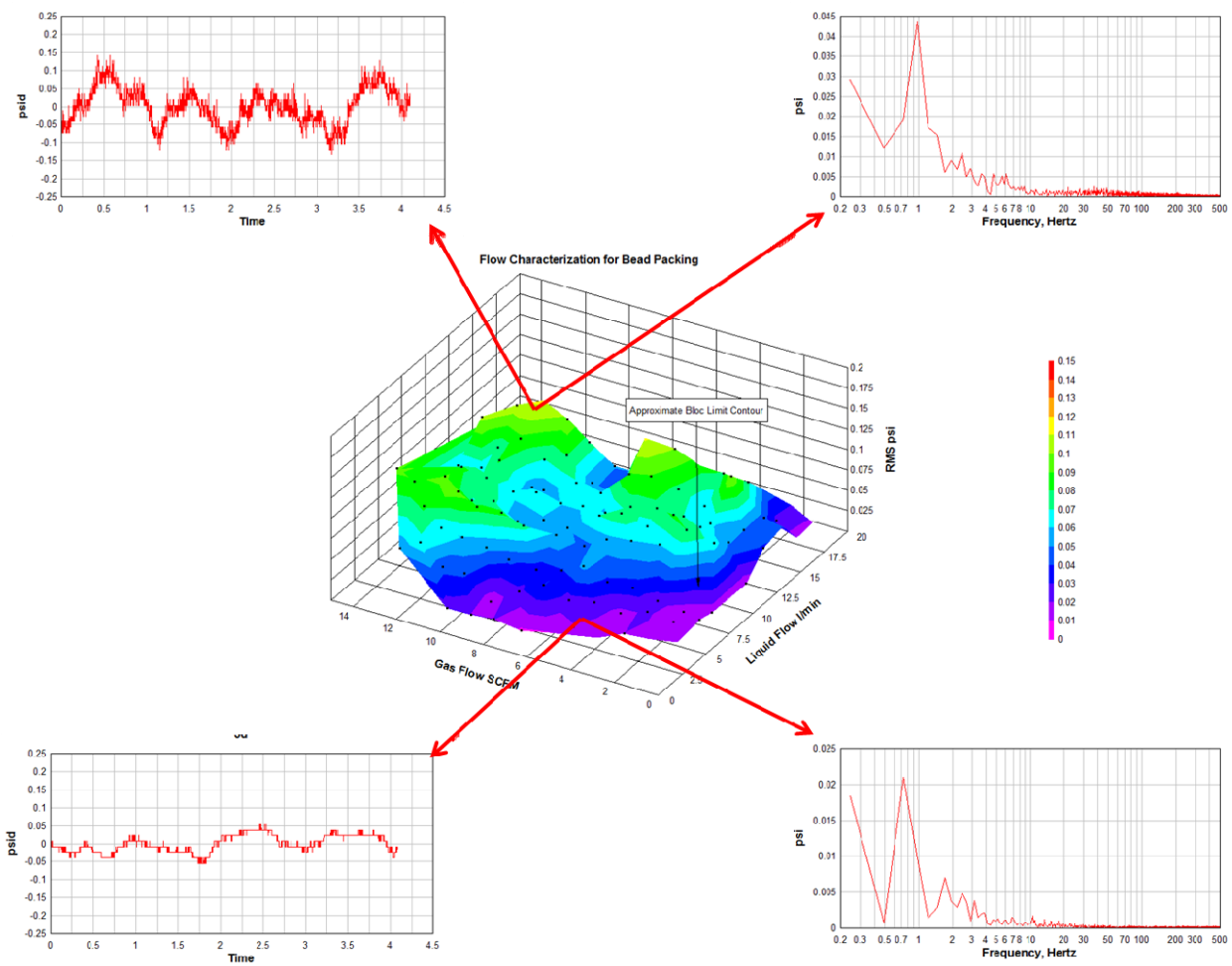

Figure 3.15. The pulse flow regime for the three phase column with water and air and 6.4 cm spheres as packing. The black dots visible in the center plot indicate the test points.

Water, isododecane and nitrogen in woven multifilament polypropylene (WMFP) packing:

Isododecane was installed in the system and the glass beads were replaced with the WMFP packing provided by CDTECH. Mapping of the pulse flow regime was obtained as shown in Figure 3.16. It is apparent in that figure that the characteristics are quite different than in those observed with sphere packing above. Much higher liquid flow rates are required to achieve pulse flow. Also, it is noted that WMFP packing cannot be modeled as small spheres, because the shift of the pulse flow regime is in the opposite direction to that predicted by the Blok correlation (see Figure 3.14)

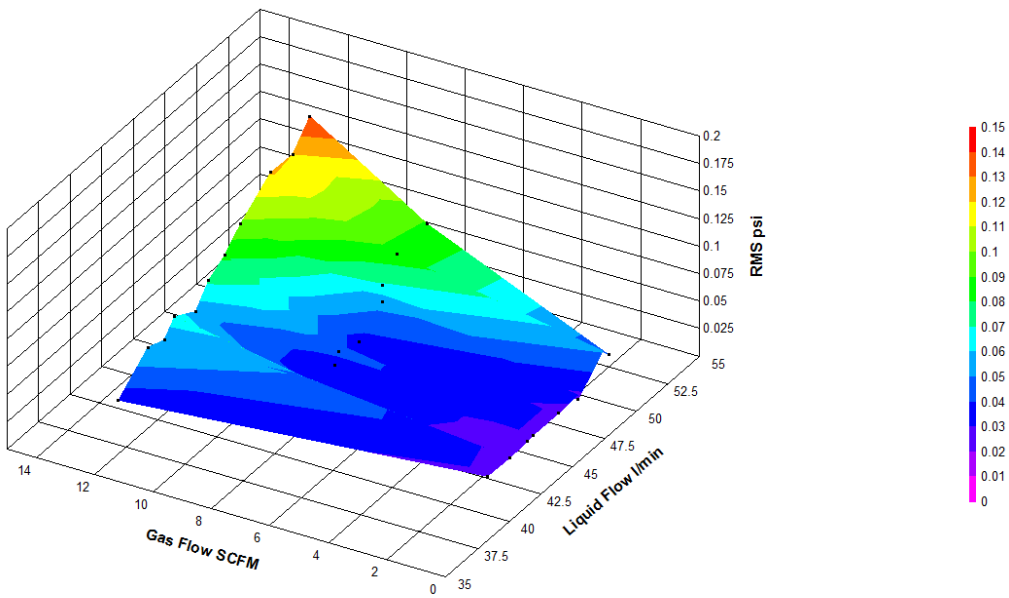

Figure 3.16. The pulse flow regime for the three phase column with water, isododecane and nitrogen. The black dots visible in the center plot indicate the test points.

II. Holdup Experiments:

Three sets of holdup experiments were completed for water and isododecane in WMFP packing: isododecane only flow, water only flow, and simultaneous flow of both fluids. A single set of experiments were conducted with the toluene, water and nitrogen. These were done as part of the mass transfer experiments discussed in a later section. Holdup was determined by setting the system to the desired flow rates then isolating the column and measuring the volume of the fluids that accumulated at the bottom of the column. The water drained almost immediately from the packing, while it took at least 4 hrs to completely drain the isododecane from the packing. A photo in Figure 3.13 shows the accumulated fluids in the bottom of the column during such a holdup determination.

Water, isododecane and nitrogen in WMFP packing:

The observed holdup for the isododecane only flow case is shown in Figure 3.17. It can be seen the holdup of isododecane is a function of both the isododecane flow rate and the nitrogen flow rate. The water holdup shows a similar dependency on the flow rate in Figure 3.18, however, there is a marked difference in the holdup range between the two liquids. The packing exhibits a definite affinity for isododecane.

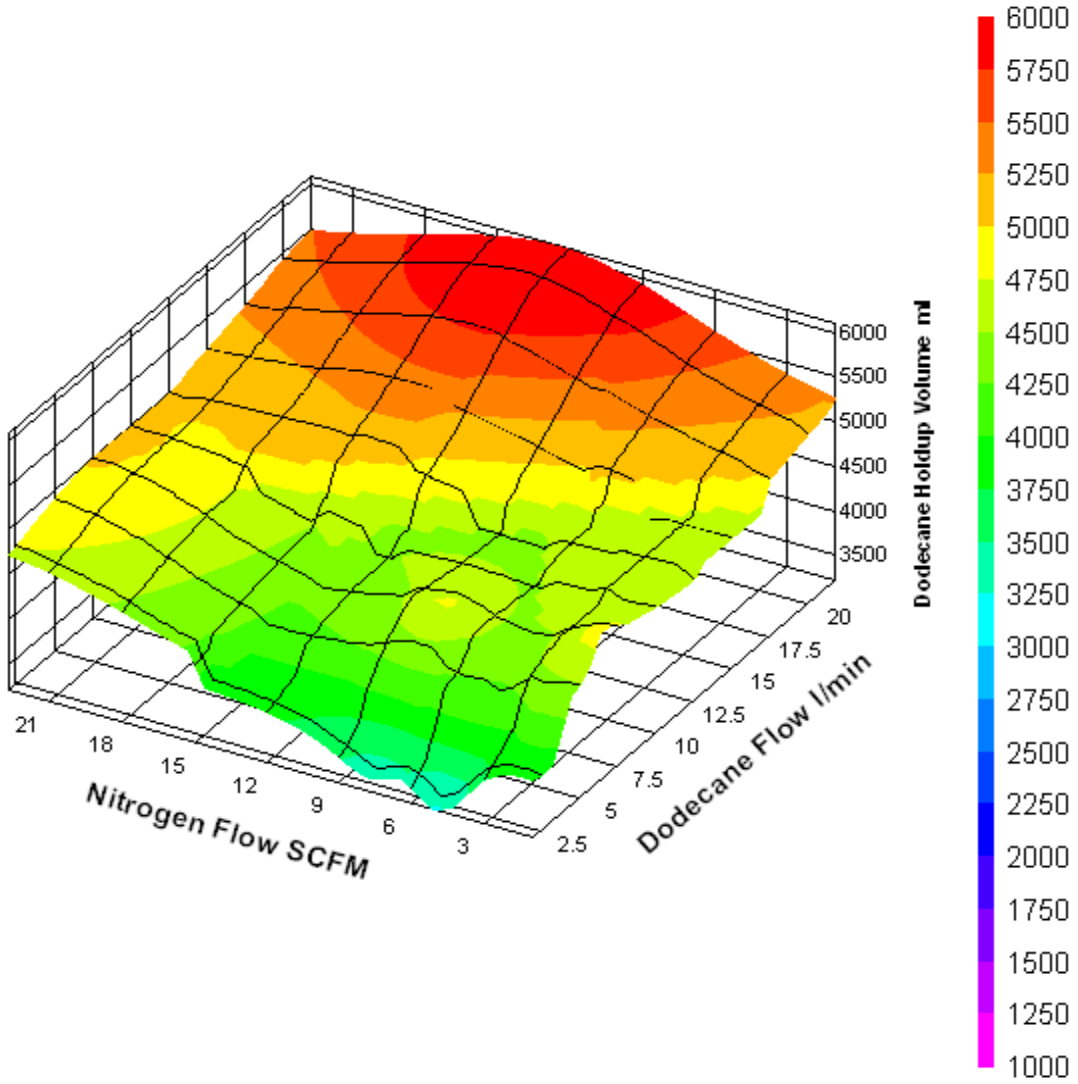

Figure 3.17. Isododecane holdup in WMFP packing when only isododecane and nitrogen are present.

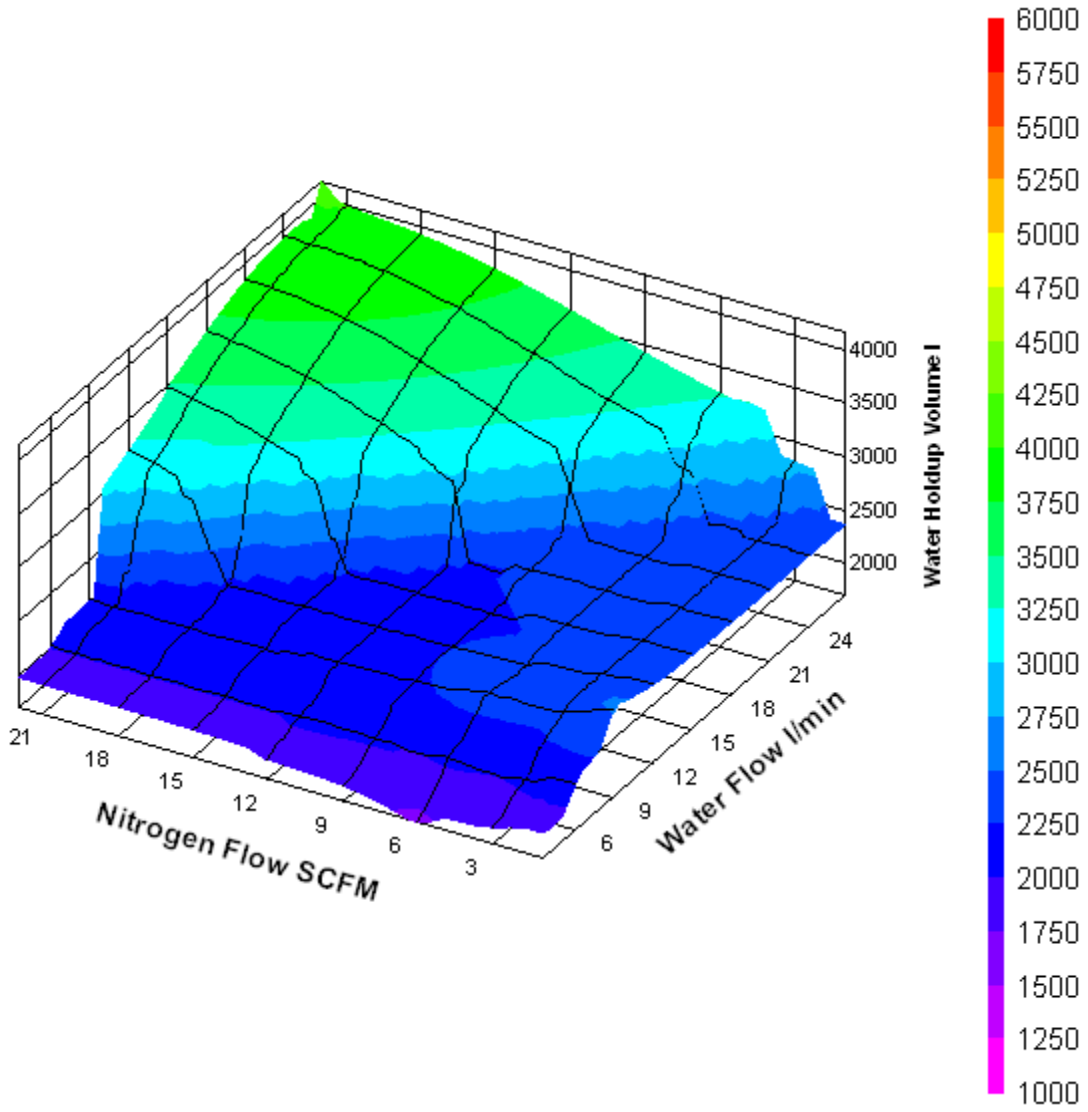

Figure 3.18. Water holdup in WMFP packing when only water and nitrogen are present. Note the color contour scale is the same as in the previous holdup figure.

With concurrent flow of isododecane, water and nitrogen the isododecane holdup shows a similar functionality with the nitrogen flow as can be seen in Figure 3.19. At low flow rates the column doesn't fill while at high flow rates there is an indication that the isododecane holdup depends on nitrogen flow. However, in Figure 3.20 it can be seen the water holdup is nearly independent of any of the other fluid flowrates. This is different than the behavior exhibited when only water was present.

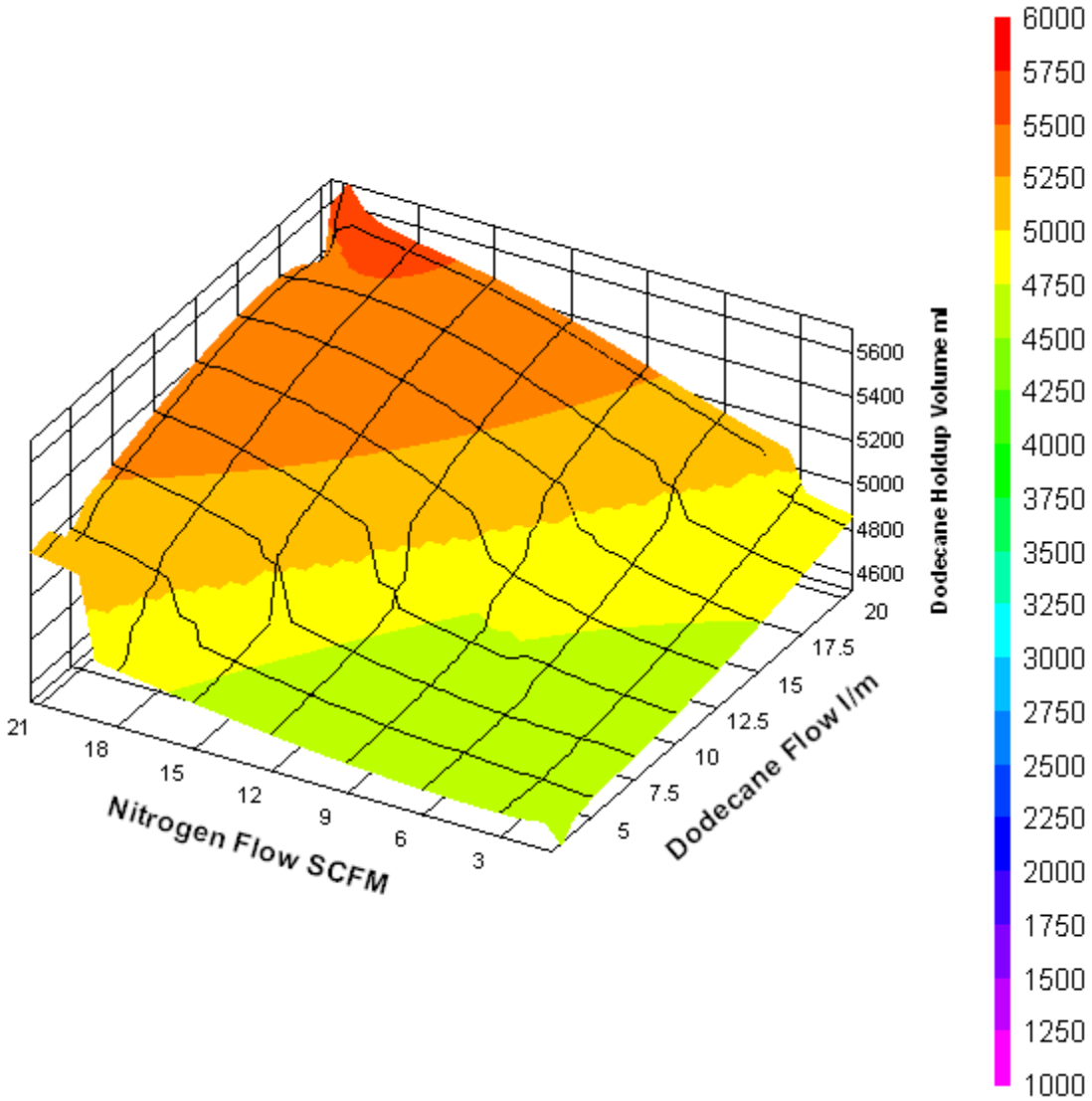

Figure 3.19. Isododecane holdup in WMFP packing when isododecane, water and nitrogen are present. Note the color contour scale is the same as in the previous holdup figures.

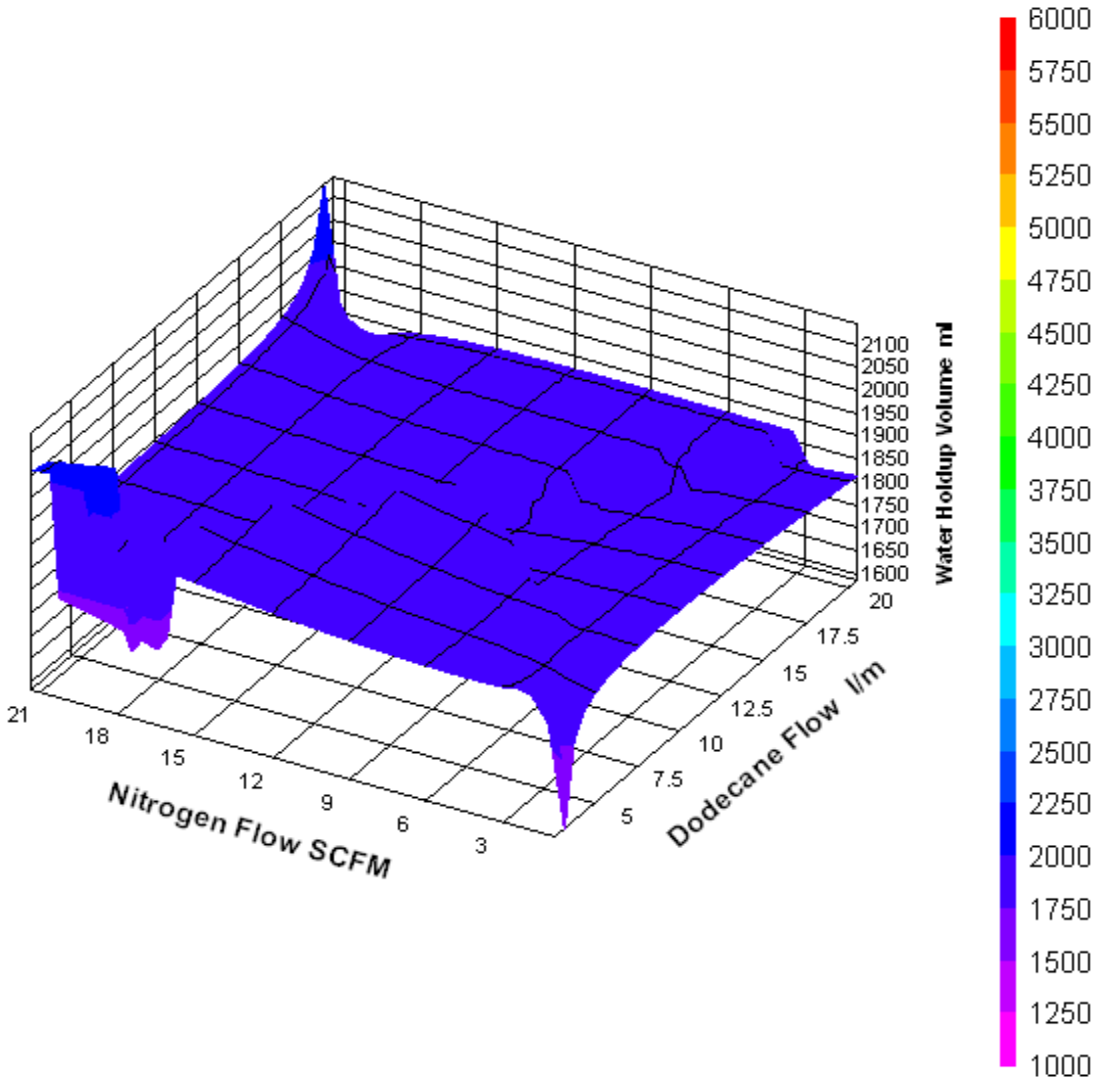

Figure 3.20. Water holdup in WMFP packing when isododecane, water and nitrogen are present. Note the color contour scale is the same as in the previous holdup figures.

Water, toluene and nitrogen in WMFP packing:

The holdup characterization for the water, toluene and nitrogen in WMFP packing was done as part of the mass transfer experiments discussed in the next section. Figure 3.21 shows the holdup for the toluene. As can be seen, there is a marked peak in holdup at a low nitrogen flow which is different than what occurred with the isododecane. This increased toluene holdup interacted with the water holdup as can be seen in Figure 3.22. In that figure, the near constant water holdup shows a marked minimum that coincides with the toluene maximum.

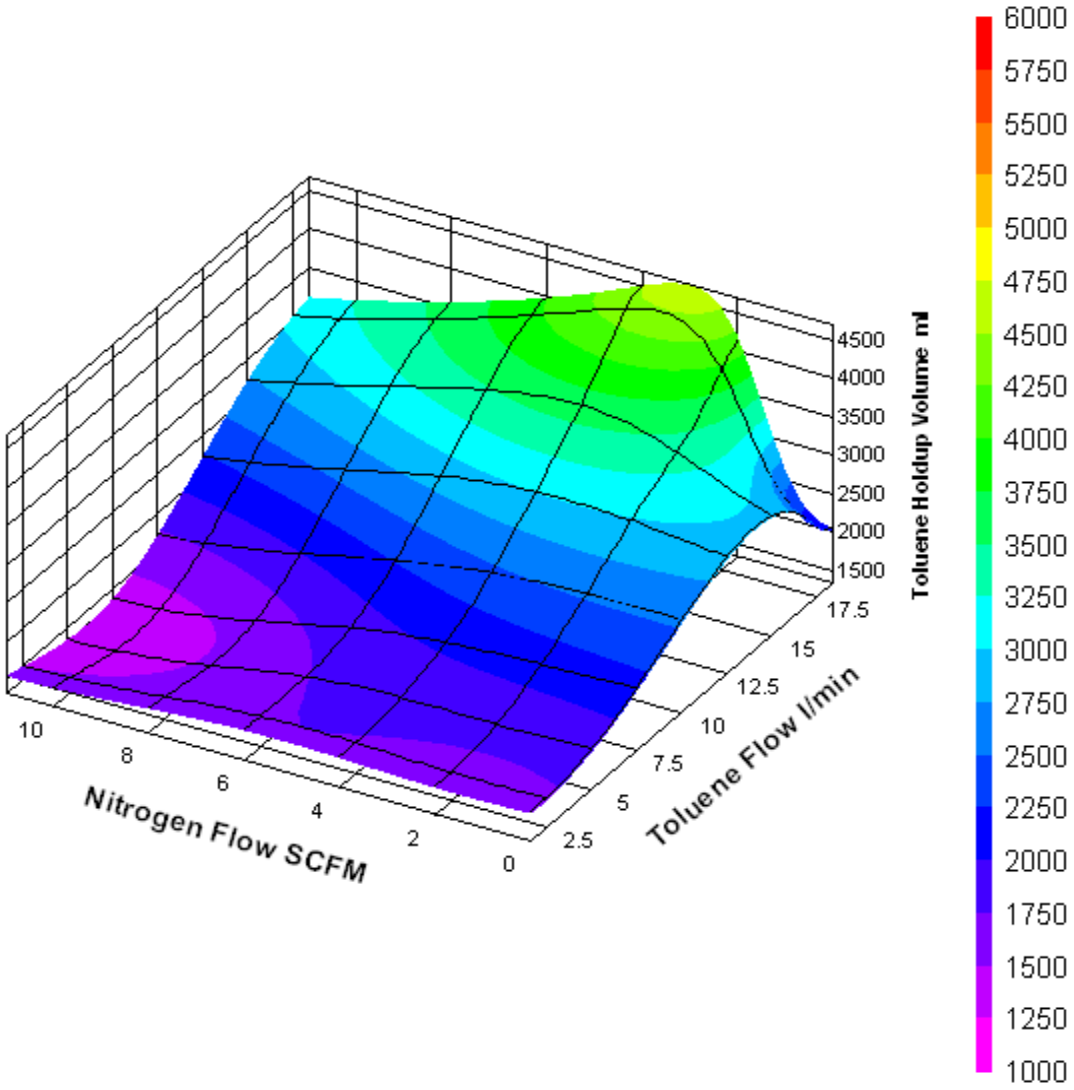

Figure 3.21. Toluene holdup in WMFP packing when toluene, water and nitrogen are present. Note the color contour scale is the same as in the previous holdup figures.

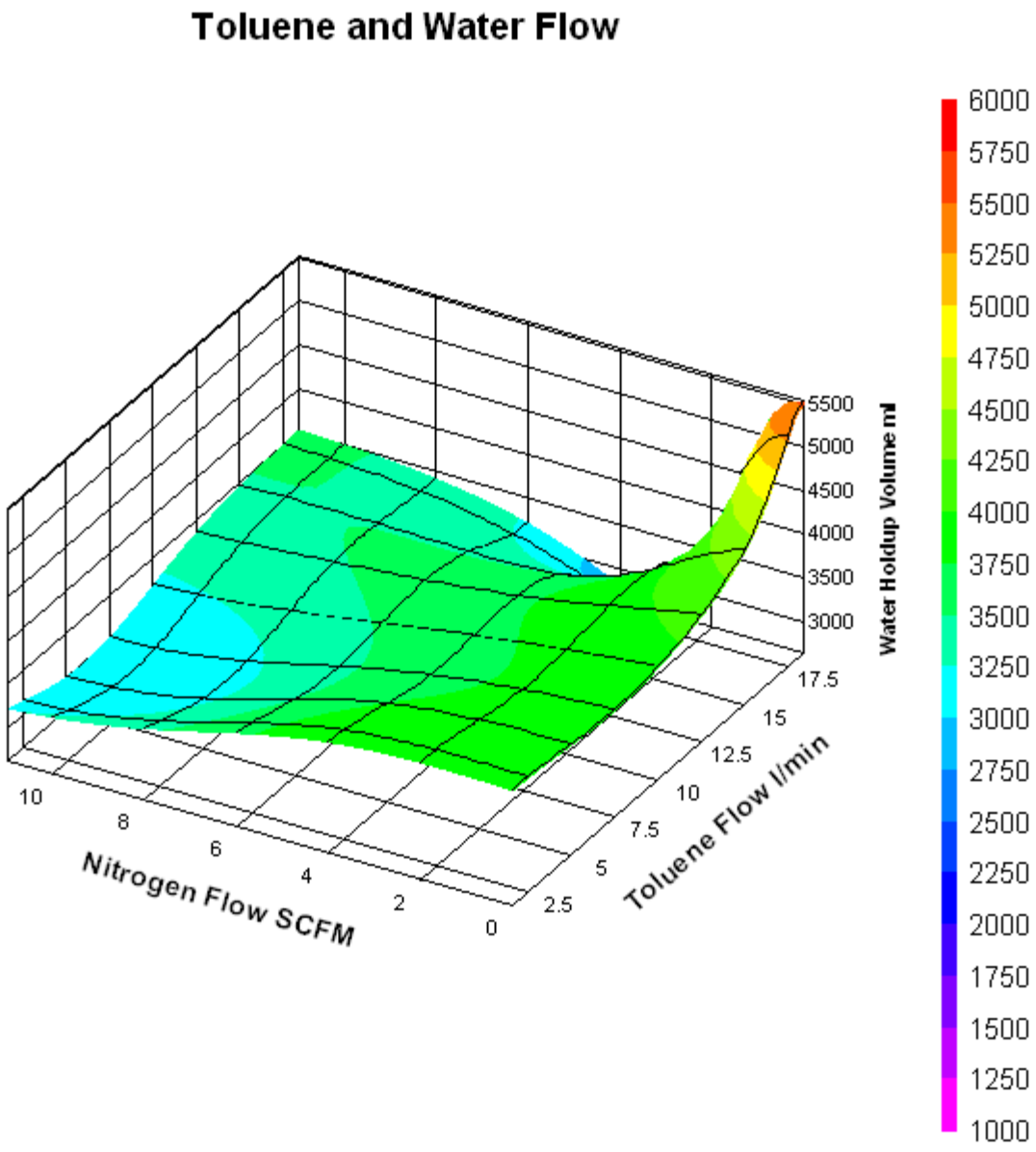

Figure 3.22. Toluene holdup in WMFP packing when toluene, water and nitrogen are present. Note the color contour scale is the same as in the previous holdup figures.

3.8.2 Mass Transfer Data

Lab Scale Tests

The mass transfer of fluorescein ion in the form of fluorescein diacetate (FDA) dissolved in toluene and transferred to an aqueous phase of sodium hydroxide, forming disodium fluorescein (NaF), has been reported in the literature for studying mass transfer across an organic to aqueous

boundary (Wenn et al., 2003). The transfer of fluorescein ion from the toluene phase to the aqueous phase is based on the hydrolysis reaction of fluorescein with sodium hydroxide:

$$\underset{\text{(FDA)}}{C_{20}H_{10}O_5(C_2H_3O_2)_2} + 2NaOH \rightarrow \underset{\text{(Disodium Fluorescein)}}{Na_2C_{20}H_{10}O_5} + 2\,C_2H_4O_2 \qquad (3.10)$$

The concentration of the fluorescein ion can be measured by spectrophotometer analysis at 291nm for FDA in toluene and 491nm for disodium fluorescein in 0.1 M sodium hydroxide.

A series of controlled lab scale tests was initially performed in order to establish an intrinsic rate constant for fluorescein. The intrinsic rate constant relates the rate of transfer of the fluorescein ion from the organic phase to the aqueous phase and is a function of the 1st order rate constant for FDA, the total organic volume and the interfacial mass transfer area between the organic and aqueous phases.

$$KV/A = (\text{intrinsic rate constant } L/mm^2/hr) \qquad (3.11)$$

Where: K – 1st Order Rate Constant = $(-\ln FDA/FDA_{t=0})/time$
V = Toluene volume in Liters
A = Interfacial mass transfer area between phases in mm^2

By experimentally determining an intrinsic rate constant, the interfacial mass transfer area between organic and aqueous phases for a 3-phase system can be calculated. This requires knowing the 1st order rate constant which is determined experimentally for a given flow condition and the holdup volume of the fluid of interest, the organic phase.

Initial lab tests followed the conversion over time of 75µM FDA in 20 ml of toluene containing 15ppm BHT to the Disodium Fluorescein (NaF) in 50 ml of 0.1M NaOH and 1M NaCl. This series of tests was run under static conditions (i.e., no mixing) at 20C and 30C in hopes to develop an Arrhenius Plot so activation energy for the FDA reaction could be calculated. However, the reaction rates at 20 C and 30 C are fairly similar so calculating activation energy over this temperature range was not possible. Using the conversion data of FDA to NaF the 1st order reaction rate constant was calculated for each test and is shown in Figure 3.23. The average 1st order rate constant calculated from these experiments was 0.0032 hr^{-1}.

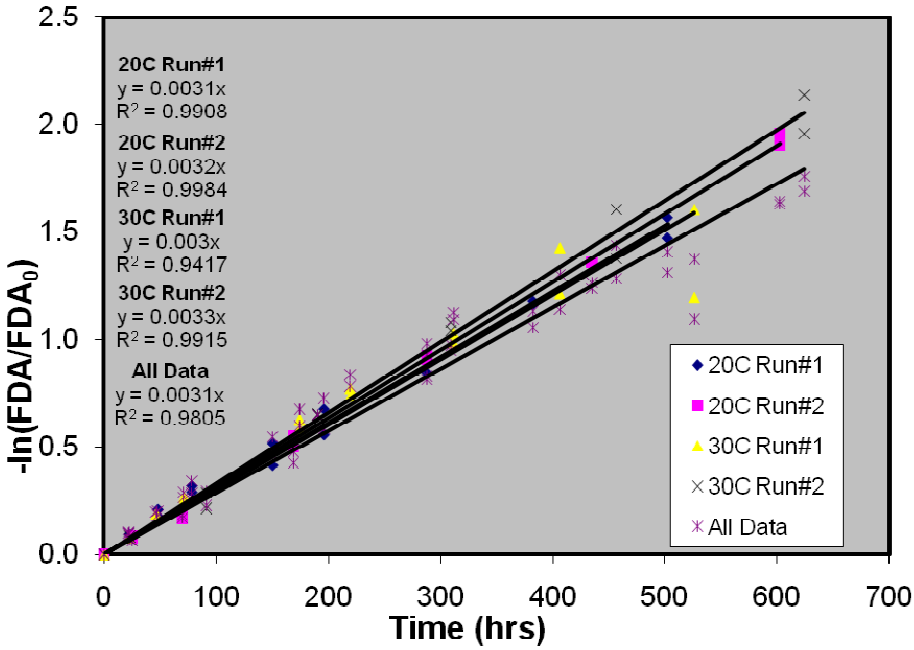

Figure 3.23. First order rate equation based on measured FDA in toluene. kt = -ln(FDA/FDA$_0$).

Another series of tests were done in which the organic volume was varied and the 1st order rate constant was calculated for each set of experiments. The results of these tests are given in Figure 3.24 and Table 3.5. Using the rate constants from each of these experiments an average intrinsic rate constant was calculated to be 9×10^{-9} +/- 4.1×10^{-10} L/mm^2/hr .

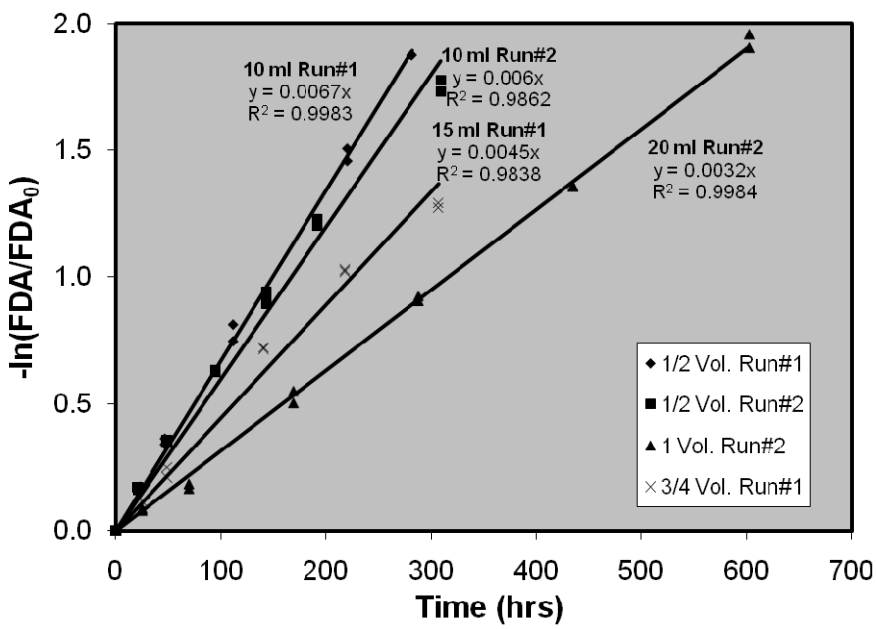

Figure 3.24. First order rate equation for varying organic volume, based on measured FDA in toluene at 20 C. kt = -ln(FDA/FDA$_0$).

Table 3.5. Data for determining Intrinsic Rate Constant

Intrinsic Rate Constant K*(V/A)			
Area (A) = $\pi D^2/4$ where D = 95mm Area (mm^2) = 7088.2			
Vol. of Organic (L)	Temperature C	1st Order Rate Constant (1/hr)	Intrinsic Rate Constant ($L/mm^2/hr$)
0.01	20	0.0067	9.4523E-09
0.01	20	0.006	8.46475E-09
0.015	20	0.0044	9.31123E-09
0.02	20	0.0031	8.74691E-09
0.02	20	0.0032	9.02907E-09
0.02	30	0.003	8.46475E-09
0.02	30	0.0033	9.31123E-09
		Average Intrinsic Rate Constant =	8.9686E-09

Using the same toluene and water that was used in the 3-phase system a lab scale test was run under the same conditions as in previous lab scale tests. This allowed for the determination of an intrinsic rate constant for the fluids used in the 3-phase tests and also for comparing to the intrinsic rate constant determined from previous lab tests. However, due to contaminate in the toluene which interfered with the hydrolysis reaction, the experimental results for FDA did not agree to previous fluorescein hydrolysis tests. Thus the disappearance in FDA did not agree with appearance in NaF as shown in Figure 3.20. However, since this lab test did show an increase in NaF over time the NaF data was used to calculate an intrinsic rate constant for use with the 3-phase test data. Using NaF concentration over time an FDA concentration was calculated and a 1st order rate constant for FDA was calculated (0.00009 hr^{-1}). This 1st order rate is almost 100 times slower than the 1st order rate constant given for the previous lab scale tests (0.0032 hr^{-1}). Using a 1st order rate constant of 0.00009 hr^{-1} an intrinsic rate constant of 3.2×10^{-10} $L/mm^2/hr$ was calculated for the 3-phase toluene and water. This intrinsic rate constant was used to calculate the interfacial transfer area using 3-phase test data.

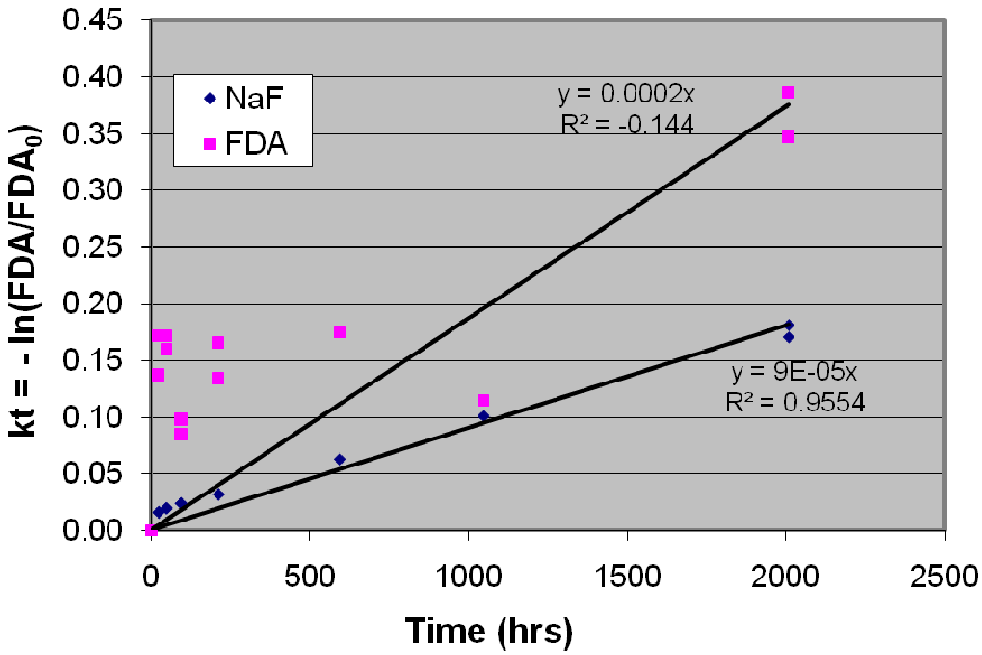

Figure 3.25. First order rate equation for fluorescein diacetate (FDA) used in 3-phase system. kt = -ln(FDA_t/FDA_0).

3-Phase Tests

Using the packed column under 3-phase co-current flow (nitrogen, toluene with FDA and aqueous sodium hydroxide with NaF) the evaluation of mass transfer of a model compound, fluorescein ion, from the organic phase to the aqueous phase was attempted for various flow conditions. The goal of testing was to determine rate as a function of flow condition and use the 1st order rates to calculate the interfacial mass transfer area generated by the packing under different flow conditions. However, the transfer rate of the fluorescein ion from FDA in the organic phase to fluorescein as NaF in the aqueous phase did not change significantly with flow and thus the interfacial mass transfer area could not be determined with any degree of confidence. As stated previously this is most likely due to a problem with contaminants in the toluene and thus interfering with FDA spectral analysis and also interfering with the hydrolysis of fluorescein.

The specific conditions used for testing fluorescein in the 3-phase system are the following:

Organic phase

25 gallons toluene
50 ppm of antioxidant BHT
60 μM FDA

Aqueous phase

55 gallons water
0.1 M NaOH
1 M NaCl

Samples were taken from the pump outlets and column outlet. However, since the mass transfer was very slow later tests samples were taken only from the column outlet.

Results

3-18-2010 Experiment: The 3-phase system was set at an aqueous flow of 28.3 L/min, a toluene flow of 18.4 L/min and nitrogen gas flow of 3 scfm. For the given flow conditions the toluene hold-up volume within the packed column was 4.69L. Samples were taken every 15 minutes for 1 hour. Results are shown in the following 2 plots. The NaF increased over time however FDA basically showed no change in concentration and actually showed an increase in concentration for some of the data points. However due to low conversion (4%) the mass balance for fluorescein based on the measured FDA at the starting condition was within 5%.

The flow conditions showed definite pulse characteristics as evidenced by the pressure column time histories shown in the Figure 3.26.

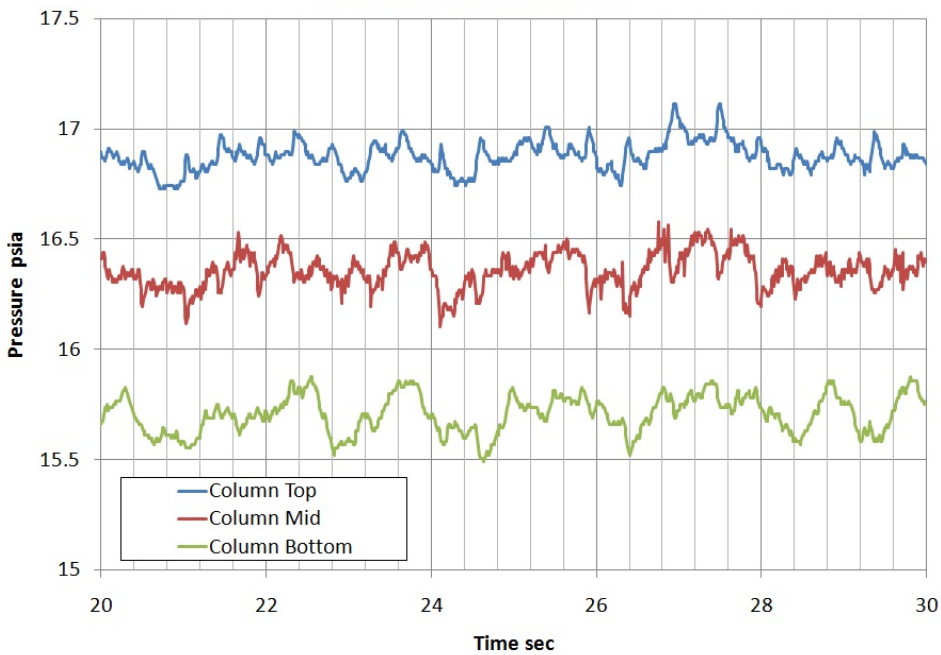

Figure 3.26. Time trace of column pressure at top, middle, and bottom of column during 3/18/2010 run. Aqueous flow 28.3 L/min, toluene flow 18.4 L/min, nitrogen gas flow of 3 scfm.

A Fourier analysis of the time-varying pressure signal shows the frequency content with 3 distinct peaks.

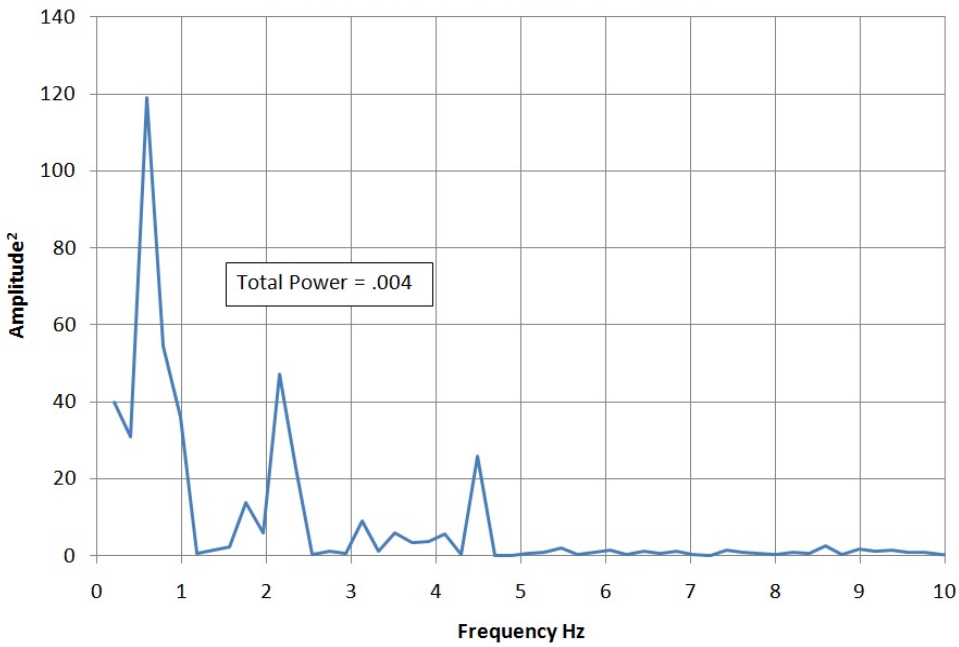

Figure 3.27. Periodogram of column pressure during 3/18/2010 run. Aqueous flow 28.3 L/min, toluene flow 18.4 L/min, nitrogen gas flow of 3 scfm.

Since the FDA data collected during the test could not be used to directly calculate a 1st order rate constant the NaF data was used instead (see Figure 3.28). Assuming the total μMoles of fluorescein at the start of the test was correct and subtracting off the μMoles of NaF an estimate of the FDA concentration could be calculated for each sample period. Using the calculated FDA concentrations a 1st order rate constant of 0.019 hr^{-1} for the hydrolysis of FDA was calculated. However, as shown in the rate plot of Figure 3.29, a regression coefficient of 0.55 is given for the entire data set. If the 1st order rate constant was calculated based on the first 4 data points, a rate constant of 0.037 hr^{-1} is given with an acceptable regression coefficient. Using these 1st order rate constants, the hold-up volume for toluene (4.69L) and an intrinsic rate constant of 3.2×10^{-10} $L/mm^2/hr$ an estimate for interfacial mass transfer area ranged from 555 m^2 to 277 m^2.

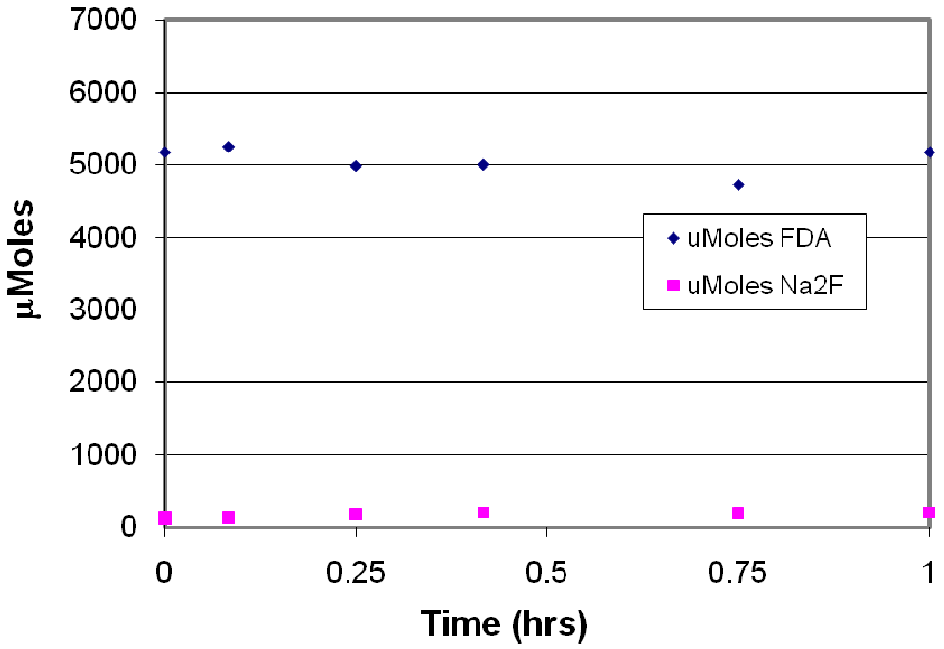

Figure 3.28. Mass transfer data showing concentration of FDA and Na2F during 3/18/2010 run. Aqueous flow 28.3 L/min, toluene flow 18.4 L/min, nitrogen gas flow of 3 scfm.

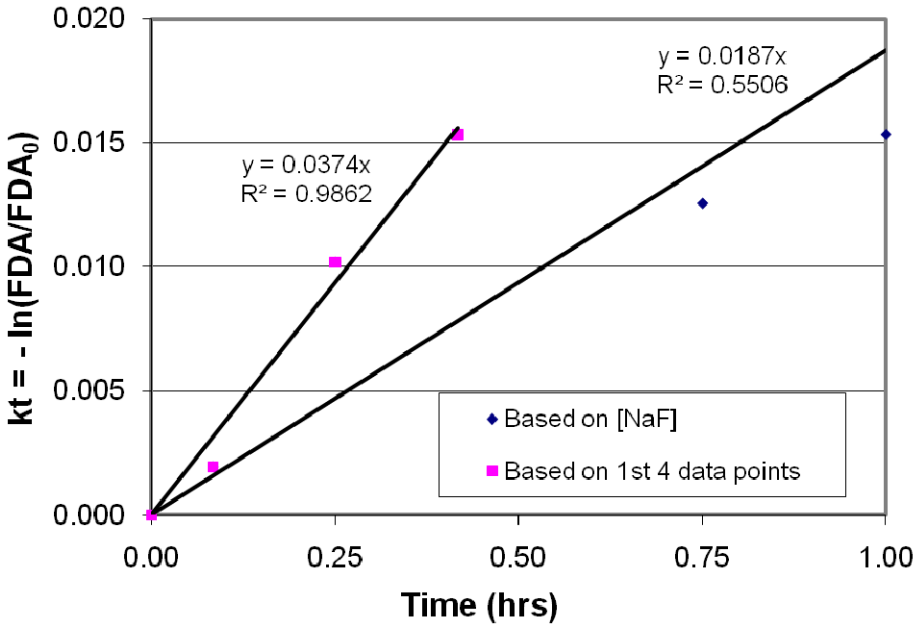

Figure 3.29. First order rate equation for FDA based on measured [NaF] during 3/18/2010 run. kt = -ln(FDA/FDA$_0$).Aqueous flow 28.3 L/min, toluene flow 18.4 L/min, nitrogen gas flow of 3 scfm.

<u>3-24-10 Experiment:</u> A repeat of the previous test (aqueous flow of 28.3 L/min, toluene flow of 18.4 L/min, nitrogen gas flow of 3 scfm) was run for 5.5 hrs. Results for fluorescein are shown in the figure below. Here again the change in FDA was hard to evaluate yet NaF increased over time. The FDA results were inconsistent and the mass balance was off by as much as 30%. Using an FDA starting concentration of 54.2 µMolar (based on measurements of FDA in the

tank), an 11.5% conversion was calculated. Using the NaF data to calculate FDA concentration a 1st order rate constant for FDA was calculated at 0.019 hr^{-1} which is similar to the data set for the tests run on 3-18-2010.

The pulsation on this test was similar to that of the previous one as can be seen in the Figures 3.30 and 3.31. The frequency peaks are not as pronounced as for the 03-18-2010 test, but the total area under the spectrum power curve is the same.

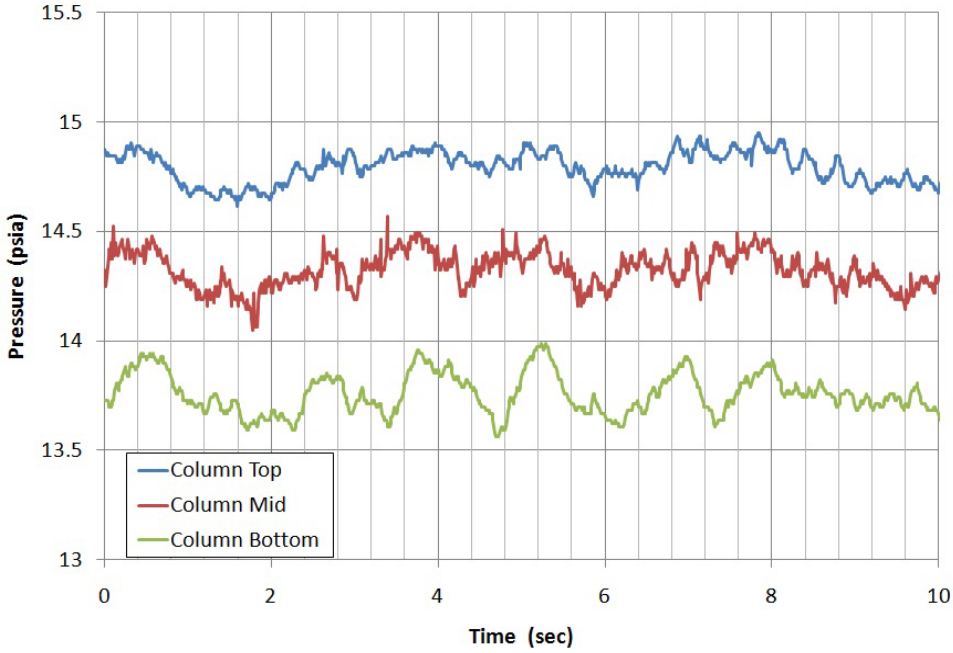

Figure 3.30. Time trace of column pressure at top, middle, and bottom of column during 3/24/2010 run. Aqueous flow 28.3 L/min, toluene flow 18.4 L/min, nitrogen gas flow of 3 scfm.

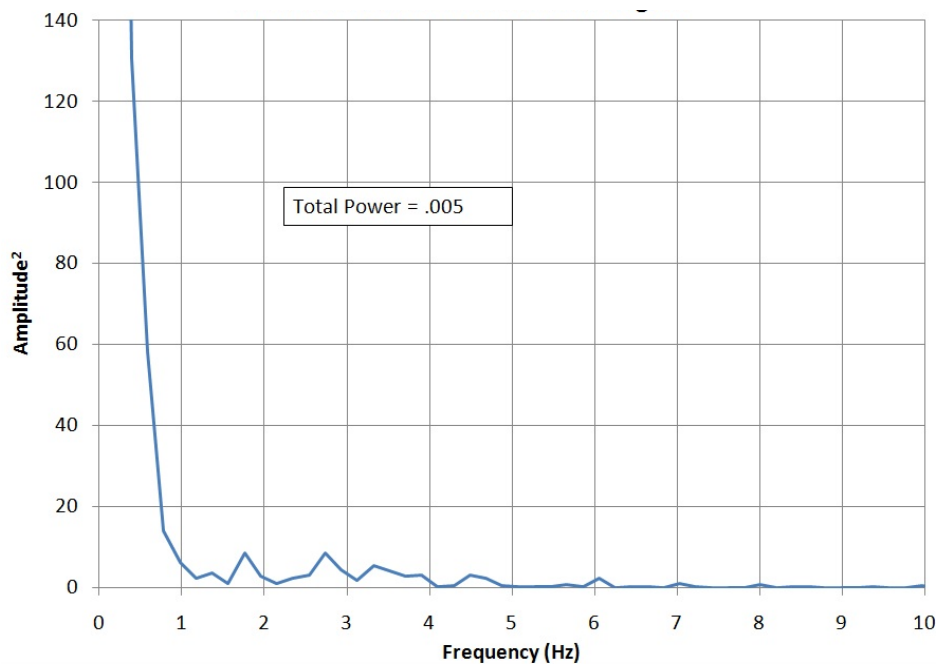

Figure 3.31. Periodogram of column pressure during 3/24/2010 run. Aqueous flow 28.3 L/min, toluene flow 18.4 L/min, nitrogen gas flow of 3 scfm.

Three hold-up tests were run with an average hold-up volume for toluene of 4.43 L. Using the toluene hold-up volume, a first order rate constant of 0.019 hr^{-1} and the intrinsic rate, 3.2×10^{-10} $L/mm^2/h^2$ constant the interfacial mass transfer area was calculated at 263 m^2.

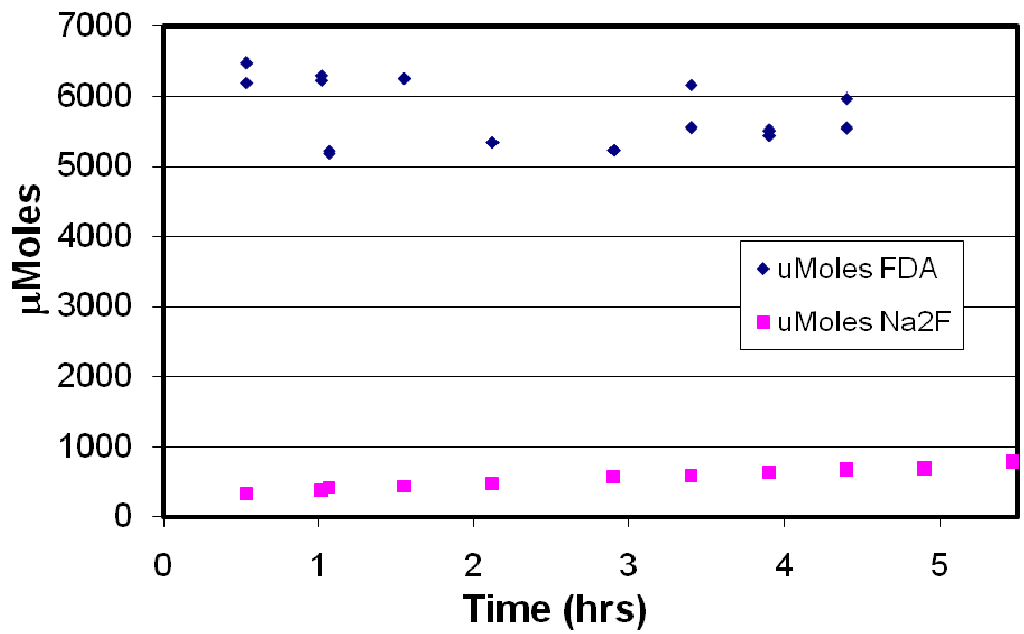

Figure 3.32. Mass transfer data showing concentration of FDA and Na2F during 3/24/2010 run. Aqueous flow 28.3 L/min, toluene flow 18.4 L/min, nitrogen gas flow of 3 scfm.

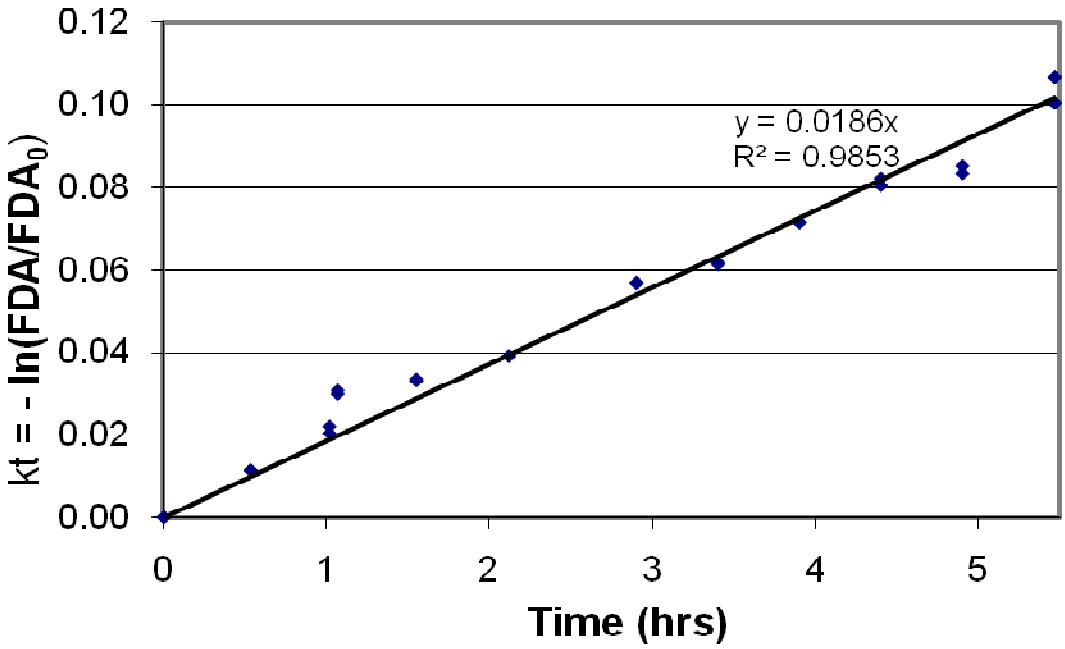

Figure 3.33. First order rate equation for FDA based on measured [NaF] during 3/24/2010 run. kt = -ln(FDA_t/FDA_0).Aqueous flow 28.3 L/min, toluene flow 18.4 L/min, nitrogen gas flow of 3 scfm.

3-25-2010 Experiments: This test was run with liquid flow only, in order to evaluate the mass transfer of fluorescein. Liquid flow rates were the same as in the previous 2 tests (aqueous flow of 28.3 L/min, toluene flow of 18.4 L/min), but there was no nitrogen flow. This test was designed to give an indication of mass transfer due to mixing without pulse flow hydrodynamics occurring. There is no pulsing present as can be seen in the column pressure time traces shown in Figure 3.34 and the frequency plot of Figure 3.35.

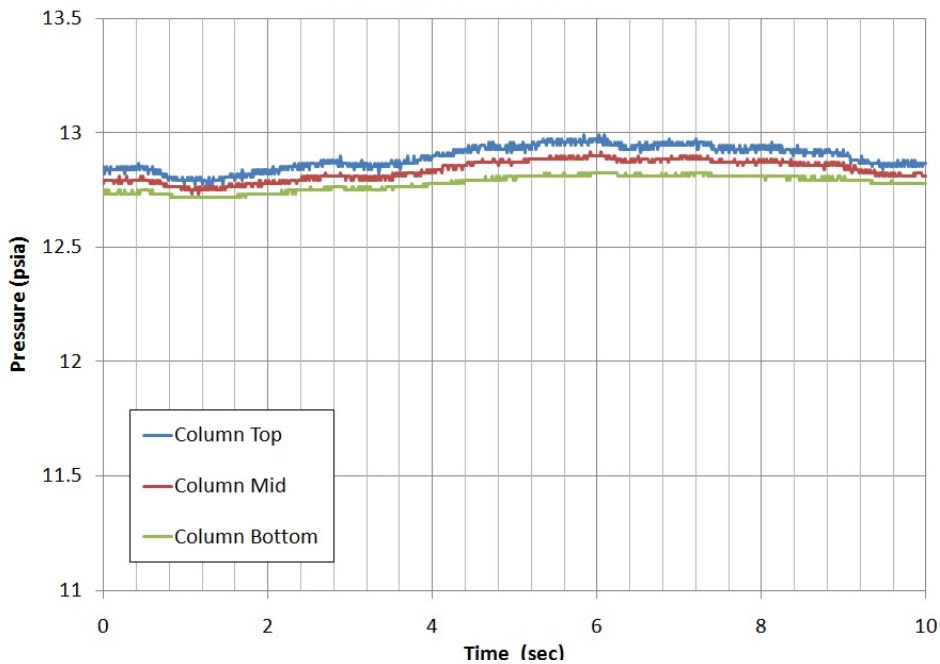

Figure 3.34. Time trace of column pressure at top, middle, and bottom of column during 3/25/2010 run. Aqueous flow 28.3 L/min, toluene flow 18.4 L/min, and no nitrogen gas flow.

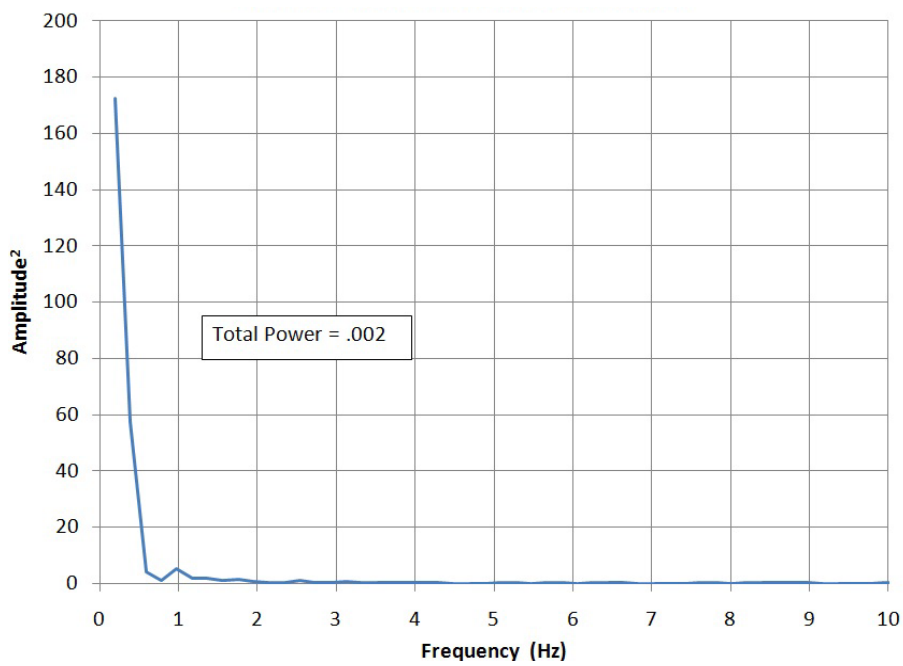

Figure 3.35. Periodogram of column pressure during 3/24/2010 run. Aqueous flow 28.3 L/min, toluene flow 18.4 L/min, no nitrogen gas flow.

Again only the NaF concentration could be used to evaluate mass transfer of fluorescein. The test data is presented in the Figures 3. 36 and 3.37.

The 1st order rate constant calculated for this set of data, 0.016 hr^{-1}, which was slightly lower than the rate for the previous tests (0.019 hr^{-1}). The average toluene hold-up volume was 2.06 L. Using the 1st order rate constant 0.0016hr^{-1}, the toluene hold-up volume and the intrinsic rate constant 3.2×10^{-10} $L/mm^2/h^2$, the interfacial mass transfer area was calculated at 103 m^2. Thus the minor amount of pulse flow which occurred in the previous tests slightly enhanced the fluorescein hydrolysis rate and reduced the mass transfer area by 60%.

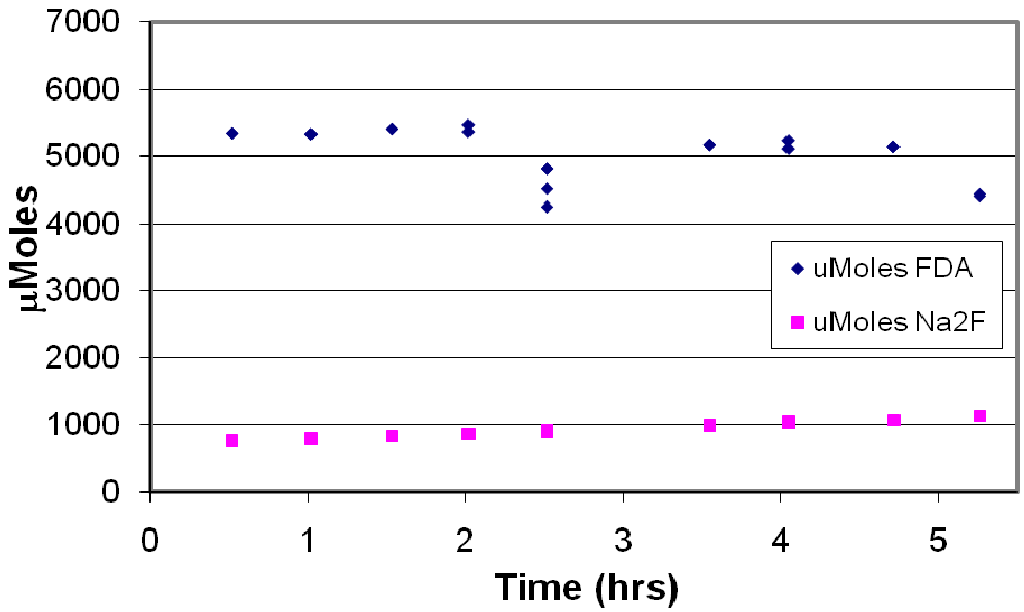

Figure 3.36. Mass transfer data showing concentration of FDA and Na2F during 3/25/2010 run. Aqueous flow 28.3 L/min, toluene flow 18.4 L/min, no nitrogen gas flow.

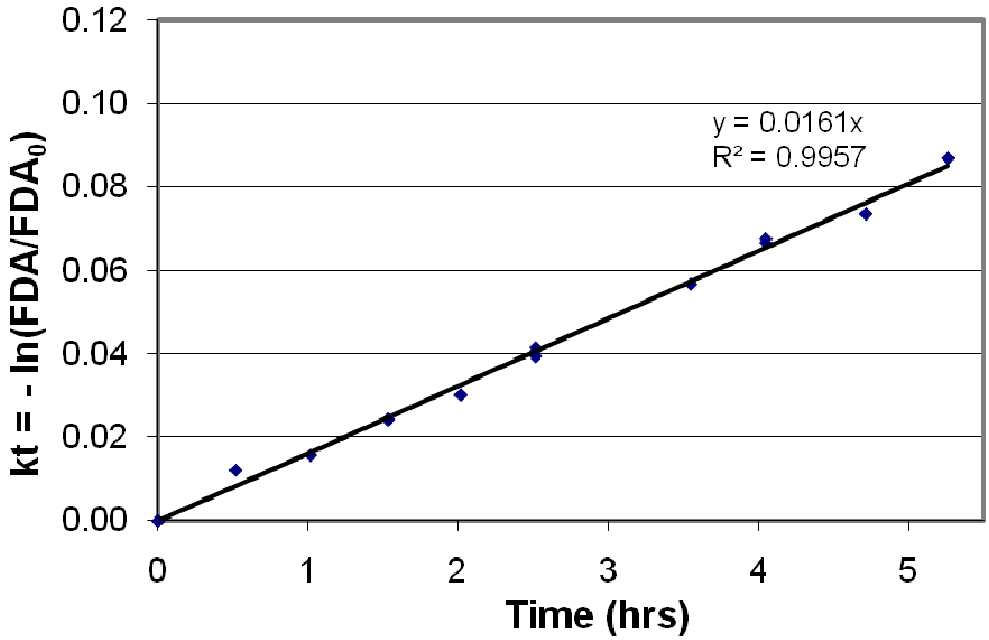

Figure 3.37. First order rate equation for FDA based on measured [NaF] during 3/24/2010 run. kt = -ln(FDA_t/FDA_0). Aqueous flow 28.3 L/min, toluene flow 18.4 L/min, no nitrogen gas flow.

4-28-2010 Experiments: A high gas flow test was attempted (~12 scfm) to try and establish the maximum amplitude in pulse flow. However, at high nitrogen gas flow toluene vapor was carried over to the compressor and condensed out in the compressor outlet, thus resulting in compressor choking due to high head pressure. This required keeping the compressor outlet line hot in an effort to keep the toluene as a vapor.

The high gas flow provoked only limited oscillations – the pressure traces being similar to the liquid only flow. There was no frequency content and the total power was lower than the liquid only case, as can be seen in Figures 3.38 and 3.39.

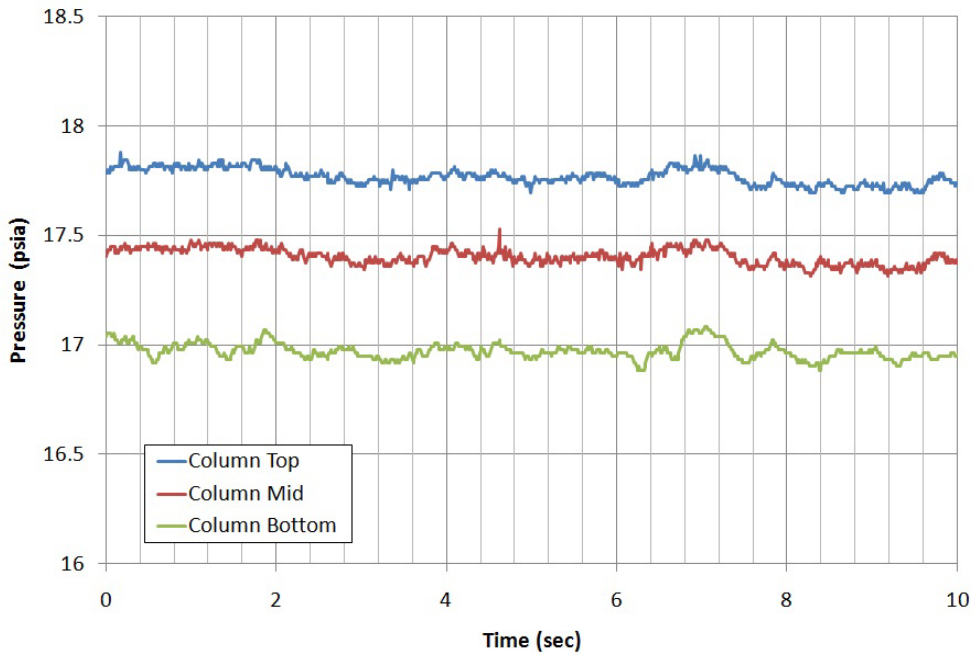

Figure 3.38. Time trace of column pressure at top, middle, and bottom of column during 4/28/2010 run. Aqueous flow 28 L/min, toluene flow 6 L/min, nitrogen gas flow 11 scfm.

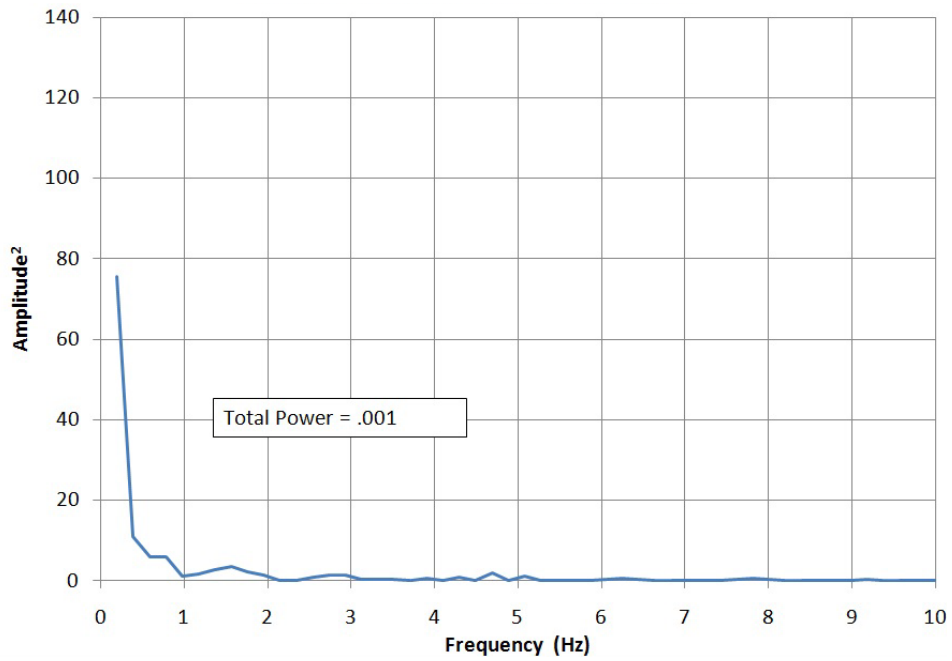

Figure 3.39. Periodogram of column pressure during 4/28/2010 run. Aqueous flow 28 L/min, toluene flow 6 L/min, nitrogen gas flow 11 scfm.

The initial high flow nitrogen test was run with a gas flow at 11 scfm, an aqueous flow set at 28L/min and toluene set at 6L/min. The results are shown in the following figure. As with previous tests the FDA data could not be used to track the fluorescein hydrolysis reaction. Also the total μMoles of fluorescein based on the initial measured values for FDA and NaF was

greater than the previous test values, 6100 μMoles vs. 5200 μMoles. However, the calculations for this data set were based on a total of 6100 μMoles fluorescein at the start of testing. Using the measured NaF over time a 1st order rate constant of $0.015hr^{-1}$ was calculated. This is a decrease from the previous tests and could be due to the compressor dropping out and requiring several restarts during testing. The compressor problem was due to high pressure head caused by toluene vapor condensing out in the outlet line. Since the compressor maintained a fairly constant nitrogen flow during the first 30 minutes of testing and did not drop out during this time period the 1st order rate constant for the first 30 minute period was calculated at $0.034hr^{-1}$ which is about double in the rate. However, there was just one data point for this time period. Using the calculated rate constants, an intrinsic rate constant of 3.2×10^{-10} $L/mm^2/hr$ and a toluene hold-up volume of 1.34L the interfacial mass transfer area ranged from 62 to 142 m^2.

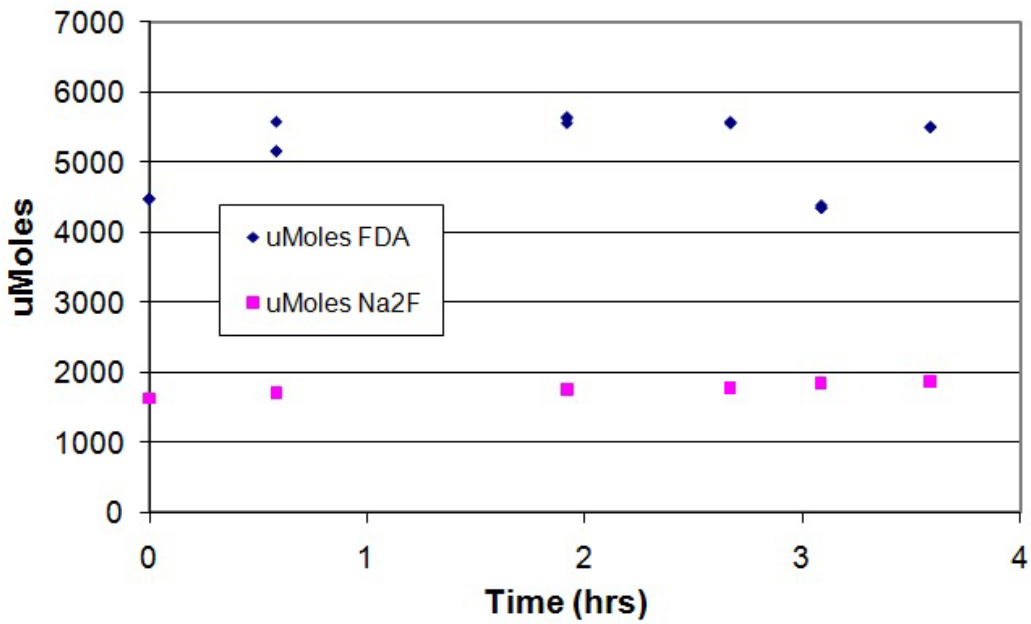

Figure 3.40. Mass transfer data showing concentration of FDA and Na2F during 4/28/2010 run. Aqueous flow 28 L/min, toluene flow 6 L/min, nitrogen gas flow 11 scfm.

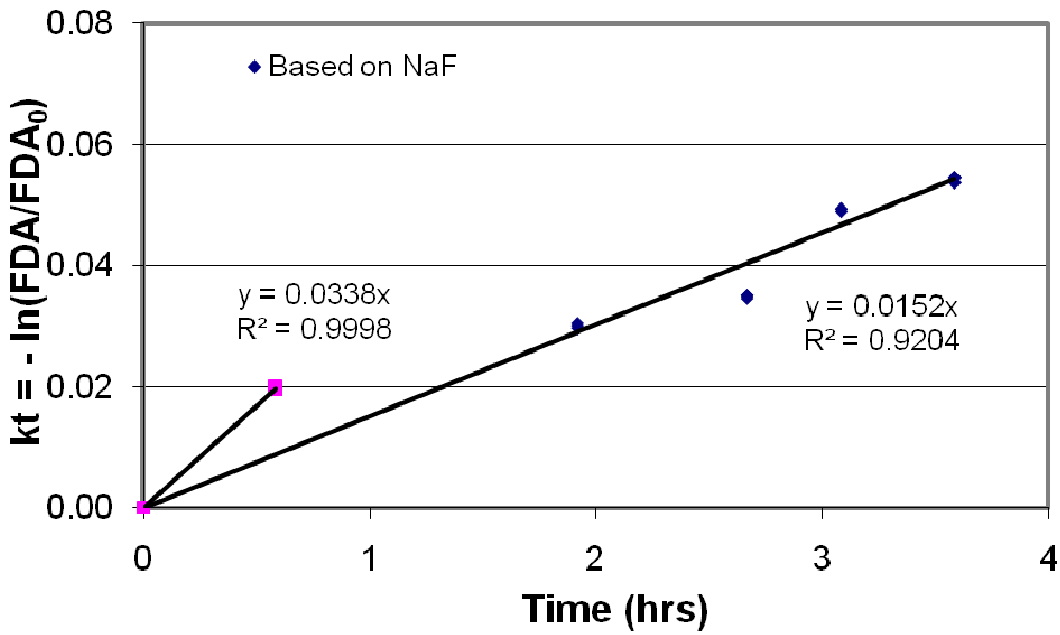

Figure 3.41. First order rate equation for FDA based on measured [NaF] during 4/28/2010 run. kt = -ln(FDA_t/FDA_0). Aqueous flow 28 L/min, toluene flow 6 L/min, nitrogen gas flow 11 scfm.

05-18-2010 Experiment: Since it was difficult to run the compressor at a high gas flow without it dropping out due to high head pressure, a test was run in which the nitrogen flow was lowered to about 4 scfm, the toluene flow lowered to a very low flow rate (1.6 L/min) and the water flow was set to 28.4 L/min. At these conditions the system could maintain pulse flow with a low toluene-to-water ratio. The toluene hold-up volume was 0.75 L. Additionally, a test was run without gas flow but keeping the toluene and water flow at the same conditions (1.6 L/min and 28.5 L/min). For the no gas flow condition the average toluene hold-up volume was 1.40L.

Little or no pressure oscillations were observed for these configurations. Therefore, no pressure data was recorded.

The results of these tests are shown in the Figures 3.42 and 3.43. As with all other tests, the FDA increased over time and could not be used to calculate the 1st order rate constant, thus the NaF was used to calculate the 1st order rate constant. The raw data plot for both flow conditions shows no real difference in the fluorescein hydrolysis. Yet for the gas flow test a slightly higher 1st order rate constant was observed (0.008 hr^{-1} vs. 0.005 hr^{-1}). However, these rates are about an order of magnitude less than the rates for the previous tests. Also, the plot for the 1st order rate for the no gas flow condition indicates a poor regression coefficient (0.77). The calculated interfacial mass transfer area for the gas flow condition was 18 m^2 and for no gas flow condition was 26 m^2.

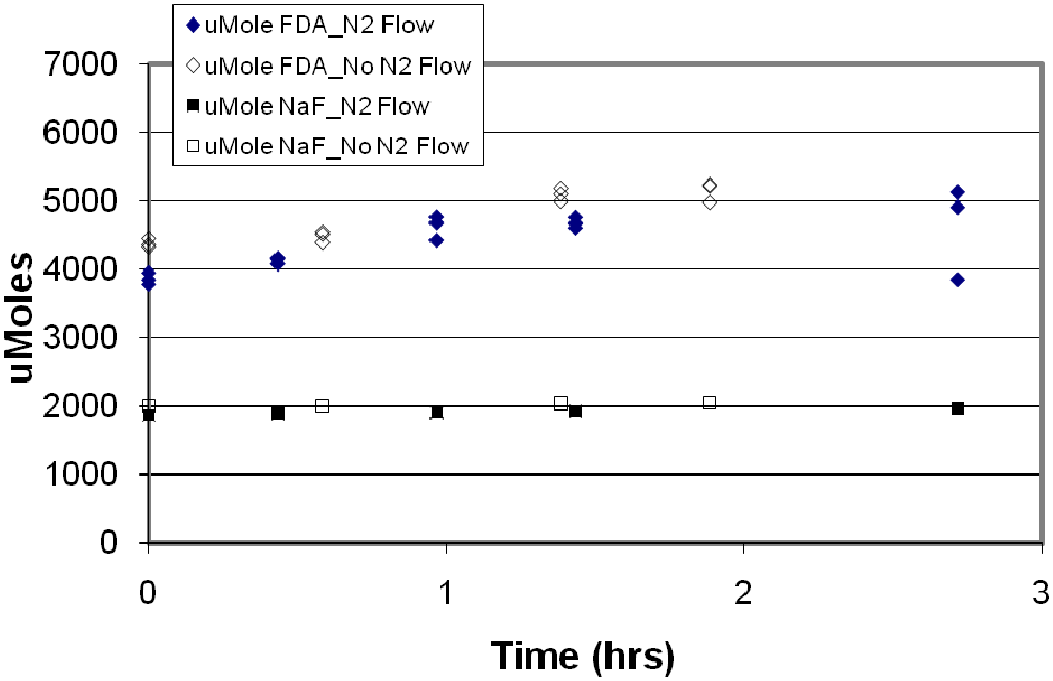

Figure 3.42. Mass transfer data showing concentration of FDA and Na2F during 5/18/2010 run. Aqueous flow 28 L/min, toluene flow 1.6 L/min, nitrogen gas flow 4 scfm.

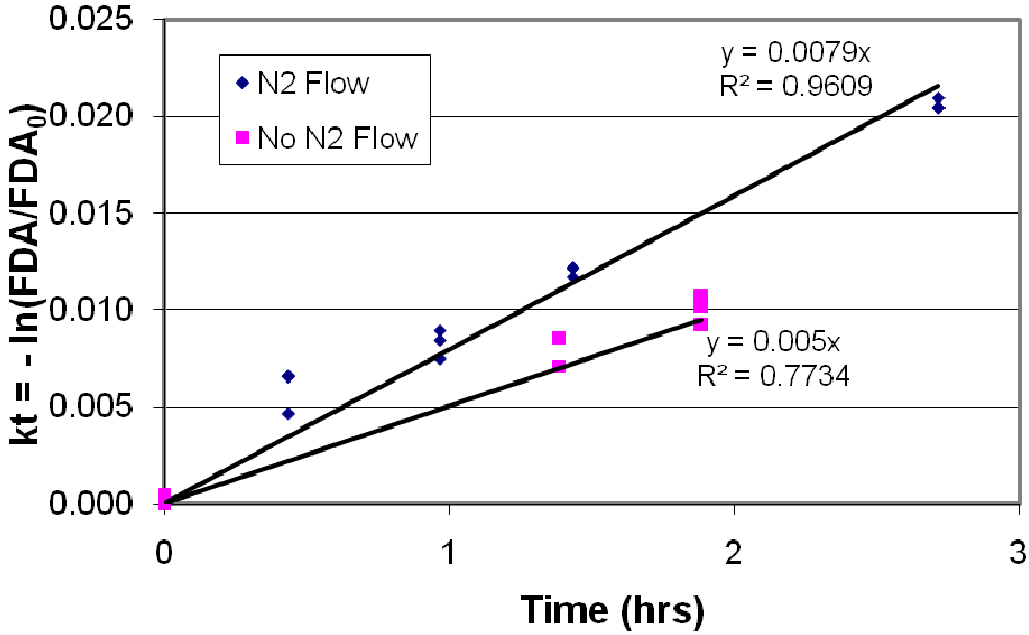

Figure 3.43. First order rate equation for FDA based on measured [NaF] during 5/18/2010 run. kt = -ln(FDA_t/FDA_0).Aqueous flow 28 L/min, toluene flow 1.6 L/min, nitrogen gas flow 4 scfm.

Discussion:

Due to the problem with fluorescein hydrolysis the calculated 1st order rate constants and the estimate of the interfacial mass transfer area should only be used as an indicator to changes in hydrolysis due to change in flow conditions in the 3 phase system. Since the formation of the hydrolysis product, disodium fluorescein, could be followed and used to calculate reasonable 1st order rate constants which are similar to the rate constant reported by Wenn et al. (2003), the change in interfacial area can be viewed as a reasonable indicator of packing performance under varying 3-phase flow conditions.

The exceptionally slow rate of hydrolysis seen for the lab scale tests using the 3-phase fluids is a clear indication there was something interfering with the reaction. This was most likely due to oxidants in the toluene that were interfering with the reaction. Since the disodium fluorescein showed an increase over time but the fluorescein diacetate did not show a uniform decrease over time the calculation of the 1st order rate constant required using the NaF values. However, since it was not practical to change out the system fluids in the 3-phase system the only alternative was to use the calculated intrinsic rate constant determined from the 3-phase lab scale test. Using this intrinsic rate constant the changes in the fluorescein hydrolysis rate and thus estimates for change in interfacial mass transfer area was determined for changes in the hydrodynamic for 3-phase flow.

For all tests water flow was kept constant at 28 L/min with varying toluene and nitrogen flow. At the high liquid flows and low nitrogen flow (aqueous:28.3 L/min, toluene: 18.4L/min, nitrogen: 2-3scfm) pulsing was present. With no pulsing (i.e., no gas flow) at high liquid flow rates the fluorescein hydrolysis decreased by about 16% with a doubling of water hold-up and a reduction by half of the toluene hold-up. This resulted in over a 50% reduction in interfacial mass transfer area.

Since the compressor dropped out at high nitrogen flow rates due to high head pressure the flow dynamics were difficult to evaluate. Taking only the first 30 minutes of testing at the high nitrogen flow, 11 scfm, with 6 L/min toluene, the hydrolysis rate increased by nearly 80%. The pulsing apparently suppressed. However a reduction in toluene hold-up, 1.34 L was observed and the interfacial mass transfer area increased slightly.

At low nitrogen flow, 4scfm, and low toluene flow, 1.6 L/min, hydrolysis decreased considerably (0.019 hr^{-1} to 0.008 hr^{-1}). Pulsing did not occur. This most likely explains the drop in rate, leading to a low toluene hold-up of 0.75 L, and an increase in the interfacial mass transfer area to 18 mm^2. At the no pulsing condition (i.e., no gas flow) with low toluene flow, 1.6 L/min, hydrolysis rate decreased even more yet interfacial mass transfer area did not change significantly. This is most likely due to little to no pulsing occurring for low gas flow and low toluene flow.

Table 3.5. Test matrix and results.

Date	Flow Condition	1st Order Rate Constant (hr^{-1})	Water: Toluene Hold-Up Volume (L : L)	Intrinsic Rate Constant ($L/mm^2/hr$)	Interfacial Mass Transfer Area (m^2)
	Lab Scale	9×10^{-5}	55 : 25[(1)]	3.2×10^{-10}	7.088×10^{-3}
3/18/10	Aq: 28.3L/min T: 18.4L/min N2: 3 scfm	0.019	2.59 : 4.69	3.2×10^{-10}	346
3/24/10	Aq: 28.3L/min T: 18.4L/min N2: 3 scfm	0.019	2.63 : 4.43	3.2×10^{-10}	263
3/25/10	Aq: 28.3L/min T: 18.4L/min N2: 0 scfm	0.016	5.53 : 2.06	3.2×10^{-10}	103
4/28/10	Aq: 28.0L/min T: 6L/min N2: 11 scfm	0.015 - 0.034	3.0 : 1.34	3.2×10^{-10}	62 to 142
5/1810	Aq: 28.L/min T: 1.6L/min N2: 4 scfm	0.008	2.8 : 0.75	3.2×10^{-10}	18
5/18/10	Aq: 28.L/min T: 1.6L/min N2:0 scfm	0.005	3.98 : 1.7	3.2×10^{-10}	26

1 – Lab scale test a static test at 55ml water to 25 ml toluene with an interfacial area of $7088m^2$ (95mm diameter)

4. Conclusions

Two-phase experiments were run over a range of conditions including gas and liquid flow rates, and with different packing materials (beads of several different diameters, woven packing, and resin beads) and liquids (water and water- ethylene glycol solutions of different viscosity). Increasing the bead diameter caused a rapid increase in the slope of the average bed pressure drop corresponding to conditions at which pulsing was visually apparent.

Higher viscosity shifted the trickle-to-pulse transition to lower gas flow rates. This effect was most significant for the woven packing.

Transition detection techniques based on pressure fluctuations were demonstrated, showing that such noninvasive measurements can be made to determine trickle-to-pulse transition when visual observations are not feasible.

In the three phase experiments, the column behaved as expected when only two phases were present with the glass bead packing. However when transitioned to organic and aqueous liquids with woven multifilament polypropylene (WMFP) packing the column behaved differently. The hydrodynamics for both pulse flow and holdup changed. The WMFP packing showed an affinity for the organic liquid and required long drain times during the holdup determinations. The WMFP packing didn't behave as glass beads. The pulse flow region moved in an unpredicted direction. The organic liquid toluene also behaved differently from the isododecane. The maximum holdup for toluene occurred at a low nitrogen flow rate and interacted strongly with the water hold up at the point. This point coincided with the conditions for maximum mass transfer.

One may conclude from all this that the use of WMFP packing removes organic liquid from the flow and thus becomes unavailable for interaction with the aqueous phase. Pulse flow occurs in the regions outside the packing where the two liquids compete for space. When the organic holdup maximizes, the contact area becomes a maximum.

Appendix A. Two-Phase Operating Procedures

Two-Phase Experiment Operating Procedures

I. Experiment preparation
   A. Power up experiment
      1. Turn on computer, DAQ unit, power strip for valves, pump power switch
      2. Verify ball valve on air to solenoid valves, to air flow meter, and to air regulator are open
      3. Verify vent valve in middle of column is closed
      4. Verify column drain valve at bottom of column is closed
      5. Verify switch on control panel is pointing to the "open" position (i.e. all three solenoid valves on column are in the open position)
   B. Install packing
      1. Open column by removing bolts securing top flange
      2. Remove top flange being sure not to lose black o-ring
      3. Place flange and o-ring on top of Unistrut
      4. support structure
      5. Use one bolt to support the top of the column in position with the support bracket
      6. Ensure ring and threaded rod support is installed in column
      7. For a packed bed of beads:
         a. Install the blue plastic filtration media and use the long tubing piece behind the experiment to push it down the column and into position against the bottom support.
         b. Select the size of beads to test
         c. Use the scale and beaker to weigh the beads to be installed in the column
         d. Use the big white bucket to rinse the beads with tap water
         e. Randomly drop the beads into the column
         f. Install the white plastic packing for water distribution at the top of the column
         g. Replace top flange making sure the o-ring is properly seated in its groove
         h. Bolt on flange following torque sequence
      8. For a bed of the woven packing:
         a. If the packing has not been used before, rinse extensively in the sink under flowing water. You will notice the water turns soapy. Rinse until water appears clean.
         b. Cut strips of the packing so that desired density is obtained
         c. Roll each strip around center rod of the threaded rod and pinwheel support (there are two pieces of the support - one with three sections and one with two sections). Try to roll the packing evenly so that it is not rolled tighter in the middle as compared to the outside. Use masking tape to keep each section rolled while you work on the other sections.
         d. Make sure that weave orientation is as desired
         e. Make sure only the ring and threaded rod packing support is in the bottom of the column (i.e. the blue plastic filtration media is not).
         f. Install the three-sectioned support with the woven packing into the column. Be careful not to squeeze the packing with your hands as it will crunch the packing causing the outer layer of the packing to not touch the inner column surface. Push the packing support down into the column by pushing on the pinwheel supports. You may have to rotate as you go to avoid getting stuck on the pressure

transducer ports. Use the long metal tube to push the packing support down until it seats on the ring and threaded rod support.

g. Install the two-section support with the woven packing on top of the three-section support. There are no pinwheel sections on the top.
h. Check to see that the packing contacts the column wall sufficiently
i. Install the white plastic packing for water distribution at the top of the column
j. Replace top flange making sure the o-ring is properly seated in its groove
k. Bolt on flange following torque sequence

C. Prime pump
1. The liquid pump must be primed prior to turning it on. Failure to do this will ruin the inner magnet and impeller assembly!
2. Verify orange needle valve on liquid supply line to column is closed
3. Verify ball valve on bypass line is open
4. Connect water hose from the chilled water supply on the north wall to the tubing extension usually sitting on the top of the water holding tank
5. Insert the extension tubing into the pump suction line a few inches - not too far or you have trouble removing it quickly
6. Attach the clear tubing section used for the holdup experiments to the exit of the bypass line so that it extends below the water level in the tank
7. Turn on the water supply about 3/4 open
8. Use your hand to prevent water backflow from around the tubing extension so that most water is sent through the pump and bypass line
9. Hold until water is continuously flowing through the bypass line and has pushed all the air out of the clear tubing that extends below the tank water line
10. When the pump is primed, remove the chilled water tubing from the pump suction line
11. Turn off water supply and remove water hose from tank
12. Start liquid pump with a LabVIEW setting about 2 gpm
13. Remove clear plastic tubing from exit of bypass line. Water should be flowing through bypass line
14. Open needle valve slightly (~1-2 turns)
15. Increase pump setting until power is about 25 Hz (~ 3-4gpm)
16. Slowly close ball valve while continuing to open the needle valve
17. Verify flow has started to the top of the column

D. Flush packing
1. Start water flow (see II.A) and increase to desired setting
2. Start air flow (see II.B) and increase to desired setting
3. Run continuously for approximately 10 minutes
4. Record pressures for 10 seconds
5. Stop air flow and water flow (see II.C)
6. Check bed pressure drop against data at the same operating condition - the pressure drop will be high if the water has been sitting overnight or the beads have not been used before
7. If the bed pressure drop is outside the range of what is acceptable then the water in the holding tank should be flushed
8. Put a paper cup under the pump suction line so the water level remains higher than the tubing entrance
9. Use the plastic tubing section to siphon most of the water out of the tank into the big white bucket

10. Fill up one of the Nalgene bottles with deionized water
11. Pour the fresh water into the holding tank. Remove paper cup
12. Repeat steps 1-11 until measured bed pressure drop is acceptable (usually 2-3 flushes). During extended testing the bed pressure drop may increase. It should be checked periodically and the water flushed if necessary.

II. Perform experiment

A. Start liquid flow (pump already primed)
   1. Enter a water setting of 3 or 4 in LabVIEW
   2. Click the "change" button in LabVIEW
   3. Go to pump motor control unit and hit the start button
   4. Watch the motor speed increase and open needle valve as speed increases from around 18 to 24 Hz
   5. Verify water flow has started to top of column

B. Start air flow
   1. Click on "start" and enter filename to initialize data collection (nothing is written to the file until the box to save data is checked)
   2. Increase setting of air flow in LabVIEW and click "change" to change value

C. Record pressure measurements
   1. Click on "Start" data collection and enter filename to save data (#.dat)
   2. Click the box to save the data to file
   3. Record for approximately 20 seconds
   4. Click on "Stop" to stop data collection
   5. If more pressure measurements are to be taken at a different operating condition then continue:
   6. Change water and air flow to desired operating condition
   7. Let stabilize for at least 2 minutes (allow up to 10 minutes at the low flow rates)
   8. Repeat steps 1-4 to record pressures

D. Perform holdup experiment
   1. Achieve steady operation at desired water and air flows
   2. Turn switch on control panel next to pump motor control unit to close all solenoid valves
   3. Immediately hit the "Stop" button on the pump motor control unit
   4. Immediately set the air flow setting to "0" and click the "change" button
   5. Close the needle valve on the liquid supply line
   6. Open the vent valve in the middle of the column
   7. Zero the scale for the container used to collect the water (glass beaker or plastic tub)
   8. Open the drain valve and put the container on the floor to collect the water
   9. Weigh collected water
   10. Add x g of water to the measurement to account for water not drained due to drain valve location

E. Stop liquid flow
   1. Lower the water pump setting in LabVIEW to 3 or 4 gpm and turn the air flow off
   2. Close the needle valve (so as to not lose the prime on the pump)
   3. Immediately after the valve is closed, hit the "stop" button on the pump motor control unit

Things to keep in mind:

1. Make sure packing is thoroughly wetted prior to taking any data. This may require operation for a few seconds at high liquid and air flow rates, then backing off flow rates to desired operating conditions. Hysteresis in the data will be observed if this is not done. This is most noticeable in the bed pressure drop and only slightly noticeable in the holdup measurements.
2. To get very low liquid flow rates, operate the pump at a high setting (i.e. 7gpm) and throttle down the needle valve. Open the bypass valve. Search for the ideal valve arrangements to get the flow as you want but be very careful not to lose prime on the pump.

Appendix B. Two-Phase Viscosity Memo

Sandia National Laboratories
Operated for the U.S. Department of Energy by
Sandia Corporation
Albuquerque, New Mexico 87185-2554

date: February 22, 2006

to: Distribution

from: Marcia Cooper, MS-1454 (2554)

subject: Testing of different viscosity liquids in the two-phase experiment

This memo documents tests carried out with the two-phase, fixed-bed experiment at Sandia National Laboratories with two liquids having viscosities greater than one. The experiment, conducted tests, and results are described. CDTECH requested information regarding the trickle-pulse transition boundary and operating conditions of the bed when operating with liquids of greater viscosities.

The two-phase experiment (Fig. 1) consists of a polycarbonate column (I.D. 3.75-in) with water supplied to the top of the column via a Magnatex liquid pump (model MMP21-R25) and air supplied from the building via an Alicat flow controller (model MCR-1000SLPM-D/5M 5IN). In these tests, the liquid bypass line was not used and all liquid flow was directed to the top of the column.

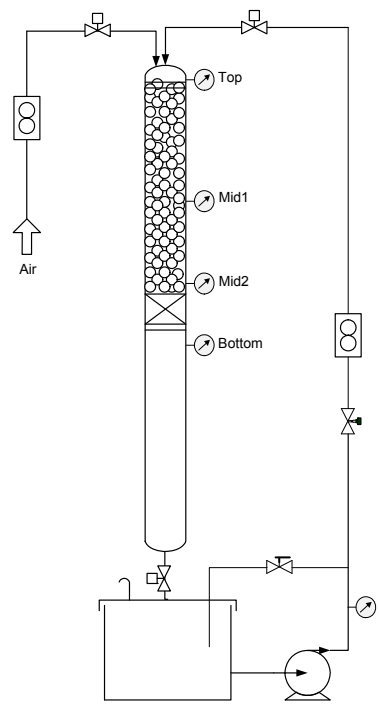

Figure 1. Schematic of the two-phase, fixed-bed experiment.

The bed was packed with either beads (1/4-in diameter) or the woven packing (supplied by CDTECH). The bed void fraction (ϕ) was calculated from the weight of beads installed in the column (w), the weight of a single bead (ρ), the bead volume (V_s), the bed height (h), and column diameter (D). A bed void fraction of 0.36 was calculated for the 1/4-in beads.

$$\phi = 1 - \frac{V_s w}{\rho(\pi/4)D^2 h}$$

The woven packing was rolled in 5 sections around a threaded rod that was mounted vertically along the column centerline. Two metal plates oriented perpendicular to each other separated each section and prevented collapse of the rolled packing. The woven packing had a bed void fraction of 0.91 determined by measuring the amount of water needed to completely flood the bed.

The liquid viscosity was modified by adding varying amounts of ethylene glycol to deionized water. Ethylene glycol was chosen based on a cost-benefits analysis of several candidate chemicals. The selection process was documented and posted to the extranet

(https://www.prod.sandia.gov/view/view-docs/mfr/2Phase/Viscosity/ViscosityTesting.doc).
The liquid viscosity was measured with a Gilmont Falling Ball viscometer, ASTM size 1 (VWR.com, PN 66062-009). Specifics of the two mixtures are given in Table 1.

Table 1. Higher viscosity liquids tested

Viscosity	Density
3.65 ± 0.28 cP	1.20 g/cc
8.25 ± 0.58 cP	1.08 g/cc

The bed pressure drop (ΔP) was measured as a function of liquid and gas mass flux. The results of the time-averaged, bed pressure drop and the time-average, normalized bed pressure drop are given in Figure 3 for a bed packed with 1/4-in beads. The baseline data with water (1 cP) are represented by solid lines.

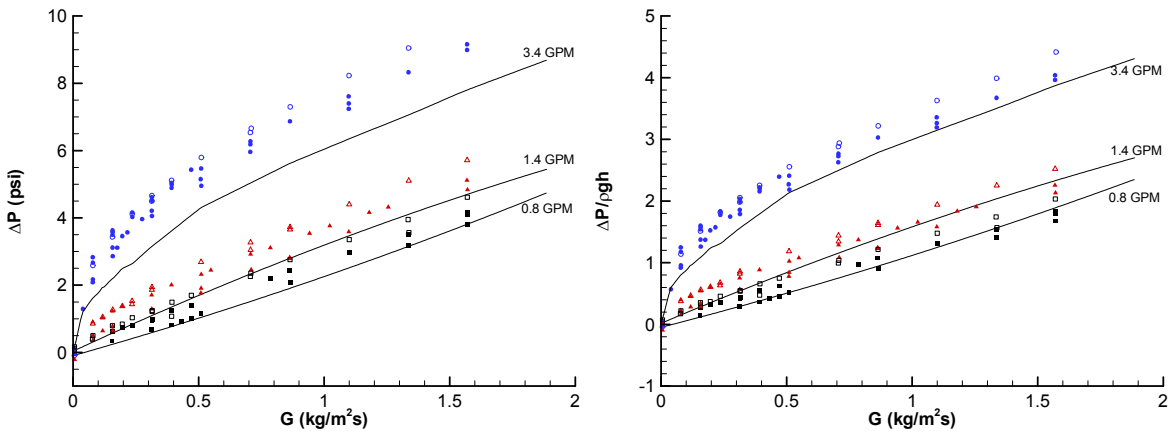

Figure 3. Time-averaged (left) and normalized (right) bed pressure drop for the bed packed with 1/4-in beads. Solid points correspond to a liquid viscosity of 3.65 cP and the open points correspond to a liquid viscosity of 8.25 cP. Black points correspond to 0.8 GPM, red points correspond to 1.4 GPM, and blue points correspond to 3.4 GPM.

The results of the time-averaged, bed pressure drop and the time-average, normalized bed pressure drop are given in Figure 4 for a bed of the woven packing. The baseline data with water (1 cP) is represented by solid lines.

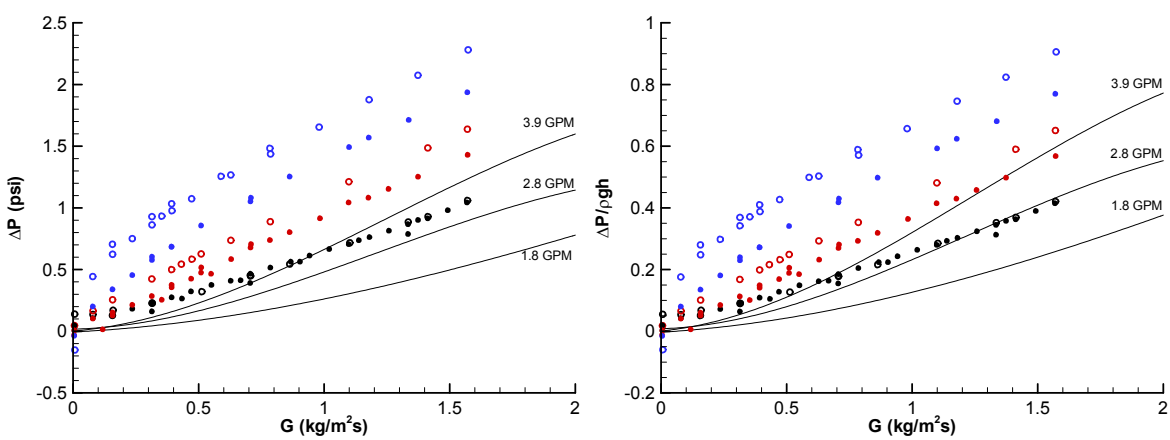

Figure 4. Time-averaged (left) and normalized (right) bed pressure drop for the bed with the woven packing. Solid points correspond to a liquid viscosity of 3.65 cP and the open points correspond to a liquid viscosity of 8.25 cP. Black points correspond to 1.8 GPM, red points correspond to 2.8 GPM, and blue points correspond to 3.9 GPM.

Increasing the liquid viscosity shifted the trickle-pulse transition boundary to lower gas flow rates. The change in the transition boundary for the different liquid flow rates and packed beds are given in Table 2. The shift in the transition boundary was greater for the woven packing.

Table 2. Gas flow rate (SCFM) at the trickle-pulse transition

Packing, GPM	1 cP	3.65 cP	8.25 cP
1/4-in, 0.8	9.0	3.0	3.0
1/4-in, 1.4	2.0	2.0	2.0
1/4-in, 3.4	1.5	4.0	2.0
Woven, 1.8	> 24.0	18.0	15.0
Woven, 2.8	14.5	6.5	5.0
Woven, 3.9	10.5	4.5	4.0

In conclusion, the effect of viscosity on the time-averaged bed pressure drop is modest. A greater effect was observed with the woven packing and is likely due to the higher surface area. The pressure results for a bed of beads compare to the literature. The increase in viscosity shifted the trickle-pulse transition boundary to lower gas flow rates. This effect was most significant for the woven packing.

Distribution (electronic):

W. Cross, CDTECH
R. Foley, CDTECH
L. Smith, CDTECH
1349 1815 Evans, L.R.
0834 1512 Grasser, T.W.
0834 1512 O'Hern, T.J.
0834 1512 Tachau, R.D.M.
0826 1513 Torczynski, J.R.
1349 1815 Miller, J.E.

Appendix C. Two-Phase Resin Memo

Sandia National Laboratories
Operated for the U.S. Department of Energy by
Sandia Corporation
Albuquerque, New Mexico 87185-0834

date: November 9, 2005

to: Distribution

from: Marcia Cooper, MS-0834 (1512)

subject: Testing of Amberlyst 15 packing in two-phase experiment

This memo documents tests carried out with the two-phase, fixed-bed experiment at Sandia National Laboratories with resin packing supplied by CDTECH of Pasadena, Texas. The experiment, conducted tests, and results are described. CDTECH requested information regarding the trickle-pulse transition boundary and operating conditions of the bed when operating in the pulse-flow regime. Pulse flow was not observed with this packing.

The two-phase experiment (Fig. 1) consists of a polycarbonate column (I.D. 3.75-in) with water supplied to the top of the column via a Magnatex liquid pump (model MMP21-R25) and air supplied from the building via an Alicat flow controller (model MCR-1000SLPM-D/5M 5IN). A liquid return line at the pump discharge was present for all tests. A pressure transducer was installed downstream of the pump to measure the liquid discharge pressure for the tests listed in Table 3. A needle valve was located between the inlet to the liquid return line and the column inlet and a ball valve was located in the liquid return line. Both valves aided in throttling the flow to the column.

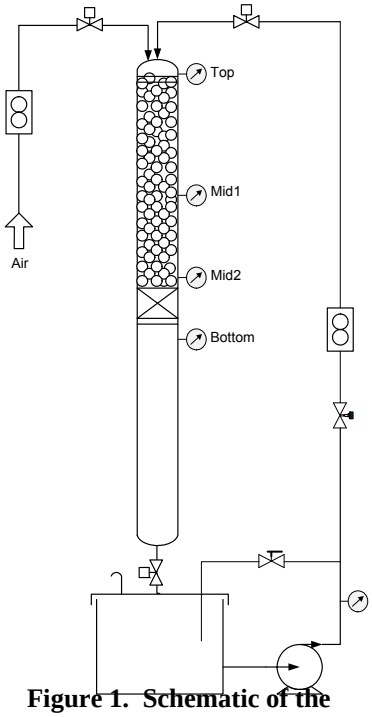

Figure 1. Schematic of the two-phase, fixed-bed experiment.

The bed (Fig. 2) was packed with Amberlyst 15 (A-15) resin manufactured by Rohm and Haas. The bead diameter is not conclusively known from the product literature. A-15 is specified as either wet or dry on the Rohm and Haas website. The MSDS supplied by CDTECH with the resin was for A-15Wet but the "Wet" was blacked out. Rohm and Haas product literature for A-15Wet specifies a harmonic mean particle size of 0.600 to 0.850 mm with 1.0% max smaller than 0.355mm and 5.0% max larger than 1.180 mm. No information was found regarding the harmonic mean particle size for A-15Dry. Bruce Hern (CDTECH) said that A-15 is a dried form of A-35. The harmonic mean particle size of A-35Wet is stated to be 0.700-0.950 mm and shrinks 40% when dried. From these various size ranges and resin types it was not clear exactly what was being used and so the bead diameter was measured.

Figure 2. Photograph of a section of the packed bed.

Micrographs of the resin beads (Fig. 3) were taken to conclusively measure their diameter. The width of each image represents 1.2mm and the range of bead sizes can be seen. These beads were initially soaked in tap water overnight (where no significant swelling was observed) before being installed in the column for the first sets of experiments. After the first two sets of experiments, the slightly damp beads were put back into the 5-gallon bucket they were shipped in and the lid was sealed. Upon re-opening the bucket for the third set of experiments, the beads were observed to have swelled so that the lid was slightly bulging (estimated to be less than a 5% increase in total volume).

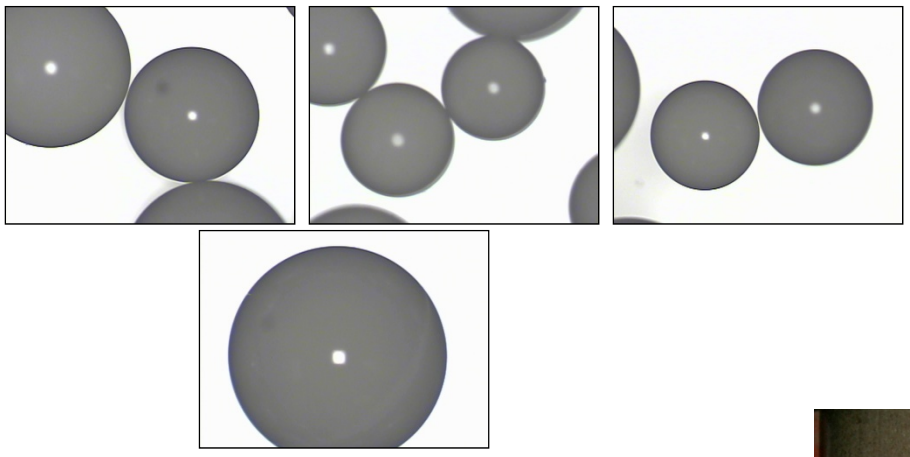

Figure 3. Micrographs of the Amberlyst packing

The diameters of 13 randomly selected beads were measured (0.711, 0.471, 0.670, 0.463, 0.421, 0.711, 0.545, 0.512, 0.512, 0.884, 0.760, 0.446, 0.471 mm) yielding an average bead size of 0.583 mm. This value for the average bead diameter was used during data analysis.

Figure 4. Photograph of the packing support.

A fixture (Fig. 4) was constructed to support the bottom of the packed bed approximately 48-in from the bottom of the column. The fixture consisted of an aluminum ring with a wire mesh spanning the inner open area. An o-ring groove was machined into the ring's outer circumference. The two o-

rings and a flat gasket fit within this groove and seal against the column's inner surface.

The first two sets of experiments (Table 1) were carried out with a 100x100 wire mesh (openings of 0.149 mm), which was readily available in the lab, and two different bed heights (43.5 and 55 in). The third set of experiments (Table 2) was carried out with a 40x40 wire mesh (openings of 0.420mm, McMaster-Carr, PN85385T864) and a single bed height (36.5 in). A larger mesh was used for the later experiments because it was thought the 100x100 mesh may be resulting in an excessive pressure drop limiting the operational flow rates. The 40x40 mesh had the largest openings that still supported most of the beads (50x50 mesh has openings of 0.595mm).

The method previously used to measure void fraction with the polypropylene beads and woven packing was to close the holdup valve at the bottom of the column, remove the flange at the top of the column and fill the entire column with water. The amount of water needed to fill the packed portion of the column was recorded. This method was not possible with the resin packing because the small bead size and water surface tension prevented the air trapped below the packed bed from being displaced by the added water. Instead, the bed void fraction was measured by pressurizing the bed with air. The initial pressure, final pressure, and mass of air added to the column were recorded for the column containing the packed bed and an empty column. Using the ideal gas law, the void fraction of the resin-packed bed was calculated to be 0.261. This value is reasonable since a randomly packed bed of uniform diameter spheres has a void fraction of 0.36 and bead non-uniformity acts to decrease the void fraction (Song et al., 1998). The amount of decrease in the void fraction depends on the loading fraction of small-to-large diameter spheres. The loading fraction is not documented for the resin packing, but could be estimated by taking micrographs of a larger sample of beads.

Several factors of the experiment limited the operating conditions when the resin packing was installed. The building supplied air at a pressure of 90psi which was regulated down to 40psi upstream of the flow controller. The maximum allowable working pressure of the polycarbonate column without holes for the wall-mounted pressure transducers was 60 psi based on ASME calculations. However, cracks in the column near the pressure transducer mounts developed while carrying out the first two sets of experiments (Table 1) where the column pressure exceeded 30psi in some cases. The cracks were sealed with epoxy, gasket material, and hose clamps in order to keep the facility operational, yet the maximum allowable working pressure can no longer assumed to be as high as 60psi. The regulated air pressure is the most immediate limitation that prevents testing to higher column pressures. This value could be increased, yet due to the compromised strength of the cracked polycarbonate column this has not been attempted.

Visual observation of the flow through the resin packing was extremely difficult due to the opaque beads and packing density. Only when the bed was flooded could water be observed along the inner column walls. During low gas flow rates, all the water appeared to flow through the center of the packed bed and emerge as a continuous stream from the packing support. At higher gas flow rates, the water

emerged from the bottom of the packing more uniformly distributed along the column cross-section but did so in many continuous streams. In either case, flow of liquid within the bed was not observable.

In an attempt to fully describe these visual observations, digital photos and movies were taken of the bed during operation at the lowest liquid flow rates and varying gas flow rates (Table 2). However, they are of limited usefulness since on-site visualization of the flow was extremely difficult.

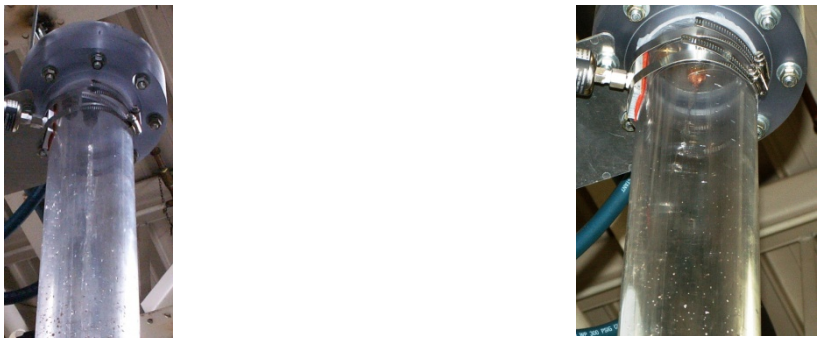

Figure 6. Photos of the inlet water stream for experiments 2131 (left) and 2133 (right).

Four movies of the column operating with the resin packing have been uploaded to the extranet. To view, click on the "Movies" link from the "Two-Phase Experiment" main page. Brief descriptions of the movies follow.

- PICT0017.MOV (16.2M) illustrates operation with a low air flow rate of 1 SCFM (experiment 2129). The water streams out of the bottom of the bed and is not well distributed across the column cross-section.

- PICT0021.MOV (30.9M) illustrates operation with a medium air flow rate of 3 SFCM (experiment 2131). The water still streams out of the bottom of the packing, yet is slightly more evenly distributed across the column cross-section.

- PICT0031.MOV (15.4M) and PICT0032.MOV (18.7M) illustrate operation with a higher airflow rate of 5 (experiment 2133) and 6 (experiment 2134) SCFM, respectively. The water comes out of the bottom of the packing in drops, not continuous streams as is the case with lower air flow rates, and is fairly well distributed across the column cross section.

The bed pressure drop (ΔP) was measured as a function of liquid and gas mass flux. The results are shown for all experiments in Fig. 5.

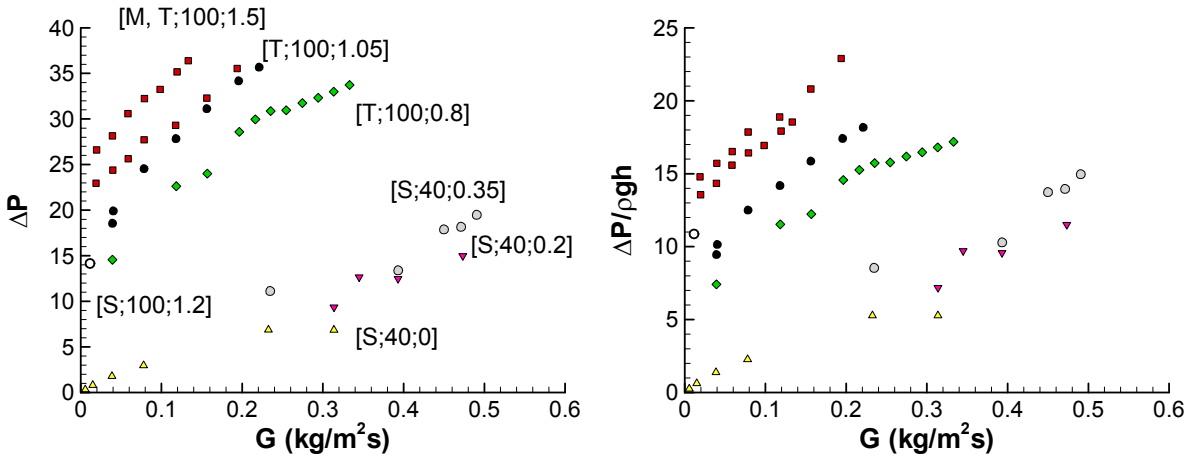

Figure 5. (A) Time-averaged and (B) normalized bed pressure drop for the resin packing. Labels: [S=36.5 in, M=43.5 in, T=55 in; 100=100Mesh, 40=40Mesh; liquid flow rate in gpm]

The effects of bed height can be observed in the two series of squares in Fig. 5A by noting the difference in absolute pressure. When normalized, this is effect is not observed (Fig. 5B) and all square points collapse to a single curve. Similarly, the one open circle at 1.2 gpm and the short bed has a lower absolute pressure than the tall bed at a lower liquid flow rate. When compared in terms of the normalized pressure, all data are ordered in terms of liquid flow rate regardless of bed height. Higher values of the gas mass flux were obtained before the pressure at the top of the bed reached the regulated air supply pressure with the third set of experiments due to the shorter bed height (and coarser packing support mesh).

Wall-mounted pressure transducers measured the local pressure at locations within the bed. In all cases, no pressure fluctuations were recorded. No experimental data was found in the literature for beds of spheres less than 3 mm. The bead diameter is an order of magnitude smaller than the ranges of applicability for existing empirical correlations. The results from beds of polypropylene beads indicate that a decrease in the particle size results in an increase in the pressure fluctuations that occur during pulse-flow. Thus, pressure fluctuations on the order of 0.5psi or greater are expected during pulse-flow operation with the resin packing.

In conclusion, pulsing was not observed within the resin packing. Additional changes to the facility (stronger column, increase in regulated air-supply pressure) are needed in order to increase the range of operating conditions. It is now recommended that experiments continue with the two-phase experiment to investigate the effect of liquid viscosity.

References:

M. Song, K.T. Chuang and K. Nandakumar. A theoretical correction of the Ouchiyama and Tanaka formula for predicting average porosity of packed beds consisting of nonuniform spheres, Ind. Eng. Chem. Res., 1998, Vol. 37, pp. 3490-3496.

Distribution (electronic):

W. Cross, CDTECH
R. Foley, CDTECH
L. Smith, CDTECH

0834	1512	O'Hern, T.J.
0826	1513	Torczynski, J.R.
1349	1815	Miller, J.E.
1349	1815	Pena, D.A.

Appendix D. AIChE 2005 two-phase paper

EXPERIMENTAL METHODS DEFINING THE TRICKLE-PULSE TRANSITION IN TWO-PHASE FLOWS THROUGH FIXED BEDS

Marcia A. Cooper, Raymond O. Cote, Timothy J. O'Hern, John R. Torczynski
Lindsey R. Evans, Donovan A. Pena
Sandia National Laboratories, Albuquerque, New Mexico 87185-5800

William M. Cross, Lawrence A. Smith
CR&L/CDTECH, Pasadena, Texas 77505

ABSTRACT

Methods to experimentally determine the conditions at which downward co-current gas-liquid flows through a fixed bed of particles confined within a cylindrical column transition from trickle flow to pulse flow are investigated. The pulse-flow hydrodynamic regime is a potentially valuable process-intensification strategy for many petrochemical applications because of the increased mass and heat transfer rates, and increased throughput without flooding compared to the trickle-flow regime. An understanding of the operating regime and, in particular, the conditions leading to trickle-pulse transition in an industrial application is of critical importance in order to exploit the benefits gained from such intensification strategies. This work is a subset of a larger experimental program being carried out jointly by Sandia National Laboratories and CR&L/CDTECH with the purpose of advancing the art of process-intensification strategies for use in multifunctional reactors.

NOMENCLATURE

D	column diameter, m
d	particle diameter, m
G	superficial mass flux of the gas phase, kg/m^{2}s
L	superficial mass flux of the liquid phase, kg/m^{2}s
N	number of particles in bed
P	pressure, Pa
P^*	normalized pulse pressure drop
r	radial location in bed, m
R	column radius, m
V_b	volume of an empty column containing the bed, m^3
V_s	volume of one particle, m^3
ϵ	experimental bed void fraction
μ_L	viscosity of liquid phase, Pa s
ρ_L	density of liquid phase, kg/m^3

INTRODUCTION

This study is part of a larger experimental effort funded by the Chemicals Subprogram of the Industrial Technologies Program at the U.S. Department of Energy to aid the development of new generations of multifunctional chemical reactors by advancing the art of process intensification, and, in particular, by exploiting the benefits of reactor operation in the pulse-flow hydrodynamic regime. Sandia National Laboratories has teamed with CR&L and ABB Lummus through their joint venture Catalytic Distillation Technologies (CDTECH), to optimize the reaction of acid-catalyzed C4 paraffin/olefin alkylation. Issues to be addressed include developing a scientific understanding of how the pulse-flow hydrodynamic regime is affected by the scale-up from bench-scale to industrially relevant sizes with fixed beds of structured packing materials. More specifically, the effects of vessel size, packing material, feed materials, and flow rates on the transition from trickle flow to pulse flow, the pulse characteristics, and the mass transfer between the liquid phases are of particular importance.

These issues are being addressed through three experimental efforts currently being carried out at Sandia National Laboratories. The first experiment consists of a two-phase, non-reactive, fixed-bed column operating with co-current downward flows of air and water. The purpose of this experiment is to investigate the hydrodynamics of the pulse-flow regime, the trickle-pulse regime transition, and how these operating regimes are impacted by the bed properties. The second experiment consists of a three-phase, reactive, fixed-bed column operating with downward flow of a surrogate chemical system. Operating the column with this surrogate chemical system enables investigation of how the hydrodynamics in and near the pulse-flow regime and the bed properties affect the chemical kinetics and mass transfer. The third experiment consists of bench-top vessels in which accurate kinetics studies are carried out.

This paper presents results from the two-phase, non-reactive experiment operating with air and water in fixed-beds of spherical particles. Several hydrodynamic regimes, which have been extensively studied over the past several decades (see the reviews of Charpentier [1], Satterfield [2], and Tosun [3]), are possible in such experiments. Our focus is on the pulse-flow regime as it is a crucial process intensification strategy due to the possibility of increased throughput without flooding [4], increased mass and heat transfer rates [5], and complete wettability of the packing [6] for petrochemical reactions and hydrotreating [7].

Industrial units sometimes operate within the pulse-flow regime or near the trickle-pulse regime transition [2], requiring an accurate definition of the transition boundary for given packed-bed properties, column dimensions, and flow streams. Previous studies defining this transition boundary have typically been carried out in beds of particles with characteristic particle dimensions orders of magnitude smaller than the confining column diameter ($D/d \gg 1$). The results presented here further investigate the trickle-pulse flow boundary and the experimental methods used to detect the transition in beds of spherical particles with values of D/d between 15 and 3.75.

PREVIOUS METHODS DETERMINING TRICKLE-PULSE TRANSITION

Several methods have been used in the laboratory to detect the trickle-pulse regime transition. The most common method is visual observation through a transparent column of either glass [8, 9] or plastic [5, 10, 11, 12, 13]. While this method is simple to implement in the laboratory, it is highly subjective resulting in different interpretations of the operating regime amongst researchers [14]. Other experimental techniques to detect pulsing consist of implementing microphones [4], video-imaging [15], light-bulb and photocells [4, 15], pressure transducers [12, 13], impact tubes [15], anemometers [5], and conductance measurements with either a point probe [16], a ring [5], or a wire mesh [10, 9].

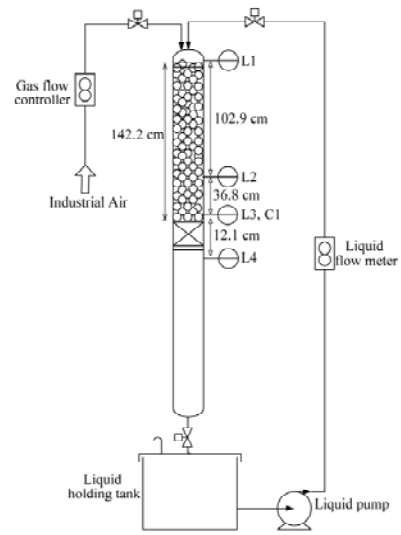

Figure 1: **Schematic of experiment**

Despite the number of studies focused on the trickle-pulse transition boundary, no quantitative measure of this important regime transition has been established. In beds of particles with large values of D/d, the transition is easily identifiable and visual observation may be acceptable. However, in the industrially relevant situations of columns operating with highly viscous fluids or with beds of large particles with low values of D/d, visual observation becomes very difficult in addition to being impractical to implement. An experimental study has been carried out with packed beds consisting of different-sized spherical beads in order to better understand how different experimental methods can be used to identify the conditions of transition from trickle flow to pulse flow. These data from wall-mounted pressure transducers and conductance probes generate a more robust definition of the trickle-pulse transition that does not currently exist in the literature.

EXPERIMENTAL FACILITY

The experiment consisted of a transparent, polycarbonate column packed with a bed of polished, solid, monodisperse, spherical, polypropylene spheres (beads), a liquid holding tank, and a liquid pump, as illustrated in Fig. 1. The experiment is capable of obtaining average bed and local pressure drop measurements and conductance probe measurements for different fixed beds.

The column had a total height of 2.5 m and an inner diameter of 9.53 cm. Four separate beds were tested (Table 1). The bed void fraction $\epsilon = 1 - N(V_s/V_b)$ was calculated from the volume

in the bed N.

The bottom of each bed was fixed 1 m from the bottom of the column and held in place by a ring supporting a 3.8-cm-thick barrier layer of highly porous filtration media (203 m^2/m^3). The beads were randomly packed by dropping them into the column from above until the bed height equaled nominally 1.4 m. Deionized water and air both entered the column at a constant flow rate through the top flange and flowed downward through the packed bed into the holding tank. The air vented to the surroundings, and the liquid was recirculated to the top of the column. A centrally-located spray nozzle at the top of the column was used to distribute the water. Table 2 shows the liquid properties and the experimental conditions examined in this work. Four pressure transducers mounted along the column wall measured pressure histories at locations L1-L4 as shown in Fig. 1. A point conductance probe was installed at location C1 near the bottom of the bed. Details of the circuitry can be found in Cho et al. [17].

Table 1: Details of packed beds

Bead diameter d (cm)	Bed void fraction ϵ	D/d
0.64	0.403	15.0
0.95	0.411	10.0
1.27	0.422	7.50
2.54	0.464	3.75

The measured pressures, conductance probe output, and flow rates were recorded by a LabView™ program. Experimental repeatability was within ±8.7% in the pressure drop (measured between locations L1 and L4 in Fig. 1), ±0.34% in the superficial mass flux of the liquid phase L, and ±0.29% in the superficial mass flux of the gas phase G. The liquid flow meter had an accuracy of ±0.20 LPM and the gas flow controller had an accuracy of ±7 SLPM based on the manufacturer's specifications.

Table 2: Experimental parameters

Liquid density, kg/m^3	ρ_L	997
Liquid viscosity, mPa s	μ_L	0.856
Liquid mass flux, kg/m^2s	L	0-66
Gas mass flux, kg/m^2s	G	0-1.88

FLOW CHARACTERISTICS AT TRICKLE-PULSE REGIME TRANSITION

Pulse flow has been described as repetitive slugs of liquid and gas [4] or a phase redistribution of a two-phase mixture [18]. At low flow rates, the liquid flows over the beads in continuous streams (trickle flow). An increase in either the liquid flow rate or the gas flow rate causes liquid-rich regions to form near the bottom of the packed bed (pulse flow). Further increases in either flow rate increase the pulse frequency and the height of pulse inception within the bed. Observations of the local pressure and conductance probe measurements at the trickle-pulse regime transition follow.

PULSE VARIATIONS WITH BED LOCATION

The pulses exhibit radial variations across the column cross-section and axial variations as they travel through the packed bed. Previous observations [19, 15] of the radial variations have shown that the center of the column ($0 < r/R < 0.1$) has a high liquid fraction within the pulse. This liquid fraction within the pulse decreases significantly to near-gas-continuous conditions in an annular

region ($0.1 < r/R < 0.6$). Conductance probe output from three different radial locations appears in Fig. 2 for a bed of 0.64-cm-diameter spheres. The results are linearly scaled so that liquid-continuous conditions yield an output of unity, while gas-continuous conditions yield an output of zero. Inspection of Fig. 2 shows that a high fraction of liquid appears near the column centerline (A), significant variations between gas-rich and liquid-rich conditions occur at a slightly larger radius (B), and a nearly constant liquid fraction exists at the column wall (C). Such a nearly constant liquid fraction is due to the increased bed void fraction at the wall, which is known to affect the flow [20, 21, 22]. This liquid fraction at the wall increases as the value of D/d decreases.

The data of Fig. 2 were taken while the pulses traveling through the bed were visually distinct. While the flow down the column walls is mostly liquid, distinct variations are observed in the conductance-probe data that match the corresponding measurements from the wall-mounted pressure transducers. It is clear that the higher concentration of liquid flow down the walls not only inhibits visual observation of the pulses but also acts to dampen the liquid-rich-to-gas-rich oscillations that occur within the bed. The difficulties associated with observing the pulses at the wall increase at higher liquid and/or gas flow rates and with beds of large particles.

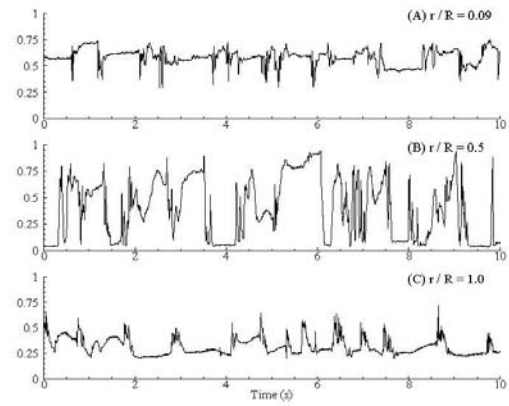

Figure 2: Conductance data showing radial variation of liquid distribution at location C1. $d = 0.64$ cm, $G = 0.236$ kg/m^{2}s, and $L = 11.6$ kg/m^{2}s.

The pulses also exhibit axial variations depending on the bed height, as previously noted by Talmor [23]. Figure 3 plots the output for the wall-mounted pressure transducers at bed locations L2 and L3 (Fig. 1) when pulses are first visually observed (A) and for pulses observed with a higher gas mass flux (B). The pressure variations are greater when measured at locations near the middle of the bed, yet the pulse profiles are more regular when measured at locations near the bottom of the bed. In determining the pulse characteristics, most researchers have taken measurements between the bottom and the middle of the bed. Measurements of pulse parameters without consistency of measurement location would likely impact agreement amongst different groups.

USING LOCAL PRESSURE MEASUREMENTS TO DETECT TRANSITION

The most versatile measurement technique to detect the trickle-pulse transition uses wall-mounted pressure transducers. However, because the axial measurement location along the bed has been shown to affect the resulting pulse characteristics, this technique is investigated further.

Chou et al. [13] used a non-transparent column made of Bakelite and relied on pressure transducers to determine the trickle-pulse transition. They report a distinct jump in the root mean

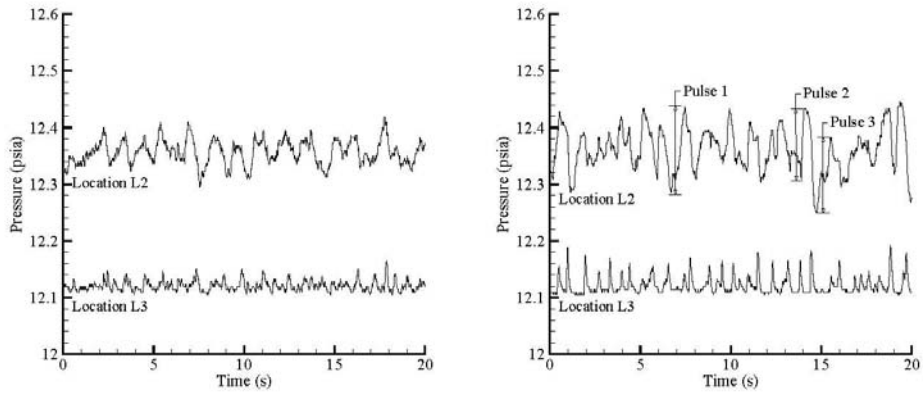

(A) $G = 0.16$ kg/m^{2}s (B) $G = 0.20$ kg/m^{2}s

Figure 3: Pressure measurements at locations L2 and L3 with $d = 0.64$ cm and $L = 11.5$ kg/m^{2}s.

square (RMS) of the time-varying pressure measured at 5% of the bed length from the bottom packing support. In this study, the RMS values of the local pressure measurements were determined at locations L2 and L3 (28.5% and 2.7% of the total bed length from the bottom packing support, respectively). The results are plotted in Fig. 4 as functions of the gas mass flux. The conditions at which pulses were first visually observed are also indicated. No correlation between the RMS values of the local pressure measurements and the conditions at which pulses were first visually observed exists. This is in agreement with the results of Tosun [3], who noted that significant pressure fluctuations appear within the flow prior to the observation of pulsing.

An alternative method to utilizing the local pressure measurements to provide an indication of the trickle-pulse regime transition is to calculate the average maximum pressure drop across a pulse at each location and compare that to the time-averaged pressure drop across the bed. This is investigated for beds with beads of different diameters.

The average maximum pressure drop across a pulse within the bed (from location L2 in Fig. 1) was determined and normalized by the time-averaged bed pressure drop ΔP, resulting in the parameter P^*, which is plotted in Figs. 5A-B as a function of the gas mass flux G. The average maximum pressure drop across a pulse is determined from the pressure history at L2 by averaging the three pulses with the greatest change in pressure (see Fig. 3B where the

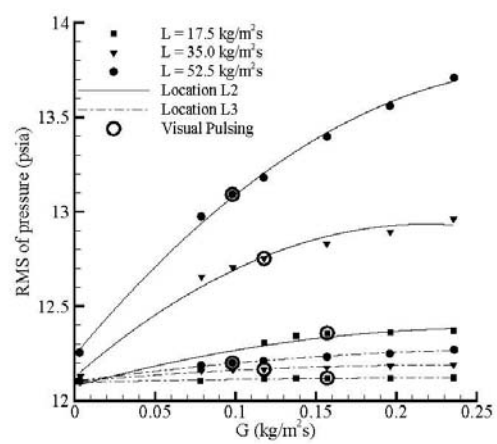

Figure 4: RMS of pressure at locations L2 and L3. $d = 0.64$ cm.

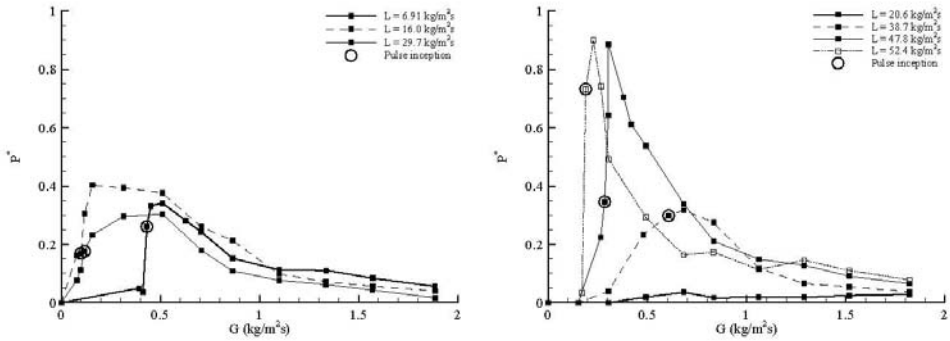

(A) $d = 0.64$ cm (B) $d = 1.27$ cm

Figure 5: Normalized pressure across pulse versus gas mass flux in a beds with different D/d values.

three pulses selected to determine the average maximum pressure drop are denoted).

The conditions at which pulses were first visually observed are noted on Figs. 5A-B by open circles. If a data series does not contain a circle (see Fig. 5B), then transition did not occur, and the bed operated in the trickle-flow regime. In the trickle-flow regime, no significant pressure oscillations were observed, as noted by values of P^* much less than the P^* values in the pulse-flow regime (Fig. 5B). When pulses occurred within the bed, pulses were first observed at lower gas flow rates as the liquid flow rate was increased. After the initial observation of pulses within the bed, the average maximum pressure drop across a pulse was found to increase to a maximum fraction of the time-averaged bed pressure drop before decreasing. Although the values of P^* decreased, pulses within the bed remained present. If the experimental capabilities enabled higher gas and liquid flow rates, the pulses would continue to be damped out until the bubble-flow regime was reached.

It is interesting to note that the conditions under which pulses became visually obvious correspond to values of $P^* = 0.2$ for beds with large values of D/d and higher values of P^* as the D/d ratio decreases. This appears to be a condition from which the transition to pulsing can be inferred. For the case of the 2.54-cm beads (not shown), the maximum values of P^* did not significantly exceed 0.2, further indicating that the pulse-flow regime was not reached.

CONCLUSIONS

A study was carried out to investigate experimental methods that can be used to determine the transition boundary between the trickle-flow and pulse-flow hydrodynamic regimes in a packed bed of spherical particles with co-current downward flows of air and water. Tests were performed with different-sized beads with D/d ratios between 15 and 3.75 and measurements obtained with wall-mounted pressure transducers and conductance probes. This trickle-pulse transition boundary has been determined for a variety of packed beds and gas and liquid flows, yet no quantitative criteria exist to experimentally determine the operating regime.

Transparent columns are impractical for industrial applications, and beds of large particles or highly viscous liquids complicate the identification of the operating regime. This work has highlighted several key considerations, such as radial and axial variations of the pulse parameters, which must be considered when using conductance probes or pressure transducers to facilitate identification of the operating regime.

ACKNOWLEDGMENTS

The financial support of the U.S. Department of Energy Office of Industrial Technologies, Brian Valentine, contract monitor, is acknowledged. The electrical conductance system was fabricated by Professor Steve Ceccio, University of Michigan. Additional support has been provided by CR&L / CDTECH. Sandia is a multiprogram laboratory operated by Sandia Corporation, a Lockheed Martin Company, for the United States Department of Energy's National Nuclear Security Administration under Contract DE-AC04-94AL85000.

REFERENCES

[1] Charpentier, J., 1976. "Recent progress in two phase gas-liquid mass transfer in packed beds". *Chemical Engineering Journal*, **11** (3), pp. 161–181.

[2] Satterfield, C. N., 1975. "Trickle-bed reactors". *AIChE Journal*, **21** (2), pp. 209–228.

[3] Tosun, G., 1984. "A study of cocurrent downflow of nonfoaming gas-liquid systems in a packed bed. 1. Flow regimes: Search for a generalized flow map". *Industrial and Engineering Chemistry Process Design and Development*, **23** (1), pp. 29–35.

[4] Blok, J. R., Varkevisser, J., and Drinkenburg, A. A. H., 1983. "Transition to pulsing flow, holdup and pressure drop in packed columns with cocurrent gas-liquid downflow". *Chemical Engineering Science*, **38** (5), pp. 687–699.

[5] Boelhouwer, J. G., Piepers, H. W., and Drinkenburg, A. A. H., 2002. "Nature and characteristics of pulsing flow in trickle-bed reactors". *Chemical Engineering Science*, **57** (22–23), pp. 4865–4876.

[6] Burghardt, A., Bartelmus, G., and Gancarczyk, A., 1999. "Hydrodynamics of pulsing flow in three-phase chemical reactors". *Chemical Engineering and Processing*, **38** (4), pp. 411–426.

[7] Sicardi, S., Gerhard, H., and Hoffman, H., 1979. "Flow regime transition in trickle-bed reactors". *Chemical Engineering Journal*, **18** (3), pp. 173–182.

[8] Wilhite, B. A., Huang, X., McCready, M. J., and Varma, A., 2003. "Effects of induced pulsing flow on trickle-bed reactor performance". *Industrial and Engineering Chemical Research*, **42** (10), pp. 2139–2145.

[9] Bartelmus, G., Gancarczyk, A., and Stasiak, M., 1998. "Hydrodynamics of cocurrent fixed-bed three-phase reactors. Part I. The effect of physicochemical properties of the liquid on pulse velocity". *Chemical Engineering and Processing*, **37** (4), pp. 331–341.

[10] Burghardt, A., Bartelmus, G., Janecki, D., and Szlemp, A., 2002. "Hydrodynamics of a three-phase fixed-bed reactor operating in the pulsing flow regime at an elevated pressure". *Chemical Engineering Science*, **57** (22-23), pp. 4855–4863.

[11] Burghardt, A., Bartelmus, G., and Szlemp, A., 2004. "Hydrodynamics of pulsing flow in three-phase fixed-bed reactor operating at an elevated pressure". *Industrial and Engineering Chemistry Research*, **43** (16), pp. 4511–4521.

[12] Helwick, J. A., Dillon, P. O., and McCready, M. J., 1992. "Time varying behavior of cocurrent gas-liquid flows in packed beds". *Chemical Engineering Science*, **47** (13/14), pp. 3249–3256.

[13] Chou, T. S., Worley, Jr., F. L., and Luss, D., 1977. "Transition to pulsed flow in mixed-phase cocurrent downflow through a fixed bed". *Industrial and Engineering Chemistry, Process Design and Development*, **16** (3), pp. 424–427.

[14] Attou, A., and Ferschneider, G., 2000. "A two-fluid hydrodynamic model for the transition between trickle and pulse flow in a cocurrent gas-liquid packed-bed reactor". *Chemical Engineering Science*, **55** (3), pp. 491–511.

[15] Weekman, Jr., V. W., and Meyers, J. E., 1964. "Fluid flow characteristics of concurrent gas-liquid flow in packed beds". *AIChE Journal*, **10** (6), pp. 951–957.

[16] Xiao, Q., Anter, A. M., Cheng, Z. M., and Yuan, W. K., 2000. "Correlations for dynamic liquid holdup under pulsing flow in a trickle-bed reactor". *Chemical Engineering Journal*, **78** (2), pp. 125–129.

[17] Cho, J., Perlin, M., and Ceccio, S. L., 2005. "Measurement of near-wall stratified bubbly flows using electrical impedance". *Measurement Science and Technology*, **16** (4), pp. 1021–1029.

[18] Talmor, E., 1977. "Two-phase downflow through catalyst beds: Part 1. Flow maps". *AIChE Journal*, **23** (6), pp. 868–874.

[19] Beimesch, W. E., and Kessler, D. P., 1971. "Liquid-gas distribution measurements in the pulsing regime of two-phase concurrent flow in packed beds". *AIChE Journal*, **17** (5), pp. 1160–1165.

[20] Winterberg, M., and Tsotsas, E., 2000. "Impact of tube-to-particle-diameter ratio on pressure drop in packed beds". *AIChE Journal*, **46** (5), pp. 1084–1088.

[21] Chu, C. F., and Ng, K. M., 1989. "Flow in packed tubes with a small tube to particle diameter ratio". *AIChE Journal*, **35** (1), pp. 148–158.

[22] Cohen, Y., and Metzner, A. B., 1981. "Wall effect in laminar flow of fluids through packed beds". *AIChE Journal*, **27** (5), pp. 705–715.

[23] Talmor, E., 1977. "Two-phase downflow through catalyst beds: Part 2. Pulsing regime pressure drop". *AIChE Journal*, **23** (6), pp. 874–878.

Appendix E. 2005 ASME two-phase paper

Proceedings of FEDSM'05
ASME Fluids Engineering Division Summer Conference
June 19-23, 2005, Houston, Texas, USA

FEDSM2005-77157

AN EXPERIMENTAL INVESTIGATION OF THE EFFECT OF WALLS ON GAS-LIQUID FLOWS THROUGH FIXED PARTICLE BEDS

Marcia A. Cooper*
Raymond O. Cote
Timothy J. O'Hern
John R. Torczynski
Lindsey R. Evans
Sandia National Laboratories
Albuquerque, New Mexico 87185-5800
*Email: macoope@sandia.gov

William M. Cross
CR&L / CDTECH
Pasadena, Texas 77505

ABSTRACT

The effect of particle diameter on downward co-current gas-liquid flow through a fixed bed of particles confined within a cylindrical column is investigated. Several hydrodynamic regimes that depend strongly on the properties of the gas stream, the liquid stream, and the packed particle bed are known to exist within these systems. This experimental study focuses on characterizing the effect of wall confinement on these hydrodynamic regimes as the diameter d of the spherical particles becomes comparable to the column diameter D (or D/d becomes order-unity). The packed bed consists of polished, solid, spherical, monodisperse particles (beads) with mean diameter in the range of 0.64-2.54 cm. These diameters yield D/d values between 15 and 3.75, so this range overlaps and extends the previously investigated range for two-phase flow. Measurements of the pressure drop across the bed and across the pulses are obtained for varying gas and liquid flow rates.

NOMENCLATURE

D	column diameter, m
d	particle diameter, m
D_h	bed hydraulic diameter, Eq. 10, m
Fr	two-phase Froude number, Eq. 5
G	superficial mass flux of the gas phase, kg/m^{2}s
g	gravitational acceleration, m/s^2
h	bed height, m
L	superficial mass flux of the liquid phase, kg/m^{2}s
N	number of particles in bed
P	pressure, Pa
P^*	normalized pulse pressure drop, Eq. 4
Re	two-phase Reynolds number, Eq. 6
Re_d	modified particle Reynolds number, Eq. 2
V_b	bed volume filled with particles, m^3
V_s	volume of one particle, m^3
v_G	specific volume of gas phase, m^3/kg
v_L	specific volume of liquid phase, m^3/kg
v_{LG}	specific volume of two-phase mixture, Eq. 9, m^3/kg
We	two-phase Weber number, Eq. 7
w_L	superficial velocity of the liquid phase, m/s
ε	mean bed void fraction
μ_G	gas phase viscosity, Pa s
μ_L	liquid phase viscosity, Pa s
μ_{LG}	viscosity of two-phase mixture, Eq. 8, Pa s
ψ	modified pressure drop, Eq. 1
ρ_G	density of gas phase, kg/m^3
ρ_L	density of liquid phase, kg/m^3
σ_L	surface tension of liquid phase, N/m

*Address all correspondence to this author.

Copyright © 2005 by ASME

INTRODUCTION

The different hydrodynamic regimes that exist in gas-liquid downward flows through fixed beds of particles have been studied for the past several decades. Much of the early work is reviewed in Charpentier [1], Satterfield [2], and Tosun [3]. More recent work has focused on a better physical understanding of the conditions leading to the transition between [4–7] and the characterization of [8–11] these different operating regimes. Those experiments have been carried out in beds of small particles so that the wall effects are negligible and the bed void fraction is considered homogeneous. Even with particle beds that can be easily characterized, the complicated fluid dynamics have typically resulted in the derivation of empirical relations for dynamic liquid holdup and bed pressure drop from experimental data. In beds of large particles, radial variation of the bed void fraction invalidates the assumption of a homogeneous bed of particles. This additional complication in characterizing the particle bed with two-phase flows has not yet been adequately addressed in the literature.

There are four generally accepted hydrodynamic regimes in two-phase, co-current flow through fixed beds: trickle flow, pulse flow, bubble flow and spray flow [3, 7]. However, other investigators have defined only two regimes (high and low interaction) [4] or up to five regimes (bubbling/pulsing flow in addition to the four listed above) [12]. The conditions for operation within each of the regimes have historically been presented on flow maps with a variety of axis coordinates. The original flow maps [2, 13] were presented in terms of the superficial mass fluxes where the two phases consisted of air and water. Charpentier [1] later accounted for liquids other than water and gases other than air with a modification to the superficial mass fluxes. Correction factors based on the ratio of liquid properties such as density, viscosity, and surface tension, as well as the ratio of the gas-to-air density, all raised to some empirical power, were developed. Talmor [12] applied a more physical understanding of the driving and resistance forces that determine the operating regime in the derivation of his flow map, instead of relying on empirical corrections as was done previously. The driving forces consist of gravity and inertia, and the resistance forces consist of viscous and surface-tension forces. The effects of the particle size and shape, if considered, are typically included in the flow map through a constant value for the bed void fraction [4] or some form of a modified hydraulic radius [12].

Of the four major flow regimes, pulse flow has gained the most attention in recent years due to the possibility of increased throughput without flooding [14], increased mass and heat transfer rates [8], and complete wettability of the packing [5] for petrochemical reactions like hydrodesulphurization and hydrotreating [4]. In the creation of the above-mentioned flow maps, particular attention was placed on the boundary between trickle flow and pulse flow due to industrial units operating in pulse flow or near the transition [2]. However, data from fixed beds operating with co-current downflows of gas and liquid have generally been collected with packing particles that have a characteristic size that is orders of magnitude smaller than the column diameter. In this case, the transition between the trickle-flow and pulse-flow regimes is distinct.

When the particle size approaches the confining column size, the mean bed void fraction is greater than the range of void fractions, 0.36-0.40 [15], of an infinite bed of randomly packed spheres. In this case, the void fraction near the wall increases and the flow is affected [16–18]. This problem is different than that of regular, high-void-fraction packings (up to 0.70) being tested due to the development of more active catalysts which are allowing commercial units to operate at higher flow rates and lower pressure drops [19]. These high-void-fraction packings are composed of many smaller empty spaces while beds of spheres with diameters on the order of the column diameter are composed of fewer, but larger, empty spaces. Rather than studying the irregular and difficult-to-characterize high-void-fraction packings, an experimental study has been carried out with packed beds consisting of different-sized spherical beads in order to better understand the effect that the walls can have on the trickling and pulsing regimes of two-phase flow. The results are illustrated in terms of the total bed pressure drop and the local pressure variations within the bed.

PREVIOUS WORK STUDYING WALL EFFECTS

The wall effect on flow through packed beds has been extensively studied for single-phase flow where the competing effects of increased void fraction near the wall and wall friction determine the resulting pressure drop. The Ergun equation, which relates the pressure drop to the rate of fluid flow through the packed bed, is typically modified for the effect of non-uniform void fraction. Below some critical value of D/d, the effect of the wall becomes significant, and the Ergun equation no longer represents the measured pressure drop. The critical diameter ratio where wall effects become important is largely disputed in single-phase flows. Mehta and Hawley [20] suggest a critical diameter ratio less than 50:1, Cohen and Metzner [18] suggest a ratio less than 30:1 for Newtonian fluids, and Chu and Ng [17] suggest that the wall effect may become important for ratios less than 25:1 and most certainly become important for ratios less than 8:1. Methods to resolve the wall effect have implemented a modified hydraulic radius [21], or a relationship for the radial variation of void fraction either through a mathematical function [16, 17] or division of the column cross-section into two [22–24] or three [18, 22] regions of different void fractions. A large collection of data was effectively correlated for D/d ratios between 1.624 and 250 for a single phase flowing through a packed bed [21] using the hydraulic radius concept. The data

Copyright © 2005 by ASME

modified pressure drop

$$\psi = \frac{\Delta P}{\rho_L w_L^2} \frac{d}{h} \frac{\bar{\varepsilon}^3}{(1-\bar{\varepsilon})} \tag{1}$$

to the modified particle Reynolds number

$$Re_d = \frac{\rho_L w_L d}{\mu_L}(1-\bar{\varepsilon}) , \tag{2}$$

where ρ_L is the liquid density, w_L is the liquid superficial velocity, μ_L is the liquid viscosity, h is the bed height, d is the particle diameter, and $\bar{\varepsilon}$ is the mean bed void fraction.

While there are many studies investigating the wall effect on the hydrodynamic behavior of single-phase flow through packed beds, only a few studies [7, 12] have mentioned this issue for downward co-current two-phase flow, and no studies have been devoted entirely to determining how the confining walls influence the hydrodynamic regimes of two-phase flow. This study addresses the lack of experimental data in columns with low D/d ratios and co-current gas-liquid downflows. Observations of the flow regimes, including pressure histories, and total bed pressure drop as a function of particle size are presented below. The scope of this study is not to develop additional empirical relations but to focus on characteristics of the operating regimes and to observe how they change as the particle size increases.

EXPERIMENTAL FACILITY

The experiment consisted of a clear polycarbonate column packed with a bed of polished, solid, monodisperse, spherical, polypropylene spheres (beads), a liquid holding tank, and a liquid pump, as illustrated in Fig. 1. The column had a total height of 2.5 m, an inner diameter of 9.53 cm, and a wall thickness of 3.2 mm. Four separate beds, composed of beads with diameters equal to 0.64, 0.95, 1.27 and 2.54 cm, were tested. Bed specifics appear in Table 1. The bed void fraction ε was calculated from the volume of the column filled with particles V_b, the volume of one particle V_s, and the number of particles in the bed N.

$$\varepsilon = 1 - N\frac{V_s}{V_b} \tag{3}$$

The bottom of each bed was fixed 1 m from the bottom of column and held in place by a ring supporting a 3.8-cm-thick barrier layer of highly porous, filtration media with a specific surface area of 203 m^2/m^3. The beads were randomly packed by dropping them into the column from above until the bed height equaled 1.4 m. Deionized water and air both entered the column at a constant flow rate through the top flange and flowed

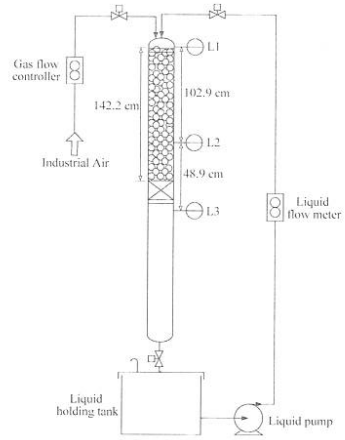

Figure 1. SCHEMATIC OF EXPERIMENT

Table 1. DETAILS OF PACKED BEDS

Bead diameter d (cm)	Bed void fraction ε	D/d
0.64	0.403	15.0
0.95	0.411	10.0
1.27	0.422	7.50
2.54	0.464	3.75

Table 2. EXPERIMENTAL PARAMETERS

Liquid density (kg/m^3)	ρ_L	997
Liquid viscosity (mPa s)	μ_L	0.856
Liquid mass flux (kg/m^2s)	L	0-66
Gas mass flux (kg/m^2s)	G	0-1.88

downward through the packed bed into the holding tank. The air vented to the surroundings and the liquid was recirculated to the top of the column. A centrally-located spray nozzle with spray holes angled at 30° to the vertical was used to distribute the water at the top of the column. Three pressure transducers were mounted along the column wall to measure pressure histories at specific locations (see Fig. 1). The measured pressures and flow rates were recorded by a LabView program for at least 15 seconds. The uncertainties for the experiment are ±8.7% in

Copyright © 2005 by ASME

15 seconds. Experimental repeatability was within $\pm 8.7\%$ in the pressure drop ΔP, $\pm 0.34\%$ in the superficial mass flux of the liquid phase L, and $\pm 0.29\%$ in the superficial mass flux of the gas phase G. The liquid flow meter had an accuracy of ± 0.20 LPM, the gas flow controller had an accuracy of ± 7 SLPM based on the manufacturer's specifications.

Measurements were obtained first with zero gas flow rate to ensure that the beads were completely wetted and maximize experimental repeatability. The gas flow rate was then increased incrementally. The bed pressure drop was determined by calculating the difference in the average pressure at the top (L1) and bottom (L3) measurement locations and was then normalized by the bed height h, gravitational acceleration g, and the water density ρ_L.

PULSE FLOW IN BEDS OF LARGE PARTICLES

Pulse flow has been described as repetitive slugs of liquid and gas [14] or a phase redistribution of a two-phase mixture [12]. Our observations and those of others [25, 26] were that, at low flow rates, the liquid flowed over the beads in continuous streams (trickle flow). An increase in either the liquid flow rate or the gas flow rate caused liquid-rich regions to form near the bottom of the packed bed (pulse flow). The liquid rich regions were pushed down the column and through the packed bed because of a pressure increase in the gas-rich region above the liquid plug. Further increases in either flow rate resulted in increases in the pulse frequency and the height of the pulse inception point, and decreases in the pulse height and the pulse pressure drop.

As stated in the introduction, the transition between the trickle-flow and pulse-flow regimes is of critical importance for the design of two-phase packed bed columns for commercial applications. Only a few models [7, 27, 28] have attempted to predict this flow-regime transition. Sicardi [4] has likened the pulsing phenomenon to the mechanism of annular two-phase flow in straight tubes in order to determine the basic conditions required for pulsing to exist. Most definitions of the flow-regime transition are based on experimental data, which has resulted in a variety of empirical relations.

In all of the above-mentioned models and empirical relations, the effect of D/d in two-phase flows has not been investigated over a sufficiently large range, unlike the case of single-phase flow in packed beds. This diameter ratio can significantly affect the flow characteristics within the packed bed. In beds with small particles or large D/d ratios, distinct pulses are observed over a wide range of flow rates. Due to the smaller voids between the particles, the liquid tends to plug these channels at relatively low flow rates.

Figure 2A shows three pressure histories at the location of L2 in the packed bed of 0.64-cm beads ($D/d = 15.0$, see Fig. 1) for the regimes of trickle flow (1) and pulse flow (2 and 3). Only minor pressure fluctuations are observed in the trickle-flow

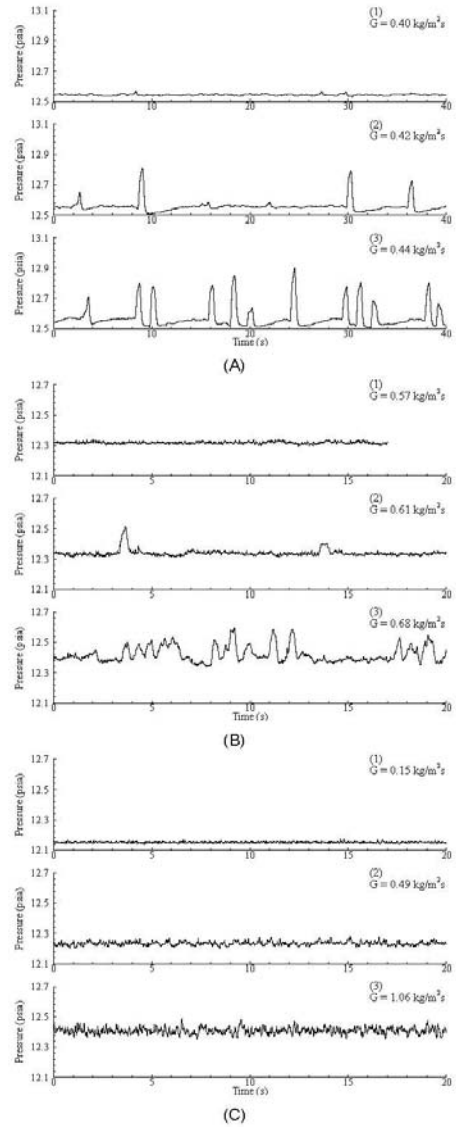

Figure 2. PRESSURE HISTORIES NEAR TRICKLE-PULSE TRANSITION FOR (A) d = 0.64 CM, L = 6.91 KG/M^{2}S, (B) d = 1.27 CM, L = 38.7 KG/M^{2}S, (C) d = 2.54 CM, L = 56.9 KG/M^{2}S.

Copyright © 2005 by ASME

regime (Fig. 2A-1) whereas the transition to pulse flow is noted by distinct pressure peaks that occur at fairly regular time intervals (Fig. 2A-2) as measured at a constant location within the packed bed. The pressure rises within the pulses are not equal. Immediately after a pulse passes, the pressure decreases to a minimum, indicating a net loss of liquid holdup [9]. The pressure then rises as the liquid holdup on the beads increases until the holdup is sufficient to span the column cross section and initiate the formation of a pulse.

Increasing the gas flow rate results in more pulses that travel through the bed per unit time (Fig. 2A-3). The induction time between pulses is intermittent and has been shown [9] to scale in a manner similar to that of turbulent bursts in a modified Taylor-Couette flow.

Increasing the bead size to 1.27 cm (D/d = 7.50) results in an increased number of small pressure oscillations in the trickle-flow and pulse-flow regimes (Fig. 2B). Additionally, the pulses become less obvious visually and in the pressure histories. The pulse irregularity is more prevalent as the bead size increases.

Finally, increasing the bead size to 2.54 cm (D/d = 3.75) results in additional increases in the small-scale pressure oscillations (Fig. 2C). No transition to pulsing was observed with the 2.54 cm beads for the experimental flow rates.

Thus, it is shown that a decrease in the D/d ratio results in higher-frequency, smaller-scale pressure oscillations within the packed bed during both the trickle-flow and pulse-flow regimes. Irregularities in the pulse height and frequency increase as the D/d ratio decreases. Significantly higher liquid and gas flow rates are required to achieve transition to pulsing in these large-particle beds.

TWO-PHASE PRESSURE DROP

The nondimensional bed pressure drop as a function of the gas mass flux is shown in Figs. 3A-C for three beds with different-sized beads and varying liquid mass fluxes. In all cases, the bed pressure drop increases with an increase in either the liquid or the gas mass flux. The data points where pulsing was first visually observed in Figs. 3A-C are noted with circles.

The smallest beads with diameters of 0.64 cm (D/d = 15.0) show a nearly constant increase in the average bed pressure drop with increasing gas mass fluxes (Fig. 3A). These trends have been previously noted in beds of particles with $D/d > 15$ [14,29]. At the lowest liquid mass flux, the pressure drop increases at a slower rate when the gas mass flux is low as compared to the rapid increase of the pressure drop at the highest liquid mass fluxes. Higher liquid mass fluxes cause the transition to pulse flow to occur at relatively lower gas mass fluxes, where the inclusion of the pulses within the bed are known to increase the average bed pressure drop over that of trickle flow [12]. The bed pressure drop for the 0.95-cm beads is not shown yet appears qualitatively similar to Fig. 3A but slightly lower in magnitude as

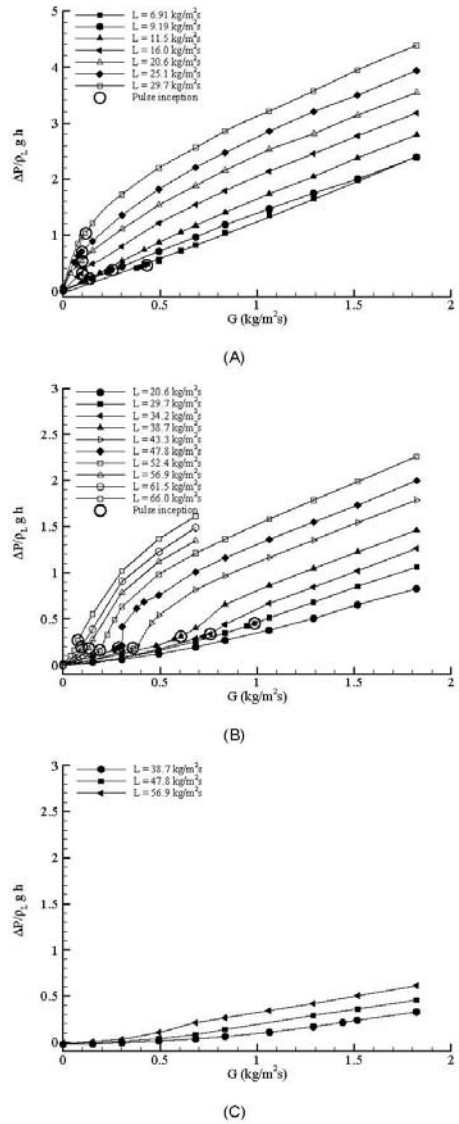

Figure 3. NORMALIZED BED PRESSURE DROP VERSUS GAS MASS FLUX FOR (A) d = 0.64 CM (B) d = 1.27 CM (C) d = 2.54 CM. CIRCLED SYMBOLS DENOTE PULSE INCEPTION.

Copyright © 2005 by ASME

expected due to the lower flow restriction provided by the larger beads and the higher bed void fraction.

The bed pressure drop for the 1.27-cm beads ($D/d = 7.50$) is plotted in Fig. 3B, and the same general trend of increasing pressure drop with either liquid or gas flow rate is shown. At the lowest liquid mass fluxes, the pressure drop increases gradually with increasing gas mass flux. As the liquid mass flux increases, a rapid change in the slope of the average bed pressure drop appears at conditions near where the pulses within the bed are visually observed. The presence of such a rapid change of the slope of the bed pressure drop as a function of the gas mass flux has not been previously noted since the literature contains only pressure drop data for two phases flowing in packed beds with larger D/d ratios.

The normalized bed pressure drop for the 2.54-cm beads ($D/d = 3.75$) is plotted in Fig. 3C for three liquid mass fluxes. Due to the large voids between particles, only trickle flow was visually observed for all of the test conditions. Higher liquid and gas flow rates that exceed the current experimental capabilities are required in order to achieve pulse flow. From the pressure data, a slight discontinuity is observed for the highest liquid flow rate tested, which indicates operation near the transition to pulse flow based on the previous results for the 1.27-cm beads. However, due to the significant flow along the inner surface of the tube, it was difficult to visually confirm the presence of pulses within the bed.

PULSE PRESSURE DROP AND TRANSITION BOUNDARY

To investigate the origin of the discontinuity in the slope of the average bed pressure drop discussed above, the magnitudes of the pressure oscillations within the bed (from location L2 in Fig. 1) were determined and compared to the total bed pressure drop. While it is known that the pulse characteristics depend on their location within the packed bed (i.e., the pulse inception point moves upward in the bed as the flow rates are increased, and the pulse velocity increases as the pulse travels downward through the bed), insight can be gained by a comparison of the flow within the bed to the behavior of the total bed.

The maximum average pressure drop across a pulse is determined from the pressure history at L2 and averaging the three pulses with the greatest change in pressure. An example pressure trace is shown in Fig. 4 with the three selected pulses used to determine the maximum average pulse pressure drop noted.

Figures 5A-C plot the parameter P^*, defined as the maximum average pressure drop across a pulse within the packed bed normalized by the total average bed pressure drop ΔP, as a function of the gas mass flux:

$$P^* = \frac{(P_1 + P_2 + P_3)/3}{\Delta P} . \qquad (4)$$

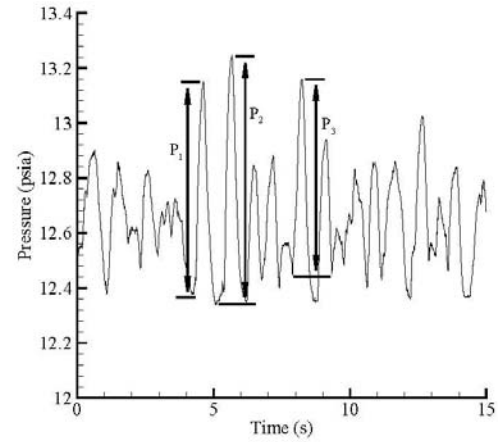

Figure 4. DETERMINATION OF MAXIMUM AVERAGE PULSE PRESSURE DROP: d = 1.27 CM, L = 43.3 KG/M^{2}S, G = 0.49 KG/M^{2}S.

The locations at which pulses were first visually observed are noted on Figs. 5A-C by circles surrounding the test conditions. If a data series does not contain a circle (see Figs. 5B and 5C), then transition did not occur, and the bed operated in the trickle-flow regime. In the trickle-flow regime, no significant pressure oscillations were observed, as noted by values of P^* much less than the P^* values in the pulse-flow regime (Fig. 5B). As noted previously, the gas-flow rate at which pulsing was first observed decreased with increasing liquid-flow rate, in cases in which pulsing did occur within the bed. After the initial observation of pulses within the bed, the maximum average pulse pressure drop was found to increase to a maximum fraction of the total bed pressure drop before decreasing. Although the values of P^* decreased, pulses remained present within the bed. If the experimental capabilities enabled higher gas and liquid flow rates, the pulses would continue to be damped out until the bubble-flow regime was reached.

It is interesting to note that the conditions under which pulsing became visually obvious correspond to values of $P^* = 0.2$ for the 0.64-cm beds and increased to $P^* = 0.3$ for the 1.27 cm beads. Transition to pulse flow seems to occur at a consistent value of P^* for a given value of D/d which increases as D/d decreases. This appears to be a condition from which the transition to pulsing can be inferred. For the case of the 2.54-cm beads, the maximum values of P^* did not exceed 0.3, further indicating that the pulse-flow regime was not reached. Values of P^* are not shown for $G < 0.5$ kg/m^{2}s due to the uncertainty in the

Copyright © 2005 by ASME

pressure measurements for the nearly-zero values of the pressure drop (see Fig. 3C).

The results of this study clearly show that the particle size can significantly impact the flow regimes, so comparisons must be made to a map that incorporates the column diameter and characteristic particle size. The flow map of Talmor [12] is chosen. The transition boundary results of this study are plotted on the flow map of Talmor [12] in Fig. 6 for the beds with the 0.64-cm, 0.95-cm, and 1.27-cm beads. The results for the 2.54-cm beads are not plotted on the flow map since no transition to pulse flow was observed either visually or by inspection of pressure histories within the bed. An increase in the experimental flow capabilities is needed in order to determine the transition location for these largest particles. The solid symbols correspond to pulse flow, and the open symbols correspond to trickle flow.

The coordinate axes consist of the volumetric gas-to-liquid ratio $(G/L)(\rho_L/\rho_G)$ on the y-axis and a ratio of nondimensional numbers $[1 + (1/Fr)] / [We + (1/Re)]$ on the x-axis. This ratio takes into account the driving forces of gravity and inertia and the viscous and surface-tension resistance forces. The gravity-to-inertia-force ratio is represented by the two-phase Froude number

$$Fr = \frac{[(L+G)v_{LG}]^2}{gD_h}, \tag{5}$$

the viscous-to-inertia-force ratio is represented by the two-phase Reynolds number

$$Re = \frac{D_h(L+G)}{\mu_{LG}}, \tag{6}$$

and the inertia-to-surface-tension-force ratio is represented by the two-phase Weber number

$$We = \frac{D_h(L+G)^2 v_{LG}}{\sigma_L}. \tag{7}$$

In these definitions, the two-phase viscosity μ_{LG} and specific volume v_{LG} correspond to the average properties of the two phases:

$$\mu_{LG} = \mu_L \frac{(L/G)}{1+(L/G)} + \mu_G \frac{1}{1+(L/G)}, \tag{8}$$

$$v_{LG} = v_L \frac{(L/G)}{1+(L/G)} + v_G \frac{1}{1+(L/G)}. \tag{9}$$

The parameter D_h is the bed hydraulic diameter:

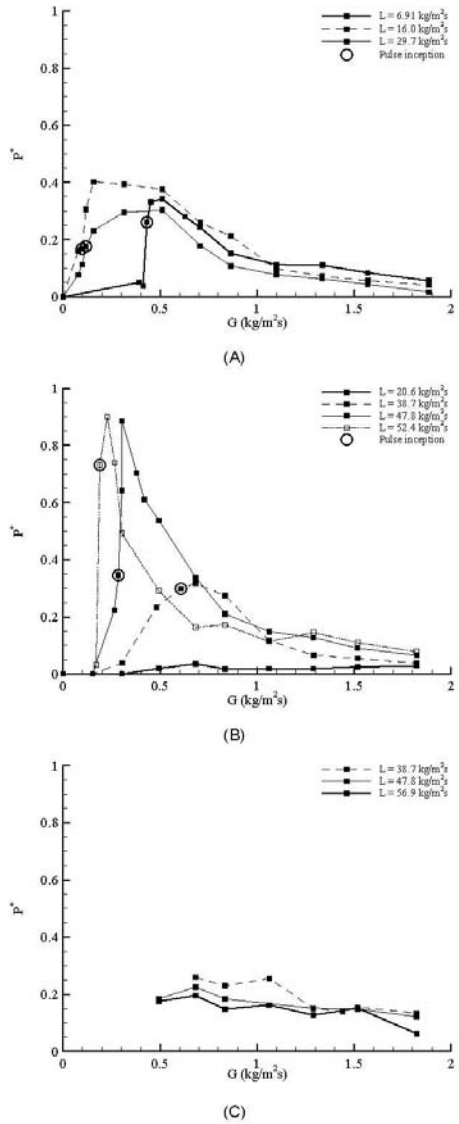

Figure 5. NORMALIZED PRESSURE ACROSS PULSE VERSUS GAS MASS FLUX FOR (A) d = 0.64 CM (B) d = 1.27 CM (C) d = 2.54 CM. CIRCLED SYMBOLS DENOTE PULSE INCEPTION.

Copyright © 2005 by ASME

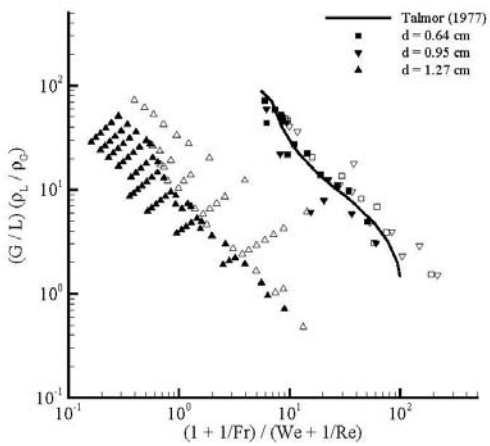

Figure 6. FLOW MAP SHOWING TRICKLE-PULSE FLOW TRANSITION FOR ALL BEADS. SOLID SYMBOLS CORRESPOND TO PULSE FLOW, AND OPEN SYMBOLS CORRESPOND TO TRICKLE FLOW.

$$D_h = \frac{2\varepsilon D}{2+3(1-\varepsilon)(D/d)}. \tag{10}$$

The trickle-pulse boundary of the flow map [12] was determined with experimental data for a range of diameter ratios D/d between 83 and 10.7. The transition points for the 0.64-cm and 0.95-cm beads match the transition line as expected since their values of D/d equal 15 and 10. Thus, wall effects and particle diameter variations are effectively captured by the relationship for the bed hydraulic diameter (Eq. 10). Near transition for the 0.64-cm and 0.95-cm beads, $(1/Fr) \sim 1$, $We \sim 0.1$, and $(1/Re) \sim 0.001$, indicating that the inertia-to-surface-tension-force ratio is dominant. The effect of the column wall is obvious for the 1.27-cm beads with $D/d = 7.5$, for which the transition boundary is shifted towards the origin. The higher-void-fraction bed is not effectively correlated by the coordinates of the flow map. Near transition for 1.27-cm beads, $(1/Fr) \sim 1$, $We \sim 1$, and $(1/Re) \sim 0.0001$, indicating that the gravity-to-inertia-force ratio is no longer negligible as comparable to the inertia-to-surface-tension-force ratio. In this case, the liquid surface tension is not sufficient to increase the holdup on the beads to enable the liquid to bridge the large open spaces between the beads, but rather this necessary process for pulse flow is inhibited by gravity.

The experimental observations of Tosun [3] do not support the trickle-pulse transition boundary of Talmor [12] even though air and water are used and the bed particles have a sufficiently large $D/d = 27$ so that wall effects are negligible. Tosun [3] does not offer an explanation for this discrepancy but instead concludes that the flow map of Talmor [12] is unreliable. Instead, Tosun [3] supports the flow map of Charpentier [1] which does not account for the bed void fraction or particle size. As stated previously, comparisons of the experimental data in this study must be made to flow map that accounts for variations in D/d, such as the flow map of Talmor [12].

CONCLUSIONS

An investigation was carried out to experimentally determine the effect that the particle size has on the transition and the characteristics of the pulse-flow regime in two-phase co-current downflow of air and water through a fixed bed of particles. Tests were performed with different-sized beads with D/d ratios between 15 and 3.75, which extended the range of previous data for two-phase flow. While the effect of this ratio has been well studied in single-phase downflow through packed beds, no previous study has systematically addressed the issue in two-phase flow.

It was shown that increasing the bead diameter generated a rapid increase in the slope of the average bed pressure drop that corresponded to the conditions at which pulsing was visually apparent within the bed. Under these conditions, the maximum average pulse pressure drop became a significant fraction of the total bed pressure drop, and the transition to pulsing occurred at almost a consistent 0.2 for the 0.64-cm beads and 0.3 for the 1.27-cm beads. While it became visually more difficult to identify when transition to pulsing occurred as the bead size increased, analysis of the pressure histories at a location within the bed can be used to determine criteria to define pulsing.

Plotting the pulse-flow-regime transition points for the different bead diameters on the existing flow map of Talmor [12] shows that the map does not effectively correlate all data with the lower D/d ratios. Further investigation is required in order to account for the increased void fraction and wall effects in fixed beds of large particles.

Thus, the effect of the D/d ratio can be significant in determining the characteristics of the pulse-flow regime and the transition boundary for pulse flow. Experiments have been carried out to illustrate the magnitude of this effect and highlight the importance of carefully determining the packing specifics required in order to achieve the desired pulse characteristics for critical commercial applications.

ACKNOWLEDGMENT

The financial support of the US Department of Energy Office of Industrial Technologies, Brian Valentine, contract monitor, is acknowledged. Additional support has been provided by CR&L / CDTECH. Sandia is a multiprogram laboratory operated by Sandia Corporation, a Lockheed Martin Company, for

Copyright © 2005 by ASME

the United States Department of Energy's National Nuclear Security Administration under Contract DE-AC04-94AL85000.

REFERENCES

[1] Charpentier, J., 1976. "Recent progress in two phase gas-liquid mass transfer in packed beds". *Chemical Engineering Journal,* **11**(3), pp. 161–181.

[2] Satterfield, C. N., 1975. "Trickle-bed reactors". *AIChE Journal,* **21**(2), pp. 209–228.

[3] Tosun, G., 1984. "A study of cocurrent downflow of nonfoaming gas-liquid systems in a packed bed. 1. Flow regimes: Search for a generalized flow map". *Industrial and Engineering Chemistry Process Design and Development,* **23**(1), pp. 29–35.

[4] Sicardi, S., Gerhard, H., and Hoffman, H., 1979. "Flow regime transition in trickle-bed reactors". *Chemical Engineering Journal,* **18**(3), pp. 173–182.

[5] Burghardt, A., Bartelmus, G., and Gancarczyk, A., 1999. "Hydrodynamics of pulsing flow in three-phase chemical reactors". *Chemical Engineering and Processing,* **38**(4), pp. 411–426.

[6] Sicardi, S., and Hofmann, H., 1980. "Influence of gas velocity and packing geometry on pulsing inception in trickle-bed reactors". *Chemical Engineering Journal and the Biochemical Engineering Journal,* **20**(3), pp. 251–253.

[7] Attou, A., and Ferschneider, G., 2000. "A two-fluid hydrodynamic model for the transition between trickle and pulse flow in a cocurrent gas-liquid packed-bed reactor". *Chemical Engineering Science,* **55**(3), pp. 491–511.

[8] Boelhouwer, J. G., Piepers, H. W., and Drinkenburg, A. A. H., 2002. "Nature and characteristics of pulsing flow in trickle-bed reactors". *Chemical Engineering Science,* **57**(22–23), pp. 4865–4876.

[9] Helwick, J. A., Dillon, P. O., and McCready, M. J., 1992. "Time varying behavior of cocurrent gas-liquid flows in packed beds". *Chemical Engineering Science,* **47**(13/14), pp. 3249–3256.

[10] Saez, A. E., and Carbonell, R. G., 1985. "Hydrodynamic parameters for gas-liquid cocurrent flow in packed beds". *AIChE Journal,* **31**(1), pp. 52–62.

[11] Xiao, Q., Anter, A. M., Cheng, Z. M., and Yuan, W. K., 2000. "Correlations for dynamic liquid holdup under pulsing flow in a trickle-bed reactor". *Chemical Engineering Journal,* **78**(2), pp. 125–129.

[12] Talmor, E., 1977. "Two-phase downflow through catalyst beds: Part 1. Flow maps". *AIChE Journal,* **23**(6), pp. 868–874.

[13] Weekman, Jr., V. W., and Meyers, J. E., 1964. "Fluid flow characteristics of concurrent gas-liquid flow in packed beds". *AIChE Journal,* **10**(6), pp. 951–957.

[14] Blok, J. R., Varkevisser, J., and Drinkenburg, A. A. H., 1983. "Transition to pulsing flow, holdup and pressure drop in packed columns with cocurrent gas-liquid downflow". *Chemical Engineering Science,* **38**(5), pp. 687–699.

[15] Valtsifer, V., and Zvereva, N., 1999. "Statistical packing of equal spheres". *Advanced Powder Technology,* **10**(4), pp. 399–403.

[16] Winterberg, M., and Tsotsas, E., 2000. "Impact of tube-to-particle-diameter ratio on pressure drop in packed beds". *AIChE Journal,* **46**(5), pp. 1084–1088.

[17] Chu, C. F., and Ng, K. M., 1989. "Flow in packed tubes with a small tube to particle diameter ratio". *AIChE Journal,* **35**(1), pp. 148–158.

[18] Cohen, Y., and Metzner, A. B., 1981. "Wall effect in laminar flow of fluids through packed beds". *AIChE Journal,* **27**(5), pp. 705–715.

[19] Miller, C., and Kaibel, G., 2004. "Packings for fixed bed reactors and reactive distillation". *Chemical Engineering Science,* **59**(22–23), pp. 5373–5379.

[20] Mehta, D., and Hawley, M. C., 1969. "Wall effect in packed columns". *I & EC Process Design and Development,* **8**(2), pp. 280–282.

[21] Eisfeld, B., and Schnitzlein, K., 2001. "The influence of confining walls on the pressure drop in packed beds". *Chemical Engineering Science,* **56**(14), pp. 4321–4329.

[22] Nield, D. A., 1983. "Alternative model for wall effect in laminar flow of a fluid through a packed column". *AIChE Journal,* **29**(4), pp. 688–689.

[23] Tosun, I., and Mousa, H., 1986. "Flow through packed beds: wall effect on drag force". *Chemical Engineering Science,* **41**(11), pp. 2962–2965.

[24] Felice, R. D., and Gibilaro, L. G., 2004. "Wall effects for the pressure drop in fixed beds". *Chemical Engineering Science,* **59**(14), pp. 3037–3040.

[25] Bartelmus, G., Gancarczyk, A., and Stasiak, M., 1998. "Hydrodynamics of cocurrent fixed-bed three-phase reactors. Part I. The effect of physicochemical properties of the liquid on pulse velocity". *Chemical Engineering and Processing,* **37**(4), pp. 331–341.

[26] Ratheesh, S., and Kannan, A., 2004. "Holdup and pressure drop studies in structured packings with catalysts". *Chemical Engineering Journal,* **104**(1–3), pp. 45–54.

[27] Iliuta, I., and Larachi, F., 2004. "Onset of pulsing in gas-liquid trickle bed filtration". *Chemical Engineering Science,* **59**(6), pp. 1199–1211.

[28] Holub, R. A., Dudukovic, M. P., and Ramachandran, P. A., 1993. "Pressure drop, liquid holdup and flow regime transition in trickle flow". *AIChE Journal,* **39**(2), pp. 302–321.

[29] Wammes, W. J. A., Mechielsen, S. J., and Westerterp, K. R., 1991. "The influence of pressure on the liquid hold-up in a cocurrent gas-liquid trickle-bed reactor operating at low gas velocities". *Chemical Engineering Science,* **46**(2), pp. 409–417.

Copyright © 2005 by ASME

Appendix F. Two-Phase Data Sets

1/4-in PP beads

Exp No.	Gas (scfm)	Liq(gpm)	P_top(psia)	P_mid2(psia)	P_bot(psia)
116	0	-0.77	12.012	------	12.208
117	0	1.829169	11.843	------	12.204
118	0.5	1.795873	13.465	------	12.2
119	1	1.860384	13.791	------	12.195
120	1.5	1.889518	13.907	------	12.194
121	2	1.889518	13.991	------	12.191
122	2.5	1.839574	14.006	------	12.189
123	3	1.829169	14.197	------	12.187
124	3.5	1.843736	14.316	------	12.188
125	4	1.837493	14.359	------	12.184
126	4.5	1.8281285	14.455	------	12.186
127	5	1.8489385	14.503	------	12.186
128	5.5	1.835412	14.6	------	12.185
129	6	1.83125	14.74	------	12.183
130	6.5	1.8531005	14.853	------	12.185
131	7	1.839574	14.949	------	12.185
132	7.5	1.839574	15.059	------	12.186
133	8	1.879113	15.229	------	12.189
134	8.5	1.839574	15.299	------	12.191
135	9	1.7823465	15.348	------	12.192
136	24	1.8052375	18.272	------	12.252
137	1	1.874951	13.567	------	12.178
138	1	1.868708	13.426	------	12.178
140	5.5	1.8406145	14.522	------	12.091
141	5.5	1.835412	14.515	------	12.093
142	3.5	1.856222	14.085	------	12.09
143	3.5	1.8531005	13.999	------	12.09
144	0.5	1.839574	13.07	------	12.091
145	0.5	1.841655	12.958	------	12.088
146	6	1.8468575	14.633	------	12.096
147	6	1.85206	14.582	------	12.097
148	12	1.8468575	15.978	------	12.111
149	15	1.8489385	16.572	------	12.121

Exp No.	Gas (scfm)	Liq(gpm)	P_top(psia)	P_mid2(psia)	P_bot(psia)
150	18	1.827088	17.117	------	12.131
151	22	1.8468575	18.005	------	12.151
153	1	4.430419	15.357	------	12.145
154	1.5	4.4647555	16.091	------	12.145
155	2	4.3960825	16.548	------	12.14
157	0	1.3224455	11.901	------	12.13
158	3	4.4481075	17.46	------	12.134
159	4	4.4335405	17.773	------	12.138
160	5	4.4564315	18.163	------	12.144
161	6	4.4668365	18.434	------	12.145
162	7	4.455391	18.684	------	12.146
163	9	4.488687	19.207	------	12.155
164	11	4.4148115	19.597	------	12.162
165	13	4.459553	20.14	------	12.167
166	15	4.459553	20.645	------	12.179
167	17	4.449148	21.11	------	12.191
168	19	4.442905	21.544	------	12.202
169	21	4.4501885	21.915	------	12.215
170	24	4.4293785	22.616	------	12.233
171	5	1.311	14.7	------	
177	0	1.8489385	26.762	------	12.142
178	1	1.8447765	28.418	------	12.148
179	2	1.827088	28.708	------	12.15
180	3	1.8489385	28.956	------	12.152
181	4	1.8343715	29.14	------	12.154
182	5	1.837493	29.36	------	12.156
183	6	1.837493	29.561	------	12.154
185	0	0.3256465	26.665	------	11.936
186	0	1.3224455	26.665	------	11.939
187	0	2.1090635	26.483	------	11.941
188	1	0.3277275	26.697	------	11.938
189	2	0.341254	26.729	------	11.94
190	3	0.3318895	26.773	------	11.944
191	4	0.318363	26.832	------	11.946
192	5	0.8021955	27.601	------	11.963
193	4	0.7897095	17.365	------	11.966

Exp No.	Gas (scfm)	Liq(gpm)	P_top(psia)	P_mid2(psia)	P_bot(psia)
194	3	0.8271675	26.97	------	11.971
195	7	0.7251985	27.797	------	11.976
196	10	0.7813855	28.64	------	11.984
197	14	0.8084385	29.519	------	12
198	2	1.325567	27.572	------	11.98
199	3	1.2933115	27.787	------	11.983
200	1	1.365106	26.757	------	11.981
201	2	3.3680685	29.771	------	11.991
202	5	3.4013645	29.771	------	12.002
203	4	2.4004035	29.771	------	12
204	5	2.370229	29.771	------	12.003
205	3	2.363986	29.658	------	12.001
206	2	2.3920795	29.341	------	12.001
207	24	2.3567025	29.771	------	12.083
209	5.002	0.8001145	13.064	------	12.229
210	4.749	0.784507	13.025	------	12.228
211	4.504	0.7938715	13.019	------	12.229
212	4.255	0.7959525	12.941	------	12.23
213	4	0.8001145	12.922	------	12.23
214	3.747	0.813641	12.856	------	12.23
215	3.495	0.8001145	12.745	------	12.228
216	3.253	0.79075	12.695	------	12.23
217	2.999	0.799074	12.663	------	12.23
218	2.751	0.796993	12.589	------	12.229
219	2.508	0.8042765	12.538	------	12.23
220	2.243	0.8063575	12.45	------	12.23
221	2	0.784507	12.361	------	12.23
222	4.997	1.0685635	13.491	------	12.233
223	4.745	1.052956	13.46	------	12.236
224	4.502	1.0519155	13.426	------	12.235
225	4.245	1.0560775	13.376	------	12.236
226	3.998	1.0498345	13.345	------	12.235
227	3.748	1.046713	13.317	------	12.235
228	3.503	1.0581585	13.264	------	12.235
229	3.25	1.0664825	13.225	------	12.234
230	3.002	1.0456725	13.167	------	12.234

Exp No.	Gas (scfm)	Liq(gpm)	P_top(psia)	P_mid2(psia)	P_bot(psia)
231	2.75	1.050875	13.133	------	12.231
232	2.504	1.0539965	13.082	------	12.234
233	2.254	1.050875	13.05	------	12.234
234	2.002	1.0623205	13.01	------	12.232
235	1.752	1.073766	12.937	------	12.232
236	1.497	1.042551	12.838	------	12.23
237	1.25	1.0581585	12.764	------	12.231
238	0.998	1.0602395	12.599	------	12.228
239	3.002	1.311	13.195	------	12.216
240	2.746	1.300595	13.178	------	12.214
241	2.5	1.306838	13.204	------	12.213
242	2.247	1.327648	13.172	------	12.212
243	2.007	1.3037165	13.127	------	12.21
244	1.747	1.3141215	13.049	------	12.212
245	1.497	1.3286885	12.974	------	12.21
246	1.25	1.311	12.9	------	12.209
247	0.999	1.325567	12.801	------	12.208
248	0.753	1.308919	12.668	------	12.208
249	0.5	1.3037165	12.468	------	12.205
250	0.244	1.329729	12.184	------	12.203
251	4.001	1.839574	14.411	------	12.209
252	3.5	1.837493	15.1	------	12.207
253	3	1.8322905	14.192	------	12.207
254	2.501	1.843736	14.097	------	12.206
255	2.247	1.8322905	14.032	------	12.204
256	1.999	1.8239665	13.967	------	12.205
257	1.748	1.822926	13.889	------	12.206
258	1.499	1.835412	13.803	------	12.204
259	1.251	1.818764	13.671	------	12.202
260	1.003	1.83125	13.534	------	12.202
261	0.752	1.841655	13.322	------	12.202
262	3.997	1.5763275	14.051	------	12.194
263	3.494	1.5638415	13.963	------	12.194
264	2.998	1.558639	13.873	------	12.193
265	2.748	1.5721655	13.848	------	12.193
266	2.504	1.569044	13.797	------	12.193

Exp No.	Gas (scfm)	Liq(gpm)	P_top(psia)	P_mid2(psia)	P_bot(psia)
267	2.249	1.571125	13.767	------	12.193
268	1.999	-0.4984295	13.706	------	12.193
269	1.749	1.587773	13.665	------	12.192
270	1.5	1.573206	13.589	------	12.191
271	1.248	1.583611	13.52	------	12.192
272	5.002	2.3515	15.525	------	12.196
273	4.001	2.3379735	15.319	------	12.195
274	3.75	2.349419	15.288	------	12.194
275	3.503	2.380634	15.241	------	12.193
276	3.255	2.3546215	15.183	------	12.191
277	3.007	2.376472	15.14	------	12.191
278	2.75	2.370229	15.087	------	12.19
279	2.501	2.3712695	15.003	------	12.189
280	2.247	2.355662	14.942	------	12.188
281	4.997	0.794912	12.881	12.528	12.227
282	5.246	0.7938715	12.915	12.543	12.227
283	5.503	0.805317	12.973	12.563	12.226
284	5.749	0.79075	13.017	12.575	12.226
285	6.499	0.801155	13.181	12.631	12.227
286	7.997	0.8063575	13.51	12.738	12.23
287	8.989	0.7876285	13.7	12.796	12.23
288	10.999	0.7980335	14.146	12.942	12.235
289	14.002	0.7917905	14.767	13.143	12.241
290	17.013	0.8021955	15.366	13.344	12.249
291	19.995	0.7959525	16.031	13.568	12.258
292	23.999	0.7876285	16.836	13.843	12.27
293	1.253	1.3162025	12.365	12.377	12.223
294	1.5	1.3162025	12.426	12.397	12.222
295	1.747	1.300595	12.493	12.417	12.224
296	2.002	1.313081	12.566	12.439	12.224
297	2.498	1.3016355	12.696	12.484	12.225
298	4.003	1.323486	13.123	12.615	12.226
299	5.502	1.308919	13.513	12.741	12.226
300	6.511	1.313081	13.792	12.833	12.226
301	7.997	1.3057975	14.156	12.942	12.23
302	9.001	1.308919	14.405	13.021	12.232

Exp No.	Gas (scfm)	Liq(gpm)	P_top(psia)	P_mid2(psia)	P_bot(psia)
303	11.011	1.3162025	14.874	13.173	12.237
304	13.996	1.311	15.536	13.387	12.245
305	17.005	1.304757	16.16	13.596	12.253
306	19.985	1.3162025	16.84	13.823	12.264
307	24.015	1.33181	17.675	14.116	12.278
308	1.001	1.8426955	12.56	12.449	12.225
309	1.248	1.814602	12.678	12.485	12.226
310	1.503	1.8426955	12.85	12.539	12.229
311	2.001	1.8364525	13.022	12.587	12.227
312	4.001	1.829169	13.653	12.783	12.228
313	6.501	1.8489385	14.478	13.045	12.232
314	9.003	1.8302095	15.139	13.263	12.238
315	11.002	1.825007	15.647	13.419	12.243
316	13.998	1.841655	16.348	13.643	12.252
317	17	1.8239665	16.988	13.858	12.262
318	19.999	1.843736	17.635	14.077	12.272
319	24.003	1.8426955	18.461	14.369	12.289
320	6.505	0.8001145	13.11	12.618	12.215
321	0.01	0.794912	12.051	12.25	12.21
322	0.01	1.313081	12.054	12.254	12.21
323	0.01	1.8343715	12.051	12.25	12.214
324	0.01	2.3587835	12.052	12.249	12.207
325	0.497	2.332771	12.665	12.464	12.21
326	1.001	2.3234065	12.958	12.558	12.209
327	1.251	2.3442165	13.095	12.597	12.209
328	2.004	2.3546215	13.463	12.7	12.208
329	4.004	2.3442165	14.228	12.936	12.208
330	6.504	2.368148	15.089	13.211	12.21
331	9.004	2.349419	15.787	13.441	12.215
332	10.998	2.363986	16.34	13.618	12.22
333	13.997	2.3525405	17.087	13.856	12.229
334	17.031	2.3587835	17.67	14.05	12.239
335	20.004	2.3442165	18.337	14.276	12.251
336	24.007	2.345257	19.153	14.56	12.262
337	1.003	2.347338	12.879	12.511	12.184
338	0.01	2.8831955	12.116	12.254	12.178

Exp No.	Gas (scfm)	Liq(gpm)	P_top(psia)	P_mid2(psia)	P_bot(psia)
339	0.759	2.861345	13.028	12.555	12.179
340	1.004	2.8831955	13.232	12.623	12.177
341	1.25	2.8831955	13.386	12.672	12.177
342	1.994	2.861345	13.765	12.782	12.176
343	4.002	2.8623855	14.697	13.063	12.176
344	6.497	2.8727905	15.616	13.353	12.178
345	9.004	2.859264	16.406	13.609	12.182
346	10.989	2.853021	16.933	13.775	12.189
347	14.003	2.873831	17.709	14.036	12.198
348	17.011	2.873831	18.418	14.268	12.209
349	19.995	2.87175	19.02	14.477	12.222
350	24.006	2.867588	19.913	14.793	12.241
351	0.01	1.044632	11.993	12.194	12.16
352	1.993	1.0602395	12.433	12.368	12.159
353	3.007	1.0560775	12.676	12.43	12.159
354	3.248	1.050875	12.741	12.437	12.158
355	4.002	1.0539965	12.862	12.474	12.157
356	6.502	1.0748065	13.405	12.653	12.16
357	9.007	1.0644015	13.914	12.816	12.163
358	11.002	1.0539965	14.361	12.945	12.166
359	14.002	1.0560775	14.934	13.132	12.175
360	17.002	1.0519155	15.496	13.319	12.183
361	20.007	1.0581585	16.009	13.493	12.191
362	23.991	1.044632	16.81	13.771	12.206
363	1.004	3.3909595	13.672	12.782	12.158
364	1.497	3.410729	14.046	12.892	12.159
365	1.251	3.408648	13.903	12.852	12.159
366	2.001	3.410729	14.406	12.992	12.159
367	0.01	3.4034455	12.115	12.251	12.156
368	4.003	3.4159315	15.431	13.293	12.159
369	6.5	3.402405	16.374	13.587	12.164
370	8.999	3.389919	17.106	13.832	12.17
371	10.999	3.392	17.706	14.035	12.179
372	13.991	3.392	18.429	14.266	12.19
373	16.995	3.3826355	19.159	14.509	12.202
374	19.99	3.3992835	19.924	14.769	12.216

Exp No.	Gas (scfm)	Liq(gpm)	P_top(psia)	P_mid2(psia)	P_bot(psia)
375	24.005	3.394081	20.823	15.06	12.237
658	0.498	3.381595	13.085	12.092	12.056
659	1.001	3.408648	13.484	12.108	12.056
660	1.25	3.400324	13.602	12.113	12.056
661	1.501	3.4055265	13.79	12.119	12.056
662	1.998	3.381595	14.046	12.123	12.056
663	2.499	3.387838	14.267	12.13	12.057
664	3.002	3.3888785	14.492	12.139	12.057
665	0.064	5.462595	12.268	12.042	12.034
666	1.004	5.450109	14.215	12.137	12.058
667	1.256	5.468838	14.547	12.147	12.058
668	1.502	5.481324	14.845	12.158	12.058
669	1.999	5.470919	15.54	12.184	12.06
670	2.5	5.4990125	16.036	12.204	12.061
671	3	5.4657165	16.502	12.224	12.062
672	0.046	1.325567	11.867	12.051	1.054
673	1.002	1.340134	12.066	12.062	12.055
674	1.501	1.321405	12.354	12.072	12.054
675	1.747	1.3120405	12.487	12.075	12.055
676	1.998	1.323486	12.565	12.076	12.056
677	2.498	1.3162025	12.66	12.076	12.055
678	3.001	1.311	12.762	12.077	12.056
679	0.054	3.4076075	11.87	12.046	12.054
680	1.001	3.3930405	13.491	12.112	12.058
681	1.249	3.4034455	13.643	12.117	12.06
682	1.501	3.381595	13.803	12.122	12.06
683	2.001	3.4034455	14.108	12.13	12.059
684	2.5	3.387838	14.352	12.138	12.06
685	2.999	3.398243	14.566	12.142	12.06
686	0.052	5.4844455	12.369	12.059	12.049
687	1.002	5.485486	14.409	12.144	12.062
688	1.254	5.504215	14.694	12.157	12.064
689	1.504	5.462595	15.02	12.169	12.064
690	2.003	5.4886075	15.581	12.19	12.065
691	2.498	5.4927695	16.093	12.208	12.066
692	3	5.4823645	16.478	12.223	12.067

Exp No.	Gas (scfm)	Liq(gpm)	P_top(psia)	P_mid2(psia)	P_bot(psia)
693	0.063	1.3224455	11.871	12.055	12.059
694	1.001	1.3224455	12.085	12.064	12.059
695	1.499	1.3099595	12.431	12.078	12.059
696	1.752	1.3078785	12.555	12.081	12.06
697	2.002	1.321405	12.641	12.083	12.06
698	2.5	1.302676	12.732	12.083	12.061
699	2.999	1.300595	12.779	12.083	12.06
704	2.997	3.3930405	14.598	12.191	12.111
705	0.046	3.408648	12.024	12.1	12.108
706	1.005	3.3888785	13.538	12.159	12.11
707	1.253	3.392	13.681	12.164	12.109
708	1.5	3.404486	13.871	12.168	12.109
709	1.997	3.4159315	14.159	12.176	12.108
710	2.499	3.373271	14.356	12.18	12.108
711	3	3.400324	14.624	12.191	12.109
712	0.04	5.5468755	12.426	12.101	12.09
713	1.002	5.481324	14.352	12.188	12.11
714	1.249	5.4677975	14.666	12.2	12.109
715	1.496	5.473	14.951	12.212	12.11
716	1.999	5.466757	15.574	12.231	12.109
717	2.496	5.464676	16.156	12.25	12.11
718	3.005	5.481324	16.621	12.27	12.11
719	0.031	1.3099595	11.912	12.1	12.101
720	0.996	1.3307695	12.123	12.104	12.101
721	1.501	1.3141215	12.416	12.117	12.101
722	1.753	1.33181	12.575	12.12	12.1
723	2	1.3120405	12.63	12.121	12.101
724	2.502	1.3141215	12.753	12.121	12.099
725	3.001	1.3078785	12.819	12.123	12.1
726	0.058	1.3266075	11.871	12.082	12.088
727	1.007	1.3245265	12.085	12.091	12.088
728	1.506	1.3099595	12.237	12.097	12.087
729	1.748	1.3120405	12.339	12.101	12.087
730	2.004	1.3162025	12.463	12.104	12.087
731	2.502	1.3307695	12.621	12.105	12.088
732	3.005	1.323486	12.687	12.106	12.088

3/8-in PP beads

Exp No.	Gas (scfm)	Liq(gpm)	P_top(psia)	P_bot(psia)
72	10	2.4690224	13.875	12.157
73	10	3.699256	14.705	12.163
74	10	4.8814336	15.408	12.168
75	10	6.0564028	16.134	12.175
76	10	7.2229622	16.901	12.182
77	10	8.4700154	17.724	12.194
78	10	9.7110616	18.593	12.189
79	10	1.2351846	13.148	12.126
80	5	1.2532056	12.742	12.107
81	5	2.4666196	13.369	12.108
82	5	3.6367832	13.972	12.111
83	5	4.8742252	14.623	12.112
84	5	6.0756252	15.233	12.117
85	5	7.2566014	15.921	12.12
86	5	8.4760224	16.636	12.133
87	1	4.8598084	13.417	12.091
88	2	4.8742252	13.841	12.024
89	8	4.8742252	14.971	12.052
90	12	4.8694196	15.595	12.073
91	16	4.8622112	16.076	12.099
92	20	4.8501972	16.685	12.125
93	24	4.8610098	17.294	12.155
94	1	2.461814	12.544	12.035
95	2	2.4810364	12.779	12.036
96	8	2.4774322	13.59	12.049
97	12	2.4942518	14.092	12.067
98	16	2.4522028	14.538	12.085
99	20	2.4894462	15.043	12.109
100	24	2.4473972	15.405	12.131
102	1	1.290449	12.255	12.04
103	1	7.8657112	14.194	12.049
104	24	1.266421	14.603	12.124
105	24	7.2517958	19.379	12.189
106	24	8.444786	20.477	12.214
107	7	7.2349762	16.297	12.072

Exp No.	Gas (scfm)	Liq(gpm)	P_top(psia)	P_bot(psia)
108	14	7.2277678	17.564	12.111
109	18	7.2998518	18.221	12.138
110	5	2.4281748	13.282	12.041
111	5	2.4690224	13.245	12.042
112	5	7.2505944	15.887	12.063
113	5	7.2541986	15.882	12.066
114	20	2.455807	14.991	12.105
115	20	2.4365846	14.965	12.107
493	0.001	2.366067	11.789	12.128
494	0.495	2.3608645	12.067	12.131
495	0.753	2.357743	12.116	12.129
496	1	2.355662	12.168	12.129
497	1.999	2.3462975	12.4	12.126
498	3.998	2.359824	12.827	12.128
499	6.506	2.355662	13.249	12.133
500	9	2.3733505	13.602	12.14
501	10.996	2.3442165	13.855	12.146
502	14.002	2.341095	14.215	12.155
503	16.989	2.347338	14.605	12.165
504	20.004	2.3421355	14.996	12.177
505	24.005	2.3525405	15.534	12.194
506	0.001	1.833331	11.903	12.13
507	0.744	1.8614245	12.086	12.13
508	1.003	1.825007	12.116	12.126
509	1.245	1.85206	12.152	12.128
510	1.499	1.841655	12.183	12.127
511	2.002	1.835412	12.248	12.126
512	4	1.8302095	12.548	12.127
513	6.508	1.829169	12.912	12.129
514	8.997	1.833331	13.24	12.134
515	11.006	1.847898	13.485	12.137
516	13.99	1.835412	13.844	12.146
517	17	1.833331	14.219	12.156
518	20.003	1.8531005	14.606	12.167
519	24.005	1.8135615	15.087	12.182
520	0.001	1.288109	11.926	12.123

Exp No.	Gas (scfm)	Liq(gpm)	P_top(psia)	P_bot(psia)
521	2.002	1.304757	12.145	12.122
522	1.752	1.304757	12.113	12.121
523	3.996	1.3057975	12.335	12.122
524	2.254	1.3099595	12.163	12.121
525	6.503	1.325567	12.632	12.124
526	9.003	1.3057975	12.923	12.13
527	11.002	1.3203645	13.162	12.132
528	13.99	1.2995545	13.49	12.14
529	16.997	1.302676	13.829	12.149
530	19.989	1.3078785	14.161	12.159
531	24.005	1.298514	14.605	12.173
532	0.001	0.778264	11.906	12.123
533	2.004	0.8063575	11.963	12.119
534	4.013	0.796993	12.086	12.119
535	6.503	0.7876285	12.33	12.124
536	4.501	0.794912	12.162	12.124
537	4.745	0.7772235	12.201	12.124
538	4.993	0.784507	12.177	12.128
539	9.001	0.8063575	12.57	12.13
540	10.993	0.7959525	12.763	12.133
541	13.995	0.780345	13.057	12.14
542	17.002	0.7959525	13.369	12.148
543	20.004	0.7980335	13.691	12.157
544	23.995	0.799074	14.116	12.169
545	0.001	2.880074	11.476	12.12
546	1.001	2.8915195	12.425	12.126
547	1.257	2.8727905	12.521	12.126
548	1.497	2.8748715	12.599	12.127
549	1.998	2.859264	12.755	12.127
550	4.002	2.87175	13.228	12.128
551	6.496	2.855102	13.644	12.132
552	9.01	2.8707095	14.011	12.139
553	10.989	2.875912	14.275	12.145
554	13.982	2.867588	14.647	12.155
555	16.996	2.880074	15.02	12.167
556	19.991	2.8748715	15.417	12.18

Exp No.	Gas (scfm)	Liq(gpm)	P_top(psia)	P_bot(psia)
557	23.988	2.873831	15.98	12.197
558	0.001	3.4242555	11.247	12.131
559	1	3.402405	12.675	12.134
560	2.004	3.400324	13.118	12.135
561	1.749	3.379514	13.017	12.136
562	2.25	3.3951215	13.188	12.136
563	4.004	3.3992835	13.632	12.139
564	6.501	3.400324	14.069	12.145
565	9	3.402405	14.435	12.153
566	10.999	3.3972025	14.684	12.16
567	14.004	3.402405	15.084	12.17
568	16.99	3.392	15.496	12.182
569	20	3.4076075	15.895	12.196
570	23.985	3.394081	16.459	12.213
571	0.001	3.910169	11.065	12.114
572	1.999	3.9361815	13.41	12.12
573	3.992	3.901845	13.942	12.123

7/16-in PP beads

Exp No.	Gas (scfm)	Liq(gpm)	P_top(psia)	P_mid2(psia)	P_bot(psia)
777	0.039	3.4388225	12.012	12.133	12.136
778	1.002	3.4200935	12.082	12.14	12.138
779	2.002	3.4013645	12.161	12.142	12.141
780	2.247	3.3972025	12.179	12.144	12.142
781	2.495	3.3972025	12.21	12.146	12.142
782	2.754	3.3930405	12.26	12.15	12.142
783	2.997	3.3805545	12.297	12.156	12.143
784	3.997	3.385757	12.74	12.174	12.144
785	6.509	3.3992835	13.213	12.193	12.15
786	8.997	3.4034455	13.542	12.209	12.158
787	11.004	3.381595	13.802	12.226	12.165
788	14.008	3.4013645	14.169	12.243	12.174
789	17.015	3.3951215	14.501	12.263	12.186
790	19.998	3.398243	14.858	12.287	12.199
791	23.991	3.385757	15.296	12.318	12.22
792	0.076	2.368148	11.903	12.106	12.11
793	1.997	2.3567025	11.991	12.11	12.11
794	3.999	2.368148	12.117	12.115	12.113
795	4.997	2.3442165	12.208	12.119	12.113
796	5.25	2.3504595	12.251	12.126	12.115
797	5.498	2.3442165	12.282	12.128	12.115
798	5.744	2.361905	12.396	12.139	12.117
799	6.505	2.3421355	12.536	12.141	12.117
800	9.006	2.366067	12.859	12.156	12.123
801	10.985	2.349419	13.063	12.166	12.128
802	13.989	2.3483785	13.368	12.181	12.137
803	17.004	2.3795935	13.663	12.198	12.147
804	20.013	2.3525405	13.927	12.214	12.16
805	24.022	2.3358925	14.325	12.24	12.176
806	0.009	1.812521	12.052	12.17	12.174
807	2	1.839574	12.116	12.173	12.174
808	3.997	1.829169	12.238	12.18	12.178
809	5.493	1.8052375	12.362	12.187	12.18
810	0.066	1.83125	11.963	12.076	12.08
811	1.999	1.8426955	12.024	12.078	12.08

Exp No.	Gas (scfm)	Liq(gpm)	P_top(psia)	P_mid2(psia)	P_bot(psia)
812	3.996	1.8426955	12.146	12.086	12.081
813	5.497	1.820845	12.302	12.093	12.082
814	5.758	1.8343715	12.311	12.092	12.082
815	6.005	1.822926	12.366	12.096	12.083
816	6.498	1.83125	12.444	12.097	12.08
817	9.011	1.833331	12.719	12.108	12.084
818	11.012	1.825007	12.915	12.116	12.089
819	14	1.841655	13.17	12.128	12.095
820	16.996	1.8093995	13.444	12.141	12.104
821	20.008	1.862465	13.748	12.159	12.115
822	23.996	1.833331	14.085	12.181	12.129
823	0.062	2.8748715	11.933	12.064	12.07
824	1.003	2.8686285	11.991	12.065	12.069
825	2.003	2.8727905	12.08	12.068	12.07
826	2.242	2.85094	12.114	12.07	12.069
827	2.49	2.8540615	12.294	12.089	12.069
828	2.746	2.85094	12.502	12.097	12.068
829	4.003	2.8665475	12.825	12.102	12.069
830	0.051	2.6022605	11.933	12.058	12.064
831	2.005	2.613706	12.054	12.067	12.065
832	2.253	2.619949	12.097	12.067	12.065
833	2.5	2.6043415	12.176	12.073	12.064
834	2.75	2.605382	12.307	12.085	12.064
835	3.999	2.5918555	12.689	12.095	12.064
836	0.004	2.087213	11.901	12.026	12.031
837	1.005	2.1007395	11.932	12.026	12.028
838	1.496	2.0882535	11.961	12.027	12.026
839	2	2.083051	12.219	12.046	12.027
840	2.256	2.099699	12.292	12.048	12.07
841	3.006	2.0820105	12.468	12.049	12.027
842	3.247	2.0903345	12.508	12.048	12.024
843	4.007	2.0944965	12.602	12.049	12.025
844	6.494	2.0965775	12.846	12.057	12.026
845	8.994	2.087213	13.092	12.068	12.032
846	10.996	2.0882535	13.284	12.079	12.039
847	13.997	2.118428	13.549	12.096	12.047

Exp No.	Gas (scfm)	Liq(gpm)	P_top(psia)	P_mid2(psia)	P_bot(psia)
848	17.003	2.0944965	13.802	12.11	12.057
849	20.001	2.108023	14.055	12.126	12.066
850	24.034	2.0903345	14.415	12.153	12.084
851	0.008	2.3567025	11.871	12	12.001
852	1.007	2.368148	11.932	11.996	12
853	1.245	2.334852	12.351	12.024	12.002
854	1.496	2.3317305	12.406	12.024	12.002
855	1.764	2.370229	12.504	12.025	12.002
856	1.998	2.363986	12.541	12.027	12.003
857	2.249	2.3712695	12.536	12.026	12.003
858	2.506	2.3567025	12.605	12.028	12.002
859	2.75	2.3795935	12.606	12.028	12.002
860	3.001	2.380634	12.643	12.029	12.003
861	4.003	2.353581	12.759	12.033	12.003
862	6.492	2.3400545	12.974	12.042	12.007
863	9.002	2.3504595	13.242	12.054	12.012
864	10.988	2.3775125	13.436	12.065	12.018
865	14.007	2.3462975	13.713	12.081	12.027
866	16.995	2.353581	13.944	12.098	12.039
867	20.004	2.347338	14.224	12.116	12.05
868	23.987	2.359824	14.61	12.146	12.068
869	-0.01	2.359824	11.962	12.092	12.096
870	0.998	2.366067	11.993	12.093	12.097
871	1.997	2.324447	12.499	12.114	12.097
872	2.999	2.3712695	12.625	12.117	12.098
873	-0.006	1.825007	11.961	12.087	12.092
874	1.997	1.841655	12.273	12.105	12.095
875	2.248	1.83125	12.289	12.103	12.091
876	2.504	1.833331	12.352	12.105	12.092
877	3.001	1.8364525	12.388	12.106	12.094
878	3.953	1.8489385	12.474	12.106	12.093
879	6.501	1.8239665	12.683	12.115	12.096
880	8.998	1.8281285	12.904	12.125	12.1
881	10.996	1.8322905	13.076	12.135	12.105
882	13.997	1.83125	13.318	12.148	12.11
883	17.01	1.8551815	13.573	12.162	12.119

Exp No.	Gas (scfm)	Liq(gpm)	P_top(psia)	P_mid2(psia)	P_bot(psia)
884	20.029	1.829169	13.825	12.178	12.129
885	24.003	1.8322905	14.195	12.203	12.144
886	0.498	1.8177235	11.932	12.069	12.078
887	1.005	1.8447765	11.961	12.069	12.078
888	1.495	1.8322905	11.968	12.07	12.076
889	1.995	1.8198045	12.223	12.088	12.076
890	3	1.825007	12.367	12.09	12.075
891	-0.008	2.8769525	11.93	12.065	12.068
892	0.5	2.888398	11.959	12.063	12.069
893	0.744	2.877993	12.254	12.087	12.069
894	0.994	2.8707095	12.378	12.09	12.069
895	1.498	2.8644665	12.535	12.093	12.069
896	1.994	2.8707095	12.664	12.095	12.07
897	3.999	2.884236	12.94	12.106	12.072
898	6.495	2.8707095	13.229	12.117	12.074
899	9.008	2.869669	13.513	12.129	12.08
900	10.995	2.85094	13.719	12.14	12.086
901	14.005	2.87175	14.035	12.158	12.095
902	16.997	2.8665475	14.326	12.176	12.105
903	19.983	2.853021	14.635	12.198	12.117
904	23.983	2.8623855	15.06	12.229	12.136
905	-0.001	3.3951215	11.902	12.051	12.055
906	0.497	3.4034455	12.335	12.074	12.056
907	1.005	3.3951215	12.644	12.082	12.055
908	1.499	3.3867975	12.796	12.086	12.056
909	2.003	3.406567	12.908	12.09	12.055
910	2.502	3.396162	12.941	12.089	12.052
911	3	3.425296	13.029	12.094	12.054
912	3.5	3.392	13.126	12.098	12.056
913	3.997	3.3909595	13.189	12.098	12.055
914	6.5	3.3909595	13.508	12.111	12.059
915	9.005	3.394081	13.813	12.125	12.065
916	11.002	3.3805545	14.054	12.138	12.072
917	14.001	3.404486	14.385	12.158	12.082
918	17.006	3.4117695	14.721	12.178	12.093
919	20.004	3.400324	15.048	12.2	12.105

Exp No.	Gas (scfm)	Liq(gpm)	P_top(psia)	P_mid2(psia)	P_bot(psia)
920	24.001	3.4159315	15.469	12.228	12.12
921	0.005	2.3733505	11.901	12.032	12.037
922	0.256	2.3795935	11.901	12.031	12.037
923	0.499	2.3608645	11.901	12.028	12.035
924	0.751	2.343176	11.939	12.031	12.031
925	1	2.3421355	12.275	12.049	12.034
926	2.497	2.3546215	12.542	12.055	12.032
927	3.998	2.359824	12.707	12.06	12.031
928	6.501	2.353581	12.971	12.071	12.036
929	8.987	2.3587835	13.189	12.082	12.041
930	11.009	2.3650265	13.396	12.091	12.045
931	13.992	2.353581	13.693	12.107	12.055
932	17	2.3400545	13.98	12.126	12.066
933	20.002	2.3462975	14.252	12.145	12.078
934	23.999	2.357743	14.673	12.174	12.093
935	-0.011	2.0861725	11.871	12.017	12.02
936	0.25	2.066403	11.871	12.017	12.02
937	0.506	2.0965775	11.885	12.016	12.019
938	0.75	2.085132	12.129	12.031	12.018
939	1.001	2.0861725	12.206	12.034	12.019
940	2.497	2.083051	12.434	12.036	12.018
941	3.996	2.095537	12.584	12.041	12.016
942	6.511	2.103861	12.838	12.05	12.021
943	9	2.1153065	13.074	12.061	12.024
944	14.002	2.1049015	13.485	12.084	12.038
945	19.993	2.1007395	14.072	12.122	12.059
946	24.001	2.0986585	14.44	12.148	12.074
947	-0.017	1.3037165	11.841	12.001	12.009
948	1.007	1.288109	11.871	12.001	12.006
949	1.497	1.3057975	11.897	12.001	12.009
950	1.748	1.300595	12.034	12.011	12.004
951	2	1.3162025	12.08	12.011	12.002
952	2.495	1.294352	12.124	12.012	12
953	4.001	1.2933115	12.264	12.014	12.004
954	6.492	1.300595	12.422	12.021	12.005
955	9.009	1.333891	12.592	12.03	12.008

Exp No.	Gas (scfm)	Liq(gpm)	P_top(psia)	P_mid2(psia)	P_bot(psia)
956	14.006	1.292271	12.959	12.05	12.02
957	19.992	1.340134	13.449	12.076	12.036
958	23.972	1.3203645	13.779	12.099	12.05
959	-0.015	1.327648	11.994	12.117	12.121
960	1.001	1.3203645	12.021	12.117	12.119
961	1.502	1.3057975	12.026	12.115	12.118
962	1.755	1.306838	12.051	12.115	12.119
963	1.997	1.3349315	12.056	12.116	12.121
964	2.501	1.2912305	12.214	12.129	12.123
965	2.748	1.319324	12.244	12.128	12.12
966	3.006	1.313081	12.257	12.13	12.122
967	3.25	1.327648	12.282	12.13	12.12
968	3.499	1.308919	12.306	12.129	12.118
969	3.746	1.300595	12.327	12.129	12.118
970	3.995	1.308919	12.358	12.132	12.121
971	4.25	1.329729	12.382	12.135	12.122
972	4.501	1.321405	12.399	12.135	12.122
973	4.749	1.319324	12.41	12.136	12.124
974	5	1.311	12.428	12.134	12.121
975	6.496	1.3099595	12.522	12.14	12.125
976	8.999	1.3182835	12.718	12.15	12.127
977	13.989	1.3349315	13.102	12.171	12.137
978	19.994	1.3453365	13.586	12.194	12.152
979	23.998	1.29019	13.894	12.217	12.166
980	0.013	2.366067	11.929	12.099	12.105
981	0.497	2.341095	11.933	12.104	12.109
982	0.749	2.3567025	12.217	12.121	12.109
983	1.007	2.3462975	12.304	12.123	12.11
984	1.252	2.3671075	12.325	12.124	12.109
985	1.499	2.3608645	12.369	12.127	12.108
986	1.752	2.3275685	12.406	12.129	12.11
987	2.003	2.368148	12.448	12.129	12.109
988	2.497	2.339014	12.497	12.131	12.11
989	3.995	2.359824	12.69	12.131	12.105
990	9.002	2.341095	13.215	12.161	12.118
991	14.009	2.3400545	13.682	12.185	12.131

Exp No.	Gas (scfm)	Liq(gpm)	P_top(psia)	P_mid2(psia)	P_bot(psia)
992	23.983	2.353581	14.712	12.252	12.171
993	0.016	3.387838	11.641	12.101	12.107
994	0.505	3.387838	12.293	12.122	12.109
995	0.998	3.37119	12.525	12.134	12.111
996	1.252	3.3763925	12.598	12.139	12.113
997	1.497	3.37119	12.661	12.14	12.111
998	1.752	3.3576635	12.734	12.141	12.11
999	2.006	3.387838	12.827	12.143	12.109
1000	2.248	3.41281	12.874	12.146	12.11
1001	2.499	3.4096885	12.924	12.15	12.112
1002	2.745	3.4117695	12.962	12.151	12.112
1003	3.001	3.416972	13.012	12.153	12.113
1004	3.252	3.406567	13.072	12.155	12.114
1005	3.502	3.404486	13.091	12.152	12.11
1006	3.994	3.4221745	13.2	12.158	12.113
1007	8.997	3.410729	13.838	12.184	12.123
1008	14.003	3.3972025	14.391	12.215	12.138
1009	24.016	3.385757	15.581	12.291	12.178
1010	0.504	2.3546215	12.031	12.122	12.118
1011	0.999	2.336933	12.207	12.127	12.117
1012	1.501	2.3504595	12.271	12.132	12.117
1013	2.002	2.3400545	12.383	12.134	12.116
1014	4.003	2.3442165	12.674	12.143	12.118
1015	9.014	2.332771	13.24	12.17	12.129
1016	14.002	2.3296495	13.74	12.197	12.143
1017	24.014	2.3296495	14.809	12.26	12.18
1018	0.02	1.294352	11.901	12.106	12.113
1019	0.999	1.300595	11.932	12.107	12.117
1020	1.494	1.296433	12.087	12.118	12.114
1021	2.003	1.3141215	12.138	12.118	12.113
1022	2.245	1.3016355	12.158	12.121	12.112
1023	2.494	1.33181	12.175	12.122	12.114
1024	4.003	1.327648	12.312	12.124	12.112
1025	8.999	1.313081	12.682	12.139	12.117
1026	13.999	1.2725015	13.083	12.161	12.131
1027	24.002	1.3141215	13.924	12.216	12.161

Exp No.	Gas (scfm)	Liq(gpm)	P_top(psia)	P_mid2(psia)	P_bot(psia)
1028	-0.016	1.8260475	12.024	12.161	12.166
1029	0.997	1.8426955	12.229	12.174	12.168
1030	1.495	1.8177235	12.309	12.175	12.169
1031	1.754	1.849979	12.301	12.177	12.168
1032	2.005	1.8406145	12.305	12.178	12.168
1033	2.503	1.829169	12.386	12.179	12.167
1034	3.996	1.804197	12.563	12.186	12.17
1035	9.003	1.8531005	13.083	12.21	12.177
1036	13.998	1.8447765	13.526	12.235	12.193
1037	24.012	1.8198045	14.51	12.299	12.299
1038	-0.008	2.869669	11.809	12.16	12.17
1039	1.001	2.873831	12.39	12.183	12.168
1040	1.503	2.8623855	12.487	12.186	12.169
1041	2.004	2.8686285	12.588	12.192	12.169
1042	1.748	2.882155	12.555	12.19	12.167
1043	2.503	2.863426	12.754	12.195	12.168
1044	3.991	2.873831	13.057	12.206	12.17
1045	9	2.8748715	13.68	12.235	12.183
1046	14.015	2.877993	14.201	12.263	12.197
1047	23.986	2.89256	15.365	12.338	12.236
1048	0.01	1.862465	11.963	12.133	12.137
1049	0.505	1.8385335	12.01	12.135	12.134
1050	1	1.8260475	12.145	12.144	12.137
1051	1.251	1.8177235	12.168	12.145	12.138
1052	1.497	1.8385335	12.213	12.146	12.139
1053	1.755	1.816683	12.239	12.147	12.139
1054	1.998	1.825007	12.252	12.147	12.138
1055	2.247	1.8614245	12.31	12.147	12.137
1056	2.5	1.8260475	12.329	12.146	12.135
1057	3.001	1.833331	12.385	12.147	12.135
1058	3.499	1.812521	12.438	12.147	12.134

1.27-cm PP beads

Exp No.	Liq (gpm)	L (kg/m2s)	Air (SCFM)	G (kg/m2s)	Top (psia)	Mid1 (psia)	Bot (psia)	DP_uc (psi)	NDP_uc
376	3.398	29.7148	0.020	0.00157	11.904	12.129	12.081	-0.177	-0.089
377	3.396	29.6973	1.998	0.15687	11.964	12.141	12.084	-0.120	-0.060
378	3.383	29.5836	3.998	0.31390	12.056	12.169	12.086	-0.030	-0.015
379	3.394	29.6798	6.498	0.51019	12.220	12.228	12.096	0.124	0.062
380	3.398	29.7148	9.006	0.70710	12.431	12.290	12.102	0.329	0.165
381	3.375	29.5136	10.996	0.86334	12.610	12.348	12.108	0.502	0.251
382	3.399	29.7235	14.005	1.09959	12.965	12.451	12.122	0.843	0.422
383	3.408	29.8022	13.006	1.02116	12.830	12.415	12.117	0.713	0.357
384	3.399	29.7235	12.498	0.98127	12.773	12.399	12.116	0.657	0.329
385	3.405	29.7760	17.006	1.33522	13.305	12.556	12.136	1.169	0.585
386	3.409	29.8110	20.003	1.57052	13.668	12.677	12.150	1.518	0.760
387	3.385	29.6011	24.007	1.88489	14.107	12.825	12.170	1.937	0.969
388	2.344	20.4978	0.020	0.00157	11.933	12.129	12.087	-0.154	-0.077
389	2.343	20.4890	2.003	0.15726	11.964	12.129	12.081	-0.117	-0.059
390	2.349	20.5415	3.989	0.31319	12.026	12.151	12.083	-0.057	-0.029
391	2.338	20.4453	6.502	0.51050	12.148	12.192	12.088	0.060	0.030
392	2.354	20.5852	9.010	0.70741	12.302	12.246	12.098	0.204	0.102
393	2.372	20.7426	10.999	0.86358	12.453	12.292	12.103	0.350	0.175
394	2.366	20.6902	13.979	1.09755	12.685	12.360	12.107	0.578	0.289
395	2.339	20.4541	17.003	1.33498	12.946	12.440	12.118	0.828	0.414
396	2.355	20.5940	19.994	1.56982	13.250	12.529	12.132	1.118	0.559
397	2.382	20.8301	24.000	1.88435	13.617	12.641	12.151	1.466	0.734
398	4.441	38.8356	0.009	0.00071	11.926	12.127	12.072	-0.146	-0.073
399	4.422	38.6694	2.004	0.15734	12.005	12.159	12.084	-0.079	-0.040
400	4.408	38.5470	4.006	0.31453	12.148	12.207	12.089	0.059	0.030
401	4.438	38.8094	6.323	0.49645	12.353	12.271	12.096	0.257	0.129
402	4.435	38.7831	9.008	0.70726	12.711	12.415	12.111	0.600	0.300
403	4.451	38.9230	8.002	0.62827	12.532	12.335	12.108	0.424	0.212
404	4.445	38.8706	7.534	0.59153	12.474	12.310	12.101	0.373	0.187
405	4.445	38.8706	11.000	0.86366	13.239	12.606	12.116	1.123	0.562
406	4.447	38.8881	13.993	1.09865	13.673	12.743	12.130	1.543	0.772
407	4.445	38.8706	17.008	1.33537	14.048	12.859	12.145	1.903	0.952
408	4.428	38.7219	20.007	1.57084	14.425	12.981	12.163	2.262	1.132
409	4.439	38.8181	24.000	1.88435	14.916	13.145	12.184	2.732	1.367

Exp No.	Liq (gpm)	L (kg/m2s)	Air (SCFM)	G (kg/m2s)	Top (psia)	Mid1 (psia)	Bot (psia)	DP_uc (psi)	NDP_uc
410	2.878	25.1675	0.015	0.00118	11.904	12.120	12.076	-0.172	-0.086
411	2.863	25.0363	1.997	0.15679	11.938	12.133	12.079	-0.141	-0.071
412	2.861	25.0188	3.989	0.31319	12.025	12.161	12.081	-0.056	-0.028
413	2.869	25.0888	6.495	0.50995	12.177	12.206	12.088	0.089	0.045
414	2.875	25.1413	8.987	0.70561	12.357	12.265	12.094	0.263	0.132
415	3.924	34.3145	0.018	0.00141	11.903	12.123	12.073	-0.170	-0.085
416	3.916	34.2446	2.003	0.15726	11.964	12.147	12.080	-0.116	-0.058
417	3.915	34.2358	3.998	0.31390	12.087	12.189	12.086	0.001	0.001
418	3.883	33.9560	6.494	0.50987	12.280	12.245	12.091	0.189	0.095
419	3.905	34.1484	9.004	0.70694	12.513	12.321	12.104	0.409	0.205
420	3.917	34.2533	9.504	0.74620	12.562	12.341	12.108	0.454	0.227
421	3.922	34.2970	9.998	0.78499	12.624	12.362	12.111	0.513	0.257
422	3.911	34.2009	11.002	0.86382	12.829	12.441	12.115	0.714	0.357
423	3.919	34.2708	14.000	1.09920	13.305	12.607	12.129	1.176	0.588
424	3.904	34.1396	16.996	1.33443	13.667	12.726	12.143	1.524	0.763
425	3.903	34.1309	19.996	1.56997	14.034	12.846	12.158	1.876	0.939
426	3.938	34.4370	24.012	1.88529	14.547	13.016	12.180	2.367	1.184
427	4.948	43.2692	0.033	0.00259	12.009	12.229	12.178	-0.169	-0.085
428	4.942	43.2167	2.003	0.15726	12.136	12.273	12.190	-0.054	-0.027
429	4.946	43.2517	3.998	0.31390	12.321	12.334	12.199	0.122	0.061
430	4.955	43.3304	6.497	0.51011	13.133	12.649	12.207	0.926	0.463
431	4.961	43.3829	5.994	0.47062	12.956	12.603	12.206	0.750	0.375
432	4.940	43.1992	5.003	0.39281	12.468	12.398	12.204	0.264	0.132
433	4.943	43.2255	4.494	0.35284	12.379	12.351	12.198	0.181	0.091
434	4.952	43.3042	4.746	0.37263	12.407	12.368	12.201	0.206	0.103
435	4.957	43.3479	9.005	0.70702	13.676	12.805	12.214	1.462	0.732
436	4.950	43.2867	10.998	0.86350	13.993	12.902	12.222	1.771	0.886
437	4.949	43.2779	14.005	1.09959	14.401	13.026	12.235	2.166	1.084
438	4.953	43.3129	17.013	1.33577	14.788	13.152	12.250	2.538	1.270
439	4.952	43.3042	20.005	1.57068	15.183	13.285	12.266	2.917	1.460
440	4.961	43.3829	24.003	1.88458	15.698	13.462	12.292	3.406	1.704
441	5.469	47.8252	0.022	0.00173	11.992	12.202	12.155	-0.163	-0.082
442	5.499	48.0876	2.002	0.15719	12.165	12.265	12.175	-0.010	-0.005
443	5.455	47.7028	3.994	0.31359	12.412	12.372	12.186	0.226	0.113
444	5.461	47.7553	3.493	0.27425	12.323	12.325	12.181	0.142	0.071

Exp No.	Liq (gpm)	L (kg/m2s)	Air (SCFM)	G (kg/m2s)	Top (psia)	Mid1 (psia)	Bot (psia)	DP_uc (psi)	NDP_uc
445	5.465	47.7902	3.753	0.29466	12.365	12.349	12.185	0.180	0.090
446	5.471	47.8427	6.501	0.51042	13.525	12.751	12.193	1.332	0.667
447	5.478	47.9039	8.995	0.70624	14.024	12.899	12.199	1.825	0.913
448	5.456	47.7115	11.004	0.86397	14.337	13.000	12.208	2.129	1.065
449	5.481	47.9302	14.006	1.09967	14.756	13.136	12.222	2.534	1.268
450	5.465	47.7902	17.002	1.33490	15.142	13.260	12.237	2.905	1.454
451	5.467	47.8077	19.992	1.56966	15.530	13.389	12.254	3.276	1.639
452	5.467	47.8077	24.014	1.88544	16.083	13.579	12.281	3.802	1.903
453	5.999	52.4600	0.013	0.00102	11.944	12.182	12.132	-0.188	-0.094
454	5.990	52.3813	1.993	0.15648	12.215	12.281	12.168	0.047	0.024
455	5.991	52.3900	2.250	0.17666	12.264	12.296	12.171	0.093	0.047
456	5.976	52.2588	2.499	0.19621	12.311	12.323	12.174	0.137	0.069
457	6.002	52.4862	4.004	0.31437	13.248	12.647	12.177	1.071	0.536
458	5.988	52.3638	6.500	0.51034	13.953	12.862	12.182	1.771	0.886
459	5.995	52.4250	9.004	0.70694	14.428	13.014	12.192	2.236	1.119
460	6.000	52.4687	10.997	0.86342	14.746	13.120	12.203	2.543	1.273
461	6.000	52.4687	13.997	1.09897	15.198	13.267	12.219	2.979	1.491
462	6.013	52.5824	17.002	1.33490	15.618	13.410	12.237	3.381	1.692
463	6.001	52.4775	20.005	1.57068	16.036	13.550	12.254	3.782	1.893
464	6.009	52.5474	24.004	1.88466	16.607	13.746	12.281	4.326	2.165
465	5.980	52.2938	2.999	0.23546	12.610	12.475	12.152	0.458	0.229
466	6.011	52.5649	3.506	0.27527	12.974	12.563	12.154	0.820	0.410
467	5.466	47.7990	4.999	0.39249	13.201	12.628	12.157	1.044	0.522
468	5.494	48.0438	5.501	0.43191	13.334	12.674	12.158	1.176	0.588
469	5.479	47.9127	4.000	0.31406	12.778	12.517	12.154	0.624	0.312
470	6.534	57.1384	0.014	0.00110	11.895	12.142	12.095	-0.200	-0.100
471	6.532	57.1209	1.003	0.07875	12.118	12.223	12.134	-0.016	-0.008
472	6.527	57.0772	1.496	0.11746	12.207	12.261	12.142	0.065	0.033
473	6.530	57.1034	1.749	0.13732	12.317	12.335	12.147	0.170	0.085
474	6.528	57.0860	1.999	0.15695	12.516	12.432	12.147	0.369	0.185
475	6.532	57.1209	4.002	0.31421	13.551	12.713	12.155	1.396	0.699
476	6.501	56.8498	6.500	0.51034	14.208	12.923	12.161	2.047	1.024
477	6.525	57.0597	8.998	0.70647	14.680	13.074	12.171	2.509	1.256
478	7.018	61.3709	0.029	0.00228	11.873	12.115	12.069	-0.196	-0.098
479	7.039	61.5545	1.002	0.07867	12.198	12.260	12.135	0.063	0.032

Exp No.	Liq (gpm)	L (kg/m2s)	Air (SCFM)	G (kg/m2s)	Top (psia)	Mid1 (psia)	Bot (psia)	DP_uc (psi)	NDP_uc
480	7.054	61.6857	1.248	0.09799	12.334	12.344	12.141	0.193	0.097
481	7.030	61.4758	2.000	0.15703	12.742	12.487	12.145	0.597	0.299
482	7.035	61.5196	4.000	0.31406	13.751	12.784	12.155	1.596	0.799
483	7.026	61.4409	6.510	0.51113	14.437	12.999	12.162	2.275	1.138
484	7.053	61.6770	8.995	0.70624	14.951	13.160	12.172	2.779	1.391
485	7.585	66.3292	0.034	0.00267	11.779	12.014	11.969	-0.190	-0.095
486	7.547	65.9969	0.499	0.03918	12.141	12.227	12.127	0.014	0.007
487	7.540	65.9357	0.748	0.05873	12.274	12.297	12.135	0.139	0.070
488	7.563	66.1368	1.002	0.07867	12.473	12.366	12.138	0.335	0.168
489	7.575	66.2417	2.001	0.15711	13.049	12.555	12.145	0.904	0.452
490	7.569	66.1893	4.002	0.31421	14.000	12.860	12.154	1.846	0.924
491	7.559	66.1018	6.499	0.51026	14.694	13.075	12.161	2.533	1.268
492	7.567	66.1718	8.997	0.70639	15.211	13.245	12.176	3.035	1.519

2.54-cm PP beads

Exp No.	Liq (gpm)	L (kg/m2s)	Air (SCFM)	G (kg/m2s)	Top (psia)	Mid1 (psia)	Bot (psia)	DP_uc (psi)	NDP_uc
574	4.438	38.8094	-0.013	-0.00102	11.887	12.120	12.082	-0.195	-0.098
575	4.419	38.6432	2.019	0.15852	11.904	12.130	12.089	-0.185	-0.093
576	4.422	38.6694	4.000	0.31406	11.937	12.140	12.094	-0.157	-0.079
577	4.442	38.8443	6.496	0.51003	11.981	12.159	12.102	-0.121	-0.061
578	4.426	38.7044	9.007	0.70718	12.034	12.180	12.111	-0.077	-0.039
579	4.439	38.8181	11.004	0.86397	12.093	12.200	12.119	-0.026	-0.013
580	4.432	38.7569	14.010	1.09999	12.203	12.240	12.136	0.067	0.034
581	4.441	38.8356	16.994	1.33427	12.339	12.289	12.152	0.187	0.094
582	4.436	38.7919	18.984	1.49052	12.442	12.320	12.161	0.281	0.141
583	4.425	38.6957	19.976	1.56840	12.495	12.340	12.167	0.328	0.164
584	4.435	38.7831	23.991	1.88364	12.696	12.420	12.194	0.502	0.251
585	5.489	48.0001	-0.009	-0.00071	11.891	12.111	12.071	-0.180	-0.090
586	5.491	48.0176	2.002	0.15719	11.933	12.140	12.095	-0.162	-0.081
587	5.498	48.0788	3.998	0.31390	11.969	12.156	12.102	-0.133	-0.067
588	5.472	47.8515	6.498	0.51019	12.037	12.180	12.111	-0.074	-0.037
589	5.457	47.7203	8.993	0.70608	12.136	12.216	12.122	0.014	0.007
590	5.471	47.8427	10.997	0.86342	12.260	12.259	12.131	0.129	0.065
592	5.487	47.9826	16.986	1.33365	12.596	12.375	12.166	0.430	0.215
593	5.464	47.7815	19.997	1.57005	12.750	12.438	12.187	0.563	0.282
594	5.457	47.7203	23.980	1.88277	12.970	12.521	12.211	0.759	0.380
595	6.527	57.0772	-0.010	-0.00079	11.885	12.093	12.053	-0.168	-0.084
596	6.506	56.8936	2.007	0.15758	11.959	12.148	12.098	-0.139	-0.070
597	6.506	56.8936	3.995	0.31366	12.017	12.169	12.105	-0.088	-0.044
598	6.501	56.8498	6.502	0.51050	12.175	12.228	12.116	0.059	0.030
599	6.486	56.7187	8.992	0.70600	12.400	12.301	12.128	0.272	0.136
600	6.509	56.9198	10.993	0.86311	12.515	12.341	12.138	0.377	0.189
601	6.523	57.0422	13.976	1.09732	12.685	12.405	12.159	0.526	0.263
602	6.511	56.9373	16.996	1.33443	12.859	12.469	12.179	0.680	0.340
603	6.522	57.0335	20.007	1.57084	13.052	12.541	12.203	0.849	0.425
604	6.531	57.1122	24.007	1.88489	13.303	12.634	12.232	1.071	0.536

Woven Packing

Exp No.	Liq (gpm)	L (kg/m2s)	Air (SCFM)	G (kg/m2s)	Top (psia)	Mid1 (psia)	Mid2 (psia)	Bot (psia)	DP_uc (psi)	NDP_uc
1059	7.071	61.8344	-0.016	-0.00126	11.831	12.028	12.026	12.033	-0.202	-0.101
1060	7.061	61.7469	1.001	0.07859	12.138	12.160	12.077	12.072	0.066	0.033
1061	7.027	61.4496	1.994	0.15656	12.276	12.224	12.093	12.080	0.196	0.098
1062	7.052	61.6682	2.993	0.23499	12.395	12.273	12.106	12.086	0.309	0.155
1063	7.067	61.7994	3.999	0.31398	12.511	12.314	12.113	12.087	0.424	0.212
1064	7.005	61.2572	4.995	0.39218	12.619	12.358	12.126	12.092	0.527	0.264
1065	7.043	61.5895	5.498	0.43167	12.678	12.377	12.130	12.093	0.585	0.293
1066	7.034	61.5108	5.997	0.47085	12.742	12.401	12.137	12.096	0.646	0.323
1067	7.022	61.4059	6.993	0.54905	12.853	12.441	12.149	12.100	0.753	0.377
1068	7.034	61.5108	9.003	0.70686	13.101	12.519	12.170	12.108	0.993	0.497
1069	7.031	61.4846	14.012	1.10014	13.685	12.718	12.232	12.135	1.550	0.776
1070	6.908	60.4090	23.994	1.88387	14.687	13.081	12.349	12.198	2.489	1.245
1071	5.988	52.3638	-0.010	-0.00079	11.870	12.036	12.036	12.041	-0.171	-0.086
1072	5.989	52.3725	1.003	0.07875	12.025	12.107	12.068	12.070	-0.045	-0.023
1073	6.024	52.6786	2.500	0.19629	12.176	12.184	12.086	12.076	0.100	0.050
1074	6.016	52.6086	3.992	0.31343	12.331	12.247	12.098	12.080	0.251	0.126
1075	6.003	52.4949	5.501	0.43191	12.471	12.307	12.110	12.087	0.384	0.192
1076	5.990	52.3813	5.993	0.47054	12.521	12.328	12.116	12.089	0.432	0.216
1077	5.996	52.4337	6.501	0.51042	12.563	12.343	12.120	12.091	0.472	0.236
1078	5.975	52.2501	7.007	0.55015	12.604	12.355	12.123	12.090	0.514	0.257
1079	5.993	52.4075	7.492	0.58823	12.658	12.372	12.128	12.093	0.565	0.283
1080	6.009	52.5474	9.038	0.70961	12.773	12.405	12.140	12.095	0.678	0.339
1081	5.991	52.3900	13.999	1.09912	13.262	12.571	12.190	12.118	1.144	0.572
1082	6.005	52.5124	23.994	1.88387	14.233	12.923	12.304	12.176	2.057	1.029
1083	4.915	42.9806	-0.010	-0.00079	11.900	12.056	12.050	12.050	-0.150	-0.075
1084	4.944	43.2342	0.996	0.07820	11.993	12.090	12.063	12.066	-0.073	-0.037
1085	4.947	43.2604	2.496	0.19597	12.087	12.143	12.074	12.069	0.018	0.009
1086	4.941	43.2080	4.007	0.31461	12.210	12.195	12.083	12.072	0.138	0.069
1087	4.946	43.2517	5.492	0.43120	12.333	12.251	12.098	12.081	0.252	0.126
1088	4.957	43.3479	6.512	0.51129	12.418	12.283	12.105	12.083	0.335	0.168
1089	4.956	43.3392	7.016	0.55086	12.453	12.297	12.107	12.084	0.369	0.185
1090	4.948	43.2692	7.507	0.58941	12.489	12.311	12.110	12.086	0.403	0.202
1091	4.978	43.5315	7.994	0.62764	12.534	12.329	12.115	12.088	0.446	0.223
1092	5.005	43.7676	8.514	0.66847	12.579	12.345	12.118	12.089	0.490	0.245

Exp No.	Liq (gpm)	L (kg/m2s)	Air (SCFM)	G (kg/m2s)	Top (psia)	Mid1 (psia)	Mid2 (psia)	Bot (psia)	DP_uc (psi)	NDP_uc
1093	4.963	43.4004	9.006	0.70710	12.614	12.359	12.122	12.090	0.524	0.262
1094	4.963	43.4004	9.494	0.74542	12.653	12.377	12.128	12.094	0.559	0.280
1095	4.951	43.2954	10.011	0.78601	12.698	12.385	12.126	12.091	0.607	0.304
1096	4.937	43.1730	13.991	1.09849	12.975	12.471	12.162	12.108	0.867	0.434
1097	4.961	43.3829	24.002	1.88450	13.831	12.773	12.260	12.159	1.672	0.837
1098	7.072	61.8431	0.010	0.00079	11.727	11.885	11.876	11.881	-0.154	-0.077
1099	7.068	61.8081	2.014	0.15813	12.149	12.156	12.063	12.056	0.093	0.047
1100	7.056	61.7032	3.991	0.31335	12.394	12.265	12.086	12.067	0.327	0.164
1101	7.043	61.5895	4.495	0.35292	12.454	12.293	12.092	12.068	0.386	0.193
1102	7.033	61.5021	5.008	0.39320	12.518	12.315	12.098	12.067	0.451	0.226
1103	7.027	61.4496	5.245	0.41181	12.539	12.327	12.098	12.069	0.470	0.235
1104	6.997	61.1873	5.504	0.43214	12.566	12.336	12.101	12.068	0.498	0.249
1105	7.009	61.2922	5.996	0.47077	12.625	12.356	12.106	12.070	0.555	0.278
1106	7.031	61.4846	8.985	0.70545	12.928	12.470	12.142	12.082	0.846	0.423
1107	7.031	61.4846	13.998	1.09904	13.506	12.660	12.197	12.104	1.402	0.702
1108	7.039	61.5545	23.985	1.88317	14.570	13.050	12.322	12.170	2.400	1.201
1109	6.011	52.5649	-0.010	-0.00079	11.836	12.012	12.004	12.011	-0.175	-0.088
1110	5.986	52.3463	2.003	0.15726	12.056	12.115	12.049	12.045	0.011	0.006
1111	6.000	52.4687	4.003	0.31429	12.254	12.203	12.067	12.052	0.202	0.101
1112	5.976	52.2588	5.000	0.39257	12.354	12.247	12.075	12.055	0.299	0.150
1113	5.971	52.2151	5.496	0.43152	12.416	12.270	12.078	12.055	0.361	0.181
1114	6.000	52.4687	5.994	0.47062	12.466	12.293	12.083	12.056	0.410	0.205
1115	6.011	52.5649	6.264	0.49181	12.496	12.303	12.086	12.058	0.438	0.219
1116	5.994	52.4162	6.507	0.51089	12.519	12.310	12.087	12.056	0.463	0.232
1117	6.024	52.6786	6.751	0.53005	12.543	12.317	12.090	12.057	0.486	0.243
1118	5.994	52.4162	6.990	0.54882	12.560	12.322	12.092	12.058	0.502	0.251
1119	5.980	52.2938	9.006	0.70710	12.707	12.372	12.108	12.065	0.642	0.321
1120	5.976	52.2588	13.995	1.09881	13.190	12.543	12.160	12.086	1.104	0.552
1121	6.017	52.6174	24.017	1.88568	14.197	12.899	12.267	12.140	2.057	1.029
1122	6.529	57.0947	0.004	0.00031	11.848	11.976	11.965	11.967	-0.119	-0.060
1123	6.495	56.7974	0.998	0.07836	11.993	12.037	12.008	12.009	-0.016	-0.008
1124	6.505	56.8848	2.510	0.19707	12.114	12.081	12.020	12.018	0.096	0.048
1125	6.535	57.1472	3.995	0.31366	12.237	12.127	12.037	12.026	0.211	0.106
1126	6.512	56.9460	5.495	0.43144	12.364	12.185	12.054	12.031	0.333	0.167
1127	6.537	57.1647	5.994	0.47062	12.424	12.221	12.060	12.030	0.394	0.197

Exp No.	Liq (gpm)	L (kg/m2s)	Air (SCFM)	G (kg/m2s)	Top (psia)	Mid1 (psia)	Mid2 (psia)	Bot (psia)	DP_uc (psi)	NDP_uc
1128	6.568	57.4357	6.501	0.51042	12.478	12.247	12.067	12.030	0.448	0.224
1129	6.547	57.2521	6.996	0.54929	12.522	12.271	12.074	12.033	0.489	0.245
1130	6.517	56.9898	7.245	0.56884	12.540	12.279	12.075	12.033	0.507	0.254
1131	6.522	57.0335	7.509	0.58956	12.575	12.293	12.080	12.036	0.539	0.270
1132	6.509	56.9198	7.747	0.60825	12.594	12.302	12.082	12.034	0.560	0.280
1133	6.518	56.9985	7.998	0.62796	12.616	12.316	12.085	12.036	0.580	0.290
1134	6.540	57.1909	8.496	0.66706	12.661	12.332	12.089	12.038	0.623	0.312
1135	6.519	57.0073	9.019	0.70812	12.703	12.352	12.093	12.040	0.663	0.332
1136	6.511	56.9373	13.999	1.09912	13.152	12.538	12.146	12.061	1.091	0.546
1137	6.533	57.1297	23.996	1.88403	14.116	12.917	12.260	12.119	1.997	0.999
1138	5.446	47.6241	0.009	0.00071	11.849	11.993	11.988	11.991	-0.142	-0.071
1139	5.464	47.7815	0.994	0.07804	11.933	12.029	12.007	12.008	-0.075	-0.038
1140	5.465	47.7902	2.499	0.19621	12.025	12.057	12.010	12.012	0.013	0.007
1141	5.494	48.0438	3.997	0.31382	12.114	12.093	12.023	12.016	0.098	0.049
1142	5.468	47.8165	5.501	0.43191	12.217	12.144	12.036	12.022	0.195	0.098
1143	5.465	47.7902	6.511	0.51121	12.301	12.179	12.044	12.024	0.277	0.139
1144	5.479	47.9127	7.496	0.58854	12.379	12.216	12.052	12.026	0.353	0.177
1145	5.467	47.8077	7.765	0.60966	12.413	12.232	12.056	12.027	0.386	0.193
1146	5.474	47.8690	8.000	0.62812	12.429	12.243	12.058	12.027	0.402	0.201
1147	5.488	47.9914	8.241	0.64704	12.453	12.254	12.060	12.028	0.425	0.213
1148	5.483	47.9477	8.488	0.66643	12.473	12.266	12.064	12.031	0.442	0.221
1149	5.468	47.8165	8.998	0.70647	12.516	12.286	12.068	12.032	0.484	0.242
1150	5.475	47.8777	13.989	1.09834	12.910	12.447	12.111	12.048	0.862	0.431
1151	5.479	47.9127	23.985	1.88317	13.752	12.771	12.210	12.094	1.658	0.830
1152	6.513	56.9548	0.013	0.00102	11.895	12.066	12.057	12.061	-0.166	-0.083
1153	6.501	56.8498	1.003	0.07875	11.995	12.097	12.077	12.080	-0.085	-0.043
1154	6.538	57.1734	2.495	0.19589	12.086	12.137	12.089	12.091	-0.005	-0.003
1155	6.527	57.0772	3.994	0.31359	12.188	12.177	12.102	12.097	0.091	0.046
1156	6.520	57.0160	5.508	0.43246	12.306	12.227	12.118	12.104	0.202	0.101
1157	6.517	56.9898	6.494	0.50987	12.393	12.262	12.127	12.105	0.288	0.144
1158	6.530	57.1034	6.998	0.54944	12.445	12.280	12.133	12.105	0.340	0.170
1159	6.530	57.1034	7.251	0.56931	12.472	12.295	12.139	12.106	0.366	0.183
1160	6.549	57.2696	7.500	0.58886	12.492	12.311	12.144	12.109	0.383	0.192
1161	6.523	57.0422	7.762	0.60943	12.530	12.330	12.154	12.110	0.420	0.210
1162	6.529	57.0947	7.990	0.62733	12.547	12.339	12.156	12.111	0.436	0.218

Exp No.	Liq (gpm)	L (kg/m2s)	Air (SCFM)	G (kg/m2s)	Top (psia)	Mid1 (psia)	Mid2 (psia)	Bot (psia)	DP_uc (psi)	NDP_uc
1163	6.525	57.0597	8.497	0.66714	12.598	12.365	12.164	12.113	0.485	0.243
1164	6.515	56.9723	8.983	0.70529	12.643	12.387	12.171	12.115	0.528	0.264
1165	6.499	56.8324	13.986	1.09810	13.104	12.579	12.221	12.134	0.970	0.485
1166	6.510	56.9285	23.992	1.88372	14.031	12.954	12.335	12.195	1.836	0.919
1167	5.460	47.7465	0.018	0.00141	11.887	12.061	12.060	12.069	-0.182	-0.091
1168	5.481	47.9302	0.998	0.07836	11.933	12.083	12.072	12.078	-0.145	-0.073
1169	5.509	48.1750	2.495	0.19589	12.023	12.111	12.082	12.081	-0.058	-0.029
1170	5.482	47.9389	3.993	0.31351	12.113	12.150	12.093	12.087	0.026	0.013
1171	5.479	47.9127	5.496	0.43152	12.218	12.196	12.108	12.093	0.125	0.063
1172	5.458	47.7290	6.989	0.54874	12.330	12.246	12.121	12.097	0.233	0.117
1173	5.473	47.8602	7.274	0.57111	12.358	12.264	12.125	12.099	0.259	0.130
1174	5.478	47.9039	7.495	0.58847	12.375	12.275	12.126	12.098	0.277	0.139
1175	5.479	47.9127	7.743	0.60794	12.396	12.285	12.129	12.099	0.297	0.149
1176	5.473	47.8602	7.987	0.62709	12.424	12.298	12.131	12.099	0.325	0.163
1177	5.473	47.8602	8.244	0.64727	12.438	12.304	12.133	12.099	0.339	0.170
1178	5.454	47.6941	8.493	0.66682	12.456	12.314	12.135	12.100	0.356	0.178
1179	5.467	47.8077	8.765	0.68818	12.488	12.331	12.140	12.103	0.385	0.193
1180	5.478	47.9039	8.997	0.70639	12.515	12.342	12.144	12.103	0.412	0.206
1181	5.465	47.7902	14.018	1.10061	12.896	12.496	12.188	12.120	0.776	0.388
1182	5.505	48.1400	23.994	1.88387	13.720	12.808	12.287	12.171	1.549	0.775
1183	7.018	61.3709	0.010	0.00079	11.810	11.994	11.983	11.987	-0.177	-0.089
1184	7.046	61.6158	1.005	0.07891	12.048	12.150	12.124	12.130	-0.082	-0.041
1185	7.032	61.4933	2.498	0.19613	12.148	12.186	12.135	12.138	0.010	0.005
1186	7.013	61.3272	3.994	0.31359	12.279	12.244	12.156	12.146	0.133	0.067
1187	7.017	61.3622	4.495	0.35292	12.332	12.266	12.164	12.148	0.184	0.092
1188	7.051	61.6595	4.756	0.37341	12.367	12.287	12.172	12.147	0.220	0.110
1189	7.062	61.7557	4.991	0.39187	12.406	12.302	12.179	12.148	0.258	0.129
1190	7.045	61.6070	5.249	0.41212	12.450	12.321	12.185	12.151	0.299	0.150
1191	7.048	61.6332	5.490	0.43104	12.474	12.336	12.190	12.152	0.322	0.161
1192	7.045	61.6070	6.001	0.47116	12.529	12.362	12.198	12.152	0.377	0.189
1193	7.044	61.5983	6.993	0.54905	12.637	12.413	12.215	12.158	0.479	0.240
1194	7.049	61.6420	8.990	0.70584	12.835	12.501	12.240	12.166	0.669	0.335
1195	7.036	61.5283	14.006	1.09967	13.348	12.712	12.291	12.186	1.162	0.581
1196	7.054	61.6857	24.018	1.88576	14.479	13.106	12.398	12.244	2.235	1.118
1197	5.983	52.3200	0.014	0.00110	11.918	12.100	12.097	12.106	-0.188	-0.094

Exp No.	Liq (gpm)	L (kg/m2s)	Air (SCFM)	G (kg/m2s)	Top (psia)	Mid1 (psia)	Mid2 (psia)	Bot (psia)	DP_uc (psi)	NDP_uc
1198	5.995	52.4250	1.005	0.07891	11.995	12.149	12.123	12.127	-0.132	-0.066
1199	6.003	52.4949	2.502	0.19644	12.104	12.199	12.138	12.132	-0.028	-0.014
1200	5.979	52.2851	3.993	0.31351	12.238	12.263	12.155	12.137	0.101	0.051
1201	5.989	52.3725	5.000	0.39257	12.333	12.314	12.167	12.140	0.193	0.097
1202	6.002	52.4862	5.247	0.41196	12.365	12.327	12.169	12.139	0.226	0.113
1203	5.988	52.3638	5.510	0.43261	12.397	12.341	12.173	12.141	0.256	0.128
1204	5.978	52.2763	5.764	0.45256	12.421	12.353	12.175	12.142	0.279	0.140
1205	6.005	52.5124	5.988	0.47014	12.445	12.365	12.179	12.141	0.304	0.152
1206	6.013	52.5824	6.500	0.51034	12.494	12.386	12.184	12.144	0.350	0.175
1207	5.995	52.4250	7.000	0.54960	12.543	12.407	12.189	12.145	0.398	0.199
1208	5.985	52.3375	9.001	0.70671	12.725	12.485	12.208	12.153	0.572	0.286
1209	5.962	52.1364	13.999	1.09912	13.181	12.654	12.253	12.170	1.011	0.506
1210	6.016	52.6086	24.033	1.88694	14.106	12.968	12.356	12.225	1.881	0.941
1211	4.952	43.3042	-0.010	-0.00079	12.012	12.165	12.154	12.163	-0.151	-0.076
1212	4.949	43.2779	0.990	0.07773	12.056	12.184	12.164	12.172	-0.116	-0.058
1213	4.946	43.2517	2.493	0.19574	12.117	12.205	12.173	12.176	-0.059	-0.030
1214	4.928	43.0943	3.996	0.31374	12.191	12.234	12.181	12.181	0.010	0.005
1215	4.927	43.0856	5.003	0.39281	12.240	12.257	12.188	12.183	0.057	0.029
1216	4.957	43.3479	5.995	0.47069	12.305	12.287	12.196	12.187	0.118	0.059
1217	4.954	43.3217	6.504	0.51066	12.346	12.302	12.201	12.188	0.158	0.079
1218	4.976	43.5140	7.000	0.54960	12.393	12.326	12.207	12.191	0.202	0.101
1219	4.952	43.3042	7.246	0.56892	12.419	12.344	12.211	12.192	0.227	0.114
1220	4.976	43.5140	7.493	0.58831	12.435	12.353	12.212	12.191	0.244	0.122
1221	4.955	43.3304	7.748	0.60833	12.456	12.364	12.215	12.192	0.264	0.132
1222	4.941	43.2080	7.992	0.62749	12.484	12.379	12.216	12.192	0.292	0.146
1223	4.939	43.1905	9.014	0.70773	12.554	12.412	12.226	12.196	0.358	0.179
1224	4.933	43.1380	13.992	1.09857	13.003	12.598	12.273	12.213	0.790	0.395
1225	4.949	43.2779	24.006	1.88482	13.907	12.879	12.360	12.255	1.652	0.827
1226	5.455	47.7028	-0.001	-0.00008	11.994	12.150	12.146	12.155	-0.161	-0.081
1227	5.486	47.9739	1.008	0.07914	12.056	12.195	12.167	12.173	-0.117	-0.059
1228	5.462	47.7640	2.497	0.19605	12.147	12.234	12.177	12.178	-0.031	-0.016
1229	5.497	48.0701	3.993	0.31351	12.245	12.289	12.190	12.182	0.063	0.032
1230	5.481	47.9302	5.015	0.39375	12.349	12.346	12.204	12.186	0.163	0.082
1231	5.460	47.7465	5.246	0.41189	12.373	12.360	12.207	12.187	0.186	0.093
1232	5.458	47.7290	5.501	0.43191	12.415	12.383	12.210	12.187	0.228	0.114

Exp No.	Liq (gpm)	L (kg/m2s)	Air (SCFM)	G (kg/m2s)	Top (psia)	Mid1 (psia)	Mid2 (psia)	Bot (psia)	DP_uc (psi)	NDP_uc
1233	5.470	47.8340	6.001	0.47116	12.463	12.407	12.216	12.189	0.274	0.137
1234	5.476	47.8864	7.500	0.58886	12.610	12.476	12.234	12.196	0.414	0.207
1235	5.457	47.7203	9.000	0.70663	12.757	12.535	12.248	12.200	0.557	0.279
1236	5.477	47.8952	14.014	1.10030	13.222	12.683	12.295	12.218	1.004	0.502
1237	5.471	47.8427	23.997	1.88411	14.143	12.955	12.378	12.260	1.883	0.942
1238	6.009	52.5474	0.029	0.00228	11.903	12.119	12.118	12.126	-0.223	-0.112
1239	6.015	52.5999	1.005	0.07891	11.988	12.155	12.139	12.149	-0.161	-0.081
1240	6.001	52.4775	2.513	0.19731	12.056	12.186	12.151	12.155	-0.099	-0.050
1241	5.972	52.2239	3.996	0.31374	12.148	12.226	12.162	12.161	-0.013	-0.007
1242	5.992	52.3987	4.999	0.39249	12.217	12.258	12.172	12.166	0.051	0.026
1243	5.988	52.3638	5.245	0.41181	12.249	12.272	12.175	12.165	0.084	0.042
1244	6.005	52.5124	5.499	0.43175	12.275	12.286	12.177	12.165	0.110	0.055
1245	6.007	52.5299	5.753	0.45169	12.301	12.304	12.182	12.168	0.133	0.067
1246	5.996	52.4337	6.002	0.47124	12.333	12.319	12.184	12.166	0.167	0.084
1247	6.000	52.4687	6.245	0.49032	12.362	12.338	12.186	12.166	0.196	0.098
1248	5.981	52.3026	6.497	0.51011	12.396	12.356	12.191	12.166	0.230	0.115
1249	5.993	52.4075	7.000	0.54960	12.456	12.390	12.197	12.167	0.289	0.145
1250	6.006	52.5212	9.000	0.70663	12.673	12.489	12.221	12.175	0.498	0.249
1251	5.988	52.3638	13.993	1.09865	13.202	12.674	12.276	12.196	1.006	0.503
1252	5.997	52.4425	23.978	1.88262	14.224	12.992	12.377	12.251	1.973	0.987
1253	6.533	57.1297	0.031	0.00243	11.903	12.138	12.137	12.150	-0.247	-0.124
1254	6.497	56.8149	0.998	0.07836	12.000	12.189	12.169	12.180	-0.180	-0.090
1255	6.522	57.0335	2.508	0.19691	12.105	12.231	12.185	12.186	-0.081	-0.041
1256	6.537	57.1647	4.007	0.31461	12.237	12.287	12.200	12.192	0.045	0.023
1257	6.533	57.1297	4.499	0.35324	12.286	12.322	12.206	12.193	0.093	0.047
1258	6.514	56.9635	5.001	0.39265	12.357	12.358	12.213	12.192	0.165	0.083
1259	6.501	56.8498	5.501	0.43191	12.421	12.391	12.219	12.193	0.228	0.114
1260	6.504	56.8761	5.747	0.45122	12.458	12.413	12.223	12.193	0.265	0.133
1261	6.472	56.5962	5.999	0.47101	12.506	12.435	12.228	12.194	0.312	0.156
1262	6.508	56.9111	6.255	0.49111	12.540	12.453	12.232	12.195	0.345	0.173
1263	6.516	56.9810	6.489	0.50948	12.576	12.471	12.235	12.194	0.382	0.191
1264	6.513	56.9548	6.992	0.54897	12.638	12.501	12.241	12.196	0.442	0.221
1265	6.506	56.8936	9.007	0.70718	12.882	12.598	12.262	12.203	0.679	0.340
1266	6.488	56.7362	13.997	1.09897	13.417	12.756	12.312	12.225	1.192	0.596
1267	4.437	38.8006	0.031	0.00243	11.935	12.156	12.161	12.166	-0.231	-0.116

Exp No.	Liq (gpm)	L (kg/m2s)	Air (SCFM)	G (kg/m2s)	Top (psia)	Mid1 (psia)	Mid2 (psia)	Bot (psia)	DP_uc (psi)	NDP_uc
1268	4.450	38.9143	1.000	0.07851	11.975	12.175	12.169	12.176	-0.201	-0.101
1269	4.439	38.8181	2.500	0.19629	12.028	12.198	12.171	12.178	-0.150	-0.075
1270	4.431	38.7481	3.996	0.31374	12.089	12.224	12.180	12.181	-0.092	-0.046
1271	4.431	38.7481	4.988	0.39163	12.148	12.248	12.189	12.187	-0.039	-0.020
1272	4.436	38.7919	6.000	0.47109	12.209	12.277	12.198	12.191	0.018	0.009
1273	4.435	38.7831	6.512	0.51129	12.240	12.291	12.200	12.192	0.048	0.024
1274	4.459	38.9930	6.999	0.54952	12.270	12.304	12.203	12.193	0.077	0.039
1275	4.435	38.7831	7.256	0.56970	12.290	12.312	12.204	12.193	0.097	0.049
1276	4.448	38.8968	7.495	0.58847	12.321	12.325	12.208	12.195	0.126	0.063
1277	4.432	38.7569	7.756	0.60896	12.337	12.338	12.213	12.199	0.138	0.069
1278	4.433	38.7656	8.018	0.62953	12.366	12.352	12.220	12.204	0.162	0.081
1279	4.421	38.6607	8.250	0.64774	12.392	12.365	12.228	12.210	0.182	0.091
1280	4.435	38.7831	8.504	0.66769	12.418	12.375	12.227	12.208	0.210	0.105
1281	4.415	38.6082	8.770	0.68857	12.435	12.383	12.228	12.207	0.228	0.114
1282	4.429	38.7307	9.003	0.70686	12.466	12.397	12.231	12.208	0.258	0.129
1283	4.460	39.0017	9.249	0.72618	12.490	12.410	12.234	12.211	0.279	0.140
1284	4.437	38.8006	9.496	0.74557	12.512	12.416	12.236	12.209	0.303	0.152
1285	4.446	38.8793	9.997	0.78491	12.551	12.432	12.237	12.208	0.343	0.172
1286	4.435	38.7831	13.977	1.09740	12.895	12.557	12.270	12.219	0.676	0.338
1287	4.456	38.9668	23.989	1.88348	13.757	12.831	12.358	12.263	1.494	0.748
1288	5.248	45.8926	0.018	0.00141	11.994	12.150	12.144	12.149	-0.155	-0.078
1289	5.199	45.4641	1.006	0.07899	12.050	12.173	12.156	12.162	-0.112	-0.056
1290	5.212	45.5778	2.492	0.19566	12.104	12.196	12.162	12.165	-0.061	-0.031
1291	5.216	45.6128	4.008	0.31469	12.178	12.228	12.170	12.169	0.009	0.005
1292	5.233	45.7615	5.003	0.39281	12.239	12.253	12.178	12.173	0.066	0.033
1293	5.212	45.5778	6.015	0.47226	12.308	12.288	12.186	12.176	0.132	0.066
1294	5.221	45.6565	6.523	0.51215	12.359	12.311	12.191	12.177	0.182	0.091
1295	5.222	45.6653	6.752	0.53013	12.376	12.321	12.193	12.178	0.198	0.099
1296	5.215	45.6041	6.994	0.54913	12.404	12.337	12.197	12.180	0.224	0.112
1297	5.216	45.6128	7.255	0.56962	12.437	12.355	12.201	12.182	0.255	0.128
1298	5.212	45.5778	7.497	0.58862	12.457	12.366	12.203	12.182	0.275	0.138
1299	5.213	45.5866	7.999	0.62804	12.518	12.395	12.209	12.184	0.334	0.167
1300	5.226	45.7002	8.997	0.70639	12.625	12.443	12.219	12.185	0.440	0.220
1301	5.186	45.3505	14.000	1.09920	13.117	12.618	12.271	12.205	0.912	0.456
1302	5.162	45.1406	23.999	1.88427	14.049	12.907	12.362	12.254	1.795	0.898

Exp No.	Liq (gpm)	L (kg/m2s)	Air (SCFM)	G (kg/m2s)	Top (psia)	Mid1 (psia)	Mid2 (psia)	Bot (psia)	DP_uc (psi)	NDP_uc
1303	5.722	50.0377	0.019	0.00149	11.939	12.106	12.132	12.141	-0.202	-0.101
1304	5.736	50.1601	1.012	0.07946	12.055	12.183	12.155	12.161	-0.106	-0.053
1305	5.726	50.0726	1.997	0.15679	12.063	12.186	12.157	12.159	-0.096	-0.048
1306	5.739	50.1863	3.995	0.31366	12.181	12.229	12.167	12.165	0.016	0.008
1307	5.730	50.1076	4.994	0.39210	12.269	12.270	12.178	12.169	0.100	0.050
1308	5.724	50.0551	5.493	0.43128	12.314	12.290	12.183	12.169	0.145	0.073
1309	5.708	49.9152	6.001	0.47116	12.364	12.319	12.188	12.171	0.193	0.097
1310	5.725	50.0639	6.245	0.49032	12.397	12.336	12.191	12.171	0.226	0.113
1311	5.720	50.0202	6.494	0.50987	12.434	12.356	12.196	12.173	0.261	0.131
1312	5.718	50.0027	6.758	0.53060	12.459	12.368	12.199	12.173	0.286	0.143
1313	5.733	50.1338	6.994	0.54913	12.494	12.387	12.202	12.173	0.321	0.161
1314	5.738	50.1776	7.497	0.58862	12.555	12.418	12.211	12.175	0.380	0.190
1315	5.747	50.2563	9.002	0.70679	12.753	12.504	12.229	12.181	0.572	0.286
1316	5.745	50.2388	14.008	1.09983	13.285	12.677	12.279	12.202	1.083	0.542
1317	5.728	50.0901	24.014	1.88544	14.240	12.972	12.371	12.250	1.990	0.996
1318	3.919	34.2708	0.021	0.00165	11.876	12.102	12.096	12.110	-0.234	-0.117
1319	3.888	33.9997	1.007	0.07906	11.903	12.111	12.103	12.115	-0.212	-0.106
1320	3.932	34.3845	2.500	0.19629	11.964	12.130	12.106	12.117	-0.153	-0.077
1321	3.916	34.2446	4.000	0.31406	12.015	12.152	12.113	12.121	-0.106	-0.053
1322	3.914	34.2271	5.515	0.43301	12.082	12.177	12.118	12.124	-0.042	-0.021
1323	3.919	34.2708	6.999	0.54952	12.148	12.205	12.129	12.125	0.023	0.012
1324	3.894	34.0522	7.996	0.62780	12.209	12.229	12.136	12.129	0.080	0.040
1325	3.909	34.1834	8.996	0.70632	12.270	12.254	12.142	12.131	0.139	0.070
1326	3.906	34.1571	14.016	1.10046	12.659	12.416	12.185	12.150	0.509	0.255
1327	3.936	34.4195	23.995	1.88395	13.479	12.687	12.270	12.191	1.288	0.645
1328	2.885	25.2287	0.028	0.00220	11.889	12.100	12.097	12.110	-0.221	-0.111
1329	2.873	25.1238	0.999	0.07844	11.902	12.106	12.100	12.113	-0.211	-0.106
1330	2.846	24.8877	2.502	0.19644	11.933	12.117	12.101	12.110	-0.177	-0.089
1331	2.882	25.2025	3.999	0.31398	11.964	12.132	12.105	12.111	-0.147	-0.074
1332	2.869	25.0888	5.498	0.43167	12.012	12.148	12.110	12.113	-0.101	-0.051
1333	2.873	25.1238	6.993	0.54905	12.056	12.166	12.116	12.115	-0.059	-0.030
1334	2.898	25.3424	9.013	0.70765	12.134	12.194	12.125	12.120	0.014	0.007
1335	2.873	25.1238	14.020	1.10077	12.391	12.289	12.154	12.136	0.255	0.128
1336	2.885	25.2287	23.996	1.88403	13.028	12.523	12.226	12.175	0.853	0.427
1337	3.915	34.2358	-0.010	-0.00079	11.943	12.128	12.119	12.133	-0.190	-0.095

Exp No.	Liq (gpm)	L (kg/m2s)	Air (SCFM)	G (kg/m2s)	Top (psia)	Mid1 (psia)	Mid2 (psia)	Bot (psia)	DP_uc (psi)	NDP_uc
1338	3.909	34.1834	3.003	0.23578	12.025	12.165	12.134	12.145	-0.120	-0.060
1339	3.899	34.0959	5.992	0.47046	12.147	12.213	12.151	12.149	-0.002	-0.001
1340	3.903	34.1309	9.001	0.70671	12.320	12.289	12.169	12.158	0.162	0.081
1341	3.886	33.9822	9.505	0.74628	12.359	12.305	12.173	12.158	0.201	0.101
1342	3.913	34.2183	10.002	0.78530	12.398	12.326	12.176	12.159	0.239	0.120
1343	3.915	34.2358	10.487	0.82338	12.445	12.345	12.181	12.161	0.284	0.142
1344	3.915	34.2358	10.997	0.86342	12.487	12.367	12.187	12.163	0.324	0.162
1345	3.931	34.3757	12.000	0.94217	12.573	12.403	12.196	12.166	0.407	0.204
1346	3.901	34.1134	14.036	1.10203	12.735	12.465	12.212	12.171	0.564	0.282
1347	2.887	25.2462	0.017	0.00133	11.937	12.129	12.122	12.138	-0.201	-0.101
1348	2.887	25.2462	2.998	0.23539	12.013	12.156	12.131	12.136	-0.123	-0.062
1349	2.881	25.1937	6.009	0.47179	12.116	12.197	12.142	12.142	-0.026	-0.013
1350	2.889	25.2637	8.994	0.70616	12.229	12.243	12.155	12.148	0.081	0.041
1351	2.853	24.9489	11.993	0.94162	12.387	12.304	12.172	12.158	0.229	0.115
1352	2.869	25.0888	12.997	1.02045	12.447	12.327	12.177	12.159	0.288	0.144
1353	2.877	25.1587	13.471	1.05767	12.464	12.336	12.179	12.160	0.304	0.152
1354	2.877	25.1587	13.997	1.09897	12.503	12.348	12.183	12.162	0.341	0.171
1355	2.865	25.0538	14.492	1.13783	12.526	12.359	12.185	12.164	0.362	0.181
1356	2.868	25.0800	15.006	1.17819	12.563	12.373	12.189	12.165	0.398	0.199
1357	2.879	25.1762	15.998	1.25607	12.630	12.396	12.196	12.169	0.461	0.231
1358	2.855	24.9664	19.992	1.56966	12.876	12.484	12.222	12.181	0.695	0.348
1359	1.828	15.9855	0.026	0.00204	11.872	12.087	12.086	12.103	-0.231	-0.116
1360	1.824	15.9505	2.504	0.19660	11.902	12.097	12.089	12.100	-0.198	-0.099
1361	1.849	16.1691	5.013	0.39359	11.936	12.117	12.091	12.099	-0.163	-0.082
1362	1.828	15.9855	7.497	0.58862	11.994	12.139	12.100	12.104	-0.110	-0.055
1363	1.838	16.0729	9.994	0.78467	12.063	12.165	12.111	12.108	-0.045	-0.023
1364	1.816	15.8805	12.499	0.98135	12.148	12.197	12.122	12.115	0.033	0.017
1365	1.847	16.1516	14.992	1.17709	12.240	12.230	12.133	12.122	0.118	0.059
1366	1.819	15.9068	17.515	1.37518	12.332	12.264	12.143	12.128	0.204	0.102
1367	1.836	16.0554	20.022	1.57201	12.454	12.309	12.158	12.137	0.317	0.159
1368	1.783	15.5920	24.003	1.88458	12.639	12.378	12.180	12.152	0.487	0.244
1369	6.522	57.0335	-0.010	-0.00079	11.916	12.094	12.088	12.095	-0.179	-0.090
1370	6.497	56.8149	1.001	0.07859	12.056	12.155	12.124	12.130	-0.074	-0.037
1371	6.545	57.2346	2.502	0.19644	12.171	12.210	12.140	12.138	0.033	0.017
1372	6.515	56.9723	3.994	0.31359	12.396	12.348	12.165	12.144	0.252	0.126

Exp No.	Liq (gpm)	L (kg/m2s)	Air (SCFM)	G (kg/m2s)	Top (psia)	Mid1 (psia)	Mid2 (psia)	Bot (psia)	DP_uc (psi)	NDP_uc
1373	6.513	56.9548	3.505	0.27519	12.337	12.323	12.160	12.143	0.194	0.097
1374	6.524	57.0510	3.000	0.23554	12.282	12.293	12.153	12.141	0.141	0.071
1375	6.504	56.8761	4.995	0.39218	12.532	12.413	12.183	12.149	0.383	0.192
1376	6.512	56.9460	6.990	0.54882	12.772	12.508	12.209	12.157	0.615	0.308
1377	6.509	56.9198	9.001	0.70671	12.983	12.590	12.231	12.165	0.818	0.409
1378	6.539	57.1821	14.013	1.10022	13.479	12.778	12.289	12.193	1.286	0.644
1379	6.514	56.9635	23.989	1.88348	14.624	13.125	12.404	12.253	2.371	1.186
1380	5.486	47.9739	0.004	0.00031	11.933	12.112	12.104	12.115	-0.182	-0.091
1381	5.475	47.8777	1.000	0.07851	12.029	12.150	12.122	12.132	-0.103	-0.052
1382	5.481	47.9302	2.501	0.19636	12.116	12.184	12.133	12.135	-0.019	-0.010
1383	5.472	47.8515	4.000	0.31406	12.208	12.233	12.145	12.141	0.067	0.034
1384	5.478	47.9039	5.004	0.39289	12.299	12.282	12.156	12.145	0.154	0.077
1385	5.467	47.8077	5.250	0.41220	12.342	12.307	12.161	12.146	0.196	0.098
1386	5.486	47.9739	5.505	0.43222	12.380	12.327	12.165	12.146	0.234	0.117
1387	5.464	47.7815	6.005	0.47148	12.437	12.356	12.173	12.149	0.288	0.144
1388	5.474	47.8690	9.000	0.70663	12.717	12.470	12.206	12.161	0.556	0.278
1389	5.455	47.7028	13.983	1.09787	13.167	12.641	12.254	12.180	0.987	0.494
1390	5.472	47.8515	24.041	1.88756	14.181	12.954	12.351	12.231	1.950	0.976
1391	4.424	38.6869	-0.005	-0.00039	11.972	12.119	12.112	12.120	-0.148	-0.074
1392	4.430	38.7394	1.011	0.07938	12.025	12.141	12.122	12.130	-0.105	-0.053
1393	4.441	38.8356	2.495	0.19589	12.069	12.164	12.128	12.133	-0.064	-0.032
1394	4.420	38.6519	4.003	0.31429	12.123	12.193	12.136	12.136	-0.013	-0.007
1395	4.436	38.7919	5.502	0.43199	12.209	12.230	12.145	12.139	0.070	0.035
1396	4.427	38.7132	5.983	0.46975	12.238	12.243	12.148	12.141	0.097	0.049
1397	4.452	38.9318	6.494	0.50987	12.270	12.261	12.154	12.144	0.126	0.063
1398	4.440	38.8268	6.742	0.52934	12.288	12.268	12.155	12.144	0.144	0.072
1399	4.440	38.8268	6.995	0.54921	12.304	12.277	12.157	12.145	0.159	0.080
1400	4.440	38.8268	7.239	0.56837	12.329	12.291	12.161	12.147	0.182	0.091
1401	4.441	38.8356	7.491	0.58815	12.347	12.298	12.162	12.147	0.200	0.100
1402	4.434	38.7744	9.013	0.70765	12.467	12.355	12.176	12.152	0.315	0.158
1403	4.421	38.6607	14.003	1.09944	12.854	12.508	12.220	12.168	0.686	0.343
1404	4.419	38.6432	24.001	1.88442	13.729	12.788	12.305	12.214	1.515	0.758
1405	6.522	57.0335	0.015	0.00118	11.840	12.072	12.068	12.078	-0.238	-0.119
1406	6.514	56.9635	0.994	0.07804	11.995	12.150	12.114	12.119	-0.124	-0.062
1407	6.537	57.1647	2.012	0.15797	12.088	12.196	12.124	12.123	-0.035	-0.018

Exp No.	Liq (gpm)	L (kg/m2s)	Air (SCFM)	G (kg/m2s)	Top (psia)	Mid1 (psia)	Mid2 (psia)	Bot (psia)	DP_uc (psi)	NDP_uc
1408	6.525	57.0597	2.999	0.23546	12.210	12.264	12.137	12.127	0.083	0.042
1409	6.501	56.8498	3.251	0.25525	12.253	12.291	12.141	12.127	0.126	0.063
1410	6.502	56.8586	3.497	0.27456	12.290	12.313	12.145	12.127	0.163	0.082
1411	6.525	57.0597	3.998	0.31390	12.367	12.348	12.152	12.129	0.238	0.119
1412	6.512	56.9460	8.998	0.70647	12.918	12.569	12.213	12.148	0.770	0.385
1413	6.516	56.9810	13.994	1.09873	13.388	12.750	12.267	12.172	1.216	0.608
1414	6.533	57.1297	23.988	1.88340	14.524	13.089	12.377	12.231	2.293	1.147
1415	6.012	52.5736	0.018	0.00141	11.840	12.052	12.070	12.086	-0.246	-0.123
1416	5.985	52.3375	0.996	0.07820	11.983	12.138	12.106	12.113	-0.130	-0.065
1417	5.962	52.1364	1.996	0.15671	12.072	12.183	12.115	12.115	-0.043	-0.022
1418	5.999	52.4600	2.994	0.23507	12.171	12.237	12.126	12.120	0.051	0.026
1419	5.992	52.3987	3.496	0.27449	12.238	12.270	12.130	12.118	0.120	0.060
1420	5.987	52.3550	3.746	0.29411	12.264	12.280	12.132	12.117	0.147	0.074
1421	6.002	52.4862	4.003	0.31429	12.300	12.295	12.134	12.116	0.184	0.092
1422	5.989	52.3725	6.513	0.51136	12.564	12.404	12.165	12.126	0.438	0.219
1423	5.987	52.3550	9.008	0.70726	12.809	12.496	12.190	12.135	0.674	0.337
1424	5.988	52.3638	13.983	1.09787	13.294	12.668	12.241	12.157	1.137	0.569
1425	6.016	52.6086	23.990	1.88356	14.329	12.996	12.341	12.209	2.120	1.061
1426	4.933	43.1380	0.014	0.00110	11.986	12.120	12.113	12.120	-0.134	-0.067
1427	4.964	43.4091	1.001	0.07859	12.053	12.149	12.126	12.134	-0.081	-0.041
1428	4.965	43.4179	2.507	0.19684	12.115	12.179	12.134	12.136	-0.021	-0.011
1429	4.955	43.3304	3.993	0.31351	12.178	12.214	12.143	12.140	0.038	0.019
1430	4.954	43.3217	4.998	0.39241	12.242	12.244	12.152	12.143	0.099	0.050
1431	4.946	43.2517	5.491	0.43112	12.292	12.268	12.157	12.147	0.145	0.073
1432	4.983	43.5753	6.009	0.47179	12.342	12.297	12.165	12.150	0.192	0.096
1433	4.962	43.3916	6.243	0.49017	12.367	12.312	12.167	12.151	0.216	0.108
1434	4.954	43.3217	6.510	0.51113	12.398	12.330	12.172	12.153	0.245	0.123
1435	4.966	43.4266	6.996	0.54929	12.457	12.359	12.179	12.156	0.301	0.151
1436	4.955	43.3304	9.007	0.70718	12.619	12.426	12.200	12.161	0.458	0.229
1437	4.933	43.1380	13.999	1.09912	13.057	12.593	12.247	12.181	0.876	0.438
1438	4.951	43.2954	24.010	1.88513	14.018	12.887	12.337	12.229	1.789	0.895
1439	7.038	61.5458	0.028	0.00220	11.852	12.048	12.073	12.078	-0.226	-0.113
1440	7.036	61.5283	1.005	0.07891	12.055	12.191	12.159	12.170	-0.115	-0.058
1441	7.016	61.3534	2.003	0.15726	12.117	12.222	12.174	12.175	-0.058	-0.029
1442	7.057	61.7119	2.997	0.23531	12.202	12.259	12.186	12.180	0.022	0.011

Exp No.	Liq (gpm)	L (kg/m2s)	Air (SCFM)	G (kg/m2s)	Top (psia)	Mid1 (psia)	Mid2 (psia)	Bot (psia)	DP_uc (psi)	NDP_uc
1443	7.025	61.4321	3.501	0.27488	12.261	12.294	12.191	12.181	0.080	0.040
1444	7.047	61.6245	3.247	0.25494	12.236	12.282	12.186	12.178	0.058	0.029
1445	7.030	61.4758	3.996	0.31374	12.377	12.369	12.197	12.180	0.197	0.099
1446	7.032	61.4933	8.993	0.70608	13.080	12.649	12.260	12.201	0.879	0.440
1447	7.056	61.7032	13.998	1.09904	13.669	12.863	12.315	12.226	1.443	0.722
1448	7.012	61.3184	24.000	1.88435	14.788	13.262	12.434	12.284	2.504	1.253
1449	6.504	56.8761	0.063	0.00495	11.803	12.030	12.043	12.049	-0.246	-0.123
1450	6.496	56.8061	1.003	0.07875	11.964	12.146	12.113	12.117	-0.153	-0.077
1451	6.537	57.1647	1.997	0.15679	12.026	12.170	12.119	12.119	-0.093	-0.047
1452	6.527	57.0772	2.996	0.23523	12.098	12.201	12.129	12.123	-0.025	-0.013
1453	6.533	57.1297	3.254	0.25549	12.118	12.209	12.132	12.124	-0.006	-0.003
1454	6.529	57.0947	3.500	0.27480	12.145	12.218	12.133	12.125	0.020	0.010
1455	6.524	57.0510	3.751	0.29451	12.162	12.226	12.135	12.124	0.038	0.019
1456	6.499	56.8324	4.003	0.31429	12.199	12.247	12.139	12.125	0.074	0.037
1457	6.527	57.0772	4.499	0.35324	12.267	12.286	12.145	12.128	0.139	0.070
1458	6.494	56.7886	9.001	0.70671	12.853	12.533	12.194	12.145	0.708	0.354
1459	6.526	57.0685	14.000	1.09920	13.432	12.740	12.250	12.170	1.262	0.632
1460	6.480	56.6662	24.001	1.88442	14.470	13.111	12.360	12.226	2.244	1.123
1461	5.994	52.4162	0.047	0.00369	11.902	12.089	12.101	12.109	-0.207	-0.104
1462	6.015	52.5999	1.006	0.07899	12.001	12.166	12.145	12.150	-0.149	-0.075
1463	6.011	52.5649	2.004	0.15734	12.055	12.191	12.153	12.155	-0.100	-0.050
1464	5.997	52.4425	2.997	0.23531	12.116	12.216	12.160	12.158	-0.042	-0.021
1465	5.994	52.4162	3.497	0.27456	12.148	12.230	12.162	12.158	-0.010	-0.005
1466	5.979	52.2851	3.995	0.31366	12.184	12.247	12.166	12.159	0.025	0.013
1467	6.013	52.5824	4.265	0.33486	12.212	12.262	12.169	12.161	0.051	0.026
1468	5.989	52.3725	4.496	0.35300	12.240	12.274	12.172	12.162	0.078	0.039
1469	5.983	52.3200	4.996	0.39226	12.307	12.309	12.178	12.164	0.143	0.072
1470	5.988	52.3638	9.025	0.70859	12.788	12.525	12.221	12.176	0.612	0.306
1471	6.004	52.5037	13.988	1.09826	13.349	12.718	12.271	12.197	1.152	0.576
1472	5.969	52.1976	23.998	1.88419	14.370	13.067	12.370	12.248	2.122	1.062
1473	5.471	47.8427	0.046	0.00361	11.855	12.069	12.093	12.103	-0.248	-0.124
1474	5.467	47.8077	0.995	0.07812	11.936	12.129	12.110	12.124	-0.188	-0.094
1475	5.479	47.9127	1.992	0.15640	11.994	12.149	12.118	12.122	-0.128	-0.064
1476	5.469	47.8252	2.999	0.23546	12.053	12.171	12.124	12.123	-0.070	-0.035
1477	5.479	47.9127	4.000	0.31406	12.117	12.202	12.132	12.127	-0.010	-0.005

Exp No.	Liq (gpm)	L (kg/m2s)	Air (SCFM)	G (kg/m2s)	Top (psia)	Mid1 (psia)	Mid2 (psia)	Bot (psia)	DP_uc (psi)	NDP_uc
1478	5.490	48.0089	4.248	0.33353	12.133	12.211	12.132	12.127	0.006	0.003
1479	5.469	47.8252	4.500	0.35331	12.148	12.216	12.133	12.126	0.022	0.011
1480	5.466	47.7990	4.997	0.39234	12.200	12.240	12.139	12.129	0.071	0.036
1481	5.458	47.7290	5.494	0.43136	12.256	12.273	12.143	12.130	0.126	0.063
1482	5.461	47.7553	9.003	0.70686	12.626	12.434	12.176	12.140	0.486	0.243
1483	5.476	47.8864	14.002	1.09936	13.138	12.619	12.222	12.158	0.980	0.490
1484	5.472	47.8515	23.993	1.88380	14.119	12.954	12.317	12.208	1.911	0.956
1485	4.960	43.3741	0.052	0.00408	11.875	12.094	12.089	12.098	-0.223	-0.112
1486	4.971	43.4703	0.996	0.07820	11.934	12.121	12.103	12.109	-0.175	-0.088
1487	4.970	43.4616	2.498	0.19613	12.022	12.149	12.108	12.113	-0.091	-0.046
1488	4.960	43.3741	3.999	0.31398	12.107	12.186	12.118	12.115	-0.008	-0.004
1489	4.976	43.5140	4.997	0.39234	12.172	12.211	12.121	12.116	0.056	0.028
1490	4.948	43.2692	4.759	0.37365	12.138	12.204	12.121	12.116	0.022	0.011
1491	4.960	43.3741	5.241	0.41149	12.177	12.222	12.122	12.115	0.062	0.031
1492	4.953	43.3129	5.501	0.43191	12.195	12.230	12.125	12.117	0.078	0.039
1493	4.956	43.3392	8.997	0.70639	12.499	12.370	12.153	12.125	0.374	0.187
1494	4.926	43.0768	13.980	1.09763	12.984	12.549	12.199	12.145	0.839	0.420
1495	4.959	43.3654	23.986	1.88325	13.896	12.857	12.285	12.191	1.705	0.853
1496	4.433	38.7656	0.010	0.00079	11.994	12.140	12.134	12.140	-0.146	-0.073
1497	4.437	38.8006	1.006	0.07899	12.025	12.153	12.144	12.152	-0.127	-0.064
1498	4.429	38.7307	2.508	0.19691	12.055	12.172	12.151	12.164	-0.109	-0.055
1499	4.451	38.9230	3.993	0.31351	12.107	12.190	12.155	12.156	-0.049	-0.025
1500	4.449	38.9055	5.001	0.39265	12.148	12.207	12.162	12.159	-0.011	-0.006
1501	4.451	38.9230	5.498	0.43167	12.177	12.215	12.164	12.160	0.017	0.009
1502	4.453	38.9405	6.002	0.47124	12.179	12.223	12.167	12.163	0.016	0.008
1503	4.427	38.7132	6.489	0.50948	12.209	12.231	12.168	12.164	0.045	0.023
1504	4.446	38.8793	6.751	0.53005	12.214	12.236	12.170	12.164	0.050	0.025
1505	4.420	38.6519	7.012	0.55054	12.239	12.243	12.172	12.165	0.074	0.037
1506	4.418	38.6345	7.248	0.56907	12.254	12.251	12.174	12.166	0.088	0.044
1507	4.446	38.8793	7.495	0.58847	12.271	12.260	12.176	12.167	0.104	0.052
1508	4.423	38.6782	7.740	0.60770	12.294	12.267	12.178	12.168	0.126	0.063
1509	4.435	38.7831	8.000	0.62812	12.302	12.273	12.179	12.168	0.134	0.067
1510	4.429	38.7307	8.265	0.64892	12.327	12.281	12.181	12.168	0.159	0.080
1511	4.420	38.6519	8.496	0.66706	12.335	12.288	12.181	12.168	0.167	0.084
1512	4.432	38.7569	9.010	0.70741	12.370	12.302	12.187	12.172	0.198	0.099

Exp No.	Liq (gpm)	L (kg/m2s)	Air (SCFM)	G (kg/m2s)	Top (psia)	Mid1 (psia)	Mid2 (psia)	Bot (psia)	DP_uc (psi)	NDP_uc
1513	4.449	38.9055	13.985	1.09802	12.846	12.527	12.231	12.187	0.659	0.330
1514	4.426	38.7044	24.006	1.88482	13.759	12.816	12.312	12.229	1.530	0.766

0.03-cm Resin beads

Exp No.	Liq (gpm)	L (kg/m2s)	Air (SCFM)	G (kg/m2s)	Top (psia)	Mid1 (psia)	Mid2 (psia)	Bot (psia)	DP_uc (psi)	NDP_uc
1515	1.501	13.1259	0.507	0.03981	36.503	15.063	14.390	12.109	24.394	15.714
1516	1.477	12.9160	0.241	0.01892	35.060	15.063	14.164	12.109	22.951	14.785
1517	1.419	12.4088	-0.038	-0.00298	28.216	15.064	13.682	12.111	16.105	10.375
1518	1.470	12.8548	0.749	0.05881	37.757	15.064	14.574	12.109	25.648	16.522
1519	1.456	12.7324	1.000	0.07851	39.830	15.065	14.783	12.110	27.720	17.857
1520	1.445	12.6362	1.498	0.11761	41.424	15.065	15.032	12.110	29.314	18.884
1521	1.456	12.7324	1.989	0.15617	44.405	15.065	15.064	12.110	32.295	20.804
1522	1.488	13.0122	2.468	0.19377	47.651	15.065	15.064	12.109	35.542	22.896
1524	1.432	12.5225	-0.099	-0.00777	32.029	15.064	13.953	12.211	19.818	10.097
1525	1.457	12.7412	0.250	0.01963	38.816	15.064	14.264	12.211	26.605	13.555
1526	1.454	12.7149	0.501	0.03934	40.359	15.064	14.411	12.210	28.149	14.342
1527	1.460	12.7674	0.745	0.05849	42.805	15.065	14.656	12.212	30.593	15.587
1528	1.455	12.7237	1.005	0.07891	44.452	15.065	14.808	12.211	32.241	16.427
1529	1.445	12.6362	1.253	0.09838	45.454	15.065	14.937	12.207	33.247	16.939
1530	1.457	12.7412	1.520	0.11934	47.380	15.065	15.063	12.207	35.173	17.921
1531	1.496	13.0822	1.697	0.13324	48.596	15.065	15.064	12.207	36.389	18.540
1532	1.073	9.3832	-0.071	-0.00557	26.118	15.065	13.300	12.206	13.912	7.088
1533	1.000	8.7448	0.502	0.03941	30.768	15.064	13.764	12.206	18.562	9.457
1534	1.095	9.5755	0.999	0.07844	36.753	15.064	14.281	12.205	24.548	12.507
1535	1.072	9.3744	1.503	0.11801	40.048	15.066	14.571	12.206	27.842	14.185
1536	1.101	9.6280	1.990	0.15624	43.335	15.065	14.822	12.207	31.128	15.860
1537	1.069	9.3482	2.492	0.19566	46.386	15.065	14.957	12.206	34.180	17.415
1538	1.048	9.1645	2.816	0.22110	47.880	15.065	15.064	12.206	35.674	18.176
1539	0.981	8.5786	0.515	0.04043	32.100	15.064	13.922	12.187	19.913	10.146
1540	0.738	6.4537	0.500	0.03926	26.745	15.065	13.513	12.187	14.558	7.417
1541	0.826	7.2232	1.508	0.11840	34.814	15.064	14.257	12.185	22.629	11.529
1542	0.710	6.2088	1.998	0.15687	36.190	15.067	14.347	12.185	24.005	12.231
1543	0.818	7.1532	2.503	0.19652	40.777	15.065	14.769	12.184	28.593	14.568
1544	0.825	7.2144	2.756	0.21639	42.138	15.064	14.895	12.183	29.955	15.262
1545	0.848	7.4156	2.998	0.23539	43.049	15.065	14.929	12.184	30.865	15.726
1546	0.804	7.0308	3.241	0.25447	43.137	15.065	14.959	12.184	30.953	15.771
1547	0.815	7.1270	3.496	0.27449	43.927	15.067	15.001	12.184	31.743	16.173
1548	0.810	7.0833	3.748	0.29427	44.505	15.066	15.043	12.181	32.324	16.469
1549	0.845	7.3893	3.992	0.31343	45.173	15.067	15.032	12.181	32.992	16.809

Exp No.	Liq (gpm)	L (kg/m2s)	Air (SCFM)	G (kg/m2s)	Top (psia)	Mid1 (psia)	Mid2 (psia)	Bot (psia)	DP_uc (psi)	NDP_uc
1550	0.801	7.0046	4.242	0.33306	45.914	15.066	15.065	12.180	33.734	17.187

Appendix G. Three-Phase Equipment List

Subsystem	PI&D Notation (Figure 3.1)	Component	Supplier	Part No.
Liquid - Aqueous	LP-1	Liquid pump	Magnatex	MMP21-R25
	MFM-1	Liquid flow meter	MicroMotion	F050
Liquid - Organic	LP-2	Liquid pump	Magnatex	MMP21-R25
	MFM-2	Liquid flow meter	MicroMotion	F050
Column	Column	Glass Column	Chem Flowtronics	custom
	P-1 through P-8	Pressure transducers	Omega	PX305-050AI
Separator and knockout tank	Chiller	Chiller	NESLAB	HX-150, CP-55, TC-400
	Separator	Separator	Brown-Minneapolis Tank	custom
Gas	Compressor	Compressor	RIX Air-cooled, oil-free N2 compressor	2TX1
	HE-1, 2	Heat exchanger	Exergy LLC	00256-1
	MFC-1	Air mass flow controller	Alicat	MCR-1000SLPM-D
	Vacuum Pump	Vacuum pump	Varian	CD-1400
Ventilation	Fan	Ventilation fan	Nederman N16	N16
	Toluene Sensor	Toluene Sensor	Rae Systems, Inc., MiniRae 2000	011-0201-000
Data Acquisition			National Instruments	SCXI and DAQ card

Appendix H. Three-Phase Safety Considerations

H.1 Pressure Ratings

The manufacturer specified that the glass column sections have a pressure rating from full vacuum to 30 psig. The sections were periodically inspected for cracks and deep scratches which would affect this pressure rating.

For additional insight into the column pressure ratings, material strength calculations were conducted. The column was designed to withstand external pressure during the initial evacuation period as well as internal pressure during general operation. Design guidelines specified that the column should be able to withstand between 4.35 psia (30 kPa) to 42.2 psia (290.9 kPa) of external pressure. To carry out this analysis the material properties for borosilicate glass (surrogate system) were used (Table H.1).

Table H.1. Borosilicate glass material properties (Avallone and Baumeister, 1996)

Material	Property	Value
Borosilicate - Pyrex	allowable stress (psi)	1,000
	Young's Modulus (psi)	8.7×10^6
	Poisson's Ratio	0.3

The failure mode for cylinders under external pressure depends on the wall thickness and column slenderness. Cylinders with internal-diameter-to-thickness *D*/*t* ratios greater than 10 are usually considered to be thin-walled and the radial stresses are assumed to be uniform. Thick-walled cylinders must be analyzed to integrate the stresses through the wall thickness. The column sections considered in the following analyses consist of the column segment with the longest length (*L* = 57 inches), an inner diameter of 4 in and a 17/64-in wall thickness. Thus, the *D/t* ratio is 15.06 and so the column is considered to be thin-walled such that the radial stresses are uniform.

Additionally, the slenderness ratio, $S_y = L/K$, determines whether the column could be considered a compression block or if it is considered a long column which is likely to bend. A value less than 120-150 implies that the column is sufficiently short that bending is unlikely. Calculating the slenderness ratio starts with a calculation of the radius of gyration, *K*.

$$K = \sqrt{I/A} = \frac{\sqrt{D^2 + d^2}}{4} = 1.51 \quad \text{in} \tag{H.1}$$

The area moment of inertia *I* for a circular cross section is

$$I = \frac{\pi(D^4 - d^4)}{64} = 8.12 \quad \text{in}^4 \tag{H.2}$$

The cross sectional area is

$$A = \frac{\pi}{4}(D^2 - d^2) = 3.56 \quad \text{in}^2 \tag{H.3}$$

The slenderness ratio of this particular column is S = L/K = 57 in / 1.51 in = 37.7 implying that bending is unlikely.

H.1.1. Internal Pressure

Design for internal pressure is straightforward for thin-walled vessels. The circumferential (hoop) stress is equal to $S = Pr/t$ under internal pressure P. If the cylinder is closed at both ends then a longitudinal stress $S = Pr/2t$ results. For an external pressure of 30 psi, and a radius of 2 in, the longitudinal stress equals 113 psi. Thus, the hoop stress is 226 psi which is less than the allowable stress of 1000 psi.

H.1.2. External pressure

Cylinders exposed to external pressure may collapse. This collapsing pressure was derived by R. G. Sturn assuming the theory of elasticity (Avallone and Baumeister, 1996).

$$W_c = KE\left(\frac{t}{D}\right)^3 \tag{H.4}$$

The factor of K is determined from empirical data yet at the limit of very slender columns the value of K approaches $2/(1-\nu^2)$. Thus, $K = 2.198$ for the borosilicate column considered here and $W_c = 3{,}852$ psi. This is substantially more than the pressure of a full vacuum and so the column is not expected to collapse radially due to external pressure.

The column was analyzed for buckling due to external pressure. The slenderness of a column experiencing external pressure will affect its failure mode. Long, slender columns will buckle as the first failure mode and are analyzed with Euler's column formula.

$$P_{cr} = \frac{n\pi^2 EI}{L^2} = \frac{4\pi^2(8.7\times10^6 \quad \text{psi})(8.12 \quad \text{in}^4)}{(57 \quad \text{in})^2} = 857{,}500 \quad \text{lbs} \tag{H.5}$$

where a factor of 4 is used for n because both ends are assumed fixed. The Euler relation says that buckling is not the mode of failure if

$$\frac{P_{cr}}{A} > \sigma_y \tag{H.6}$$

Since $P_{cr}/A = 240{,}871$ psi is greater than a working yield stress of 1000 psi then strength rather than buckling causes failure. This reinforces the fact that the column is not long and is unlikely to buckle.

To determine the factor of safety that exists under conditions of external pressure, the longitudinal stress for a column with capped ends is calculated (Young and Budynas, 2002).

$$S = \frac{\text{Pr}}{2t} = \frac{(12.2 \quad \text{psi})(2 \quad \text{in})}{2(17/64 \quad \text{in})} = 46 \quad \text{psi} \tag{H.7}$$

which is less than the allowable stress for glass of 1000 psi. Thus, a safety factor of approximately 20 is implied.

If the column is assumed sufficiently short, then an empirical relation for buckling may be used. The critical pressure for buckling of a free ring (the circumference of the circular column) is

$$S = \frac{2E}{(1-\nu^2)(D/t-1)^3} = 4{,}617 \quad \text{psi} \tag{H.8}$$

This is compared to the expected hoop stress in the cylinder

$$S_h = \frac{\Pr}{t} = 92 \quad \text{psi} \tag{H.9}$$

Implying a factor of safety of approximately 50.

These calculations were carried out assuming a perfect vacuum inside the column during column evacuation processes, so that the pressure difference between the inside and outside of the column equals the atmospheric pressure of 12.2 psi. This is a worst case scenario and it illustrates that the material strength is sufficient. When using a glass column, surface flaws and their impact on material strength are critical. Proper consultation and pressure testing by the glass column manufacturer was done to alleviate this issue. In addition, the glass column was surrounded by a plastic shield to prevent broken glass shards from becoming flying debris in the event of failure (which did not occur).

In the cases of internal and external pressure, a borosilicate column does have the required strength if the wall thickness is equal to 17/64 in and the diameter is close to 4in.

H.1.3. Separator Tank Pressure Ratings

The vessel was designed to ASME standards but was not certified, but was hydrostatically tested to 25 psig by the manufacturer. The vessel, like the glass column, was exposed to internal and external pressure. The internal pressure is not expected to exceed 30 psig.

Table H.2. Properties of 304 stainless steel.

Young's Modulus (psi)	2.8×10^7
Poisson's Ratio	0.29
Density (lb/in^3)	0.289
Yield Strength (psi)	31,200

The analysis for the end plates does not depend on whether the force is acting internal or external to the vessel. In either case, the situation is that of a circular plate with clamped edges and uniform loading. The operating pressure of 30 psig is the design pressure analyzed. The analysis will also apply to vacuum conditions during column evacuation steps, where the maximum pressure applied external to the lid would equal 12.2 psi (local atmospheric pressure in Albuquerque). The end plates are considered to be flat and are either bolted (top plate) or welded (bottom plate) to the cylinder.

Assume plane stress in endplates in order to use the plate bending equations using the Love-Kirchhoff assumptions (Young and Budynas, 2002). Consider the situation of a circular plate of radius R, thickness t, and clamped around the edges. It is subject to a uniform distributed load $P=P(r)$. The deflection pattern that satisfied the boundary conditions ($r=R$: $w=w'=0$, $r=0$: $w=$ finite) is

$$w(r)=k(R^2-r^2)^2 \tag{H.10}$$

where $k=P/64D$ and D is the bending rigidity

$$D=\frac{Et^3}{12(1-\nu^2)} \tag{H.11}$$

ν is the Poisson's ratio and E is the Young's Modulus.

Calculations for stress and strain were performed and the maxima determined. The maximum stress occurs along the external plate surface ($z=t/2$).

$$\sigma_{rr}^{max} = \frac{3}{2}\frac{PR^2}{t^2} \tag{H.12}$$

The maximum deflection is

$$Y_{max} = \frac{0.171PR^4}{Et^3} \tag{H.13}$$

Given different plate thicknesses t, the maximum stresses and deflections were calculated assumed a plate diameter of 3 ft. Based on these calculations the end plates should be at least 1 in thick, which helped determine the equipment requirements.

Table H.3. Required end plate thicknesses.

t (in)	0.5	0.75	1	1.25	1.5	1.75	2
σ_{rr}^{max} (psi)	79380	35280	19845	12700.8	8820	6480	4961.25
Max defl (in)	0.286	0.085	0.036	0.018	0.011	0.007	0.004
FS = YS / σ_{rr}	0.4	0.9	1.6	2.5	3.5	4.8	6.3

As was done with the glass column, the slenderness ratio of the separator vessel was calculated. The slenderness ratio ranges between 0.058 and 0.064 depending on the wall thickness. In this case, it is a short compression block and is not expected to bend. The end plate mass is considered in the longitudinal stress calculation.

$$S=PR/2t \tag{H.14}$$

The thickest plate of 2 in and vacuum conditions results in the worst case stress to be applied to the wall thickness of the cylinder. Assuming this situation, the longitudinal stresses are calculated for the different cylinder wall thicknesses in Table . All of these stresses are sufficiently below the yield stress.

Table H.4. Longitudinal stresses in cylinder due to vacuum and 2-in thick end plate.

t (in)	0.125	0.25	0.5	0.75	1	1.25	1.5	1.75	2
Longitudinal stress (2" end plate)	5115	1538	514	286	193	145	115	95	81

H.2 Chemical Hazards and Mitigation

H.2.1 Occupational Exposure Limits and Ventilation System

SNL uses the lower between OSHA/NIOSH and ACGIH occupational limits. The limits applicable to toluene are as follows:

- 8 hr time weighted average = 50 ppm (ACGIH)
- 15 minute short term exposure limit = 150 ppm (NIOSH)
- There are no exposure limits for isododecane. However, the NFPA health hazard ranking for isododecane is 0 which is a designation given to materials that, on exposure under fire conditions, offer no hazard beyond that of ordinary combustible material.

The experiment requires a ventilation system to provide personal protection when entering the components, to exhaust components such as the pressure relief valves and the sample valves.

Numerous discussions were held with the Sandia Industrial Hygiene department regarding the required ventilation for the toluene experiment. A work area must meet the regulations of a Hazardous Occupancy if 125 gallons or more of hazardous materials are used. The isododecane is not considered a hazardous material. Thus, our experiment was run with only 20-30 gallons of liquids that are considered hazardous (i.e. toluene).

- Another option is to use an elephant trunk-like vent that can be moved to pull vapors from a specific area. While filling the separator the vent trunk was moved over the inlet port or repositioned for various maintenance procedures. This provided ventilation at the point of release and could easily be moved out of the way so as to not become cumbersome to work around.

The ventilation system selected and installed was the Wallcart stationary wall filter from Nederman (http://www.nederman.com/). It consists of an elephant trunk for positioning over different experimental components, an activated carbon filter unit, and a fan. A manifold can be constructed to enable two carbon filters to be mounted in addition to multiple ports for connection to the various pressure relief valves of the experiment.

H.2.2 Vacuum purge requirements

The experiment was evacuated (by pulling a coarse vacuum) and purged with nitrogen to remove the room air prior to adding toluene. Nitrogen was supplied from standard cylinders.

H.2.3 Flammability limits

The surrogate system utilized toluene, which is a flammable liquid. As a result, the flammability hazards need to be considered. For any flammable mixture there are two flammability limits, an upper limit and a lower (lean) limit. Between the two limits a mixture is considered flammable. These limits are affected by temperature, pressure, and mixture composition. The next sections calculate estimates of the flammability hazard for the surrogate system during the initial process of air removal and the introduction of the volatile liquids.

Flammability of the components: toluene and isododecane

The upper and lower flammability limit for a substance must be experimentally determined. The flammability limits of isododecane, one of the experimental components, have not been previously measured in the literature (to the author's knowledge). To carry out this analysis isododecane is substituted for isododecane in all cases. Isododecane and isododecane have the same number of H and C atoms yet are structurally different. Benzene has a similar structure to isododecane yet different numbers of H and C atoms.

The upper and lower flammability limits for toluene, isododecane, and benzene in air at standard pressure are given in H.5.

The stoichiometric reaction of toluene with air is

$$C_7H_8 + 9(O_2 + 3.76\ N_2) \rightarrow 7CO_2 + 4H_2O$$

For this reaction the concentration C_{tol} of toluene in the reactant mixture is

$$C_{tol} = \frac{1\times 100}{1+9\times 4.76} = 2.28\ volpct \qquad \text{(H.15)}$$

Table H.5. Properties of volatile compounds: toluene, isododecane, benzene. † 100°C

	Toluene	Isododecane	Benzene
Formula	C_7H_8	$C_{12}H_{26}$	C_6H_6
LFL (vol pct)	1.2†	0.6	1.3†
UFL (vol pct)	7.1†	5.0	7.9†
Autoignition T (°C)	480	205	560
ΔH_c (kcal/mol)	901.5	1810.5	-
Density (kg/m^3)	867	755	-
MW (g/gmol)	92.1	170.3	-

Thus, the toluene volume percent in a stoichiometric mixture with air is between the flammability limits of 1.2 and 7.1 vol pct.

The stoichiometric mixture of isododecane with air is

$$C_{12}H_{26} + 18.5(O_2 + 3.76\ N_2) \rightarrow 12CO_2 + 13H_2O$$

For this reaction the concentration C_{dod} of isododecane in the reactant mixture is

$$C_{dod} = \frac{1\times 100}{1+18.5\times 4.76} = 1.12\ volpct \tag{H.16}$$

Thus, the isododecane volume percent in a stoichiometric mixture with air is between the flammability limits of 0.6 and 5.0 vol pct. The upper limit was calculated from the lower limit as determined by Zabetakis (1965) mixtures in air at atmospheric pressure and 25°C.

$$U_t = 6.5\sqrt{L_t} \tag{H.17}$$

The LFL for toluene and isododecane both depend slightly on temperature as shown in Figure H.1. The relationship illustrating this dependence by the modified Burgess-Wheeler Law suggested by Zabetakis et al. (1959).

$$L_t = L_{ref} - \frac{0.75}{\Delta H_c}(T - T_{ref}) \tag{H.18}$$

where L_{ref} is the LFL at temperature T_{ref} and ΔH_c is the net heat of combustion in kilocalories per mole (Table H.5).

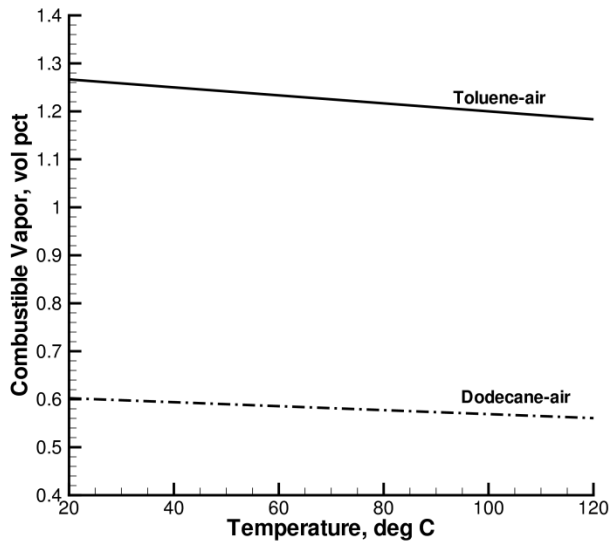

Figure H.1. Lower flammability limit of toluene and isododecane in air at standard pressure as a function of temperature.

The intended operating conditions are room temperature. However, the purge process will be carried out before system operation and so the system temperature is not expected to exceed the ambient air temperature of approximately 25°C.

The effect of pressure on the flammability limits is slight within the intended range of operation. Generally, the LFL and UFL increase as the pressure decreases. The LFL is only slightly affected where the UFL is affected more significantly. Empirical relations can predict the effect of pressure on the flammability limits. These relations are of the form (Vidal et al., 2002)

$$LFL = A_1 - A_2 \log P \tag{H.19}$$

$$UFL = B_1 + B_2 \log P \tag{H.20}$$

for changes in the mixture pressure where P is in atm. For this hazard analysis, the flammability limits at standard atmospheric pressure are considered as a worst-case scenario.

H.2.4. Creating a nonflammable mixture with a single component fuel

Adding an inert component

The concentration of the combustible vapor determines if a mixture is flammable. The concentration of any species in the mixture can be adjusted so that the fraction of combustible component is either less than the LFL concentration or higher than the UFL concentration. It is common practice to "inert" a mixture by adding a species that does not participate in chemical reaction such as N2, CO2, Ar, water vapor, etc. In our situation, the separator vessel contains a mixture of toluene and water. Thus, the water vapor acts to inert the combustible mixture. Water vapor is not as effective at inerting a combustible mixture as is nitrogen, but it is a better inerting chemical than carbon dioxide.

Consider the effect of adding inert N2 to a stoichiometric mixture of toluene-air at standard pressure to render the vapor mixture nonflammable. As noted before the concentration of toluene

in the stoichiometric mixture is 2.25 vol pct which is within the flammability range dictated by the LFL and UFL (7.1 and 1.2 vol pct). Thus, the stoichiometric mixture is flammable.
Consider adding 10% N2. The reactant mixture is then

$$C_7H_8 + 9(O_2 + 3.76\ N_2) + 4.38N_2$$

and the concentration of toluene in this mixture is

$$C_{tol} = \frac{1\times100}{1+9\times4.76+4.38} = 2.07\ volpct \tag{H.21}$$

The mixture is now lean yet does not have a concentration of toluene that is less than the LFL. If 50% N2 is added, the reactant mixture becomes

$$C_7H_8 + 9(O_2 + 3.76\ N_2) + 21.92N_2$$

and the concentration of toluene in this mixture is

$$C_{tol} = \frac{1\times100}{1+9\times4.76+21.92} = 1.52\ volpct \tag{H.22}$$

This concentration of toluene is close to the LFL so the mixture is nearing the LFL and becoming nonflammable. The variation of toluene concentration in the mixture with percent added N2 appears in H.2(a) and the in H.2(b) for isododecane mixtures.

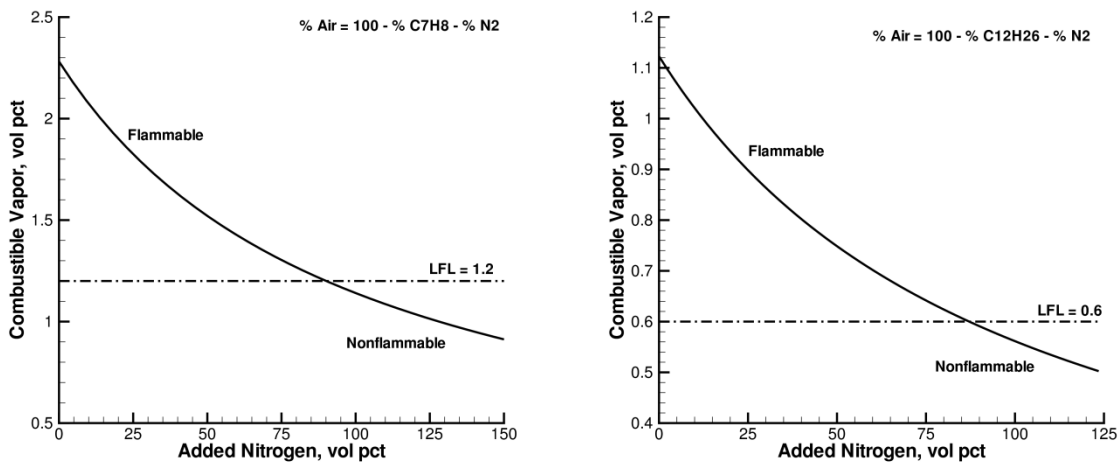

(a) (b)

Figure H.2. Concentration of a) toluene and b) isododecane in reactant mixture as a function of added nitrogen.

These results show that approximately 91 vol pct N_2 must be added to stoichiometric toluene-air and 88 vol pct must be added to stoichiometric isododecane-air to yield a combustible vapor concentration that is nonflammable. Another way to view the problem is the concentration of oxygen in the mixture. Adding 91 vol pct of N_2 to the toluene-air mixture results in an oxygen concentration of 10.7%. Adding 88 vol pct to the isododecane-air mixture results in an oxygen concentration of 11%. Thus, adding N_2 such that the nitrogen concentration in the gaseous phase such that the oxygen concentration is less than approximately 10% can render the mixture nonflammable.

Subtracting Air

Now consider the experiment for which these flammability issues are a concern. In this case, the system initially contains atmospheric air to which the liquids of toluene and isododecane are added. The vapor of the volatile liquids will diffuse into the air, possibly creating a flammable mixture. Because the system initially contains air and the combustible components are added in a second step, the mass of air can be initially decreased by applying a vacuum to the system. In an ideal experiment, the system plumbing could be at a perfect vacuum such that when the toluene and isododecane are installed the resulting mixture is nonflammable. However, such a vacuum is difficult to obtain in the lab. Thus, the minimum amount of air that should be removed from the system to make the resulting mixture nonflammable is desired.

The effect of decreasing the amount of air in the system is investigated. This can similarly be thought of as adding combustible vapor to increase its concentration above the UFL in the mixture. This is first investigated for each pure substance assuming that we can subtract only air from an initial mixture that is stoichiometric. We ignore the effect of pressure on the flammability limit.

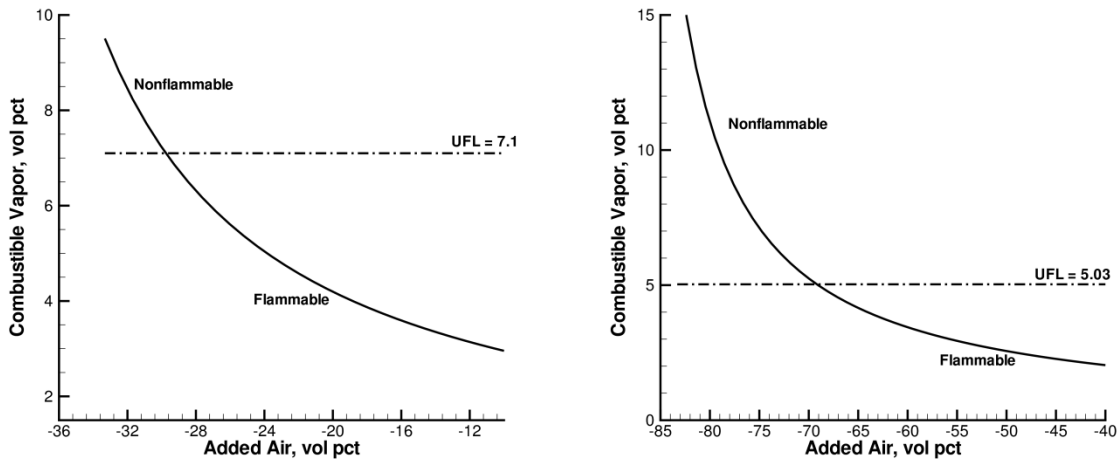

(a) (b)

Figure H.3. Concentration of a) toluene and b) isododecane in reactant mixture as a function of subtracted air.

These results show that approximately 30 vol pct air must be subtracted to stoichiometric toluene-air and 69 vol pct must be subtracted to stoichiometric isododecane-air to yield a combustible vapor concentration that exceeds the UFL and is nonflammable. Subtracting 30 vol pct of air from the toluene-air mixture results in an oxygen concentration of 19.5%. Subtracting 69 vol pct from the isododecane-air mixture results in an oxygen concentration of 20%. Thus, subtracting air such that the oxygen concentration exceeds approximately 20% can render the mixture nonflammable.

H.2.5. Component concentrations in the vapor blend

The next step consists of determining the concentration of each component in the liquid blend and in the vapor blend that is in phase equilibrium. The anticipated liquid blend consists of 40 gal of toluene and 40 gal of the NaOH solution which we will consider to be pure water. The resulting total moles in the liquid blend along with the component properties are listed in Table H.6.

Table H.6. Concentration of components in experimental blend.

	Toluene	Isododecane	Water
Volume (gal)	40		40
Mass (kg)	131.2		151.0
Moles (kmol)	0.713	0.336	8.387
X_i in liquid solution (%)	7.55	3.56	88.89
P_i^0 at 25°C (mmHg)	21.86	0.215	17.544
P_i^0 at 50P_{vi} at 25°C (mmHg)	1.65	0.00765	15.59
P_{vi} at 50°C (mmHg)	6.96	0.04	82.33

This information is used to determine the relative concentration of these parameters in the vapor phase that is in equilibrium with the liquid phase. Assuming an ideal mixture, Raoult's law is used to determine the component vapor pressure in the blend to the vapor pressure of each pure component. This was predicted for the relative fraction of each component expected in the experiment (Table H.6).

$$P_{vi}(25^oC)=X_iP_i^0 \tag{H.23}$$

Use of Raoult's law assumes an ideal mixture. This is often not the case and then the empirical Henry's constants can be used to replace P_i^0 in the above equation. This is out of the scope of this flammability analysis.

With the vapor pressure of each component in the blend, the mole fraction of each component can be determined given the total pressure. Given the partial pressure of air in the system and knowing each component vapor pressure in the blend the combustible mixture concentration can be determined. For example, when the system is initially at atmospheric pressure of 760 mmHg and the liquid components are added, the vapor pressure of the blend at 20°C is 17.25 mmHg. Thus, the gaseous mixture consists of

$$0.212\ C_7H_8+9.84E\text{-}4\ C_{12}H_{26}+2.006\ H_2O+97.78\ (0.21\ O_2 + 0.77\ N_2)$$

and a concentration of fuel vapor (toluene and isododecane) in the mixture of

$$C_{fuel}=\frac{(0.212+9.84E-4)\times 100}{0.212+9.84E-4+2.006+97.78}=0.213\ volpct \tag{H.24}$$

This flammable mixture concentration is low and is likely in the nonflammable region below the LFL. However, for operation of the chemical reactor, the air needs to be evacuated in order to fill with nitrogen. If air is removed, the combustible vapor concentration will increase and likely pass into the flammable mixture range. To ensure that enough air is evacuated, the LFL and UFL of the vapor blend needs to be determined.

Flammability limits of vapor blend

Based on these values of the volume percent of each vapor phase component, the resulting lower flammability limit for the blend is determined from Le Chatelier's law (Coward and Jones, 1979). This law states that the flammability of the blend is dictated by the flammability of each component at their proportion in the vapor blend in air at standard conditions.

$$\sum_{i}^{k} \frac{n_i}{L_i} = 1 \tag{H.25}$$

Where k is the number of component species in the blend and n_i is the percentage of component i in the blend (i.e. $\sum_{i}^{k} n_i = 100$). L_i is the corresponding LFL of each pure component in air. The toluene and isododecane are present in equal volume so their relative concentration is When rewritten, the LFL (vol pct) of the mixture is determined from the components.

$$L = \frac{100}{\sum_{i}^{k} \frac{n_i}{L_i}} \tag{H.26}$$

From the parameters in Table the corresponding LFL of the toluene-isododecane blend is

$$L = \frac{100}{\frac{32}{0.6} + \frac{68}{1.2}} = 0.91\ volpct \tag{H.27}$$

The same procedure is followed to predict the UFL of the blend. The UFL is substituted for the LFL in Eq. **Error! Reference source not found.**H.26.

$$U = \frac{100}{\frac{32}{5.03} + \frac{68}{7.1}} = 6.27\ volpct \tag{H.28}$$

So it is clear now that the mixture considering the inerting with the water vapor and air at standard conditions is below the LFL.

Subtracting Air from the fuel blend

The same procedure as before was carried out to subtract air from the vapor phase prior to filling the vessel with the liquid mixture. Since the initial mixture with air at standard conditions is below the LFL, as the partial pressure of the air decreases the combustible vapor will pass through the flammable region. The UFL is not reached until the partial pressure of air is less than 1.5 kPa at 20°C. This is illustrated in H.4.

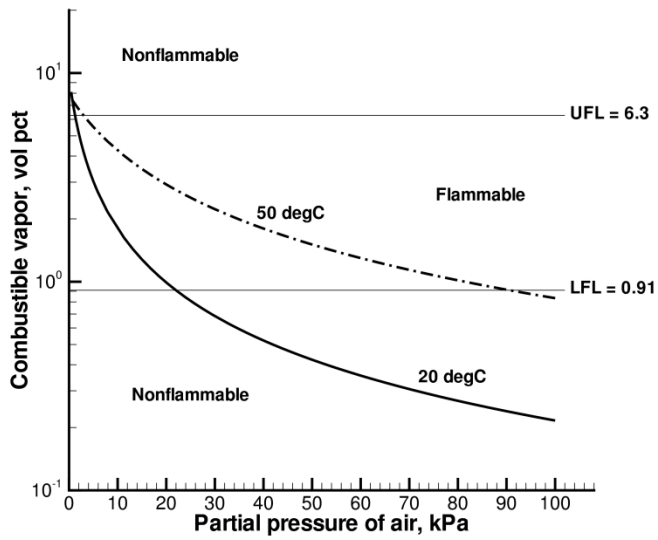

Figure H.4. Method of partial pressures and upper flammability limit.

Because such a low vacuum is difficult to obtain without exceeding the material strength of the glass column evacuating the air should be done in several steps and purging with nitrogen.

This procedure was conducted using a limiting amount of 9 vol. percent for the oxygen. For this criterion, pulling a vacuum one time to 300 mmHg (40 kPa) would yield the concentration of oxygen to be 8% and the mixture nonflammable. This estimate of the required vacuum does not consider the vapor pressure contributions of the toluene, isododecane, or water. When these are considered, reducing the air pressure one time to 300 mmHg results in a concentration of O2 equal to 20%.

If the vacuum cycle to 550 mmHg is repeated three times and the system is filled back to atmospheric pressure with nitrogen each time this is another way to obtain a nonflammable mixture. However, considering the vapor pressure of the blend this should be repeated at least 4 times to obtain an oxygen concentration less than 9%. If the vacuum cycle is carried out to 0.5 atm or 380 mmHg, and purged three times with Nitrogen. The oxygen concentration will result in about 5% which is not expected to be flammable.

H.2.6. Conclusions

The flammability hazards were analyzed for the surrogate system during the initial air purge and injection of volatile liquids. The component concentrations in the blend and the LFL, UFL, and vapor pressure of the blend were evaluated based on an equal volume mixture of toluene and isododecane. The effect of temperature and pressure were determined to be modest so that carrying out the analysis assumed standard conditions of the mixture in air is a worst case analysis. A separate analysis considered the partial pressure of the vapor phase and air in the system determined that the flammability issues can be mitigated by creating a partial vacuum of at least 38 kPa in the system prior to injection of the liquids. By repeating this process three times along with a nitrogen purge, the level of vacuum can be increased. In both case, the material strength has a factor of safety greater than 25 is the column is constructed of tempered glass with a 4 in OD and a 0.25 in wall thickness.

Appendix I. Three-Phase Operations

Operating Procedures: Normal System Startup (Labels refer to the P&ID, Figure 3.1)
Rev. 04.20.06

This procedure assumes the separator contains 20-30 gallons of a 50/50 mixture of toluene and isododecane (referred to as the organic liquid below) and 20-30 gallons of NaOH aqueous solution (referred to as the aqueous liquid below). All plumbing contains N2. Both liquid pumps are primed.

1. Verify all components are in "Normal Shutdown Mode" as specified in Table I.1.
2. Power on components:
    a. LabVIEW and DAQ
    b. LP-1
    c. LP-2
    d. MFM-1
    e. MFM-2
    f. Chiller
    g. MFC-1
    h. All pressure transducers and thermocouples
    i. Exhaust fan (when needed)
3. Apply air supply to solenoid valves:
    a. Open HV-19
    b. Regulate PRG-5 to 90 psig
4. Start flow of aqueous liquid:
    a. Open HV-1
    b. Start LP-1 using controller on wall (hit “Start” to switch from “Stop” to “Run” mode) and set to 25 Hz (minimum flow condition)
        i. LabVIEW will automatically verify (or open) SOV-5
        ii. Wait 15 sec or until pump has reached set speed
        iii. Monitor pump speed indicator on LabVIEW
    c. Verify aqueous liquid level in separator using sight glass
    d. Switch 3WV-1 to column
        i. LabVIEW will automatically open SOV-1 when P-7 reaches the user-specified "Head Pressure Set Point", units are in PSIS (relative to 14.7 psi).
        ii. Listen for SOV-1 to open and verify that green light and "open" are output on LabVIEW display
    e. Monitor MFM-1 on LabVIEW graph
    f. Wait 20 sec or until steady flow is achieved
    g. Verify aqueous liquid level in separator using sight glass
5. Start flow of organic liquid:
    a. Open HV-2
    b. Start LP-2 using controller on wall (hit “Start” to switch from “Stop” to “Run” mode) and set to 25 Hz (minimum flow condition)
        i. LabVIEW will automatically verify (or open) SOV-6
        ii. Wait 15 sec or until pump has reached set speed
        iii. Monitor pump speed indicator on LabVIEW
    c. Verify organic liquid level in separator using sight glass
    d. Switch 3WV-2 to column
        i. LabVIEW will automatically open SOV-2 when P-8 reaches the user-specified "Head Pressure Set Point", units are in PSIS (relative to 14.7 psi).
        ii. Listen for SOV-2 to open and verify that green light and "open" are output on LabVIEW display
    e. Monitor MFM-2 on LabVIEW graph

    f. Wait 20 sec or until steady flow is achieved
    g. Verify organic liquid level in separator using sight glass
6. Start compressor:
    a. Close Vent HV (was “Close PRG-3”)
    b. Start compressor using “Nitrogen Compressor” wall switch
    c. Monitor P-1 (near ambient pressure) and P-2 (approximately 18.5 psia)
    d. Open HV-6
7. Start flow of N2:
    a. Increase flow set point of MFC-1 in increments of 1 SCFM
        i. LabVIEW will automatically open SOV-3
        ii. With SOV-7 open, up to 3.5 SCFM may be obtained
    b. To achieve gas flows greater than 3.5 SCFM:
        i. Open Vent HV
        ii. Close SOV-7
        iii. Increase MFC-1
        iv. Throttle Vent HV as needed to achieve MFC-1 set point (capable up to 10 SCFM)
8. Increase LP-1, LP-2, and MFC-1 to desired set points
9. Verify all components are in “Normal Operating Mode” as specified in Table I.2.

At this point the column should be in steady operation. Next steps would include either data acquisition under steady flow conditions, holdup measurements, FDA injection, or normal shutdown.

Operating Procedures: Holdup Measurements

This procedure assumes the system is in steady operation (i.e. constant flow rates for both liquid pumps and the gas compressor). The steps listed below could be initiated by the user clicking a "virtual switch" in LabVIEW.

1. Click "Perform Holdup" button on LabVIEW. LabVIEW will automatically (and simultaneously):
    a. close SOV-1, SOV-2, SOV-3, and SOV-4
    b. Open SOV-7
    c. Switch 3WV-1 and 3WV-2 to bypass mode
    d. Lower liquid pump speed to minimum bypass flow condition (20 Hz)
    e. MFC-1 set to zero flow
2. Close Vent HV
3. Monitor P1 (near or slightly greater than ambient pressure) and P2 (approximately 18.5 psia)
4. Wait for liquid to drain to bottom of column. Record volume measurement.
    If this waiting period is significantly long, the liquid pumps and compressor may be turned off.
5. Open SOV-4
6. Restart liquid and gas flows as in the Normal Startup Procedure

Operating Procedures: Emergency Shutdown

This procedure assumes the system is in steady operation and an unexpected event occurs (i.e. overpressure or liquid leak or spill). Specifics of the scenarios that would require emergency shutdown are considered in the document “Release Scenarios”.

1. Simultaneously:
    a. Close SOV-1, SOV-2, SOV-3, SOV-5, and SOV-6
    b. Open SOV-7
    c. Set PRG-1 and MFC-1 to no flow

    d. Switch 3WV-1 and 3WV-2 to bypass mode
    e. Shut off LP-1 and LP-2
    f. PRG-3 and PRG-4 to ambient pressure
    g. Turn compressor off
2. Set PRG-5 to no flow

Operating Procedures: Normal System Shutdown

This procedure assumes the system is in steady operation.

1. Verify all components are in "Normal Operating Mode" as specified in Table I.2.
2. Shut off flow of organic liquid:
    a. Switch 3WV-2 to bypass mode (LabVIEW will automatically reduce LP-2 to minimum bypass flow condition of 20 Hz)
    b. Close SOV-2
    c. Set LP-2 to zero flow
    d. Close SOV-6
3. Shut off flow of aqueous liquid:
    a. Switch 3WV-1 to bypass mode (LabVIEW will automatically reduce LP-1 to minimum bypass flow condition of 20 Hz)
    b. Close SOV-1
    c. Set LP-1 to zero flow
    d. Close SOV-5
4. Open (or verify) SOV-7
5. Reduce MFC-1 low flow condition (1 SCFM)
6. Close (or verify closed) PRG-3
7. Close SOV-3 (LabVIEW will automatically set MFC-1 to zero flow)
8. Turn off compressor
9. Turn off chiller
10. Close HV-4
11. Close HV-6
12. Verify all components are in “Normal Shutdown Mode” as specified in Table I.1.

Operating Procedures: Replace liquids in Separator

This procedure describes the steps required to remove the spent liquid from the separator and replace with a fresh batch of liquids. This procedure does not include maintenance or other activities where the separator lid would be removed or a port on the separator would be open for an extended period of time. The surrogate chemical system is “spent” when all of the fluorescein diacetate (FDA) reactant in the organic liquid (composed of a 50/50 mixture of toluene and isododecane) has been chemically converted into the fluorescein product in the aqueous liquid (0.1M NaOH). Under most cases, only the aqueous liquid needs to be removed from the system and replaced with a fresh batch. Additional FDA can then be added to the organic liquid to replenish the reactant in the system.

The operator removing and adding the liquids would use appropriate PPE to protect against liquid splashing. The MinRae2000 Toluene sensor is located near the operator to detect vapor concentrations.

1. Verify the experiment is not operating and all components are in “Normal Shutdown Mode” as specified in Table I.1.
2. Verify P1 reads ambient pressure
3. If P1 is above ambient pressure:
    a. Open HV-14
    b. Reduce set pressure of PRG-4 to ambient pressure
    c. Wait until P1 reaches ambient pressure

    d. Close HV-14
4. Attach tubing and pump to connect drain port to waste vessel
5. Open HV-9
6. Empty vessel
7. Close HV-9
8. Follow waste procedures to dispose of spent chemicals
9. Attach tubing and pump to connect fill port to vessel containing fresh chemicals
10. Fill separator
11. Evacuate air from separator headspace
    a. Turn on vacuum pump
    b. Verify liquid level is above liquid-liquid return line
    c. Slowly and partially open HV-10
    d. Monitor P1
    e. Close HV-10 when P1 reaches 1 psia
    f. Open HV-14
    g. Fill separator headspace with N2 by opening PRG-1
    h. Monitor P1
    i. Close HV-14 when P1 reaches 0 psig
    j. Repeat steps 13.c-13.i at least 3 times

Experiment is now ready for normal startup to operation.

Operating Procedures: Replace packing in column

This procedure describes the steps required to remove the packing in the column and replace with a different type of packing and also includes any maintenance activities for the column only. It is assumed that the system has been flushed sufficiently long with nitrogen following the *System Flushing Procedure*.

The operator handling the packing removing and adding the liquids would use appropriate PPE and the MinRae2000 Toluene sensor is located near the operator to detect vapor concentrations.

1. Verify the experiment is not operating and all components are in "Normal Shutdown Mode" as specified in Table I.1.
2. Verify P1 and P2 read ambient pressure
3. Remove the top glass section containing the three inlet connections and place on the support hooks.
4. Use vacuum to suck out packing if beads, or use tool to remove woven packing sections.
5. Replace packing and top glass section

Experiment is not ready to for the fill/purge process to remove the air from the column and fill with nitrogen.

Operating Procedures: System Flush with Nitrogen

This procedure describes the steps required to flush the system with nitrogen prior to opening any component for maintenance or replacement. This ensures that no users are exposed to hazardous amounts of toluene vapor. Typically, either the column or the separator will need to be opened. Depending on the nature of the maintenance activities valve positions may vary. However, the general idea is to operate the gas system on recirculation mode through the column or flushing mode through the separator. This process may take many hours or possibly a few days. The vacuum pump can be used to facilitate this process, but should not be done until the system has been flushed for a period of time to minimize the amount of liquid that could be pulled into the vacuum pump. Check the flow stream periodically with the toluene sensor to evaluate the toluene concentrations. This will determine when the system may be opened.

Table I.1. Valve Positions of "Normal Shutdown Mode"

	Component	Name	Position	Excitation
Liquid Subsystem	SOV-6	Organic pump inlet	closed	none (NC)
	SOV-5	Aqueous pump inlet	closed	none (NC)
	LP-1	Aqueous pump	off	none
	LP-2	Organic pump	off	none
	3WV-1	Aqueous bypass 3-way	bypass mode	none
	3WV-2	Organic bypass 3-way	bypass mode	none
	HV-1	Aqueous outlet hand valve	open	n/a
	HV-2	Organic outlet hand valve	open	n/a
	SOV-1	Aqueous inlet – top of column	closed	none (NC)
	SOV-2	Organic inlet – top of column	closed	none (NC)
	MFM-1	Aqueous mass flow meter	off	none
	MFM-2	Organic mass flow meter	off	none
	S-1	Sample valve – top of column	closed	n/a
	S-2	Sample valve – top of column	closed	n/a
	SOV-4	Column base holdup valve	open	none (NO)
	HV-3	Column base drain	closed	n/a
	HV-16	Aqueous pump drain	closed	n/a
	HV-17	Organic pump drain	closed	n/a
	HV-9	Separator tank drain	closed	n/a
	S-3	Column sample valve	closed	n/a
	S-4	Column sample valve	closed	n/a
	S-5	Column sample valve	closed	n/a
	S-6	Column sample valve	closed	n/a
Gas Subsystem	SOV-3	Nitrogen inlet – top of column	closed	none (NC)
	MFC-1	Nitrogen Alicat mass flow cont.	No flow	
	SOV-7	Nitrogen bypass solenoid	open	none (NO)
	HV-4	Column vapor take off drain to knockout tank	closed	n/a
	HV-5	Separator tank vent/fill	closed	n/a
	HV-6	Knockout tank drain to separator	closed	n/a
	Chiller		off	
	Compressor		off	
	PRG-3	Temporary hand valve Vent HV	ambient pressure	n/a
	HV-7	Compressor discharge vent	closed	n/a
	HV-8	Liquid accumulator drain	closed	n/a
Vacuum Subsystem	HV-11	Vapor/liquid line to vacuum pump	closed	n/a
	HV-12	Vacuum bleed line	closed	n/a
	HV-10	Vacuum line to top of separator	closed	n/a
N_2 Supply	HV-14	N_2 supply to separator	closed	n/a
	HV-15	N_2 supply to vent	open	n/a
	PRG-4	Pressure relief N_2 supply to vent	ambient pressure	n/a
	HV-13	Room 8 - N_2 Isolation	closed	n/a
	PRG-0	Room 8 – House N_2 regulator	set 1500 psi	n/a
	PRG-1	Room 19 - N_2 supply regulator	No flow	n/a
	HV-18	Main N_2 supply isolation	closed	n/a
Air Supply	HV-19	Building air supply brass valve	open	n/a
	PRG-5	Building air supply regulator	set 85-90 psi	n/a

Table I.2. Valve Positions of "Normal Operating Mode"

	Component	Name	Position	Excitation
Liquid Subsystem	SOV-6	Organic pump inlet	open	+120VAC
	SOV-5	Aqueous pump inlet	open	+120VAC
	LP-1	Aqueous pump	off	none
	LP-2	Organic pump	off	none
	3WV-1	Aqueous bypass 3-way	to column	+120VAC
	3WV-2	Organic bypass 3-way	to column	+120VAC
	HV-1	Aqueous outlet hand valve	open	n/a
	HV-2	Organic outlet hand valve	open	n/a
	SOV-1	Aqueous inlet – top of column	open	+120VAC
	SOV-2	Organic inlet – top of column	open	+120VAC
	MFM-1	Aqueous mass flow meter	off	none
	MFM-2	Organic mass flow meter	off	none
	S-1	Sample valve – top of column	closed	n/a
	S-2	Sample valve – top of column	closed	n/a
	SOV-4	Column base holdup valve	open	none (NO)
	HV-3	Column base drain	closed	n/a
	HV-16	Aqueous pump drain	closed	n/a
	HV-17	Organic pump drain	closed	n/a
	HV-9	Separator tank drain	closed	n/a
	S-3	Column sample valve	closed	n/a
	S-4	Column sample valve	closed	n/a
	S-5	Column sample valve	closed	n/a
	S-6	Column sample valve	closed	n/a
Gas Subsystem	SOV-3	Nitrogen inlet – top of column	open	+120VAC
	MFC-1	Nitrogen Alicat mass flow cont.	desired flow	
	SOV-7	Nitrogen bypass solenoid	open (or closed)	none (or +120VAC)
	HV-4	Column vapor take off drain to knockout tank	open	n/a
	HV-5	Separator tank vent/fill	closed	n/a
	HV-6	Knockout tank drain to separator	open	n/a
	Chiller		on	
	Compressor		on	
	PRG-3	Temporary hand valve Vent HV	discharge pressure	n/a
	HV-7	Compressor discharge vent	closed	n/a
	HV-8	Liquid accumulator drain	closed	n/a
Vacuum Subsystem	HV-11	Vapor/liquid line to vacuum pump	closed	n/a
	HV-12	Vacuum bleed line	closed	n/a
	HV-10	Vacuum line to top of separator	closed	n/a
N2 Supply	HV-14	N_2 supply to separator	open	n/a
	HV-15	N_2 supply to vent	open	n/a
	PRG-4	Pressure relief N_2 supply to vent	suction pressure	n/a
	HV-13	Room 8 - N_2 Isolation	closed	n/a
	PRG-0	Room 8 – House N_2 regulator	set 1500 psi	n/a
	PRG-1	Room 19 - N_2 supply regulator	suction pressure	n/a
	HV-18	Main N_2 supply isolation	open	n/a
Air Supply	HV-19	Building air supply brass valve	open	n/a
	PRG-5	Building air supply regulator	set 85-90 psi	n/a

5. References

Al-Dahhan M.H. and Dudukovic M.P., (1994), "Pressure drop and liquid holdup in high pressure trickle-bed reactors," *Chemical Engineering Science* **49**, 5681-5698.

Adam, G. and Duncan, H., (2001), "Development of a sensitive and rapid method for the measurement of total microbial activity using fluorescein diacetate (FDA) in a range of soils," *Soil Biology and Biochemistry*, 33(7-8), 943-951.

American Chemical Society, (1996), "Technology Vision 2020: The U. S. Chemical Industry" available at http://www.chemicalvision2020.org/vision.html.

Andreussi, P., Donfrancesco, A. D. and Messia, M., (1988), "An impedance method for the measurement of liquid holdup in two-phase flow," *International Journal of Multiphase Flow* **14**(6), 777-785.

Attou, A. and Ferschneider, G., (2000), "A two-fluid hydrodynamic model for the transition between trickle and pulse flow in a cocurrent gas-liquid packed-bed reactor," *Chemical Engineering Science* **55**(3), 491-511.

Avallone, E. A. and Baumeister, T., (1996), Marks' Standard Handbook for Mechanical Engineers, 10th ed.

Bartelmus, G., Gancarczyk, A. and Stasiak, M., (1998), "Hydrodynamics of cocurrent fixed-bed three-phase reactors. Part I. The effect of physicochemical properties of the liquid on pulse velocity," *Chemical Engineering and Processing* **37**(4), 331-341.

Battin, T. J., (1997), "Assessment of fluorescein diacetate hydrolysis as a measure of total esterase activity in natural stream sediment biofilms," *The Science of the Total Environment*, **198**(1), 51-60.

Beimesch, W. E. and Kessler, D. P., (1971), "Liquid-gas distribution measurements in the pulsing regime of two-phase cocurrent flow in packed beds," *AIChE Journal* **17**(5), 1160-1165.

Blok, J. R., Varkevisser, J., and Drinkenburg, A. H., (1983), "Transition to pulsing flow, holdup, and pressure drop in packed columns with cocurrent gas-liquid downflow," *Chemical Engineering Science* **38**(5), 687-699.

Boelhouwer, J. G., Piepers, H. W., and Drinkenburg, A. A. H., (2002), "Nature and characteristics of pulsing flow in trickle-bed reactors," *Chemical Engineering Science* **57**(22-23), 4865-4876.

Boyer, C. and Fanget, B., (2002), "Measurement of liquid flow distribution in trickle bed reactor of large diameter with a new gamma-ray tomographic system," *Chemical Engineering Science* **57**(1), 1079-1089.

Breeuwer, P., Drocourt, J.-L., Bunschoten, N., Zwietering, M. H., Rombouts, F. M., and Abee, T., (1995), "Characterization of uptake and hydrolysis of fluorescein diacetate and carboxyfluorescein diacetate by intracellular esterases in *Saccharomyces cerevisiae*, which result

in accumulation of fluorescent product," *Applied and Environmental Microbiology*, **61**, 1614-1619.

Burghardt, A., Bartelmus, G., and Gancarczyk, A., (1999), "Hydrodynamics of pulsing flow in three-phase chemical reactors," *Chemical Engineering and Processing* 38(4), 411-426.

Burghardt, A., Bartelmus, G., Janecki, D., and Szlemp, A., (2002), "Hydrodynamics of a three-phase fixed-bed reactor operating in the pulsing flow regime at an elevated pressure," *Chemical Engineering Science* **57**(1), 4855-4863.

Burghardt, A., Bartelmus, G., and Szlemp, A., (2004), "Hydrodynamics of pulsing flow in three-phase fixed-bed reactor operating at an elevated pressure," *Industrial and Engineering Chemistry Research* **43**(16), 4511-4521.

Charpentier, J., (1976), "Recent progress in two phase gas-liquid mass transfer in packed beds," *Chemical Engineering Journal* **11**(3), 161-181.

Cho, J., Perlin, M., and Ceccio, S. L., (2005), "Measurement of near-wall stratified bubbly flows using electrical impedance," *Measurement Science and Technology* **16**(4), 1021-1029.

Chou, T. S., Worley, F. L., and Luss, D., (1977), "Transition to pulsed flow in mixed-phase cocurrent downflow through a fixed bed," *Industrial and Engineering Chemistry, Process Design and Development* **16**(3), 424-427.

Chu, C. F. and Ng, K. M., (1989), "Flow in packed tubes with a small tube to particle diameter ratio," *AIChE Journal* **35**(1), 148-158.

Clarke, J. M., Gillings, M. R., Altavilla, N., and Beattie, A. J., (2001), "Potential problems with fluorescein diacetate assays of cell viability when testing natural products for antimicrobial activity**,"** *Journal of Microbial Methods*, **46**(7), 261-267.

Cohen, Y. and Metzner, A. B., (1981), "Wall effect in laminar flow of fluids through packed beds," *AIChE Journal* **27**(5), 705-715.

Cooper, M. A., Cote, R. O., O'Hern, T. J., Torczynski, J. R., Evans, L. R., Cross, W. M., and Smith, L. A., (2005), "Experimental Methods Defining the Trickle-Pulse Transition in Two-Phase Flows through Fixed Beds," AICHE Spring National Meeting, Atlanta, GA, April, 2005.

Cooper, M. A., Cote, R. O., O'Hern, T. J., Torczynski, J. R., Evans, L. R., Cross, W. M., and Smith, L. A., (2005), "An Experimental Investigation of the Effect of Walls on Gas-Liquid Flows Through Fixed Particle Beds," ASME Fluids Engineering Division Summer Conference, Houston, TX, June, 2005.

Coward, H. F. and Jones, G. W., 1979, "Limits of flammability of gases and vapors," U.S. Dept of the Interior, Bureau of Mines, Bulletin 503.

Eisfeld, B. and Schnitzlein, K., (2001), "The influence of confining walls on the pressure drop in packed beds," *Chemical Engineering Science* **56**(14), 4321-4329.

Felice, R. D. and Gibilaro, L. G., (2004), "Wall effects for the pressure drop in fixed beds," *Chemical Engineering Science* **59**(14), 3037-3040.

Fogler, H. S., (1992), Elements of Chemical Reactor Engineering, Englewood Cliffs, NJ: Prentice Hall, 191-193.

Gianetta, A. and Specchia, V., (1992), "Trickle-bed reactors: state of art and perspectives," *Chemical Engineering Science* **47**(13), 3197-3213.

Grosser, K., Carbonell, R.G., Sundaresan, S., (1988). "Onset of pulsing in two-phase cocurrent downflow through a packed bed," *AIChE. Journal* **34**, 1850–1860.

Guilbault G. G. and Kramer, D. N., (1964), "Fluorometric Determination of Lipase, Acylase, Alpha-, and Gamma-Chymotrypsin and Inhibitors of These Enzymes," *Analytical Chemistry*, **36**(2), 409-412.

Helwick, J. A., Dillon, P. O., and McCready, M. J., (1992), "Time varying behavior of cocurrent gas-liquid flows in packed beds," *Chemical Engineering Science* **47**(13/14), 3249-3256.

Holub, R. A., Dudukovic, M. P., and Ramachandran, P. A., (1993), "Pressure drop, liquid holdup and flow regime transition in trickle flow," *AIChE Journal* **39**(2), 302-321.

Huang, Z., (1991), "Kinetic assay of fluorescein mono-.beta.-D-galactoside hydrolysis by .beta.-galactosidase: a front-face measurement for strongly absorbing fluorogenic substrates," *Biochemistry*, **30**(35), 8530-8534.

Huang, Z., (1991), "Kinetic fluorescence measurement of fluorescein di-.beta.-D-galactoside hydrolysis by .beta.-galactosidase: intermediate channeling in stepwise catalysis by a free single enzyme," *Biochemistry*, **30**(35), 8535-8540.

Iliuta, I. and Larachi, F., (2004), "Onset of pulsing in gas-liquid trickle bed filtration," *Chemical Engineering Science* **59**(6), 1199-1211.

Inbar, Y., Boehm, M. J., and Hoitink, H. A. J., (1991), "Hydrolysis of fluorescein diacetate in sphagnum peat container media for predicting suppressiveness to damping-off caused by *Pythium ultimum," Soil Biol. Biochem.*, **23**(5) 479-483, 1991

Invitrogen Corporation, Molecular Probes: The Handbook http://www.invitrogen.com/site/us/en/home/References/Molecular-Probes-The-Handbook.html, retrieved 03/03/2010.

Jaeger, H. M. and Nagel, S. R., (1992), "Physics of granular states," *Science* **255**, 1524.

Jorgensen, P. E., Eriksen, T., and Jensen, B. K., (1992), **"**Estimation of viable biomass in wastewater and activated sludge by determination of ATP, oxygen utilization rate and FDA hydrolysis," *Water Research*, **26**(11) 1495-1501.

Leonhardt, H., Gordon, L., and Livingston, R., (1971), "Acid-base equilibria of fluorescein and 2′,7′-dichlorofluorescein in their ground and fluorescent states," *J. Physical Chemistry*, **75**(2), 245–249.

Lindquist, L., (1960), "A flash photolysis study of fluorescein," *Arkiv. Kemi.*, **16**, 79-138.

Martin M. M. and Lindquist, L., (1975), "The pH-dependence of fluorescein fluorescence," *Journal of Luminescence*, **10**, 381-390.

Mehta, D. and Hawley, M. C., (1969), "Wall effect in packed columns," *I-and-EC Process Design* and *Development* **8**(2), 280-282.

Miller, C. and Kaibel, G., (2004), "Packings for fixed bed reactors and reactive distillation," *Chemical Engineering Science* **59**(22-23), 5373-5379.

Nield, D. A. (1983), "Alternative model for wall effect in laminar flow of a fluid through a packed column," *AIChE Journal* **29**(4), 688-689.

Nigam, K. D. P. and Larachi, F., (2005), "Process Intensification in trickle-bed reactors," *Chemical Engineering Science* **60**, 5880-5894.

Niven, R. K., (2002), "Physical insight into the Ergun and Wen & Yu equations for fluid flow in packed and fluidised beds," *Chemical Engineering Science* **57,** 527-534.

O'Hern, T. J., Gill, W., Evans, L. R., Miller, J. E., Cross, W., Foley, R., Smith, L., (2007) "Experimental Study of Flow in Trickle Beds," 2007 AICHE Spring National Meeting, Houston, TX, April, 2007.

Rao, V. G. and Drinkenburg, A. A. H., (1985), "A model for pressure drop in two-phase gas-liquid downflow through packed columns," *American Institute of Chemical Engineering Journal* **31**, 1010-1018.

Ratheesh, S. and Kannan, A., (2004), "Holdup and pressure drop studies in structured packings with catalysts," *Chemical Engineering Journal* **104**(1-3), 45-54.

Reinecke, N. and Mewes, D., (1996), "Tomographic imaging of trickle-bed reactors," *Chemical Engineering Science* **51**(10), 2131-2138.

Saez, A. E. and Carbonell, R. G., (1985), "Hydrodynamic parameters for gas-liquid cocurrent flow in packed beds," *AIChE Journal* **31**(1), 52-62.

Satterfield, C. N., (1975), "Trickle-bed reactors," *AIChE Journal* **21**(2), 209-228.

Schmit, C. E., Cartmel, D. B., and Eldridge, R. B., (2001), "The experimental application of X-ray tomography to a vapor-liquid contactor," *Chemical Engineering Science* **56**(1), 3431-3441.

Schnurer J. and Rosswall, T., (1982), "Fluorescein Diacetate Hydrolysis as a Measure of Total Microbial Activity in Soil and Litter," *Applied and Environmental Microbiology*, **43**(6), 1256-1261.

Shiney, J. and Varma, Y., (1995), "Flow pattern and pressure drop in gas-liquid cocurrent downflow through packed beds," *Bioprocess Engineering* **12**, 215-220.

Shorey, S. W. (2005), Motor-Fuel Alkylation with CDAlky^{TM} Process Technology, *in* "103rd National Petrochemical & Refiners Association (NPRA) Annual Meeting," San Francisco, CA, March.

Sicardi, S., Gerhard, H., and Hoffman, H., (1979), "Flow regime transition in trickle-bed reactors," *Chemical Engineering Journal* **18**(3), 173-182.

Sicardi, S. and Hofmann, H., (1980), "Influence of gas velocity and packing geometry on pulsing inception in trickle-bed reactors," *Chemical Engineering Journal* **20**(3), 251-253.

Specchia, V. and Baldi, G., (1977), "Pressure drop and liquid holdup for two-phase cocurrent flow in packed beds," *Chemical Engineering Science* **32**, 515-523.

Steinhaus, H., (1999), *Mathematical Snapshots*, Dover.

Talmor, E., (1977a), "Two-phase downflow through catalyst beds: Part 1. Flow Maps," *AIChE Journal* **23**(6), 868-874.

Talmor, E., (1977b), "Two-phase downflow through catalyst beds: Part 2. Pulsing regime pressure drop," *AIChE Journal* **23**(6), 874-878.

Tosun, G., (1984), "A study of cocurrent downflow of nonfoaming gas-liquid systems in a packed bed. 1. Flow regimes: Search for a generalized flow map," *Industrial and Engineering Chemistry Process Design and Development* **23**(1), 29-35.

Tosun, I. and Mousa, H., (1986), "Flow through packed beds: wall effect on drag force," *Chemical Engineering Science* **41**(11), 2962-2965.

Valtsifer, V. and Zvereva, N., (1999), "Statistical packing of equal spheres," *Advanced Powder Technology* **10**(4), 399-403.

van Woezik B.A.A. and Westerterp, K.R., (2000), "Measurement of interfacial areas with the chemical method for a system with alternating dispersed phases," *Chemical and Engineering Processing*, **39**(4) 299-314.

Vidal, M., Rogers, W. J., Holste, J. C., and Mannan, M. S., (2002) "A Review of Estimation Methods for Flash Points and Flammability Limits," *Process Safety Progress* **23**(1), 47-55.

Wammes, W. A., Mechielsen, S. J., and Westerterp, K. R., (1991), "The influence of pressure on the liquid holdup in a cocurrent gas-liquid trickle-bed reactor operating at low gas velocities," *Chemical Engineering Science* **46**(2), 409-417.

Weekman, V. W. and Meyers, J. E., (1964), "Fluid flow characteristics of cocurrent gas-liquid flow in packed beds," *AIChE Journal* **10**(6), 951-957.

Wenn, D. A., Shaw, J. E., and Mackenzie, B., (2003), "A mesh microcontactor for 2-phase reactions," *Lab on a Chip*, **3**, 180-186.

Wilhite, B. A., Huang, X., McCready, M. J. and Varma, A., (2003), "Effects of induced pulsing flow on trickle-bed reactor performance," *Industrial and Engineering Chemical Research* **42**(10), 2139-2145.

Winterberg, M. and Tsotsas, E., (2000), "Impact of tube-to-particle-diameter ratio on pressure drop in packed beds," *AIChE Journal* **46**(5), 1084-1088.

Xiao, Q., Anter, A. M., Cheng, Z. M., and Yuan, W. K., (2000), "Correlations for dynamic liquid holdup under pulsing flow in a trickle-bed reactor," *Chemical Engineering Journal* **78**(2), 125-129.

Young, W. C. and Budynas, R. G., (2002), *Roark's Formulas for Stress and Strain*, 7th ed.

Zabetakis, M., (1965), "Flammability characteristics of combustible gases and vapors," U.S. Dept of the Interior, Bureau of Mines, Bulletin 627.

Zabetakis, M. G., Lambiris, S., and Scott, G. S., (1959), "Flame temperatures of limit mixtures," *7th Symp. (Internat.) on Combustion*, Butterworths Sci. Pub., London, 484–487.

Zanker, V. and Peter, W., (1958), "The prototropic forms of fluorescein," *Chem. Ber.* **91**, 572–580.

Distribution:

Hardcopies to:

Brian Valentine
U. S. Department of Energy
Energy Efficiency and Renewable Energy
Office of Industrial Technologies
EE-20, Office of Industrial Process Systems
1000 Independence Ave. NW
Washington, DC 20585-0121

Bill Prymak
US DOE Golden Field Office
1617 Cole Blvd
Golden, CO 80401

Dickson Ozokwelu
U. S. Department of Energy
Energy Efficiency and Renewable Energy
Office of Industrial Technologies
EE-20, Office of Industrial Process Systems
1000 Independence Ave. NW
Washington, DC 20585-0121

Electronic only:

MS0899	Technical Library, 9536
MS0384	D. B. Dimos, 1500
MS0824	J. S. Lash, 1510
MS0836	C. J. Bourdon, 1512
MS0836	T. J. O'Hern, 1512
MS0836	J. D. Hartenberger, 1512
MS0346	D. J. Rader, 1513
MS0346	J. R. Torczynski, 1513
MS0826	W. Gill, 1532
MS1349	J. E. Miller, 1815
MS1349	L. R. Evans, 1815
MS1454	M. A. Cooper, 2554

Richard Foley, CDTECH
Arvids Judzis, CDTECH